Zeolite Modified Metal Oxides for Gas Sensing

Dominic Peter Mann

This thesis is submitted in partial fulfilment of the requirements for the Degree of Doctor of Philosophy

October 2005

University College London
Chemistry Department

ProQuest LLC
789 East Eisenhower Parkway
P.O. Box 1346
Ann Arbor, MI 48106-1346

Abstract

A novel method of improving the selectivity of metal oxide gas sensors has been developed by using catalytically active molecular sieve materials. They have been successfully introduced into a proprietary sensor array and a commercially available electronic nose.

The cracking patterns of various organic compound groups including alkanes, aromatics and flavours over transition metal exchanged zeolites (ZSM-5, zeolite Y, and zeolite β) have been measured using a zeolite bed/GC/MS experimental set-up within a temperature range of 200°C to 400°C. The findings have been successfully translated for the use of the zeolites as filter technology on chromium titanium oxide (CTO) sensors for the purposes of selective gas sensing. Studies have been carried out regarding the effects of metal loading, zeolite type, material fabrication techniques and operating temperature with regards to catalytic activity and selectivity. Variations in activity due to alkane chain length have been related to the ability of the molecule to enter the zeolite cavity, the quantity of supported metal complexes and their oxidation state in the zeolite pores.

The composite sensors utilising the novel zeolite materials have been used in a custom built sensor rig that houses 3 dual electrode sensors and can measure real time responses of these sensors to an introduced headspace generated from organic liquids. The response data have been utilised in a statistical software package (SPSS 12.0) to rationalise sensor discriminatory behaviour to various compound groups.

The zeolite coated CTO sensors have also been tested in a commercial electronic nose array which has provided enhanced discrimination as compared to a standard CTO sensor array for a number of active and potential commercial applications mainly involving complex flavour compound mixtures.

Table of Contents

Table of Figures

Table of Tables

Table of Abbreviations

ADC	analogue to digital converter
AHM	ammonium heptamolybdate
AQ	aqueous ion exchange
BTX	benzene, toluene, and xylenes
CTO	chromium titanium oxide
DFA	discriminant function analysis
EDAX	energy dispersive X-ray analysis
FCC	fluid catalytic cracking
GC	gas chromatograph
LPG	liquefied petroleum gas
LTA	Linde Type A
MOSFET	metal-oxide semiconductor field-effect transistor
MS	mass spectrometer
MTG	methanol to gasoline
PCA	principal component analysis
PTFE	polytetrafluoroethylene
SEM	scanning electron microscopy
SSE	solid state exchange
UCL	University College London
UMIST	University of Manchester Institute of Science and Technology
USY	ultrastable Y
VOC	volatile organic compound
XPS	X-ray photoelectron spectroscopy
ZSM	Zeolite Socony Mobil

Acknowledgements

I would like to thank my supervisors Professor David Williams and Professor Ivan Parkin for their support and assistance throughout this work. I would also like to thank Dr Keith Pratt, Dr Dewi Lewis, John Hill, Dr Steve Firth, Kevin Reeve and Simon Naisbitt for theoretical and practical assistance during this work. I have enjoyed my time at University College London and appreciate the opportunity to undertake this work.

This work was supported by the European Commission under project MICS, GRD1-2000-25288.

This thesis is dedicated to my grandfather who taught me humility.

1. Introduction

1.1 Overview of thesis

This work has involved development and characterisation of new semiconducting metal oxide sensors. Analytical assessment of these novel sensors was undertaken and the sensors integrated into an electronic nose.

Commercially available zeolite materials were chemically altered by the introduction of transition metal ions (chromium, molybdenum and tungsten) to alter the catalytic characteristics of the zeolites. This process was performed using two different ion exchange techniques (aqueous and solid state) and various loadings of the subsequent metal ion species were obtained. This was performed to compare the effects of the chemical alteration on the zeolite materials catalytic characteristics. The zeolite materials were tested in an experimental rig that was comprised of a zeolite bed, thermal desorber and GC/MS. This was utilised to establish the identity and relative quantities of the reaction products produced after a compound was passed over the heated zeolite powder in an air stream. Thus the catalytic effect of the zeolite materials could be assessed for the purposes of adding it as a filter layer on semiconducting metal oxide gas sensors.

The zeolite materials were subsequently integrated into the design of chromium titanium oxide (CTO) gas sensors as a catalytically active filter layer. An array of three sensors was set up within a proprietary gas testing rig whereby the analyte is introduced via gaseous injection into an air stream. The sensing characteristics of the zeolite filtered sensors were assessed and the transient data related to the catalytic data obtained from the GC/MS testing. The effects of the zeolite layers could clearly be assessed against a standard sensor constructed of a CTO sensing layer with no additional filter layer.

The sensors were also integrated into a commercially available electronic nose to assess their discrimination capabilities with compound mixtures. A number of like samples with subtle varying component concentrations were assessed in the electronic nose. The sensor responses were analysed by principal component analysis (PCA) and discriminant function analysis (DFA) to provide a statistical comparison of the data obtained. This

produced statistical plots of best discrimination and an assessment of the sensor's effectiveness within an array.

1.2 The demand and requirements of gas sensors

Sir Humphry Davy invented his flame safety lamp in 1816 to detect methane in coal mines. This was probably the first successful gas sensor. Although more of a safety lamp in a methane rich environment, if the flame went out it would alert to a low level of oxygen. Due to an increasingly industrialised society since the inception of this early device there has been an ever increasing need to monitor the environments in which we live and work. Therefore nowadays there are a plethora of devices offering a variety of techniques to perform a gas sensing function; electrochemical cells, quartz crystal, spectrophotometric, conducting polymer, infrared, semiconductor, pyroelectric and thermal devices. [1, 2, 3, 4]

Semiconducting metal oxide gas sensors have been used commercially for many years.[5,6] These sensors have advantages over competing technologies such as electrochemical, quartz crystal, spectrophotometric and conducting polymer sensors in terms of long term stability and/or robustness. However, metal oxide sensors suffer from one major drawback in that they are weakly selective, i.e. they respond to a wide range of gases. The relative sensitivity of a sensor to different gases can be modified slightly by variation of operating temperature and/or the addition of dopants or modification of the sensor microstructure.[7,8]

One way to take advantage of poorly selective devices is to operate an array, where the assumption is that recognition and measurement of a particular target gas can be achieved because the relative magnitude of response to that gas on the different poorly selective sensors is different, so that the gas can be recognised by a unique response pattern, similar to a spectrum. Now there comes a different problem with metal oxide gas sensors in that the variations in response pattern obtainable by simple changes of dopant or operating temperature are generally too small to allow an array with good discrimination. There is also the problem of drift in the calibration of an array, which gets worse the larger the number of sensors that are used. Also the mechanism of the discrimination at a molecular reaction level is not understood, which makes development of materials for sensors that might improve discrimination an empirical matter.

1.3 Organisation of the thesis

This thesis presents the conception, fabrication and implementation of a much improved solid state gas sensor based on existing technology, combining a known and robust sensor material with zeolites to modify selectively the gaseous environment sampled by the sensor material. Proprietary analytical equipment was assembled and utilised to provide a unique catalytic characterisation of the materials used. This has proved invaluable in providing an understanding of sensor response characteristics.

- Chapter 2 provides an insight and description of various sensor technologies, a background into zeolite materials and finishes with a description of current electronic nose technology.
- An overview of the existing solid state gas sensor technology utilised in this study is outlined in chapter 3. The construction and operation of the chromium titanium oxide (CTO) sensor is described.
- Chapter 4 describes the experimental procedure used to ion exchange the zeolite materials. The experimental set-up used to assess the catalytic properties of the zeolites is described. Sensor construction and various gas testing rigs are described along with electronic nose operation.
- The zeolite materials characterisation is reported in chapter 5. Scanning electron microscopy (SEM) and energy dispersive X-ray analysis (EDAX) were used to assess the materials.
- Chapter 6 discusses the results obtained from the gas chromatograph / mass spectroscopy (GC/MS) experimental set-up to assess relative catalytic activity of the zeolites towards various organic compounds.
- Chapter 7 details sensor transient data and the direct effects of the zeolite layer by sensor normalisation to a control in an injection gas rig apparatus.
- In the final results chapter, Chapter 8, the electronic nose data are collated and interpreted for the purposes of sensor array and development. Testing of commercial samples is also shown, to assess the improved discriminatory potential over the existing metal oxide sensor array.

• A general discussion of the analytical methods utilised and the results obtained is provided in chapter 9. An overview of the results is provided to show continuity in development from materials characterisation to instrumental analysis.

• Chapters 10 and 11 respectively provide the conclusions and future directions for this technology.

2. Literature Review

2.1 Introduction

The main premise of this study hinges on the functionality and adaptability of the zeolite materials which, when combined with a gas sensor material, provide a means to selectively modify the gaseous environment sampled by the gas-sensitive material, and hence alter in a controllable and gas-specific way the sensor response. Therefore a large proportion of the literature review surveys the history, structure, chemistry, shape selectivity and catalysis of zeolites. As this is such a large subject the focus is mainly on the zeolite types which were used in this study. The section on post zeolite modifications is outlined in chapter 4. There is a section in this chapter detailing past implementations of zeolites in gas sensors and the chapter concludes with an overview of electronic noses. Thus the literature review runs linearly with the development, implementation and utilisation of zeolites in gas sensors akin to the experimental analysis in this study.

2.2 Zeolites – An Introduction

The word "zeolite" is Greek in origin, coming from the words "zein" and "lithos" meaning to boil and rock, respectively. The word was first coined by Cronstedt (Swedish Chemist) in 1756 who found that upon heating the zeolite mineral (stilbite) it produced steam.[9, 10] However it was not until the 1930s that the characterisation of zeolite structures and chemistry was explored by the modern founder of zeolite chemistry, Barrer.[11] His many papers gave details of the first method of laboratory synthesis of zeolites from silicate alumina gels, the changes that occur upon ion exchange and their use as strong environmentally friendly, shape selective catalysts. These discoveries sparked huge interest in the synthesis of shape selective zeolite catalysts in companies such as Union Carbide and Mobil. In the 1950s and early 1960s Union Carbide made several discoveries which proved to be of great economic significance and propelled them to the forefront of zeolite science. Milton and Breck of the Linde division of Union Carbide, over a period of 5 years, developed and characterised three novel zeolites Linde A, X and Y, which have become 3 of the most profitable synthetic zeolites.

The structure and types of zeolites are many and varied and there are now websites devoted to their structures[12] and journals devoted to their science, namely "Zeolites" which was later incorporated into "Microporous and Mesoporous materials" published by Elsevier. Basically zeolites can be found naturally or synthesized. They are commonly used as molecular sieves because of their lattice-type molecular structure with many internal spaces which can be occupied by atoms and molecules of other substances.

Natural zeolites are a group of hydrous aluminium silicate minerals, containing varying amounts of group I or II cations that are present in the surrounding environment, e.g. K^+, Na^+, Ca^{2+} and Mg^{2+}. They occur as veins or as in-fillings of voids within basic igneous rocks such as basalt, which is the commonest type of lava.

Structurally within zeolites, the isomorphous replacement of silicon with aluminium gives rise to a charge imbalance due to the different atomic valencies which must be neutralised. Also aluminium has lower co-ordination ability than silicon leading to a structural alteration. The neutralisation is achieved in two ways:

1. The Al-O bond length becomes slightly longer.
2. A co-ordination site is made available for the cation to counter the excess negative charge.

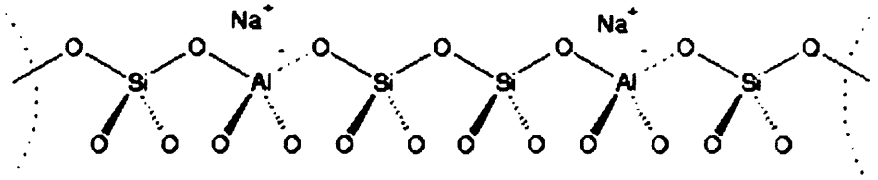

Figure 2.2.1 Neutral sodium balanced zeolite framework. Na^+ balances the negative charge at co-ordination site.

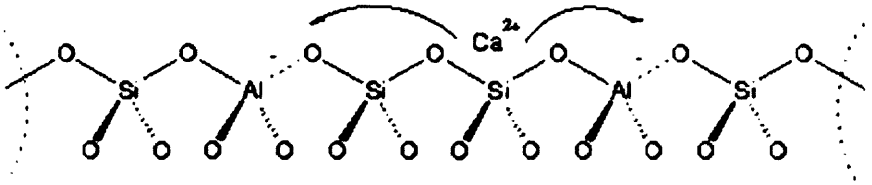

Figure 2.2.2 Neutral calcium balanced zeolite framework. Ca^{2+} balances the negative charge at two co-ordination sites.

Zeolites are found in everyday household products such as cat litter to absorb odorous compounds, and they are a constituent of washing powder to soften the water and prevent the precipitation of surfactants. In washing powder the Na^+ version of zeolite A

(LTA structure) is used which readily swaps the Na^+ ion for Ca^{2+} and Mg^{2+} ions. Zeolite A is also used for the treatment of radioactive waste where radioactive caesium and strontium are removed from nuclear waste into the zeolite cavity. The zeolites are stable even under the highest levels of radiation, a fact proven after the fission reactor meltdowns at both Three Mile Island and Chernobyl where zeolites (mainly bentonite) were used to remove radioactive ions from contaminated water.[13]

Synthesized zeolites are largely based around the structures of natural zeolites, e.g. zeolite Y has a Faujasite structure.[12] Large mesoporous materials which are not based on natural structures have also been synthesized e.g. MCM-41 (approximately 40 Å pore diameter). Possible structures and synthesis routes can be assessed computationally before being made. The cation in the structure can be a variety of types depending on the template molecules used to create the pores during synthesis. Also many post synthesis techniques can be applied to alter the chemical characteristics and structure of the zeolite.

Industrially zeolites have typically been used as a catalytic and/or filtering agent in various chemical production processes, especially in the petrochemical industry. Their importance to industrial catalysis can be attributed to them possessing a unique combination of the following properties:

- High internal surface areas (>600 m^2/g)
- Uniform pores with one or more discrete sizes
- Presence of ion exchangeability produces highly dispersed catalytically active sites, such as highly acidic sites when the exchangeable cations are replaced by protons.
- Good thermal stability
- Ability to sorb and concentrate hydrocarbons

The uses of zeolites are increasing at a substantial rate, as advantage is being taken of their filtering ability in a wide range of pollution control applications. They are used for odour control in waste materials and for removing unwanted wastes in effluents from agricultural and industrial processes.

2.3 Zeolite Structures and Chemistry

Zeolites have the chemical formula $M_{2/n}OAl_2O_3.xSiO_2.yH_2O$, where the charge-balancing nonframework cation M has valence n, x is 2.0 or more, and y is the number of moles of water in the voids. The primary building unit of zeolites are cations coordinated tetrahedrally by oxygen. These tetrahedra are connected via corners, thus forming the crystal structure of the specific zeolite.

A number of zeolites are used as catalysts either as the parent aluminosilicate, de-aluminated or with metal ions substituted in the framework. The type of counter ion used to balance the charge plays an important part in the use of the zeolite. A typical aluminosilicate zeolite can act as a solid acid since for each Al^{3+} substituted for Si^{4+} in the structure, a proton can be used to maintain the overall neutrality. The cation is replaced by hydrothermal treatment to form a hydroxyl group at the oxygen bridge as shown in figure 2.3.1. The acid site formed behaves as a classic Brønsted, proton donating acid site.

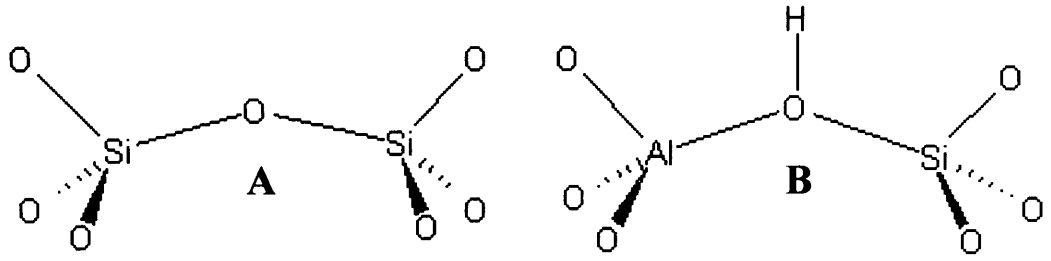

Figure 2.3.1 Diagrams representing A) Siliceous zeolite B) Zeolite Brønsted acid site.

In many zeolites the Si/Al ratio is often increased to improve stability through dispersion of the Al sites. Furthermore this dispersion can actually increase the catalytic effect of the zeolite as the acidic sites are more effectively spread over the framework and isolated Si-O-Al sites are believed to be more acidic. When acid sites are close together they can dehydrate becoming Lewis acid sites. Isolated sites are stronger due to higher electric field gradients. When acidic sites are near to each other the electric fields overlap and there is less loss of potential between sites as opposed to isolated sites. There are a number of methods by which the Si/Al ratio can be increased. For example by treatment with $SiCl_4$, the Al is leached from the framework and replaced by Si. Aluminium can also be removed hydrothermally by a treatment with steam at 500°C. Aluminium remains as an extra-framework (octahedral) species which can contribute to acidity (Lewis) and

subsequent catalysis. Si moves into the framework vacancies left from other parts of the crystal (bulk). The Al remains in the sample, either as intracrystalline oxidic or cationic aluminium species or as intercrystalline material i.e. as a separate crystalline or amorphous aluminium oxide phase.

The microporous nature of zeolites allows for the selective absorbtion of reactants, which is dependant on the aperture size of the cavities produced by the arrays of tetrahedra within the molecular framework. This 3-D lattice array when built up consists of channels through which certain small molecules can pass and react inside by a process called shape selectivity. Bulky molecules cannot enter the channels and reaction of smaller molecules to larger ones is hindered by the size of the channels.

A major progress in the field of shape selective catalysis was the discovery of the medium pore zeolite ZSM-5. (The framework of this zeolite and others are shown in Appendix 1). The importance of ZSM-5 is due to its unique channel structure with dimensions approaching those of many organic molecules resulting in diffusional differences between linear and branched hydrocarbons.[14] It is also thermally stable at the temperatures (up to 600°C) used in this work.

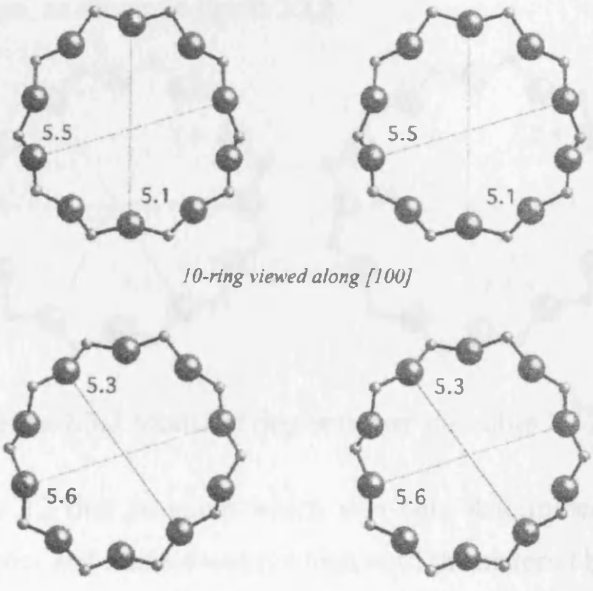

Figure 2.3.2 Models of the ring structure in ZSM-5 showing both pore systems.[12]

In ZSM-5 there are two intersecting pore systems as shown in figure 2.3.2,[12] one consisting of zigzag channels of near-circular cross-section (bottom pair in figure 2.3.2) and another of straight channels of elliptical shape (top pair in figure 2.3.2). In figure 2.3.2 for each set of pores indicated the ring on the left indicates the pore size at the start of the channel on one side of the unit cell and the ring on the right indicates the pore size at the end of the channel on the other side of the unit cell. The intersection of the two sets of channels creates a supercage cavity with a diameter about 9 Å. Its water content is low which is in contrast to the hydrophilic nature of most other zeolites.[15 16]

Zeolite Y is used commercially for the catalytic cracking of hydrocarbons in the production of transportation fuels from crude oil. As prepared zeolite Y is thermally unstable above 500°C and hence is usually modified by a hydrothermal treatment, or steaming. This increases thermal stability as mentioned earlier and leads to an increase in the hydrocarbon cracking activity due to the isolated Al atoms being more acidic. It has also been suggested that the large enhancement in activity is partly due to the increased surface area of the zeolite caused by destruction of crystallinity upon steaming.[17] The channels of zeolite Y are composed of 12 oxygen atoms forming a ring of diameter 7.4 Å, referred to as supercages, as shown in figure 2.3.3.

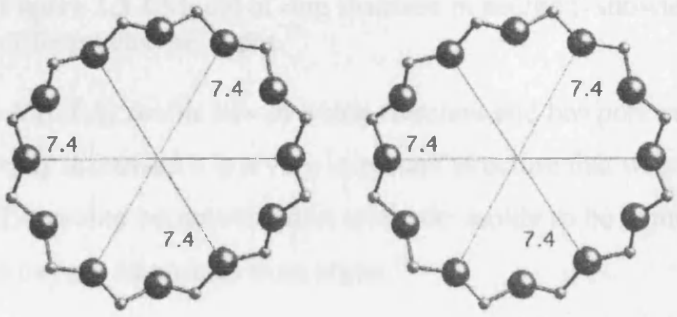

Figure 2.3.3 Model of ring structure in zeolite Y.[12]

Zeolite β has a 12 ring structure which was only determined in the late 1980's because it is very complex and interest was not high until the material became important for some de-waxing operations. De-waxing is the absorption of wax-like, long chain normal paraffins from oil feed stock and subsequent selective conversion into branched paraffins. Zeolite β consists of an intergrowth of two distinct structures termed polymorphs A and B, which grow as two-dimensional sheets that randomly alternate. Both polymorphs have a

three dimensional network of 12-ring pores, and whilst the intergrowth of the polymorphs does not significantly affect the pores in two of the dimensions, in the direction of the faulting the pore becomes tortuous, but not blocked. Therefore zeolite β is composed of two types of channels along different axes as shown in figure 2.3.4.

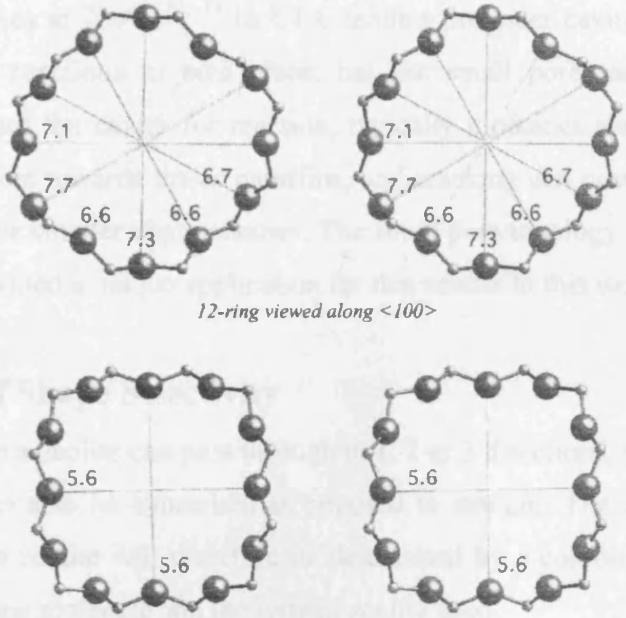

Figure 2.3.4 Model of ring structure in zeolite β showing different channel types.[12]

Linde Type A (LTA) zeolite has an 8 ring structure and has pore sizes ranging from 3 Å to 10 Å. As already discussed it is a very important structure that was one of the first to be characterised, LTA zeolite became the first synthetic zeolite to be commercialised as an adsorbent to remove oxygen impurities from argon.[18]

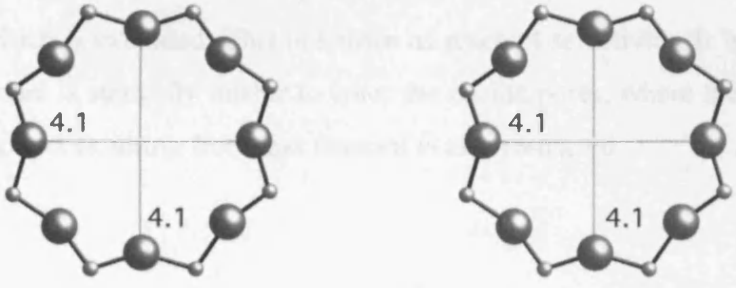

Figure 2.3.5 Model of ring structure in LTA zeolite.[12]

The size of the largest pore in a zeolite is determined by the number of oxygen ions rimming the pore and its shape; e.g. a planar, circular eight-ring (8R) pore rimmed by eight oxygen ions has a diameter of 4.1 Å as can be seen in the LTA zeolite. It has a void volume fraction (ratio of solid to intracrystalline space) of 0.47, with a high Si/Al ratio of 1.0. It thermally decomposes at 700°C.[12, 19] In LTA zeolites the inner cavity is large enough for structure changing reactions to take place, but the small pore means only a specific structure can get into the cavity for reaction, typically n-alkanes and alkenes. The small entry pore is selective towards linear paraffins, and cracking can occur on sites within the supercage to produce smaller chain alkanes. The small pore topology of LTA coupled with its stability has provided a unique application for this zeolite in this work.

2.4 Principles of Shape Selectivity

The pores in a zeolite can pass through in 1, 2 or 3 directions, vary in size and in the case of ZSM-5, can also be sinusoidal as opposed to straight. The rate of diffusion of a molecule through a zeolite will therefore be determined by a combination of the size and shape of the diffusing molecule and the type of zeolite used.

2.4.1 Molecular exclusion

The first type of selectivity is reactant selectivity. For example, only molecules equal or smaller in dimension in their straight dimensions than straight hydrocarbons and alcohols can pass through the pores of an 8-membered oxygen ring small pore zeolite. Therefore it is possible to selectively catalyse the reaction of these molecules in a mixture of other branched and cyclic molecules over small pore zeolites. For example, figure 2.4.1.1 shows the selectivity between heptane which is accepted into the zeolite pore and methyl-hexane which is excluded. This is known as reactant selectivity. It is also useful to note that if a reactant is sterically unable to enter the zeolite pores, where the reaction takes place, then the product resulting from that reactant is also restricted.

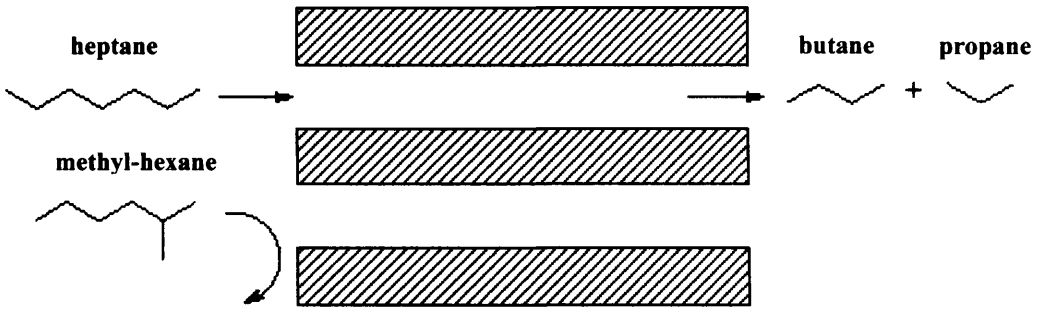

Figure 2.4.1.1 Schematic diagram of reactant shape selectivity: Rejection of branched chained hydrocarbons.

Hence the availability of more than 50 different aluminosilicate zeolite structures with pore openings ranging in size from less than 5 Å to larger than 10 Å offers a variety of possibilities for carrying out selective reactions by size exclusion.

The second type of selectivity is product selectivity. Larger product molecules may be produced in the supercages of the zeolite and then undergo secondary reactions to produce smaller molecules which then escape, slow down the reaction and in some cases deactivate the zeolite by carbonisation. Figure 2.4.1.2 describes the conversion of methanol and benzene to para-xylene (1,4-dimethylbenzene).

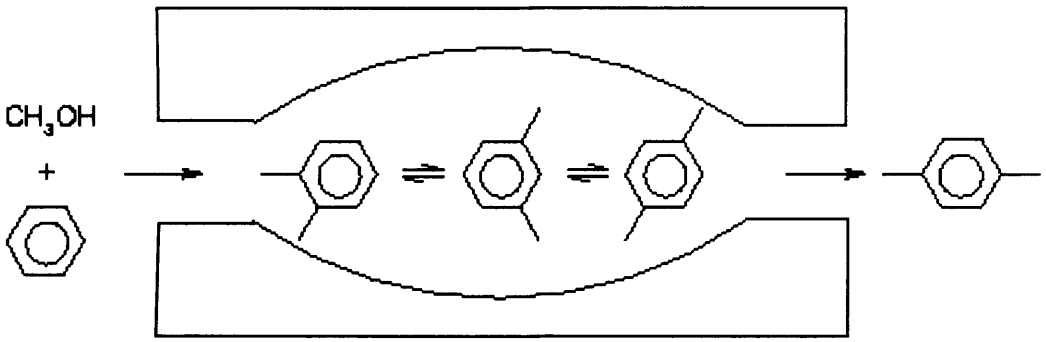

Figure 2.4.1.2 Schematic diagram of product shape selectivity: Para-xylene diffuses preferentially out of the zeolite channels.

Of particular interest to us here is the observation of Jacobs et al.[20] who found major differences in isomer distribution obtained on hydroisomerisation of C_9 – C_{10} n-alkanes with ZSM-5 compared to a larger pore zeolite, ultrastable Y (USY), a lot less dibranched and tribranched isomers were produced through the ZSM-5.

2.4.2 Coulombic Field Effects

Zeolites have unique pore sizes and more intense coulombic fields that leads to higher intracrystalline reactant concentrations than in other amorphous solids.

The size of the pore or channel system in a zeolite has a large influence on the strength of sorption. Butanes and hexanes, for example, are much more strongly sorbed in medium pore zeolites such as ZSM-5 than in large pore zeolites such as ultrastable-Y. High alumina (low Si/Al ratio), cationic zeolites possess strong electrostatic fields and are hydrophilic. They sorb polar molecules such as water or alcohols in preference to non polar hydrocarbons. In contrast the sorbate interaction in high silica (high Si/Al ratio) zeolites is essentially due to dispersion forces with little contribution from polarization forces. Such materials are hydrophobic and do not show such preferences in sorption.

Zeolites containing alkali metal cations more strongly adsorb aromatic molecules. For example in Na-zeolite, benzene is more strongly adsorbed than cyclohexane. Replacing the Na cations with protons generates the undissociated hydroxyl groups and almost eliminates the electrostatic field leaving only the dispersion forces. As a result in the H-zeolite, cyclohexane is now more strongly sorbed than benzene because it contains more hydrogen atoms.

2.4.3 Transition State Selectivity

Transition state selectivity occurs when both the reactant molecule and the product molecule are small enough to diffuse through the intracrystalline channels, but the reaction intermediates are larger than either the reactant or product. This is especially important for ZSM-5. The effect is independent of crystal size, activity, or Si to Al ratio, and depends only on the zeolite structure and pore diameter. For example, because 3-methylpentane is a bulkier molecule than n-hexane its transition state complex has a significantly larger cross-sectional area, giving rise to the constraint index test, which measures the relative rate of cracking of the pair over different zeolites. The index decreases for medium pore zeolites with temperature as the role of bimolecular cracking diminishes.

2.4.4 Other effects

Configurational diffusion controlled selectivity - Selectivity is controlled by configurational diffusion when the rate of diffusion of the slower species either reactant or product cannot keep up with the rate of conversion.

Reverse Molecular Selectivity – Cavities formed at the intersection of a zeolitic channel system are often larger than the pores. Large product molecules, which then either go through a further reaction or get trapped and can act as a precursor to coke formation, can be formed in these cavities.

Confinement or surface curvature effects – This term encompasses various interacting forces between the host and the guest molecules, including chemisorption, physisorption, and molecular orientation within the zeolite. It has been speculated that in the case of molecular diffusion the relationship between the guest and the host depends on the curvature of the intracrystalline host surface and the shape and size of the guest molecule. Diffusion rates increase, acquiring supermobility as the guest molecule, and the zeolite pore size match each other more intimately.

2.5 Principles of Zeolite Catalysis

The number and location of active sites in a catalyst are known to determine the catalytic activity. The location of active sites becomes especially critical in zeolite catalyst systems since zeolites are made up of crystalline arrays of cages and channels with dimensions close to molecular size, ultimately rendering some or all active sites inaccessible to reactant molecules.

The catalytic activity of zeolite materials, in hydrocarbon conversion reactions for example, is based on the presence of acidic centres, especially strong Brønsted acid sites in the zeolite framework. The O-H bond in a Brønsted acid site is mainly covalent in nature and the acid strength is affected by the Si-O-Al angle, the amount of aluminium in the first coordination sphere and the concentration of protons in the framework.[14] Therefore, if we consider H-ZSM-5 which has a high Si to Al atomic ratio, it also has a high acid strength due to the low concentration of structural aluminium atoms. If the Si to Al ratio is high the acidic centres are therefore isolated and high in acidic strength leading to low rates of bimolecular hydrogen transfer reactions, such as between a carbocation and a feed paraffin

molecule. This factor, as well as the advantageous channel structure in ZSM-5 are the reasons for its use as a large octane boosting component in a modern fluid catalytic cracking (FCC) catalyst.

If we take the example of linear alkane cracking, there are a number of mechanisms by which cracking can occur. At elevated temperatures, non-catalytic, thermal cracking can occur. Thermal cracking proceeds via primary radicals, which crack at the C-C bond located β to the carbon atom having the unpaired electron. Such a mechanism would typically lead to large amounts of ethene being produced and small amounts of methane and other alkenes.

Catalytic cracking can occur either via hydrogenolysis (breaking of a chemical bond in an organic molecule with the simultaneous addition of a hydrogen atom to each of the resulting molecular fragments) of hydrocarbons over, e.g. Pt in a metal substituted zeolite, or via acid catalysis. In acid catalysed conversion of hydrocarbons, the reaction proceeds via positively charged carbocations, i.e. carbenium ions ($C_nH^+_{2n+1}$) and/or carbonium ions ($C_nH^+_{2n+3}$) as reaction intermediates.[21] If cracking proceeds via the protolytic monomolecular route, the formation of lighter linear alkanes can be accounted for by a simple cleavage of a penta-coordinated carbonium ion ($C_kH^+_{2k+3}$) into a smaller alkane (C_mH_{2m+2}) and a carbenium ion ($C_nH^+_{2n+1}$) where m + n = k.

Therefore the reaction is thus:

$$C_kH_{2k+2} + H\text{-}Z \rightarrow C_kH^+_{2k+3} + Z^- \rightarrow C_nH^+_{2n+1} + C_mH_{2m+2} + Z^- \quad \textbf{(1)}$$

Where H-Z denotes a proton site in the zeolite framework. If k = 6 for example (n-hexane), n = 2 to 5 and m = 1 to 4. The production of hydrogen is also possible. The carbenium ion (which may be linear or branched) in this reaction will then proceed and may lose a proton to form the corresponding alkene:

$$C_nH^+_{2n+1} + Z^- \rightarrow C_nH_{2n} + H\text{-}Z \quad \textbf{(2)}$$

Also the formation of alkenes may occur simultaneously from equation (1) and not via the consecutive reaction (2).

$$C_kH_{2k+2} + H\text{-}Z \rightarrow C_kH^+_{2k+3} + Z^- \rightarrow C_nH_{2n} + C_mH_{2m+2} + Z \quad \textbf{(3)}$$

The carbenium ion can also be involved in secondary reactions rather than the one detailed in reaction (2). These routes are termed bimolecular. By using n-hexane as the feed molecule it can lead to:

• Isomerisation to branched, tertiary carbenium ions and subsequent H-transfer followed by β-scission. "i" indicates branched and "n" indicates linear alkanes.

$(i,n)\text{-}C_4H^+_9 + n\text{-}C_6H_{14} \rightarrow (i,n)\text{-}C_4H_{10} + n\text{-}C_6H^+_{13}$ **(4a)**

then: $n\text{-}C_6H^+_{13} \rightarrow C_3H^+_7 + C_3H_6$ **(4b)**

• Alkylation of an alkene with a small carbenium ion followed by β-scission of the formed carbenium ion.

$C_nH^+_{2n+1} + C_mH_{2m} \rightarrow C_{m+n}H^+_{2m+2n+1}$ where $(m+n) \geq 6$ **(5a)**

$C_{m+n}H_{2m+2n+1} \rightarrow$ cracked products via β-scission. **(5b)**

• Isomerisation followed by H-transfer.

$n\text{-}C_6H^+_{13} \rightarrow i\text{-}C_6H^+_{13}$ **(6a)**

$i\text{-}C_6H^+_{13} + n\text{-}C_6H_{14} \rightarrow i\text{-}C_6H_{14} + n\text{-}C_6H^+_{13}$ **(6b)**

As a final secondary reaction, H-transfer reactions between alkenes formed in reaction (2) yield alkanes, cycloalkenes, and ultimately aromatics.

The carbenium ions will always rearrange to the most stable form:

tertiary > secondary > primary > methyl carbenium ion

$R_1\text{-}^+CR_3\text{-}R_2 > R_1\text{-}^+CH\text{-}R_2 > R_1\text{-}^+CH\text{-}H > {}^+CH_3$

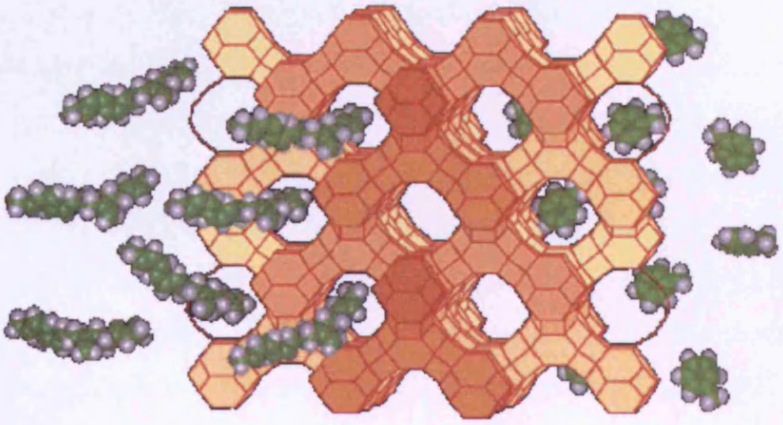

Figure 2.5.1 Model of catalytic activity within zeolite Y structure.[12]

Figure 2.5.1 shows a 3-dimensional model of the catalytic cracking process to smaller molecules from a larger feedstock molecule.

In summary, carbenium ions, once formed on zeolites, may (a) desorb as alkenes from the catalyst, (b) undergo double-bond-, cis/trans-, and skeletal isomerisation, (c) crack further into smaller alkenes and carbenium ions. The extent to which these processes occur depends on the acidity of the catalyst and on the shape and concentration of the alkenes.[22]

2.6 Zeolite Catalysis "in action"

An example of the effect of shape selective catalysis is the methanol to gasoline (MTG) process[23] developed by the Mobil Oil Company but discovered by accident. The zeolite H-ZSM-5 was being used to convert methanol into a fuel additive. The process instead produced di-methyl-ether, which underwent further reaction to produce alkenes, alkanes and aromatics, the final mixture of paraffins and aromatics being similar to that in gasoline. The MTG process is highly dependent on the presence of the Brønsted proton. If the catalytic H-ZSM-5 is replaced by the purely siliceous analogue of ZSM-5 which has no Brønsted protons, the reaction does not take place at all. In the MTG process a stream of gaseous methanol is passed over an H-ZSM-5 catalyst bed and a dehydration-polymerisation reaction takes place inside the pore. The resulting effect is a sharp cut off of product distribution at C_{11} (gasoline) length fractions, the largest length of hydrocarbon that can fit inside the zeolite pore. The impact of this has been immense, countries with no natural source of crude oil such as New Zealand are generating their own gasoline via the MTG process.

Zeolites are used for the purposes of catalytic cracking in the petroleum refining process. In petroleum refineries the heavy fractions such as gas oil are fed to fluid catalytic cracking (FCC) units or fixed bed hydrocracking units, which utilise catalyst particles containing zeolite Y or other zeolites. They convert the higher molecular weight hydrocarbons to lighter ones suitable for gasoline and other uses.

There are many catalytic processes in petroleum refining for which zeolites are used such as hydrocracking, catalytic dewaxing, paraffin hydroisomerisation and various aromatic production e.g. ethylbenzene, para-xylene, cumene. Of particular interest is the production of aromatics from light hydrocarbons. Various modified ZSM-5 zeolites have been used to convert LPG (propane, butanes) or feedstocks containing alkenes and alkanes liquid aromatic products, particularly BTX (benzene, toluene, and xylenes).[24] For example, a Zn doped H-ZSM-5 zeolite is used in the Alpha process to convert light hydrocarbons containing a high percentage of olefins into BTX.[25]

2.7 Post-synthesis zeolite modifications

After synthesis from the primary precursors, the unadulterated zeolite frameworks are often unsuitable for many of the catalytic purposes for which they are intended and require modifications. Often the objective is to produce more hydrophobic zeolites that are more "organophilic" and therefore have different sorption selectivities. Often simple methods can be employed to alter the Al content such as steaming to alter the acidic strength as mentioned previously. However because of the selective nature of the molecular framework, zeolites are often employed to support metal ions for more effective catalysis. After synthesis negative charges are present in the microstructure due to the framework aluminium. These negative charges on the framework get balanced by the positive charges of extra framework cations or via the interaction of the framework oxygen atoms with protons under formation of acid hydroxyls, the Brønsted centres. Usually Na^+, K^+ or other template cations are present from the synthesis and play the role of charge compensating species. However these or the protons can be replaced by other cations. A simple example of this is exhibited by the different pore sizes obtainable in the Linde Type A (LTA) zeolite which is a commonly used molecular sieve. After synthesis LTA with Na^+ cations has a pore size of 4 Å, if 75% of the Na^+ cations are replaced by larger K^+ cations the pores become more restrictive producing a pore size of 3 Å, and if 75% of the Na^+ cations are replaced by divalent Ca^{2+} cations the pores become more open attaining a pore size of 5 Å.

There are a variety of different types of post-synthesis modifications possible; ion exchange in aqueous solution, solid state ion exchange, dealumination, and impregnation are the main methods.[26]

Ion exchange in aqueous solutions is carried out by suspending the zeolite powder in aqueous solutions of salts containing the cation for exchange. After stirring the suspension for a period of time, usually at elevated temperature the zeolite powder and the solution must be separated. The separation process may need to be repeated for a high level of exchange. Problems are encountered when the cation complexes are too bulky to enter the zeolite pores. This method was the one used in our study to exchange Cr cations. The process was initially performed by T. Paraskeva[27] and was based on a method utilised successfully by Chintawar and Greene.[28, 29] The method was repeated and is detailed in chapter 3.

In solid-state ion exchange dry powders of zeolites and salts or oxides containing the cation for exchange are reacted. It can be done in one step, and cations can be incorporated into narrow pore zeolites.

Dealumination can be performed by a variety of techniques which involve either the extraction of framework aluminium by chemical agents, hydrothermal dealumination, and the substitution of framework silicon for aluminium.

Once the ion exchange has been performed, depending on the method and the zeolite used the catalytic properties of the zeolite and the position of the exchanged cations can be markedly different. Hence, a structural analysis of a given zeolite catalyst to locate actual sites is very useful in understanding its activity. Parillo et al. [30] looked at the characteristics of Cu exchanged ZSM-5 and Y. They found that even when each zeolite has comparable Si/Al ratios and Cu content there is a large difference in activity, the Cu-Y being much less active. They found that in Cu-Y the ion-exchanged Cu does not remain at the tetrahedral Al sites upon heating but is replaced by a proton which results in Brønsted acidity, with Cu migrating to less accessible locations. They proposed that this instability of the Cu in the Y resulted in the difference in activity due to the more open structure of Y zeolites and the lack of 5 member ring pockets present in ZSM-5, therefore making it easy for the Cu to migrate.

With regard to Cr exchanged zeolites, Rachapudi et al. [31] looked at the interactions of Cr-ZSM-5 with chlorinated volatile organic compounds (VOCs). They found that chromium sites (S_{II}, S_{III} – as illustrated in figure 2.7.1) within the straight channels or near channel intersections were the most active, but were most prone to migration and/or loss. These sites are most accessible to the chlorinated VOCs but their loss is also due to their weak association to the zeolite framework. However, chromium sites (S_I, S_{IV}) located in the sinusoidal channels were found to be less active, but more persistent during deactivation because of their increased coordination with zeolite framework atoms and reduced accessibility to incoming molecules. Interestingly these authors did not encounter any visible coking of the material or any significant carbonaceous material on the catalyst surface. Obviously the conditions involved here are quite harsh but it gives us an idea of site importance of the Cr cations and points to problems that might occur during testing to other feed molecules.

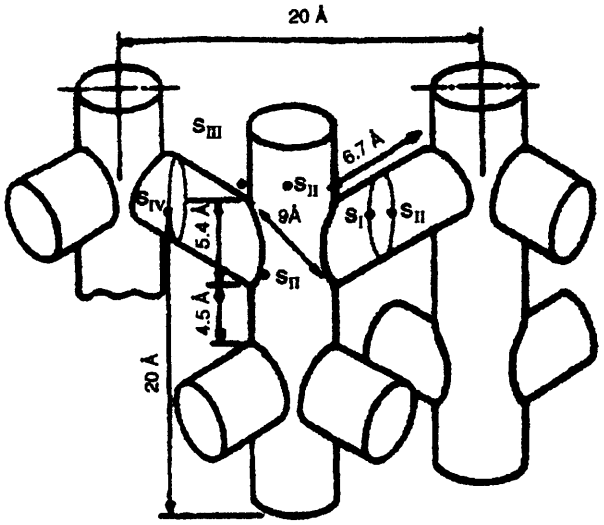

Figure 2.7.1 Possible site locations of Cr ions after exchange.[31]
Key:
S_I – midway along the surface of the sinusoidal channels
S_{II} – within the open straight channel cross section, near the intersections
S_{III} – subsurface, top and bottom edges of sinusoidal channels, near intersections
S_{IV} – 2/3 of the way along the surface of the sinusoidal channels.

An alternative approach to the introduction of Cr into a zeolite structure has been developed by Gianetto et al.[32] who introduced the Cr at the zeolite synthesis stage thus hoping for more dispersed chromium species. Their concern was that with conventional methods of exchange the chromium species may be in the form of supported oxides rather than in the framework. They found that extensive oxidation of occluded Cr(III) clusters to Cr(VI) species occurred after calcination and also the presence of structural and non-structural Cr(V) species was detected.

Wechhuysen et al.[33, 34], performed a large study on various metal ions exchanged into ZSM-5 by impregnation and solid state exchange. They found that activity to convert methane into aromatics decreased in the following order: Mo > W > Fe > V > Cr, and that impregnated materials had higher activity than solid state ion-exchanged materials. The catalytic effects depended heavily on the presence of Brønsted acid sites, the distribution of the transition metal ions in the zeolite material, and the pre-treatment of the material. They proposed that the supported transition metal ions were mainly located in the zeolite channels of the solid state ion materials which had only a small amount of Brønsted acidity. In the sample prepared by impregnation the supported transition metal ions were mainly

located at the outer surface, and only a fraction diffused into the channels of the zeolite material. After XPS analysis of the Cr impregnated materials they found that Cr(VI) with some traces of Cr(V) was the main species in what was a yellow coloured catalyst. After reaction in methane (oxygen free atmosphere) for 3.5 h they found that Cr_2O_3 was starting to be formed. After reaction in methane for 10 h they found that either coke was forming over the Cr_2O_3 clusters or that the clusters were growing in size.

Several attempts using a variety of techniques have been made to introduce molybdenum cations into zeolite Y.[35, 36, 37, 38] There has also been some interest in creating binary Ni-Mo zeolite Y catalysts for the purposes of hydrocracking.[38, 39] Aqueous ion exchange has been a popular method to introduce Mo into zeolites using solutions of ammonium heptamolybdate (AHM),[40] although there are problems due to the large aqueous molybdate ions not exchanging directly onto the cation exchange sites because they fail to penetrate the zeolite cavities.[36] This problem can be overcome by thermal decomposition of these species under low vapour pressures of water to produce a redispersion of molybdenum due to solid-state exchange of $MoO_2(OH)_2$ within the zeolite pores.

For the solid state exchange of molybdenum into a zeolite, the hydrogen form of the zeolite is physically dry mixed with MoO_3 and subsequently heat treated.[35, 41, 42] During the heat treatment isolated MoO_x species migrate into zeolite channels via gas phase or surface diffusion, and react with H^+ atoms at exchange sites to form $(MoO_2(OH))^+$ species, which can condense with another one to form a $(Mo_2O_5)^{2+}$ dimer and H_2O. The dimer formed will be most prevalent in zeolites with a low Si/Al ratio such as the zeolite Y (Si/Al = 5.2). The reaction pathway is outlined below: [43]

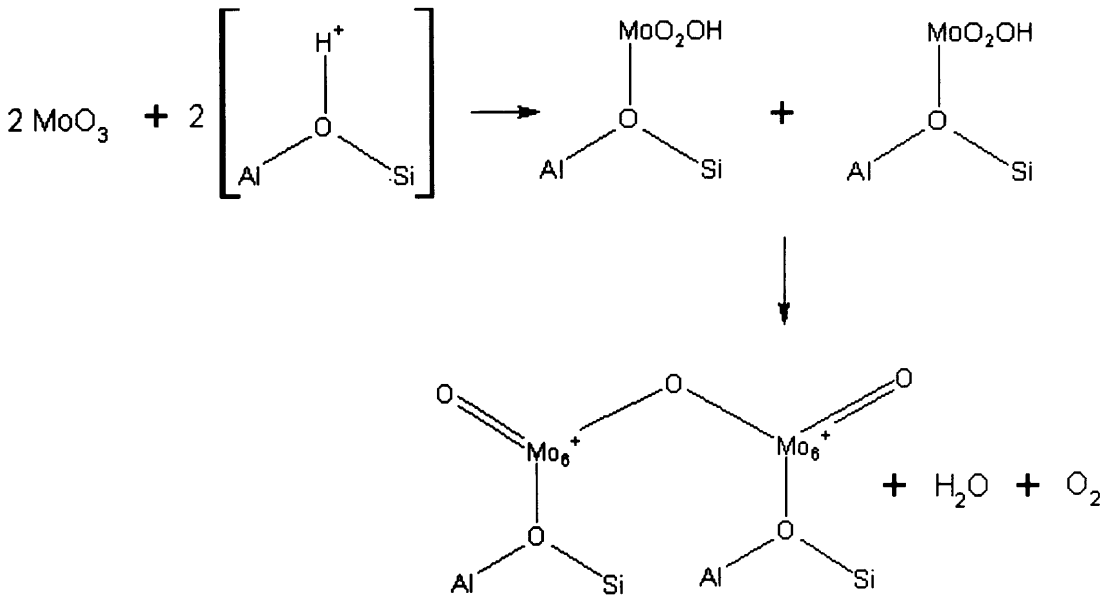

Figure 2.7.2 Reaction scheme of MoO_3 introduction into a hydrogen zeolite via solid state ion exchange.

Pt-mordenite catalysts have been used for the hydroconversion of linear alkanes.[44] In this process the metallic function converts the linear alkane into the corresponding alkene at a high enough rate to ensure the permanent establishment of the thermodynamic equilibria:

n-alkane $\leftrightarrow$ n-alkene + H_2

isoalkene + $H_2 \leftrightarrow$ isoalkane

The acid function performs the isomerisation of the linear alkene into the corresponding isoalkene. Thermodynamics anticipate favoured cracking as the temperature is increased. It is therefore most important that the acid function be as strong as possible to convert the intermediate alkene into the corresponding carbenium ion at the lowest possible temperature to favour isomerisation against cracking.

Tungsten exchanged H-ZSM-5 catalysts have been characterised for the partial oxidation of methane to formaldehyde.[45, 46] In this instance an aqueous ion exchange is performed on the H-ZSM-5 by ammonium metatungstate. It was found that both monomeric and polymeric tungsten species are present in the material after exchange. The monomeric species (isolated tetrahedra WO_4^{2-}) join to the Brönsted acid sites of the zeolite.

The samples with the highest W loading had the highest amount of polymeric species (polyoxotungstate and WO_3 crystallites) which were located on the external surface due to their large size causing the blockage of channels to some extent. However relative acidity did not drop off with these samples. The increase in the amount of polymeric species is observed above a W loading of 4.0%. There was a dramatic reduction in the BET surface area above a loading of 7.1%. Therefore at low contents of tungsten, tetrahedral species predominate and they are mainly located in the zeolite channels. For higher loading, the amount and size of the polytungstate species increases gradually causing a decrease in the dispersion and the partial blocking up of the H-ZSM-5 zeolite.

2.8 Catalysis utilising transition metal exchanged zeolites

Supported metal catalysts have been used for many years for reactions involving hydrogen, such as hydrogenation, hydrogenolysis, and catalytic reforming. In these applications metal particles are highly dispersed on inert aggregate supports. However if the metal is dispersed in the form of ionic complexes or oxide clusters on a solid acid zeolite support, the relative rates of parallel or sequential reactions ought to be affected by the number, arrangement and type of sites on the catalyst. These in turn will be affected by site positioning in relation to the zeolite pore structure, determining access of the analyte to the catalytic sites. Finally, there is the question of how the residence time within the volume of material is affected by these factors to produce the resultant reaction products.

There are many catalytic applications for metal-exchanged zeolites. If we take a look at ZSM-5 as the zeolite support, then depending on the metal exchange a number of different reactions can be achieved.[47]

- Pd-ZSM-5 - water tolerant catalyst for NH_3 oxidation to N_2

$$2NH_3 + 3/2O_2 \rightarrow N_2 + 3H_2O$$

- Pd-ZSM-5 - catalyst for CH_4 combustion.
- Co-ZSM-5 – catalyst for wet N_2O decomposition
- Cu-ZSM-5 – catalyses the decomposition of NO_x into its elements.

Bifunctional catalysts such as these comprise a combination of acid and hydrogenation-dehydrogenation functions. The conventional reaction mechanism for the conversion of an alkane on a bifunctional catalyst is as follows - the metal phase dehydrogenates the alkanes into alkenes which are protenated at the Brønsted acid sites yielding alkylcarbenium ions. After rearrangements and/or scissions, these alkylcarbenium ions desorb from the acid sites as alkenes and are hydrogenated at the metal phase to yield saturated reaction products.[48]

2.9 Use of zeolites in gas sensing technology

The use of zeolites as filter materials in gas sensor technology is almost unheard of. However there have been a couple of instances where zeolites were used to solve a specific problem regarding gas sensing.

The most pertinent use of zeolites in gas sensor technology with relation to this study was instigated by Müller and Lange.[49] They utilised 3 zeolites with differing pore sizes (Type A - 3 Å, Type A - 4 Å and Type X - 9 Å) and deposited a 40 μm thick layer onto MOSFET type devices. A 4 sensor array was constructed including one sensor with no zeolite coating. The system was used to identify small species such as methanol, acetone and benzene and the zeolites were not catalytically modified. Thus the zeolites were utilised as molecular sieves in this instance.

Interestingly a zeolite has been used directly before on an interdigitated electrode structure (see figure 2.9.1) similar to the ones used in this study. Plog et al.[50] used a platinum exchanged NaY zeolite for the possible detection of butane, CO or H_2. They found that only butane showed any useful response. They proposed that the increase in resistance caused by the butane was due to the mobility of the sodium ions being reduced by the catalytic reaction rate of butane. Figure 2.9.1 shows the basic construction of this sensor with a cross section showing the zeolite coating on the interdigitated electrode.

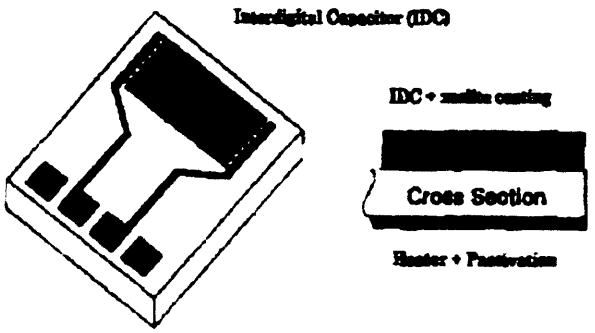

Figure 2.9.1 Construction of zeolite Y gas sensor.[50]

A CO sensor has been developed that uses a siliceous (Si to Al ratio above 5) zeolite coating on top of a La_2O_3-Au/SnO_2 based sensor. The sensor was a pellistor type sensor where the coil is both the heater and the electrode, see figure 3.5.1. The La_2O_3 suppressed sensitivity to H_2, CH_4, i-C_4H_{10} and C_2H_4. The zeolite is integrated into the sensor design to depress the high ethanol sensitivity.[51]

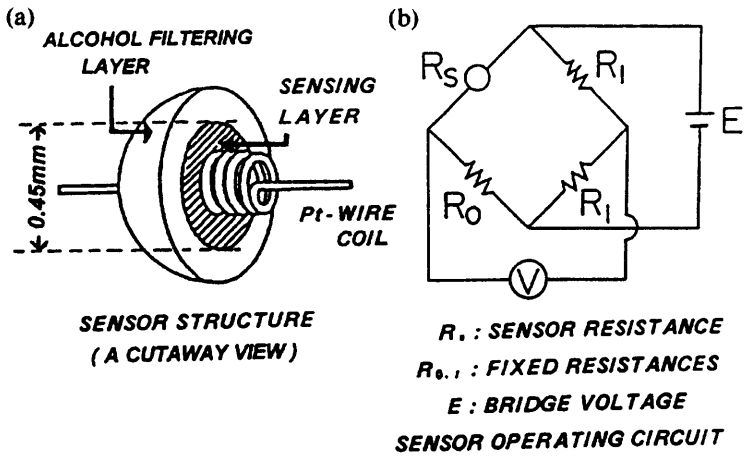

Figure 2.9.2 Diagram of metal oxide based gas sensor with zeolite filter technology. a) sensor structure, b) bridge circuit for operation. [51]

ethylene within the zeolite layer that covers the sensing layer, which has a low sensitivity to ethylene. The siliceous zeolites used were ferrierite and two types of zeolite Y which all have a hydrophobic nature and good thermal stability. Ferrierite had the largest Si to Al ratio and thus a large acid amount and strong acid strength, and was the best filter. The sensor was operated at 300°C.

2.10 Current technology in electronic noses

The human nose tends to become desensitized and tire after a short period. Aromas detected initially by a human will begin to fade after varying lengths of time, dependant on the odours involved. Therefore it is the ideal to produce an instrument which is the "ultimate nose". One that detects every odour does not become desensitised and always gives the same description to a specific odour. However as ever, even with the technology available it is not an easy task.[52]

There are several commercial instruments described as electronic noses. They are basically volatile chemical sensor arrays which detect most vapours, odorous and non-odorous including water vapour. Sensitivity is highly variable to various volatiles dependent on the type of sensor used - usually arrays of semiconducting metal oxide sensors or conducting polymer sensors. However despite the unspecificity of the array these instruments have a good classification capability. A trained instrument (i.e. running large numbers of known samples) can classify odours 'like', 'unlike' and varying degrees of

similarity in between. However this also requires a skilled operator who still has to input various known properties of the sample concerned. Thus to date electronic noses are still very much in development but have found a market in quality control.

An electronic nose is an instrument, which comprises a sampling system, an array of chemical gas sensors with differing selectivity, and a computer with an appropriate pattern-classification algorithm, capable of qualitative and/or quantitative analysis of simple or complex gases.

There are a number of different types of electronic noses in development and available commercially. The two main types are either based on metal oxide sensors or conducting polymer sensors.

As mentioned before, selectivity is the main problem for the electronic nose and the sensor array as it will have to either produce a different chemical "note" between different gases and/or distinguish one gas from a number of different gases in a sample for commercial viability.

Faia et al.[53] proposed a unique way of trying to resolve selectivity and sensitivity issues with a SnO_2 and Fe_2O_3 sensor array. The basic premise was to shape the nose chamber conically similar to the real human nostril, with 16 sensor elements placed uniformly around the inside of the surface. It was designed in such a way that all the sensors had the same exposure area to the gas, which may have different flow characteristics due to the conical shape of the chamber. They also looked at porosity control to enhance sensitivity and perhaps selectivity as sensors are based on the adsorption/desorption and chemical reactions on the surface of the material. However this approach seems inadequate for complex selectivity of a variety of target gases and it could be doubtful whether the shape of the chamber will have any real significant discernible impact to the selectivity.

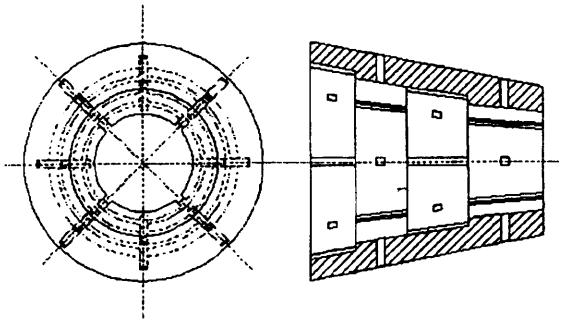

Figure 2.10.1 Schematic of novel electronic nose sensor chamber showing basic dimensions.[53]

An electronic nose was developed at UMIST by Hatfield et al. using electrically conducting organic polymers based on heterocyclic molecules.[54] They display reversible changes in conductivity when exposed to polar volatile chemicals. One of the benefits of these sensors is the rapid adsorption and desorption kinetics observed at ambient temperatures. They do not show high specificity to individual gases but they can be chemically tailored to enhance differences in response to particular classes of polar molecules. Identification of a specific chemical thus makes use of an array of sensors of different specifities. The compound of interest is identified when the entire response pattern of such an array is identical to that stored on a computer.

Up to 20 different polymer materials were utilised in the Hatfield array, and changes in resistance could be measured for individual sensors within that array. Each sensor responds to a volatile compound, for example, to varying degrees depending on the type, thus enabling a pattern of the resistance change to be produced unique to that substance regardless of concentration as the responses can be normalised to represent relative changes. They successfully discriminated between various amines using this approach.

To improve the effectiveness of an electronic nose Muenchmeyer et al.[55] used a trap and thermal desorption unit in conjunction with an electronic nose to enhance selectivity towards flavour compounds. A schematic of the apparatus used is shown in figure 2.10.2 showing the transition of the analyte from sample to trap and thermal desorber and through onto the electronic nose. The nose consisted of metal oxide semiconductor sensors. Their objective was to limit the effect of ethanol on the sensors, which is a major component in perfumes for example but is not important for the aroma. With the trap and thermal desorption unit they were hoping to lower the detection limit for organic compounds thus

minimising the cross sensitivity to any very volatile compounds. Thus in this case they studied limonene in a background of mainly ethanol. The basic function of the trap and thermal desorption is shown in figure 2.10.3.

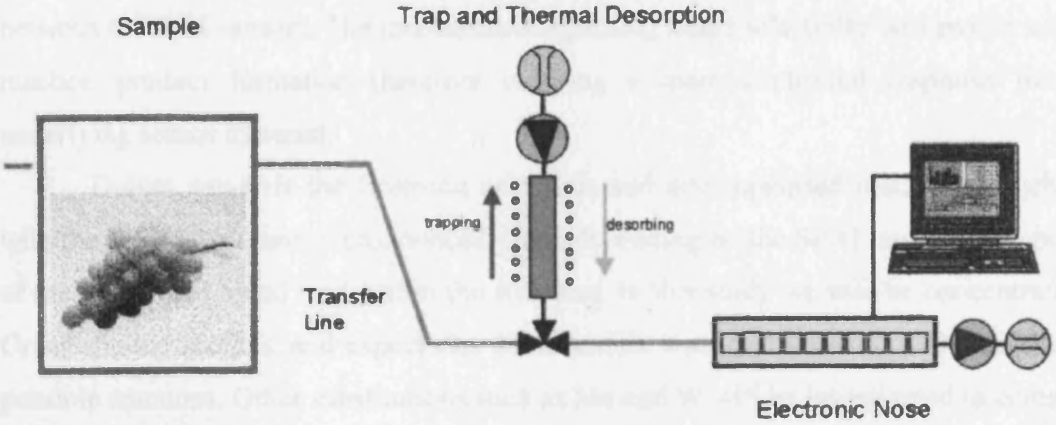

Figure 2.10.2 Diagram showing set-up of thermal desorber with electronic nose used by Muenchmeyer et al.[55]

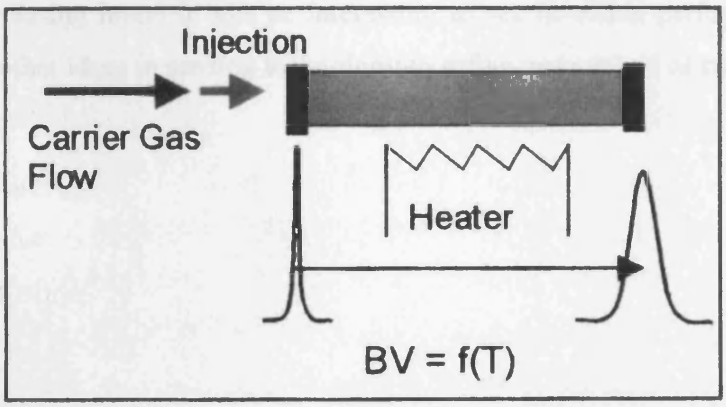

Figure 2.10.3 Principles of operation of thermal desorber. Analytes are injected into carrier gas flow and collected by absorbent bed. Subsequent controlled heating of the bed releases compounds in pulses from absorbent bed dependant on volatility for analysis.

2.11 Literature Review Summary

The structures of the various zeolites used in this study have been identified. They exhibit differences in structure that can be exploited to enable discriminatory effects between the final sensors. The mechanisms regarding shape selectivity will enable selective reaction product formation therefore ensuring a more controlled response from the underlying sensor material.

During catalysis the Brønsted acid sites and any supported metal ions exchanged with the zeolite will have a pronounced effect depending on the Si/Al ratio and the position of the exchanged metal ions within the structure. In this study we will be concentrating on Cr substituted zeolites, and expect that the oxidation state of chromium will also affect the possible reactions. Other substitutions such as Mo and W will be investigated to compare to the Cr substituted zeolites.

The sensor will be made with a zeolite layer deposited directly on top of the gas sensing layer. It will be interesting to see how this performs and whether we can utilise other ideas in sensing technology to refine our method of construction.

3. Background to the existing solid state sensor technology utilised in this study

3.1 Introduction

This chapter will give an overview of the technology that is utilised in this study as it draws upon a large amount of prior art both in the gas sensing field and application of these gas sensing devices in electronic noses. This will provide a base of knowledge upon which the subsequent experimental and results chapters will build.

3.2 Principles of gas sensing by metal oxide semiconductors

The response of semiconducting metal oxides as gas sensors is due to the change in surface oxygen concentration invoked by oxidising or reducing reactant species interacting with the oxygen surface ion. Therefore for the sensor to function in an atmosphere containing oxygen it is clear that the surface of the oxide is not in equilibrium with the gas phase.

Most early work on gas sensors was performed on tin dioxide, an n-type bulk semiconductor. In an n-type semiconducting oxide, oxygen adsorption decreases the charge carrier density at the interface between grains. The surface charge is balanced by the charge carried on the ionised donors. In contrast, for a p-type semiconducting oxide, oxygen adsorption increases the charge carrier density at the interface. The charge is balanced by additional holes in the valence band. In the case of tin dioxide, under normal sensor operating conditions the surface conductivity is much less than that of the bulk due to excess oxygen at the surface. The formation of surface ions and a near surface depletion layer leads to the development of Schottky barriers at interparticle contacts which has a critical effect on the conductivity of porous thick films of semiconducting oxide as used in a typical gas sensor.[56] (See figure 3.2.1).

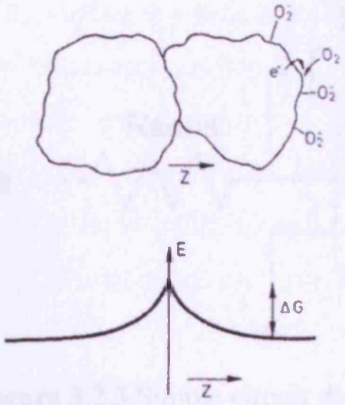

Figure 3.2.1 Schematic diagram of the formation of interparticle Schottky barriers as a result of the trapping of charge at surface oxygen ions (here represented as O_2^-).

Therefore the nature and concentration of the surface oxygen species on semiconducting oxides needs to be known to understand fully the mechanisms of gas response.

In a typical gas sensor utilising these materials (figure 3.2.2) the sensing element comprises a semiconducting metal oxide layer formed on an alumina substrate of a sensing chip together with an integrated heater to maintain an optimum operational temperature. In the presence of a detectable gas, the sensor conductivity changes depending on the gas concentration in the air. A simple electrical circuit (figure 3.2.3) can convert the change in conductivity to an output signal that corresponds to the gas concentration.

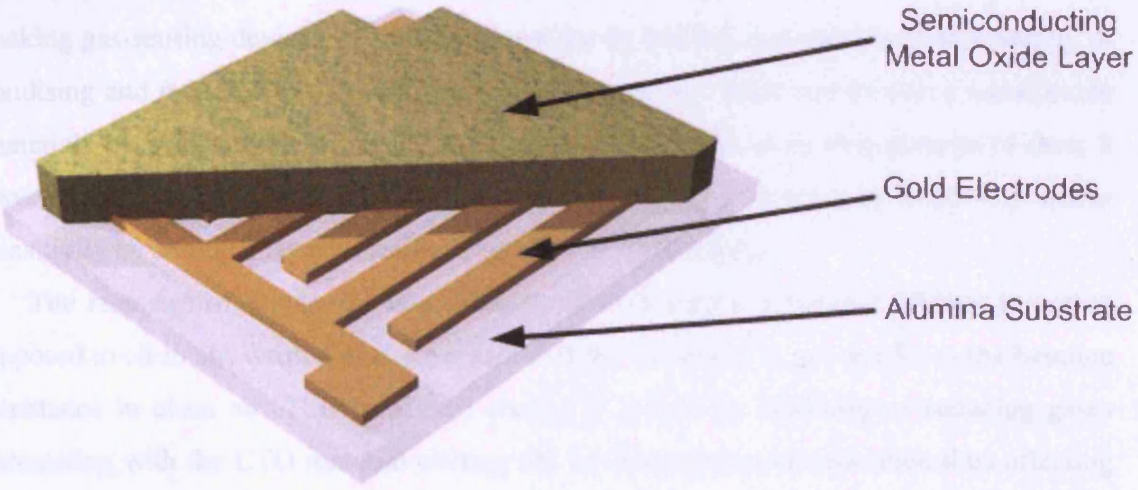

Figure 3.2.2 Cut-away diagram of semiconducting oxide sensor showing principal construction. Picture courtesy of City Technology.[5]

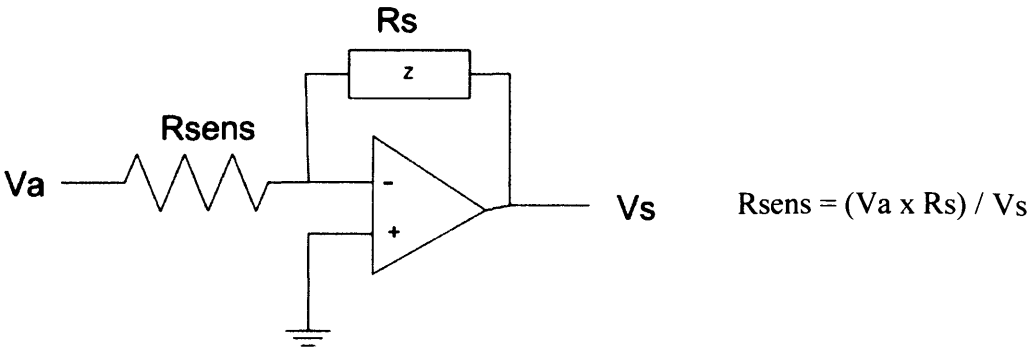

Figure 3.2.3 Simple circuit diagram to illustrate the measurement circuit for the sensor's resistance (Rsens).

3.3 Chromium titanium oxide gas sensors in operation

The use of metal oxides in gas detection devices involves different characteristics for the resulting sensor or arrays of sensors. The important characteristics of such a device are sensitivity, selectivity and stability of the sensing device(s). Sensitivity is the capacity that a material has for detecting a certain type of gas. Selectivity is the capacity that a sensor has to discriminate between different types of gases. Stability refers to the capacity that a sensor has to give the same information under certain conditions, independently of the number of times this sensor has already been used or of any time left idle. The sensing material will remain the same throughout this work and is chromium titanate, $Cr_{2-x}Ti_xO_y$, (CTO), which has been relatively recently introduced commercially as a material for making gas-sensing devices,[7, 57] and is known for its stability and sensitivity to a variety of oxidising and reducing gases. CTO has an advantage over other gas sensitive metal oxide materials by being relatively insensitive to water and stable over long periods of time. I have concentrated on the development of the sensor itself to increase its selectivity and/or sensitivity by adding a layer of zeolite over the CTO sensing layer.

The response of the sensor is a measure of its electrical resistance change in gas as opposed to clean air, written as R/Ro where R is the resistance in gas and Ro is the baseline resistance in clean air. This resistance change is caused by oxidising or reducing gases interacting with the CTO material altering the surface oxygen concentration thus affecting

the charge carrier density. Oxygen adsorbed from the air acts as an electron acceptor state, lying within the band gap of the oxide but located at the surface of the material. Reactions at the surface result in a change in the fractional surface coverage of this acceptor state and hence a change in conductivity. As CTO acts as a p-type semiconductor (holes are the majority carriers, electrons the minority carriers) the resistance increases when reducing gases are present such as CO, hydrogen, alcohols, ethane, propane etc. However, it is insensitive to methane and CO_2. The classification 'n' and 'p' is used to describe gas sensitive semiconductor materials because it is believed that this reflects the charge type of the majority carriers in the two cases, but this is not necessarily true. Unfortunately CTO is not particularly selective as it responds to a variety of gases in the same manner. Therefore by adding an additional layer of material, in this case zeolites, we hope to be able to improve the selectivity of the sensor by selectively modifying the local gaseous environment that is sampled by the sensor material. The zeolites will exhibit two useful properties. They should show some sieving properties enabling size and shape selectivity due to the aperture size of the pores in its microstructure. Most should also exhibit some chemical activity towards the organic compounds passing through hence altering, cracking, or combusting the target molecule in some way to produce a particular response on the sensor. Using a zeolite as a filter layer for a gas sensor array has been attempted before as mentioned in section 2.9, [49] albeit in this instance, the array used by the authors consisted of the same zeolite type (LTA) but with different pore sizes on a number of MOSFET type devices. The system was used to identify small species such as methanol, acetone and benzene and the zeolites were not catalytically modified.

To provide further discrimination by utilising the gradient in composition of the gaseous environment through the device, the sensing material will be interrogated at two different depths by means of a pair of electrodes on the one sensor. On the multiple electrode structure the wide electrode gap (160 μm) and the narrow electrode gap (40 μm) interrogate both the top and the bottom of the CTO layer, respectively. This array is referred to as the SEMDEC electrode type pattern and is illustrated in figure 3.3.1.

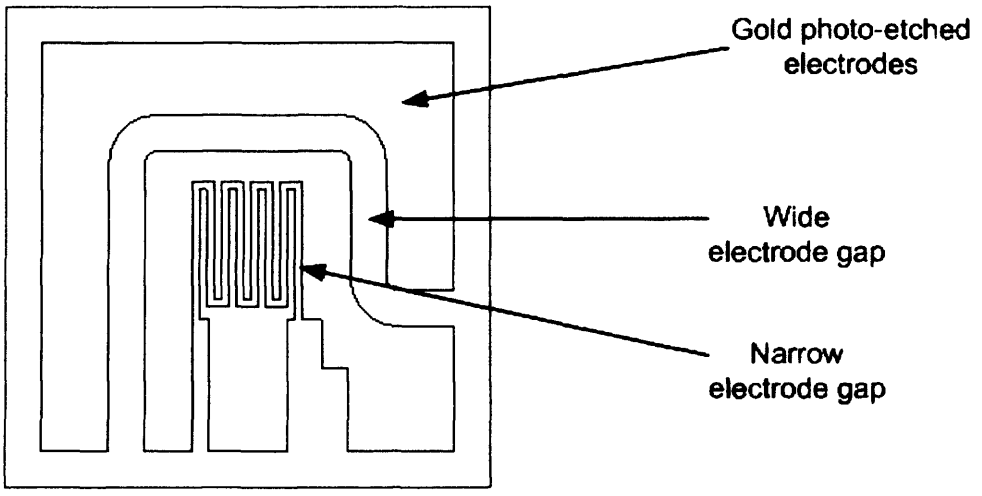

Figure 3.3.1 Diagram of gold electrode array supported on 2x2mm alumina tile.

The basic construction of the proposed sensor is shown below in figure 3.3.2. The zeolite layer will be screen-printed directly on top of the CTO and the chip fired as one unit.

There may be problems of adhesion between the zeolite and the CTO because of differing thermal expansion coefficients of the two materials so there may be a need for an intermediate layer in some instances. This is a fabrication problem due to the large contact area between the two materials relative to the material thickness. Thus when the sensors are fired at 600°C and above the difference in size between the green and sintered product for each material will affect the adherence of the zeolite layer.

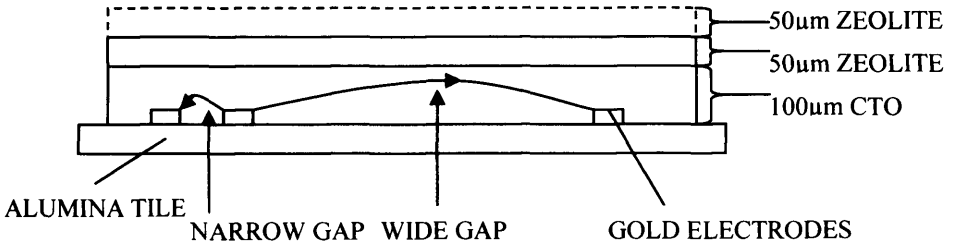

Figure 3.3.2 Schematic of sensor construction

With reference to figures 3.3.1 and 3.3.2 the SEMDEC electrode pattern provides differing electrode gaps so different areas of the CTO can be interrogated within the layer. The wide gap electrode has a distance of 200 µm between electrodes so a long field path is taken in the upper region of the CTO layer. The narrow gap electrode has a distance of 40 µm between electrodes and a shorter field path taken in the lower region of the CTO layer.

3.4 Sensor arrays for the use as an electronic nose

As has been mentioned earlier many gas sensors have poor selectivity especially when used singly so it is therefore advantageous to use sensor arrays. The first use of a sensor array was reported with semiconductor sensors.[58]

Arrays of relatively unspecific sensors are used commercially in what are termed electronic noses.[59, 60, 61] A variety of statistical signal processing techniques such as principal component analysis (PCA) and discriminant function analysis (DFA) are used to extract and utilise the limited selectivity of the sensors within the array. Neural networks have also been used to analyse sensor array data which provides a non-parametric approach to multivariate data analysis. The application of an electronic nose involves the selectivity of the individual sensors within the array to distinguish certain chemical notes that are apparent when the sensor responses are cross-referenced with each other. Currently, within most electronic noses that use metal oxide sensors, discrimination is achieved by using various metal oxide sensing materials and/or operating them at varying temperatures. However, when complex mixtures of compounds need to be compared with each other the system is limited because the sensors are sensitive to a large variety of gases and have a similar response pattern to the usual target gases, so no discrimination of gas mixtures is determined by the sensors. One approach to dealing with this problem has been to use very large arrays, but then stability of the array characteristics becomes a problem. Currently in electronic noses it is the post sensor response signal processing that is used to provide a means of pattern recognition between groups of samples. This can be very limiting and unnecessarily complex and in practise with the devices currently used commercially relies primarily on the relative volatilities of the differing samples to provide discrimination on the PCA plots. If you take a look at a typical PCA plot as described in figure 3.4.1 it can be seen how different wine samples have been separated out into little clusters. The bigger the distance between these clusters basically means the better the discrimination. This method of sensor array analysis is further explained in chapter 4.9.

PCA and DFA are ways of identifying patterns in data, and expressing the data in such a way as to highlight their similarities and differences. Since patterns in data can be hard to find with many variables (e.g. sensor responses) these methods are a powerful way of analysing and displaying the data graphically.

The goal of PCA is to reduce an original set of variables into a smaller set of uncorrelated components that represent most of the information found in the original variables. By reducing the dimensionality, you interpret a few components rather than a large number of variables.

DFA is useful for situations where you want to build a predictive model of group membership based on observed characteristics of each case. The procedure generates a discriminant function, or a set of discriminant functions, based on linear combinations of the predictor variables that provide the best discrimination between the groups. The functions are generated from a sample of cases for which group membership is known. The functions can then be applied to new cases with measurements for the predictor variables but unknown group membership.

Therefore PCA is useful for determining variance from the smallest possible array of best fit, and hence can be utilised to determine which sensors in an array are performing the best in terms of discrimination. The DFA is useful for determining the arrays performance in identification of samples after training the nose.

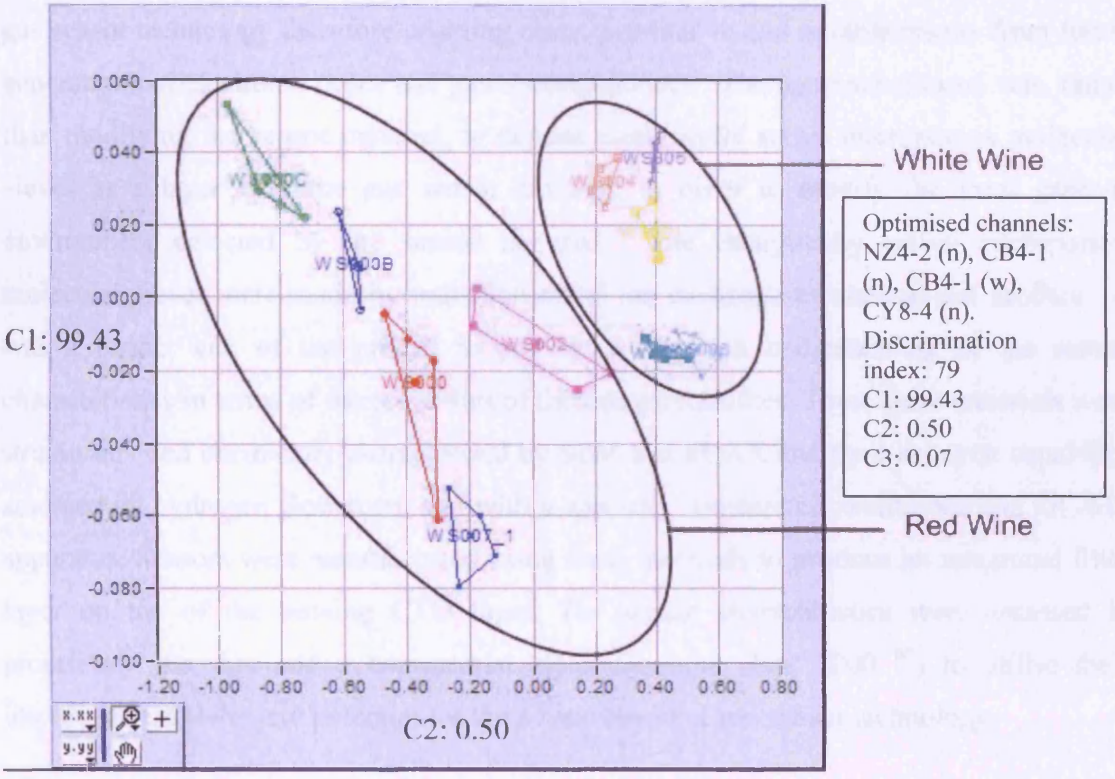

Figure 3.4.1 Example of PCA plot describing wine testing. 3 sensors operating at 400°C – control CTO, Cr-zeolite β (50 μm), Cr-zeolite Y (100 μm). PCA plot constructed using unprocessed sensor response data.

A Fox 2000 electronic nose supplied by Alpha M.O.S. was utilised for this work. The nose uses an array of 6 single electrode gap type sensors or 3 SEMDEC type sensors. The unit is automated to analyse a number of samples in a cycle. The sample is contained in a sealed vial, which is then put into the autosampler's oven to be heated and agitated in order to generate the headspace. The headspace is then taken from the vial and injected into the instrument containing the sensor array. The sensor responses are then processed to provide the various response values for the sensors and the differences between the sensor responses within the array to ascertain a fingerprint for the analyte. However this type of system usually can only determine the variations from the ideal based on the system response. Therefore by developing the selectivity of the sensor the aim is to enhance this effect and perhaps increase the analytical capacity of the device, rather than relying on qualitative variations.

3.5 Aims of the project

The aim of the project was to improve the selectivity of semiconducting metal oxide gas sensor technology therefore enabling more quantitative and reliable results from future generations of electronic noses and gas sensing devices. The approach chosen was, rather than modifying the sensor material, to deposit catalytically active microporous molecular sieves as a layer over the gas sensor material, in order to modify the local gaseous environment detected by the sensor material. The catalytically active microporous molecular sieves were made by transition metal ion exchange of commercial zeolites. It was a further aim of the project to provide a thorough understanding of the sensor characteristics in terms of the properties of the catalytic zeolites. Thus, these materials were structurally and chemically characterised by SEM and EDAX and their catalytic capability assessed by hydrogen flow tests, and with a specially constructed zeolite bed and GC/MS apparatus. Sensors were manufactured using these materials to produce an integrated filter layer on top of the sensing CTO layer. The sensor characteristics were assessed in proprietary gas rigs and a commercial electronic nose (Fox 2000 [61]) to utilise their improved selectivity and potential for the advancement of gas sensor technology.

4. Experimental Methods

4.1 Introduction

The purpose of this chapter is to detail the experimental methods used to develop the discriminatory sensor array. The methods detail the zeolite material fabrication by introduction of a transition metal complex into the zeolite framework using two different ion exchange methods. The subsequent characterisation of the material by SEM/EDAX and proprietary zeolite bed flow tests to determine the catalytic properties. The sensor construction is detailed including the integration of the zeolite layer. The testing method and evaluation of the sensors in a proprietary injection gas sensing rig and electronic nose are also detailed.

The zeolites used for this study were of an aluminosilicate structure, namely zeolite Y (Faujasite structure), zeolite β (*BEA structure), ZSM-5 (MFI structure) and LTA (Linde Type A). Zeolites have framework structures constructed by joining together $[SiO_4]^{4-}$ and $[AlO_4]^{5-}$ coordination polyhedra. These tetrahedral are assembled together such that the oxygen at each tetrahedral corner is shared with that in another tetrahedron (Si or Al).[62]

In order to increase the catalytic activity of the zeolites ion exchange methods are described in this chapter to decorate transition metal complexes within the zeolite cavity. All zeolites were subjected to an aqueous ion exchange, for the Mo system solid state exchange was also studied.

To characterise the transition metal zeolites SEM and EDAX were used to determine the structure and chemical composition of the zeolites. A proprietary hydrogen testing rig was developed to assess catalytic reactivity by monitoring the output of hydrogen gas flow using a CTO gas sensor after the gas had passed over a heated zeolite bed. The majority of the catalytic analysis was performed using a similar concept. Known analytes were added into an airflow which then passed over a heated zeolite bed where reaction took place and the reaction products were then collected using a thermal desorber. The thermal desorber then desorbed these reaction products into a GC/MS which could identify the reaction products and give qualitative proportional amounts of each compound.

Sensors were then constructed using the catalytic zeolite materials and assessed in a proprietary gas rig based on the same concept as the GC/MS set-up to allow for a correlation of results. Initially a zeolite bed was used in the airflow before zeolite coated sensors were introduced so the reaction products from a zeolite bed on its own could be assessed before the zeolite filtered sensors were introduced into the rig.

Finally testing of the sensors was performed in an electronic nose and assessed using PCA and DFA. The ultimate goal was to assess the sensors discriminatory capability to headspace generated compound mixtures and see how improved sensor properties can aid the electronic nose operation.

4.2 Materials preparation

Zeolite Y, zeolite β and ZSM-5 were obtained from Zeolyst International and zeolite LTA was obtained from Sigma-Aldrich. All were in powder form and their properties are outlined in Table 4.2.1

Zeolite Type	Form of cation	Formula with respect to Al	Pore Size (Å)	Si/Al ratio	Surface Area (m^2/g)
ZSM-5	NH_4	$Si_{80}Al_1O_{161.5}$	(5.5 x 5.1),(5.3 x 5.6)	80	425
Y	H	$Si_{5.2}Al_1O_{11.9}$	7.4	5.2	730
β	H	$Si_{75}Al_1O_{151.5}$	5.6, (7.1 x 7.7 x 6.6 x 7.3 x 6.6 x 6.7)	75	680
LTA	Na	$Si_1Al_1O_4$	4.1 x 4.1	1	350

Table 4.2.1. Summary of zeolites structural properties. [63]

Depending on the method and type of transition metal ion to be exchanged with the cation of the zeolite it was sometimes necessary to convert the cation from NH_4^+ to H^+ and vice versa.

For the conversion of H-zeolite to NH_4-zeolite two ammonium exchanges were performed at 60°C using ammonium chloride (NH_4Cl) solution (1 M) in water (1200 ml).

For conversion of NH_4-zeolite to H-zeolite a simple thermal decomposition was performed in air at 500°C for 12 h with a precursory treatment at 100°C for 8 hrs to remove adsorbed water.

4.2.1 Preparation of Cr-zeolites

H-Zeolite Y was initially converted to the ammonium form. The NH_4-Zeolite (amount used varied depending on correct stoichiometric ratio required) generated was then subjected to chromium exchange with chromium nitrate nanohydrate solution (42.9 mM $Cr(NO)_3$ $9.H_2O$) as a source of chromium cations, at 60°C for 48 hours. The initial pH of the solution was adjusted to 4.0 by the addition of a few drops of aqueous ammonium hydroxide (NH_4OH). After the chromium exchange, the resulting catalyst was washed with deionised and double distilled water, dried at 100°C and then calcined at 500°C for 12 h. After the initial ion exchange Cr^{3+} and Cr^{2+} ions were present as hexaaquo complexes in the cages and channels of the zeolite. The drying decreases the ligand field strength of the $Cr(H_2O)_6^{3+}$ complex and there is a replacement of the water molecules with lattice oxygens of the zeolite which is outline in equation 4.1. [64]

$$Cr(H_2O)_6^{3+} + (n)\ ^{-}O\text{-Zeolite} \rightarrow Cr^{3+}\text{-}(O\text{-Zeolite})_n(H_2O)_m + (6\text{-}m)H_2O \qquad (4.1)$$

The calcination oxidizes the hydrated Cr^{3+} and Cr^{2+} complexes to chromate, dichromate or polychromate (Cr^{6+}), chromyl cations (Cr^{5+}), and some Cr_2O_3 clusters.[64]
The zeolite β and ZSM-5 went through the same process except for the initial exchange with ammonium chloride as they are already in the ammonium form.

4.2.2 Preparation of Mo-zeolites

Two methods were employed to produce molybdenum decoration within the zeolite cavity - an aqueous ion exchange and a solid state exchange. This gave a comparison in catalytic properties based upon the method of introduction of the transition metal species.

For the aqueous ion exchange[65] H-zeolite Y was initially converted to the ammonium form as outlined in section 4.2. Then the NH_4-Zeolite was subjected to molybdenum exchange with ammonium heptamolybdate (AHM), $(NH_4)_6Mo_7N_6O_{24}.H_2O$ as a source of molybdenum cations, at 333 K for 48 hours. The initial pH of the solution was adjusted to 4.0 by the addition of a few drops of aqueous ammonium hydroxide (NH_4OH). After the molybdenum exchange, the resulting catalyst was washed with deionised and

double distilled water, dried in a vacuum at 383 K for 12 h and then calcined at 773 K for 12 h.

For the solid state exchange (SSE)[66, 67]; zeolite H-Y (or H-β) and the MoO_3 were physically mixed for 0.1 hours to intimately mix the sample in suitably determined proportions that gave a stoichiometric Mo/Al ratio. These were Mo/Al of 0.2, 0.5, 1.0 and 2.0 for zeolite Y, and an Mo/Al of 0.2, 0.5, 1.0 for zeolite β. All the samples were then given a heat treatment in air as outlined in figure 4.2.2.1. The first step of the heat treatment in air at 623K for 12 hrs drives off physisorbed H_2O and puts MoO_x species onto the external surface, the next stage is at 773K for 12 hrs at which temperature MoO_x crystallites spread at lower vapour pressures than bulk MoO_3. Finally a step at 973K for 2 hours was performed to allow zeolite pore penetration by the MoO_x crystallites.

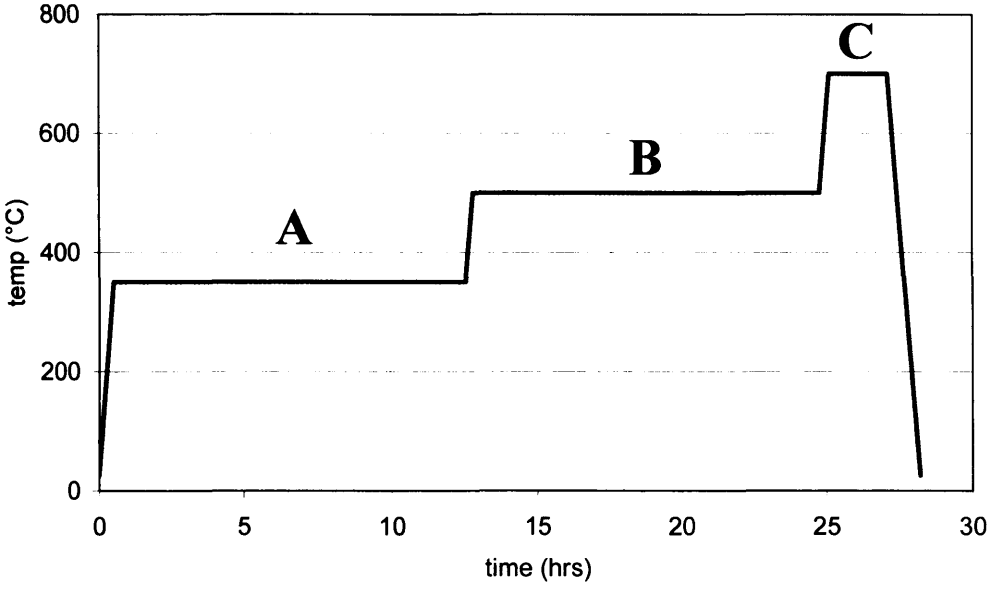

Key:
A – 350°C, drive off physisorbed H_2O, MoO_x onto external surface
B – 500°C, MoO_x crystallites spread at lower vapour pressures than bulk MoO_3
C – 700°C, zeolite pore penetration

Figure 4.2.2.1 Heat treatment for MoO_3/zeolite Y mixture to promote solid state ion exchange

4.2.3 Preparation of W-zeolites

An aqueous ion exchange was performed on the zeolites.[68] H-zeolite Y was converted to the ammonium form as outlined in chapter 4.2. Then the NH_4-Zeolite was subjected to tungsten exchange with ammonium (para)tungstate (APT), $(NH_4)_{10}W_{12}O_{41}.5H_2O$ as a source of tungsten cations, at 333 K for 48 hours. The initial pH of the solution was adjusted to 4.0 by the addition of a few drops of aqueous ammonium hydroxide (NH_4OH). After the molybdenum exchange, the resulting catalyst was washed with deionised and double distilled water, dried in a vacuum at 383 K for 12 hrs and then calcined at 773 K for 12 h.

4.3 Characterisation of zeolites by EDAX and SEM

After exchange the levels of transition metal in the zeolites were ascertained by energy dispersive X-ray analysis (EDAX) over a number of spots and areas to check for homogeneity of the dispersion. The analysis was performed by an Oxford Instruments INCA Energy system in conjunction with a JEOL JSM 6301F scanning electron microscope. Samples were carbon coated for EDAX analysis and separate samples were prepared and gold sputter coated for detailed SEM images to be taken. For EDAX analysis the samples were referenced against a cobalt standard before each sample was analysed.

4.4 Zeolite bed and GC/MS set-up for catalytic testing

The apparatus (figure 4.4.1), in sequence consists of a heated sample inlet to allow analyte entry via a syringe with an appropriate airflow to transport the analyte in the vapour phase. The analyte then passes into a reaction chamber holding the zeolite, which is held at a steady temperature. The reaction products then flow into the adsorbent trap in a Markes Unity™ thermal desorber which maximises the concentration of these reaction products. This enables a controlled flow of these reaction products in a stream of Helium to enter the Varian 3400 gas chromatograph (GC) via a heated silica transfer line by temperature ramped controlled desorption. After the products have condensed within the column (fused silica coated with dimethyl polysiloxane) of the GC, the subsequent GC temperature ramp passes the reaction products into the Finnigan 4500 mass spectrometer (MS) for analysis. All exposed interconnected tubing between the various components of the apparatus are

temperature controlled by rope heaters where accessible to prevent condensation of the vapours on the inside walls of the tubing. The Finnigan 4500 MS is controlled by a computer running Teknivent Vector 2 software on an OS/2 operating system. The resulting spectra were analysed using a Wiley spectral database. The thermal desorber was controlled by a PC running Unity control software on Windows NT. The Unity software controlling the thermal desorber is also in communication with the GC via the thermal desorber for uninterrupted throughput of sample.

The zeolite bed was set-up as follows; a tube furnace was mounted on a wooden stand so as to have the tube oriented vertically. A glass tube was made with glass frit at the centre to contain the zeolite and a suitable thermocouple was placed around the tube in the centre of the furnace to monitor the temperature.

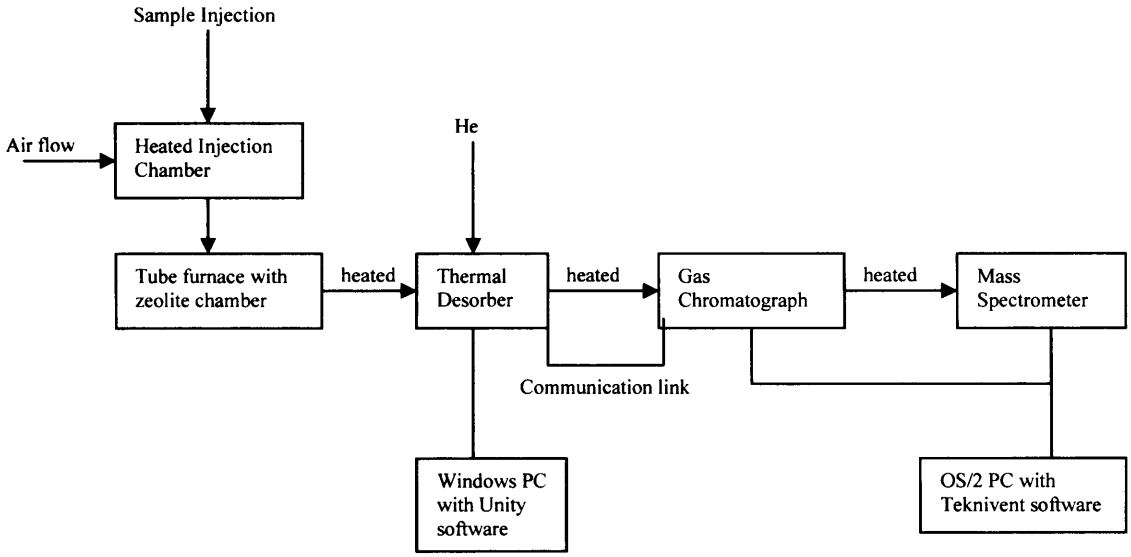

Figure 4.4.1 Schematic of the zeolite bed apparatus with thermal desorber and GC/MS arrangement.

The injection unit accepts a single direct injection from a syringe that is not rate controlled. The amount of liquid used in each case was 3 µl unless stated. The injection rig is heated to the temperature required to vaporise the analyte concerned and is controlled by a thermocouple. The analyte is taken in a carrier of air at approx. 10 ml/min through to the zeolite bed. The tube furnace was set at the required temperature and monitored using a separate thermocouple. There is a heated transfer line from the furnace to the thermal

desorber whereupon the products from the zeolite bed collect on an adsorbent trap. There are four main steps to the operation of the thermal desorber:

Pre-purge – Does not pass sample through the trap but clears the sampling lines to prevent carry over from previous runs and also prevents systematic error in the true volume of sample taken. Time set at 5 mins.
Sampling - The analyte is injected through the zeolite bed at this stage and in this step the resultant VOCs from the sample are trapped onto the cold trap. Time set at 3 mins.
Trap Purge – He carrier gas from the Markes Unity™ thermal desorber is purged through the cold trap to remove any residual oxygen and selectively purge off any unwanted solvents. Time set at 5 mins.
Trap Heat – Markes Unity™ injects the sample into the GC by ramping the temperature of the trap.

A control is performed periodically where no analyte is passed through the system to check for contamination. This "contamination test" is performed after specific groups of organic analytes have been tested which are also tested in increasing size. A contamination test will also be performed before the start of any run of experiments if the apparatus has been left idle for more than approx. 3 h, or there has been a part change or sample change which can cause the ingress of water or other contaminants. Once the sample has passed through the heated transfer line to the GC, the GC is on a 23 min controlled cycle as shown in figure 4.4.2. There is a controlled temperature ramp in the GC from 60°C to 260°C.

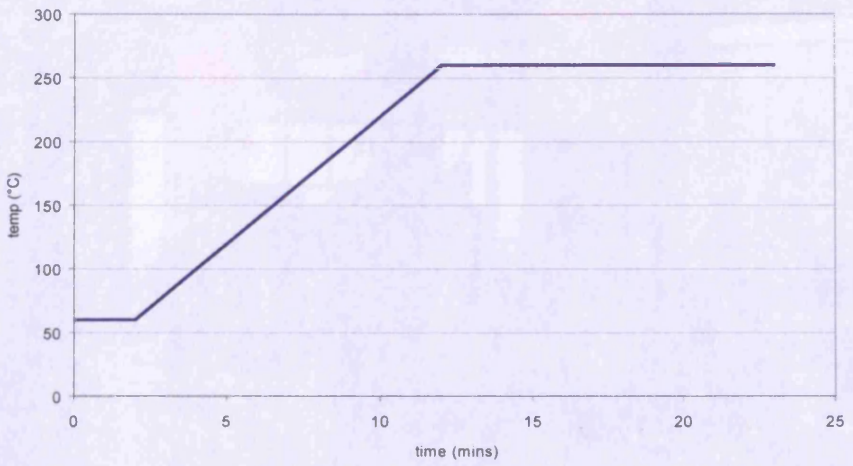

Figure 4.4.2 Gas Chromatograph temperature cycle.

The reaction products then pass through a heated transfer line to the mass spectrometer, which has been calibrated to target smaller MW components, and the software scans from a molecular weight of 12 to 250 in most instances. As well as analysing the spectra against the software database the chromatogram can also be analysed to attain compound types from column retention times established by control samples.

Figure 4.4.3 Photograph of complete apparatus set-up.
Key: A – Sample injection and zeolite chamber, **B** – Thermal Desorber, **C** – Gas Chromatograph, **D** – Mass Spectrometer Quadrupole Module, **E** – Mass Spectrometer Electronics Module, **F** – Mass Spectrometer Computer, **G** – Thermal Desorber Computer.

Figure 4.4.4 Photograph of zeolite bed apparatus (Mk. 2) with transfer to thermal desorber.
Key: A – Power supplies for injection rig
B – Injection Rig
C – Tube Furnace
D – Zeolite chamber
E – Heated transfer line to thermal desorber
F – Heated transfer line to GC.

4.5 Zeolite bed apparatus for reactivity testing

A second system was set up using a similar furnace and zeolite bed arrangement as the GC/MS apparatus but simply had a $Cr_{1.95}Ti_{0.05}O_3$ gas sensor at the outlet, which had its resistance measured using a computer controlled 16-bit data logger (Pico ADC16) with a suitable resistance in series. Power was supplied across the sensor using a 1.5 V AA battery and the Pt heater was driven at 400°C or 500°C using a suitable power supply and heater driver board. This apparatus was devised to determine how much Cr had been ion exchanged onto the zeolite structure as detailed in chapter 4.2.1. This was achieved by passing varying concentrations of hydrogen over the heated zeolite bed (400°C) in the tube furnace. Depending on the reactivity of the Cr-exchanged zeolite there will be a drop in the ppm of hydrogen as it is combusted to water. As the sensor is highly sensitive to hydrogen but not significantly to water then the response of the sensor should show a drop in hydrogen concentration as compared to a control sample of plain zeolite.

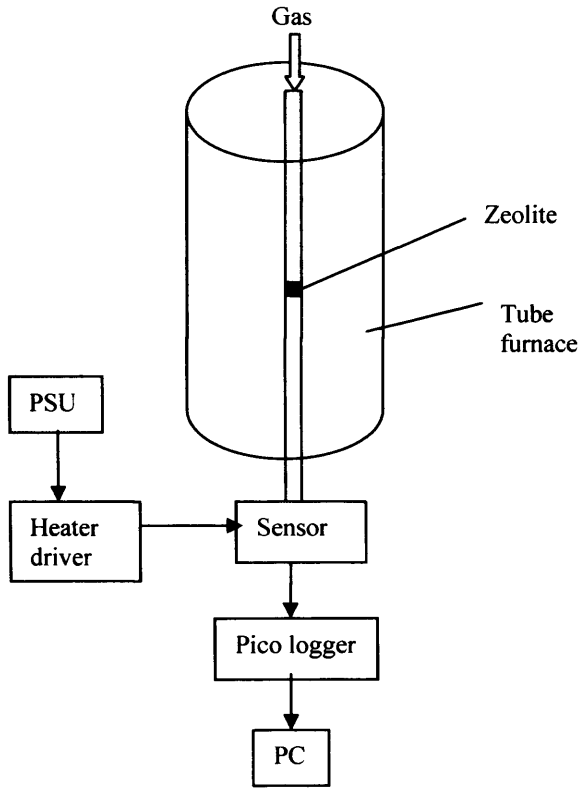

Figure 4.5.1 Schematic of zeolite bed with CTO sensor set-up.

This arrangement can also be used in the future for direct sensor testing as it emulates the situation whereupon there is a zeolite layer directly on the CTO sensor, however the arrangement is simplistic and does have certain limitations.

4.6 Sensor Fabrication

$Cr_{1.95}Ti_{0.05}O_3$ powder was prepared as detailed below.[69]

Chromia was obtained from the thermal decomposition of ammonium dichromate in air. The powder was dispersed in propan-2-ol and the required stoichiometric quantity of titanium propan-2-oxide solution in propan-2-ol was added under ultrasonic agitation. The chromia was kept in suspension by sonication while an excess amount of a 1:4 mixture of water and propan-2-ol was run in to slowly hydrolyse the isopropoxide. The resulting chromia/titania suspension is subsequently rotary evaporated under sonication (sonication maintained to prevent fractionation of titania and chromia) to dryness. The dried powder is fired at 1000°C for 4 hours (ramp rate 15°C) to produce a solid solution of CTO.

The CTO powder is then mixed with a commercial organic vehicle (ESL400)[70] in a weight: weight ratio of 1:1 then triple roll milled to ensure homogenous dispersion of the powder in the vehicle. The ink is screen printed using a DEK 1202 onto 2 x 2 mm alumina tiles with integral heater and a gold electrode pattern that has both a narrow (40 μm) and a wide (150 μm) electrode gap[71, 72]. This interrogates areas at the bottom and top of the CTO layer respectively to enable the determination of any gas concentration gradient evident within the material. The Cr-zeolite powders were also made into inks and applied on top of the CTO layer using the same process. 8 layers of CTO were printed down, to give a total thickness of 100±10 μm, followed by 4 or 8 layers of zeolite, giving zeolite layer thicknesses of 50±5 or 100±10 μm respectively. The cross-section of the chip is shown schematically in figure 4.6.1. After drying under an infra-red lamp, the sensors were bonded up using 50 μm platinum wires, which suspend the sensor on metal pins in a moulded polyphenylene sulphide housing. The sensor chips were subsequently fired in air at 600°C for 30 mins using the sensor heater. A control was also made which had no zeolite layer.

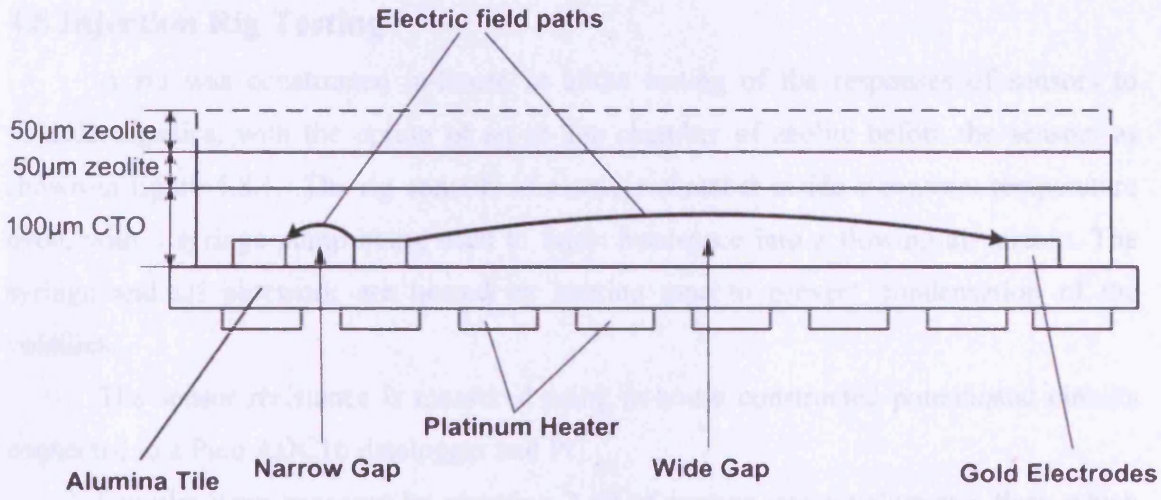

Figure 4.6.1 Schematic of sensor construction detailing integration of two different thicknesses of zeolite filter layer.

4.7 Further Sensor Designs

As well as using a single catalytic zeolite layer on top of the CTO an intermediate layer can also be used to absorb or seriously prohibit diffusion of certain molecules in the sensor design thus creating a sandwich structure.

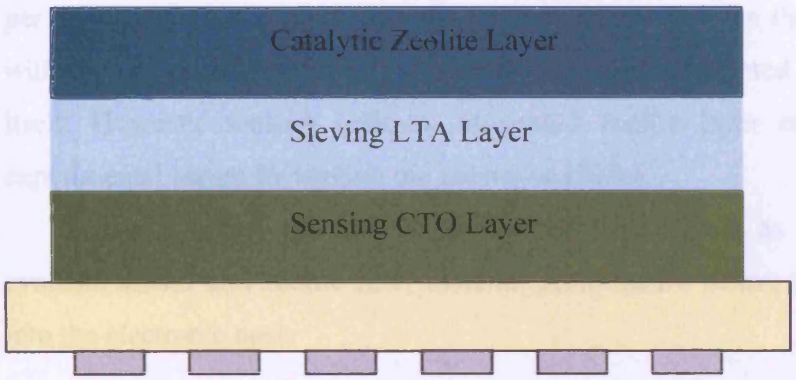

Figure 4.7.1 Schematic of "sandwich" sensor construction

The LTA zeolite is used as the sieving layer only. LTA with a pore size of 4 Å is a known adsorbent of SO_2, CO_2, H_2S, C_2H_4, C_2H_8 and C_3H_8.[12] However it will also be necessary to assess the implementation of these zeolites in situ as the temperature on the surface of the zeolites will vary with layer composition and thickness, therefore a number of sensors were made with the sieving LTA layer but without the catalytic layer.

4.8 Injection Rig Testing

A rig was constructed in-house to allow testing of the responses of sensors to volatile organics, with the option of an in-line chamber of zeolite before the sensors as shown in figure 4.8.1. The rig consists of a sensor chamber inside a constant temperature oven, with a syringe pump being used to inject headspace into a flowing air stream. The syringe and all pipework are heated by heating tape to prevent condensation of the volatiles.

The sensor resistance is measured using in-house constructed potentiostat circuits connected to a Pico ADC16 datalogger and PC.

Samples were prepared by pipetting 2 ml of analyte into a volumetric flask which was then heated to produce a known vapour pressure of the compound. If a large dilution is necessary, a sample of the headspace from the volumetric flask was transferred into a second flask of clean air via a syringe. Finally, a sample of headspace (1 ml) is taken using a heated syringe that was then attached to the syringe pump. The syringe pump was then used to inject the sample into the air stream.

The zeolite chamber was either left blank or contained a zeolite. This allowed the analysis of standard CTO sensor responses after analyte has passed over the zeolite bed as per the GC/MS set-up thus providing a comparison between the sensor response observed with the powdered zeolite as opposed to an integrated printed zeolite layer on the sensor itself. However sensors with an integrated zeolite layer can also be tested in this experimental set-up by leaving the zeolite bed blank.

The injection rig consists of a three sensor array as outlined below to help us evaluate sensor and zeolite filter material performance before and after a sensor is placed into the electronic nose.

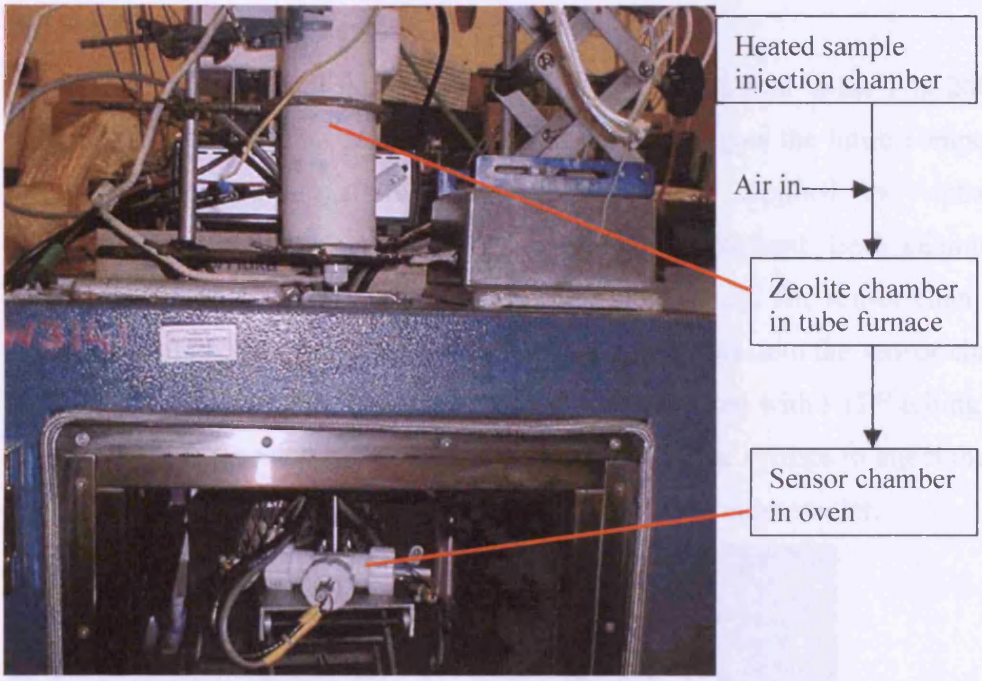

Figure 4.8.1 Schematic and photo of zeolite chamber and sensor arrangement

With the three sensor array the zeolite layer can be assessed comparatively against a control sensor. For the purposes of array development the 3 sensors usually consisted of a control with no zeolite layer, a second sensor with a 50 μm layer of zeolite material and a third sensor constructed with a 100 μm layer of the same zeolite as the second sensor. The zeolite can be assessed by comparing against both the control sensor and also as a function of depth. The method in which these results are collated is explained in detail in chapter 7.

4.9 Electronic Nose Testing

The sensors used in the injection rig were then utilised in the Fox 2000 electronic nose (supplied by Alpha M.O.S.).[73] Figure 4.9.1 highlights the basic components of the electronic nose. Two custom sensor chambers were supplied by Alpha M.O.S. to accommodate the dual electrode type sensor that was utilised. Each chamber housed 3 multiple electrode SEMDEC type sensors (see figure 4.9.2). The sensor chamber is heated to a constant temperature to prevent adsorption of analytes onto the sensor chamber which is constructed from PTFE. The chambers are interconnected with PTFE tubing which is not heated. There is a heated sample inlet which allows for the syringe to inject the sample into the air stream after collecting it from a specific vial in the autosampler.

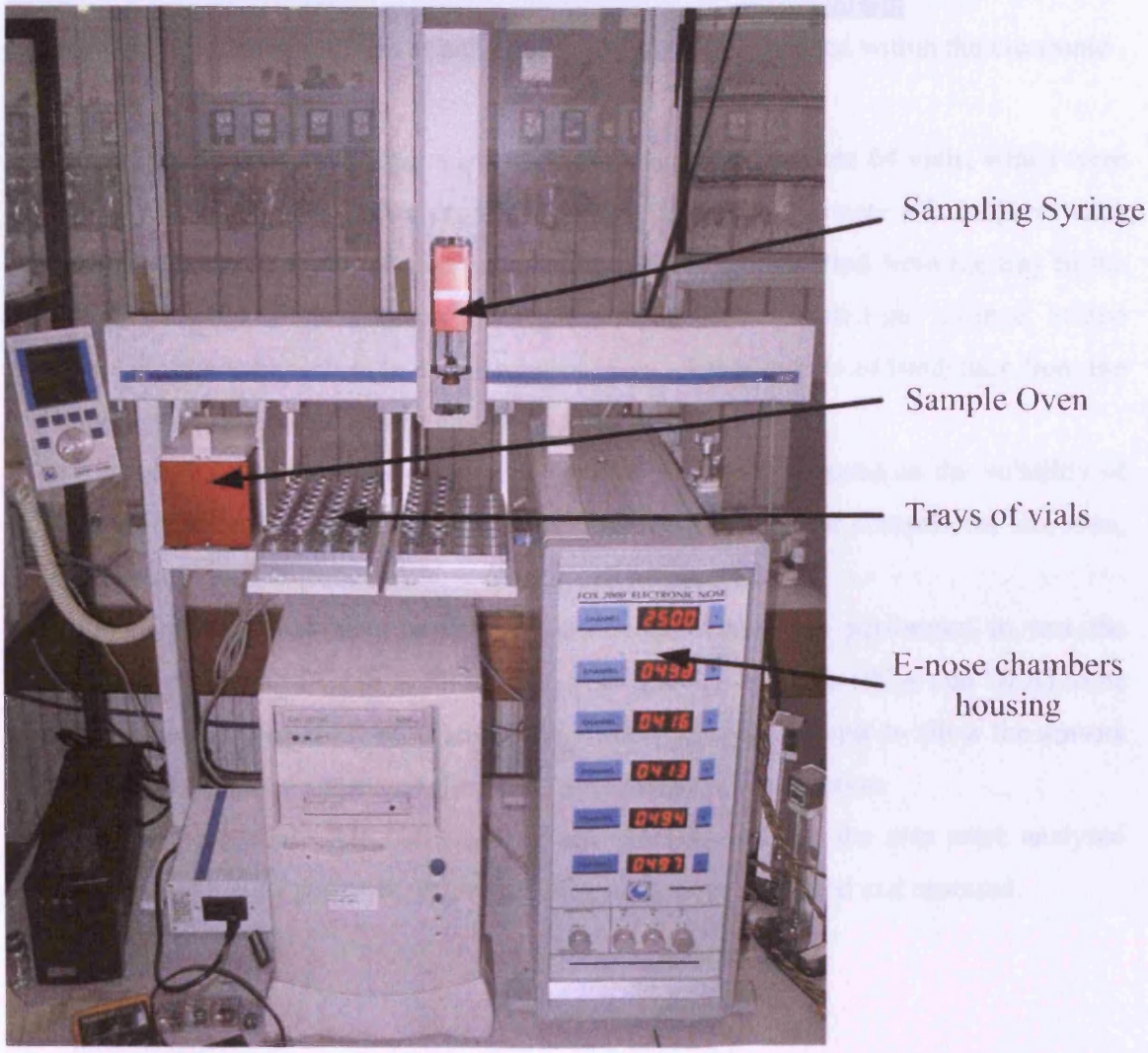

Figure 4.9.1 Photograph illustrating basic components of Fox 2000 electronic nose.

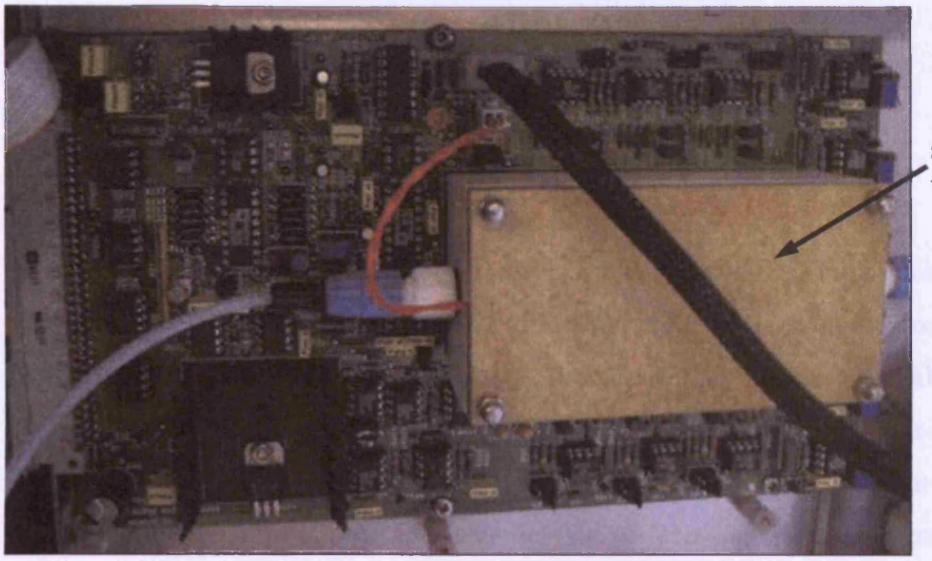

Figure 4.9.2 Photograph of sensor cell on electronics module housed within the electronic nose.

The static headspace autosampler (HS100) can accommodate 64 vials, which were capped 10 ml vials and typically contained 0.5 ml of sample to create a headspace when heated and agitated in the autosamplers oven. Each vial is transferred from the tray to the autosampler's oven to generate the headspace. A 2.5 ml automated gas syringe, heated above the sample temperature to avoid condensation, takes a sample of headspace from the vial and transfers it into the carrier gas of the instrument.

For each type of sample a sampling method is generated based on the volatility of the sample and the sensitivity of the sensor. The method sets the controls for the oven, syringe temperatures, injection volumes and speed of injection.

For each sample at least four repeated injections were performed to test the repeatability of the results and to allow statistical analysis methods (PCA and DFA) to be applied. There is a time delay of at least 30 mins between each sample to allow the sensors to recover and the gas syringe was flushed to avoid cross contamination.

Once the results were collated from an experimental run the data were analysed using Alphasoft v. 7.02 software. PCA and DFA plots were produced and assessed.

5. Materials Characterisation

5.1 Introduction

The Cr-zeolites were all fabricated using an aqueous (AQ) ion exchange on zeolites Y, β and ZSM-5. The Mo-zeolites were fabricated using an aqueous ion exchange and solid state exchange (SSE) on zeolites Y and β. Finally the W-zeolites were fabricated using an aqueous ion exchange on zeolites Y and β. By using the differing methods of ion exchange; aqueous and solid state exchange, there should be differences in the form of the transition metal complexes introduced and changes in surface and pore topography. Especially considering possible problems regarding the aqueous ion exchange in which the aqueous complexes may have difficulty in passing through the zeolite pores as mentioned in chapter 2.7. This chapter deals with the quantitative analysis of the transition metal introduced using energy dispersive X-ray analysis (EDAX), topographical observations using scanning electron microscopy (SEM), and a qualitative reactivity assessment using a proprietary experimental set-up that assesses hydrogen combustion.

5.2 EDAX analysis

After ion exchange the levels of chromium were ascertained by energy dispersive X-ray analysis (EDAX) performed by an Oxford Instruments INCA Energy system on a JEOL JSM 6301F scanning electron microscope. The analysis was performed on a total of at least 5 points and areas to check for homogeneity of the introduced transition metals dispersion on the surface. From the point analysis we can ascertain whether there are any clusters of metal oxide that have formed which would be indicated by a high level of the transition metal being present. Care has to be taken when interpreting the point analysis results as the point diameter is constant (1 μm) and is independent of magnification. For the transition metal exchanged zeolites in this study the levels have been calculated as an atomic ratio relative to the Al sites. The summary of the samples produced and their relative atomic percentages are outlined in Table 5.2.1.

Samples					Atomic percentage				Atomic ratios	
Zeolite Type	Addition	Sample	Code	Exchange Type	Si	Al	O	M	Si/Al	M/Al
Y	Cr	1	Cr-Y-1	AQ	24.9	5.3	63.5	6.3	4.7	1.19
Y	Cr	2	Cr-Y-2	AQ	36.3	6.0	57.3	1.0	6.0	0.16
Y	Cr	3	Cr-Y-3	AQ	25.0	4.9	66.3	3.8	5.2	0.79
Y	Cr	4	Cr-Y-4	AQ	30.6	7.1	61.9	0.4	4.3	0.06
β	Cr	1	Cr-β-1	AQ	47.5	0.9	51.0	0.3	53.7	0.38
ZSM-5	Cr	4	Cr-Z-4	AQ	41.3	0.8	56.4	1.6	54.3	2.04
Y	Mo	1	Mo-Y-1	SSE	28.1	8.7	61.4	1.8	3.2	0.20
Y	Mo	3	Mo-Y-3	SSE	22.4	7.2	64.6	5.9	3.1	0.83
Y	Mo	5	Mo-Y-5	AQ	32.0	9.3	58.1	0.6	3.5	0.07
β	Mo	2	Mo-β-2	SSE	47.9	0.9	50.0	1.1	53.0	1.24
β	Mo	5	Mo-β-5	AQ	31.3	0.7	68.1	0	47.6	0
Y	W	1	W-Y-1	AQ	24.6	8.0	66.5	1.0	3.1	0.10
Y	W	2	W-Y-2	AQ	26.0	7.9	65.0	1.1	3.3	0.14
β	W	1	W-β-1	AQ	61.8	0.9	37.3	0	42.5	0

Table 5.2.1 Summary of energy dispersive X-ray analysis results (EDAX) from an Oxford Instruments INCA Energy system on a JEOL JSM 6301F scanning electron microscope. M represents the transition metal introduced (indicated in the "addition" column).

There are a number of observations to be made from the EDAX results. Zeolite β was difficult to perform an aqueous ion exchange on using Mo and W complexes. It has narrow pore openings and the channels have tortuous paths so exchange within the pores and cavities will be difficult. Also it has a high Si/Al ratio therefore there are fewer sites for exchange than for the zeolite Y. The EDAX results show that for Mo-β-5 and W-β-1 the transition metal was not detected in each case. The SSE exchange of Mo with zeolite β had high levels of Mo but you would assume a high amount of MoO_3 to still be present which the point analysis did indicate.

Zeolite Y is readily exchangeable with all 3 transition metals and by using both exchange methods. It has more readily accessible pores due to a larger pore diameter than zeolite β and ZSM-5 (see table 4.2.1). Therefore a large amount of the exchange work was concentrated on zeolite Y and subsequently the Cr-zeolite Y samples have a range of Cr levels. Samples Cr-Y-4 and Mo-Y-5 have similar loadings of chromium and molybdenum respectively introduced via aqueous ion exchange into zeolite Y. Therefore a comparison of the effects of the transition metal introduced can be assessed by comparing the catalytic properties of these two materials.

For any sample with a high M/Al ratio there could be certain amounts of the metal oxide present due to the abundance of the transition metal ion complexes. This could be assessed by point analysis as the areas of metal oxide would appear like small inclusions on the surface of the zeolite particles, although this was often difficult to substantiate due to the spot size when using point analysis as discussed earlier.

5.3 SEM analysis

The following images were taken on a JEOL JSM 6301F scanning electron microscope utilising Oxford Instruments Link ISIS imaging software. There are further images that were taken during EDAX analysis which are shown in Appendix III.

Cr-zeolite sample 1 is indicated in figures 5.3.1 and 5.3.2. It exhibits a sub micron particle size and clusters of Cr_2O_3 were found to be present. The Cr/Al ratio was 1.19 for the bulk of the material and would be much higher for Cr_2O_3 clusters.

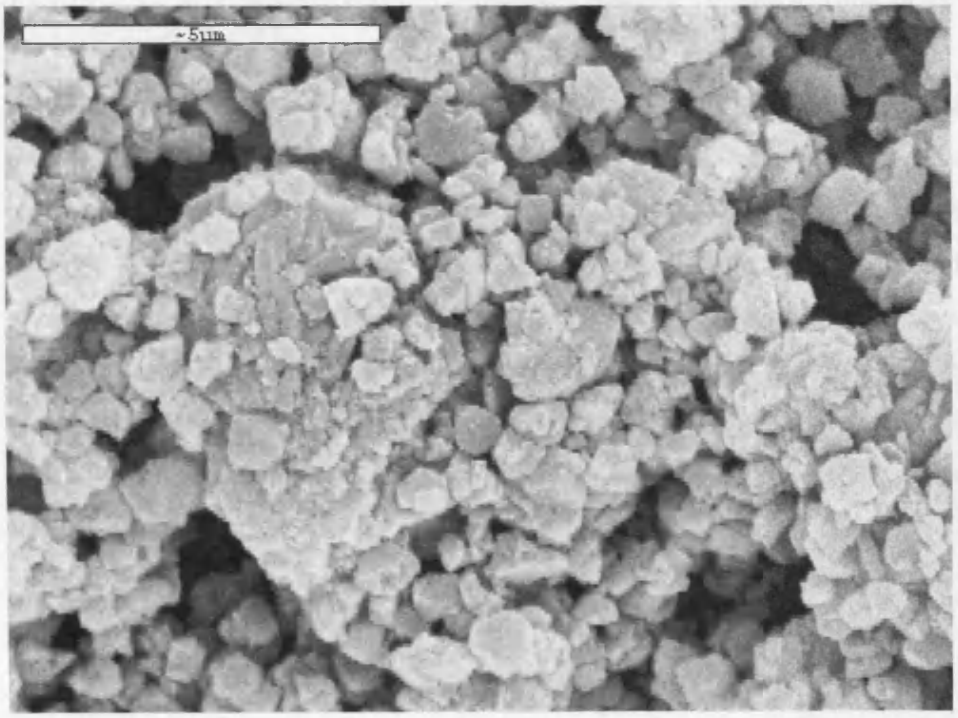

Figure 5.3.1 SEM micrograph of Cr-zeolite Y sample 1 in situ as filter layer on sensor. Magnification: x10000.

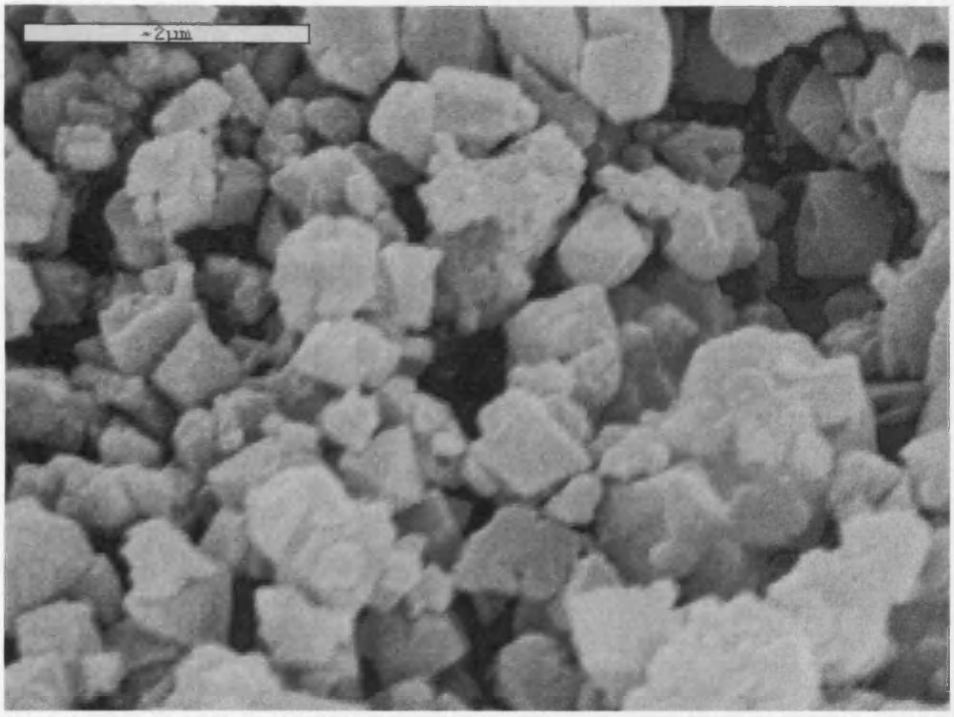

Figure 5.3.2 SEM micrograph of Cr-zeolite Y sample 1 in situ as filter layer on sensor. Magnification: x20000.

Figures 5.3.3 and 5.3.4 describe Cr-zeolite Y sample 3 integrated as a filter layer on a CTO sensor. Figure 5.3.3 gives an overall view of the sensor at a magnification of 50 to represent a sense of scale and structure looking top down on the sensor. The zeolite layer appears white in contrast to the rest of the picture. Despite being gold sputter coated, the exchanged zeolites are still acting as good insulators and due to the porous nature sputter coating was difficult. Therefore we are seeing the effects of charging by the electron beam resulting in the contrasting appearance of the zeolite filter layer.

Cr-zeolite sample 3 exhibited similar clusters of Cr_2O_3 as Cr-zeolite 1 despite the lower Cr content.

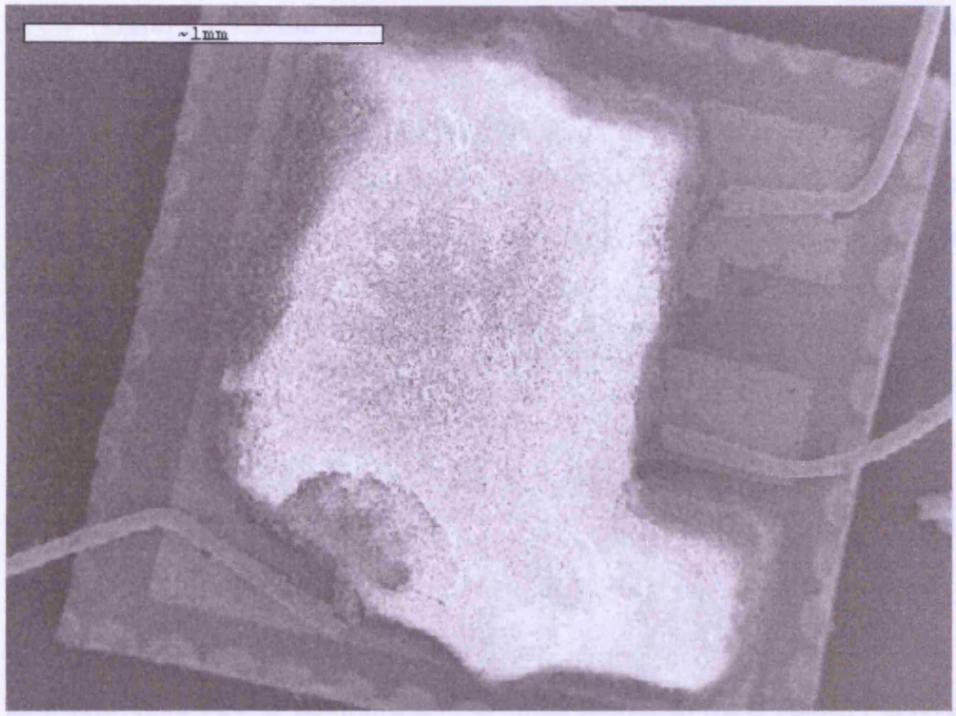

Figure 5.3.3 SEM micrograph of Cr-zeolite Y sample 3 in situ as filter layer on sensor. Magnification: x50.

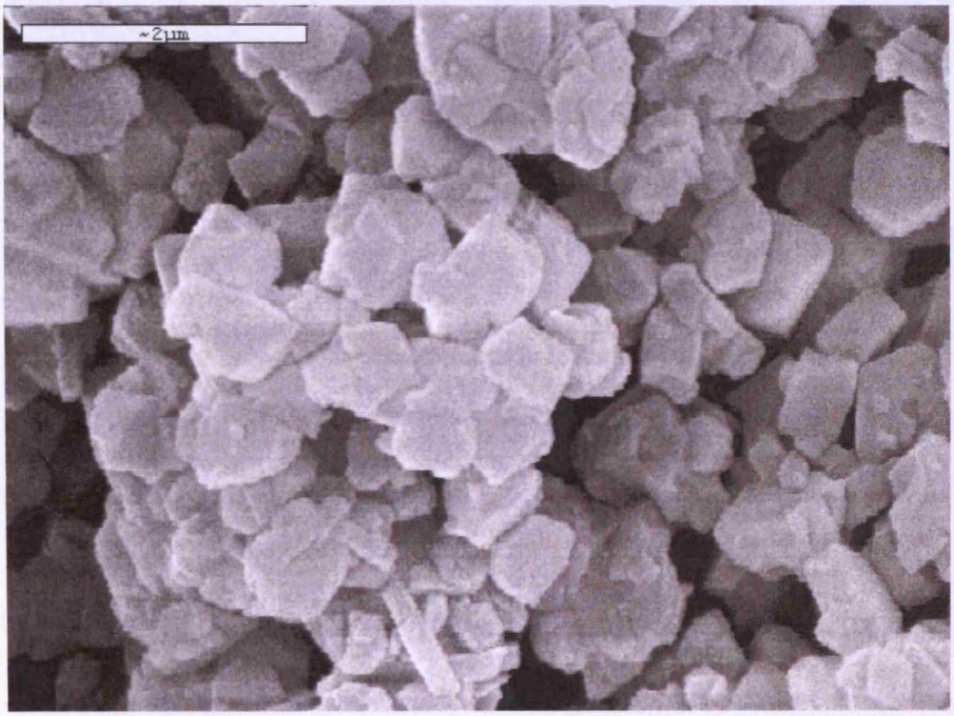

Figure 5.3.4 SEM micrograph of Cr-zeolite Y sample 3 in situ as filter layer on sensor. Magnification: x20000.

Figures 5.3.5 and 5.3.6 show the nature of Mo-zeolite Y sample 3 integrated as a filter layer on a CTO sensor. Mo-Y-3 was prepared by SSE with MoO_3 and contains a large amount of Mo (Mo/Al = 0.83). In the high magnification image (figure 5.3.6), there are a large number of inclusions which upon point EDAX analysis were detected to be deposits of MoO_3. Due to the nature of the SSE exchange a large proportion of the MoO_3 was inevitably going to end up on the surface of the sensor.

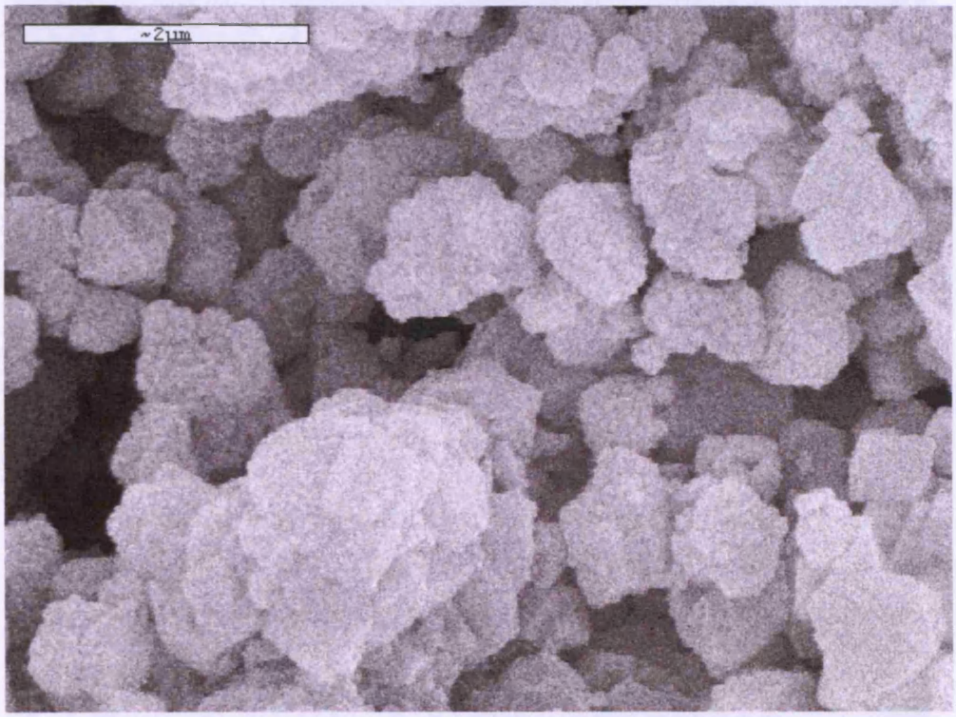

Figure 5.3.5 SEM micrograph of Mo-zeolite Y sample 3 in situ as filter layer on sensor. Magnification: x20000.

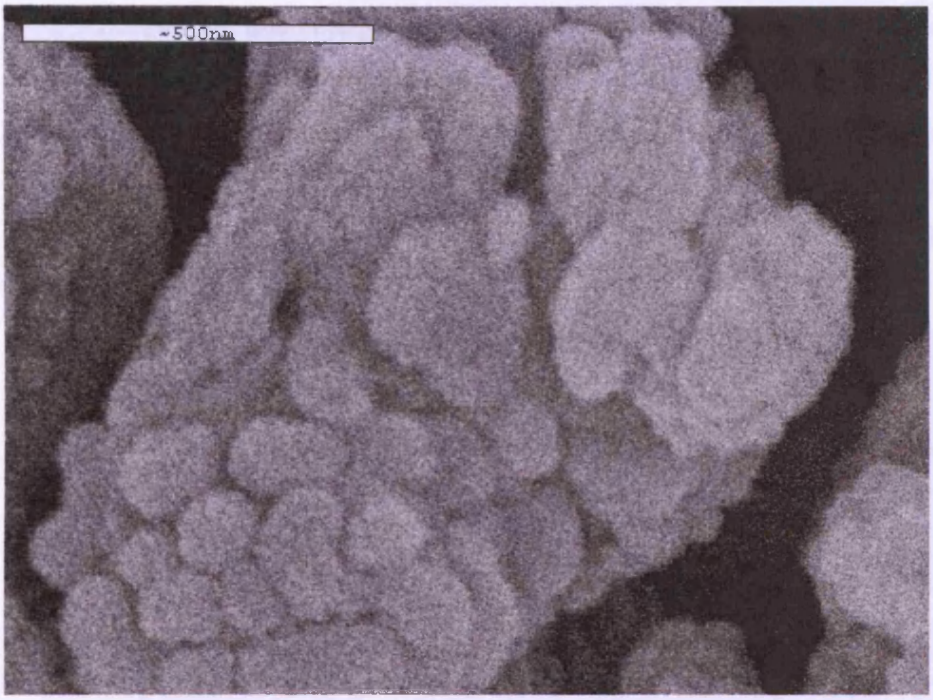

Figure 5.3.6 SEM micrograph of Mo-zeolite Y sample 3 in situ as filter layer on sensor. Magnification: x100000.

The structure of the underlying CTO sensor is outlined in figure 5.3.7, it is very porous for gas access exposing a large surface area open to gas interaction.

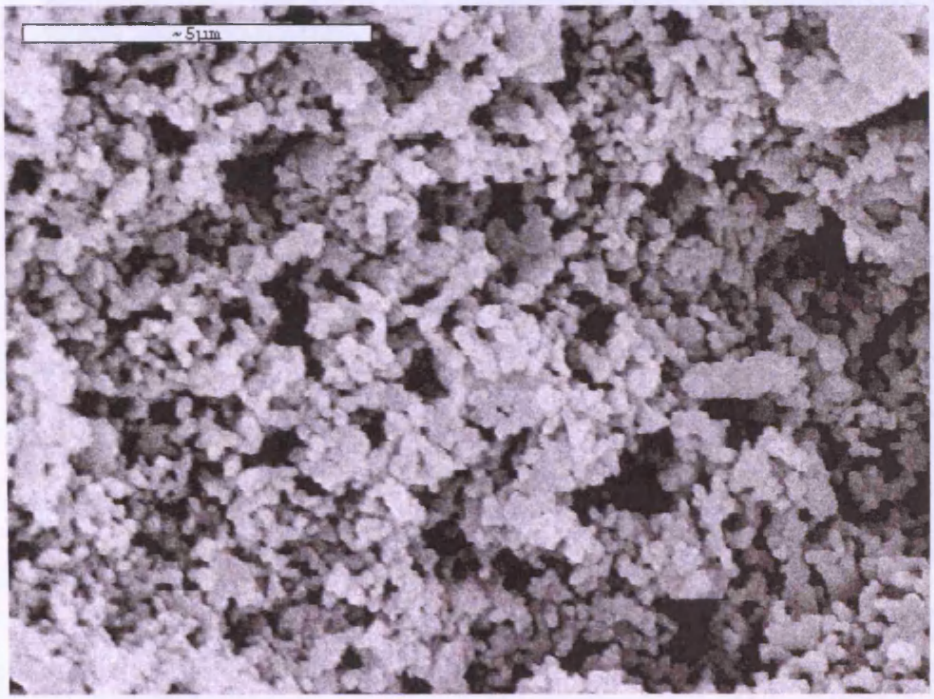

Figure 5.3.7 SEM micrograph of chromium titanium oxide on sensor. Magnification: x10000.

Further to this, images were also obtained using the Oxford Instruments INCA Energy system on a JEOL JSM 6301F scanning electron microscope. The images were taken prior to the EDAX analysis. Figure 5.3.8 describes Mo-zeolite β sample 2 where the Mo was introduced by SSE and the Mo/Al ratio was 1.24 indicating an excess of Mo. Therefore inclusions of MoO_3 are present as discussed previously for the Mo-zeolite Y samples.

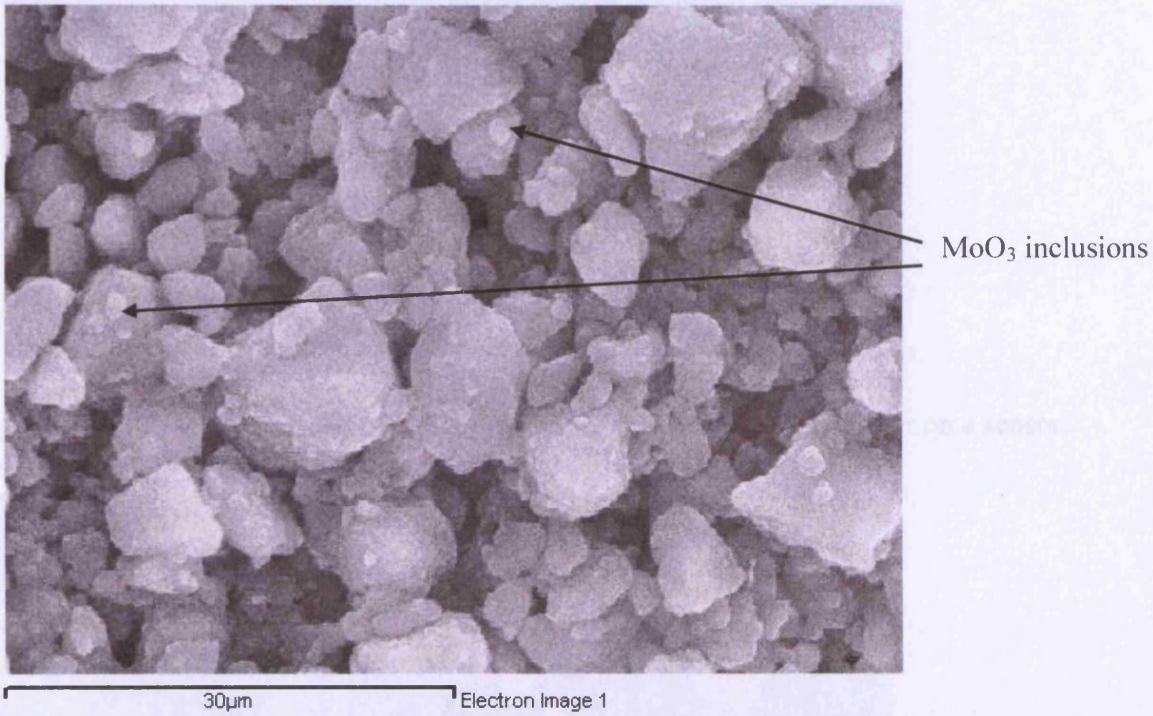

Figure 5.3.8 SEM micrograph of Mo-zeolite β sample 2 in situ as filter layer on sensor. Magnification: x2000.

Figure 5.3.9 shows the microstructure of Cr-zeolite Y once integrated as a filter layer onto a CTO sensor. There is a large amount of porosity present and the grain size is < 1 µm and the grains are uniform in size. Figures 5.3.10 and 5.3.11 are SEM micrographs of Cr-zeolite Y sample 4 and Cr-zeolite Y sample 3 respectively. The as-received powders have a sub-micron grain size and are uniform in size.

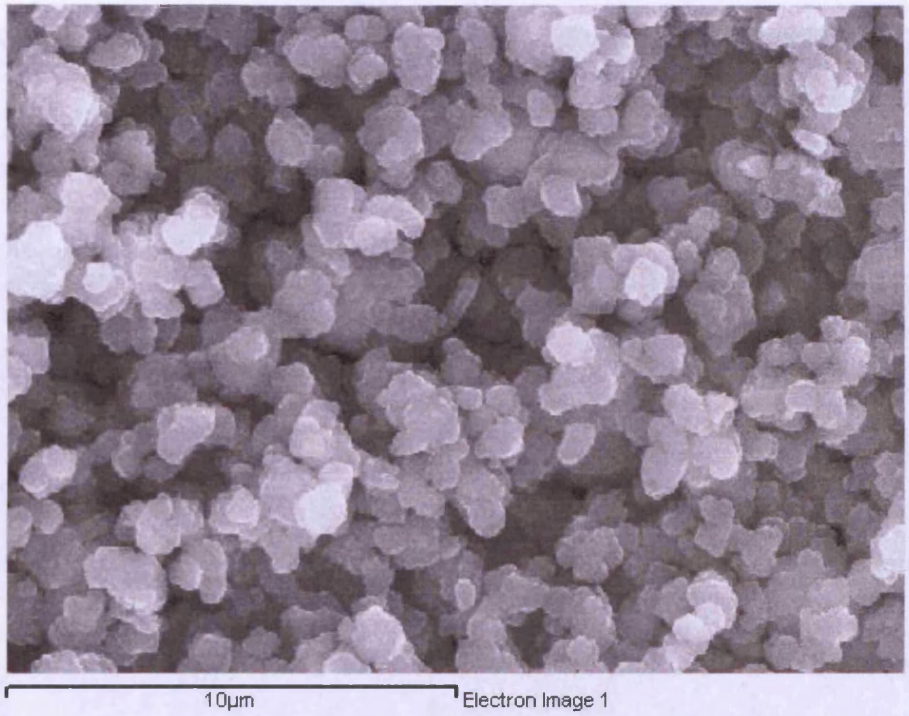

Figure 5.3.9 SEM micrograph of Cr-zeolite Y sample 2 in situ as filter layer on a sensor. Magnification: x6000.

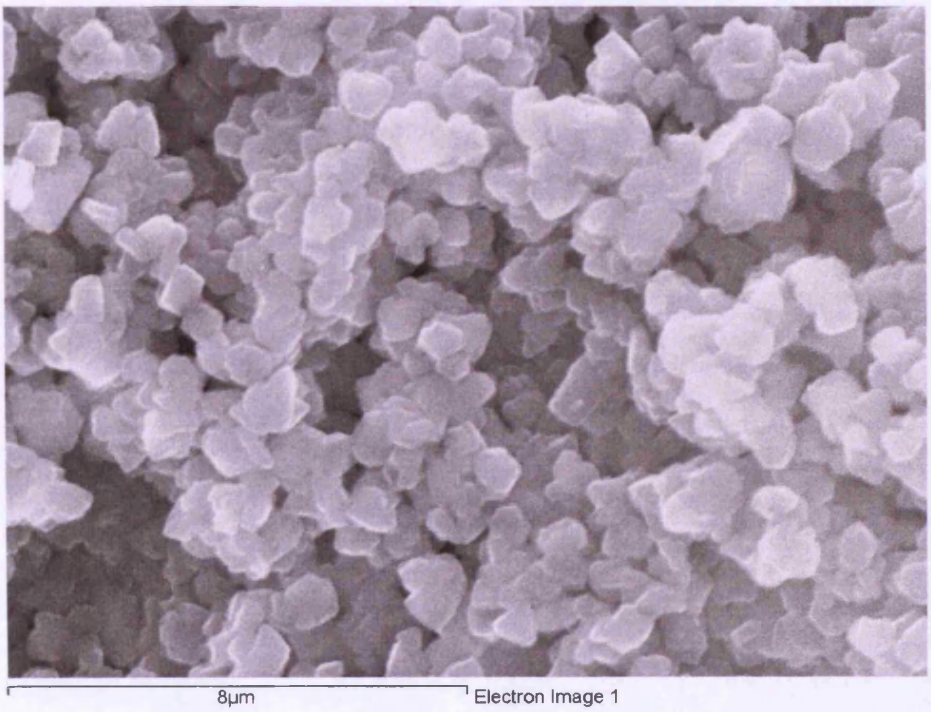

Figure 5.3.10 SEM micrograph of Cr-zeolite Y sample 4 as a powder. Magnification: x8000.

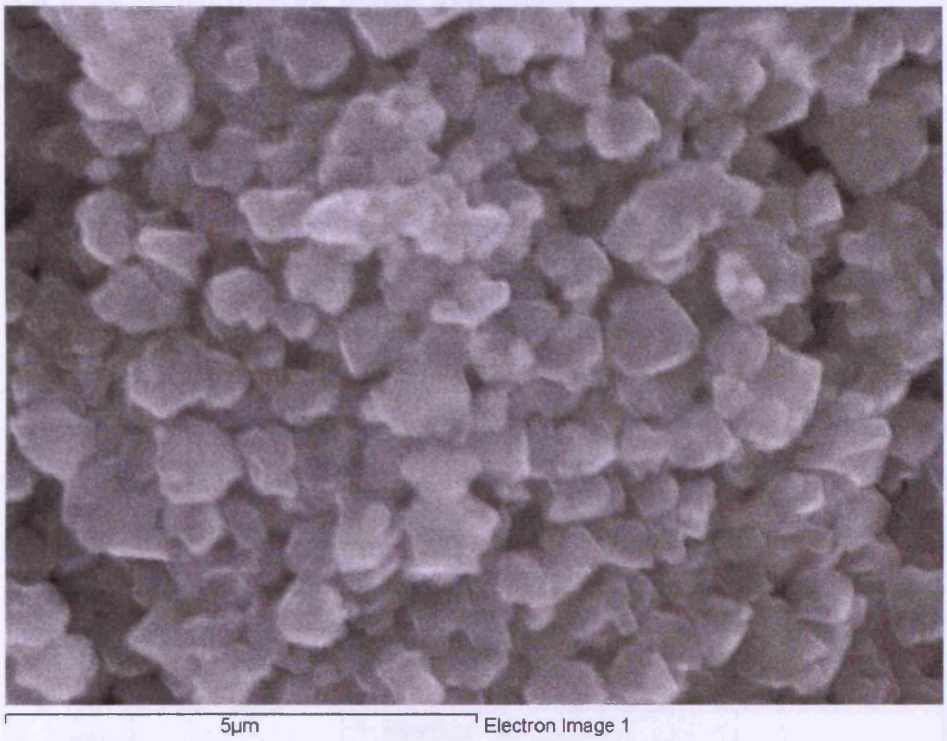

Figure 5.3.11 SEM micrograph of Cr-zeolite Y sample 3 as a powder. Magnification: x6000.

5.4 Reactivity testing using hydrogen

There was initial testing to see what actually happened to Cr-zeolite Y samples when hydrogen was passed over the surface with a temperature step ramped up to 400°C. By looking at figure 5.4.1 two effects are present. Initially on the ramp to 200°C (between 600 s and 1600 s) there is a peak in sensor resistance that has a shoulder of response at 1500 s adjacent to the main peak. This is most likely due to organic contaminants and water in the zeolite desorbing from the structure from two different sites. This is backed up by observations in the GC/MS rig when there is most likely to be water and various unknowns present in a contamination test when a fresh zeolite is placed in the chamber. It should be noted that with the Cr-ZSM5 samples there was a more pronounced second peak exhibited by this water desorption. The second effect present in figure 5.4.1 is that of the loss of sensor resistance at 400°C as expected due to the combustion of hydrogen to water as the hydrogen is passed over the zeolite powder.

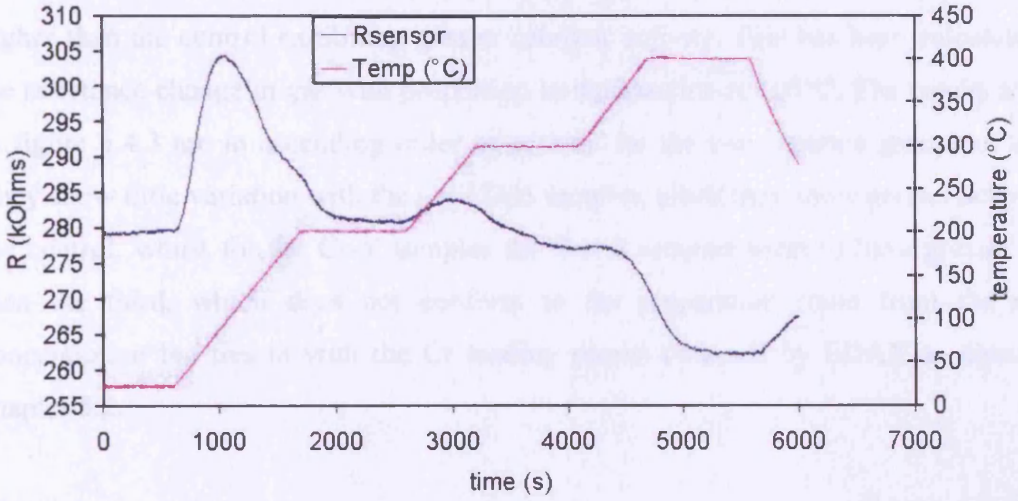

Figure 5.4.1 Sensor resistance in relation to temperature of Cr-zeolite Y sample 2 during a constant supply of 1000 ppm hydrogen in dry air. CTO sensor operating at 400°C.

Initial testing was done on the three Cr-exchanged Y zeolites and the three Cr-exchanged ZSM-5 zeolites compared to a control of no zeolite in the chamber. This was performed initially by the cycling of 1000 ppm hydrogen with the sensor at 400°C. An example of which is shown in figure 5.4.2.

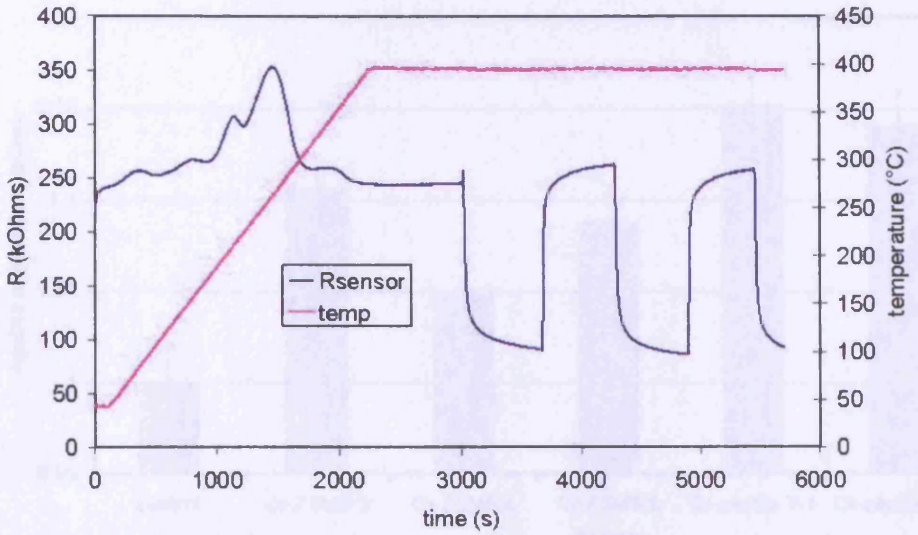

Figure 5.4.2 Cr-ZSM5-3 with continuous temperature ramp to 400°C whereupon the hydrogen is cycled between 1000 ppm and 0 ppm in dry air. CTO Sensor operating at 400°C.

The overall results have been portrayed below in relation to the control with anything higher than the control exhibiting greater catalytic activity. This has been calculated from the resistance change in gas with proportion to the baseline at 400°C. The results as shown in figure 5.4.3 are in ascending order of activity for the two separate groups of zeolites. They show little variation with the Cr-ZSM5 samples, albeit they show greater activity than the control, whilst for the Cr-Y samples the first 2 samples seem to have greater activity than the third, which does not conform to the preparation route from the aqueous concentration but ties in with the Cr loading results obtained by EDAX as discussed in chapter 5.2.

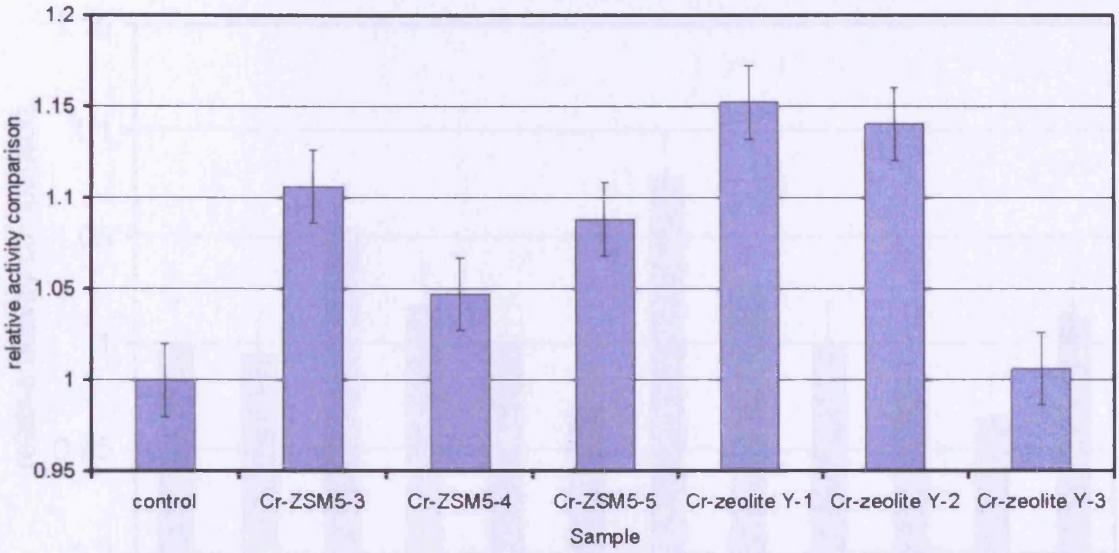

Figure 5.4.3 Comparison as a function of activity towards the combustion of hydrogen at 400°C using 1000ppm hydrogen in air

Further testing was performed to try and refine these responses, 500 ppm hydrogen was cycled at 600 s intervals to try and accentuate the loss of hydrogen and the sensor was set at 500°C. The as-received zeolites were used in this test; from figure 5.4.4 it can be seen that the Cr-ZSM5-4 sample is more active than the other Cr-ZSM-5 samples. Also Cr-Y-1 is more active than the other Cr-zeolite Y samples whilst the H-Beta shows no discernible difference. Again the zeolites are displayed in ascending Cr content from left to right within their groups as opposed from their preparation. This shows that despite the increased loading in Cr expected from the preparation route it seems the "middle" zeolite is most active. Visually the middle zeolite is greener in colour than the other two in the series.

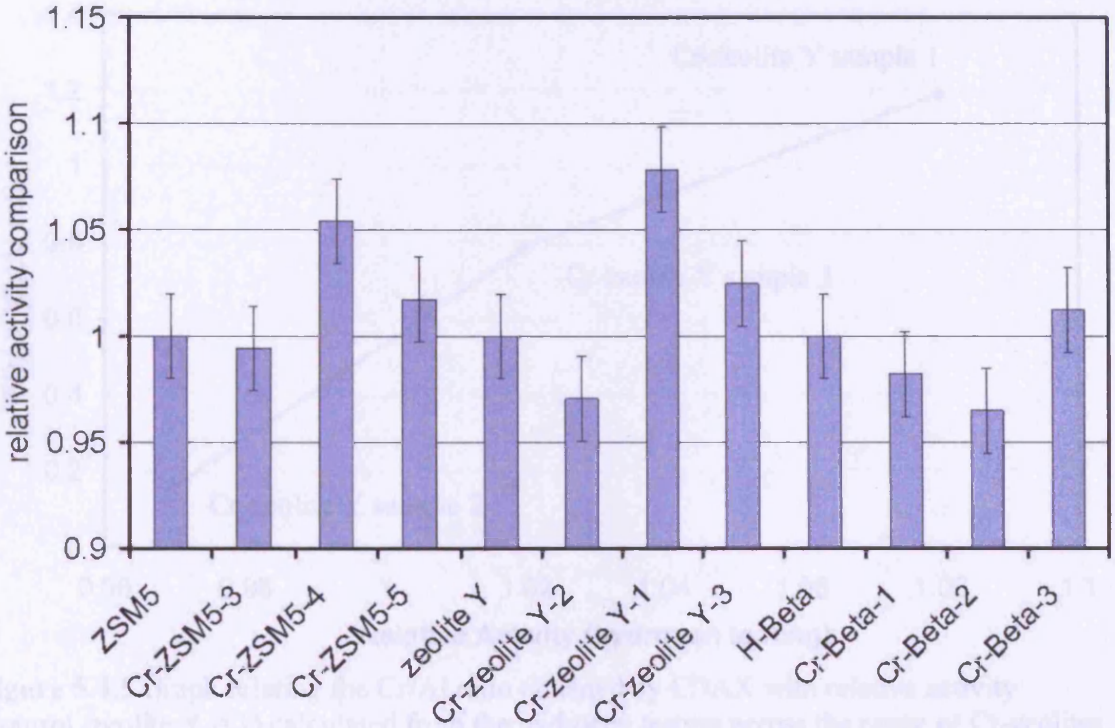

Figure 5.4.4 Comparison as a function of activity towards the combustion of hydrogen at 400°C using 500ppm and new settings. CTO sensor operating at 400°C.

In the case of the three Cr-zeolites, samples 1 to 3, the relative activity calculated from the hydrogen testing as indicated in figure 5.4.4 can relate to the EDAX results as shown in table 5.2.1. Therefore if one is plotted against the other as shown in figure 5.4.5 it can be shown that there is a correlation between the two indicating that the activity is proportional to the Cr content for the range shown.

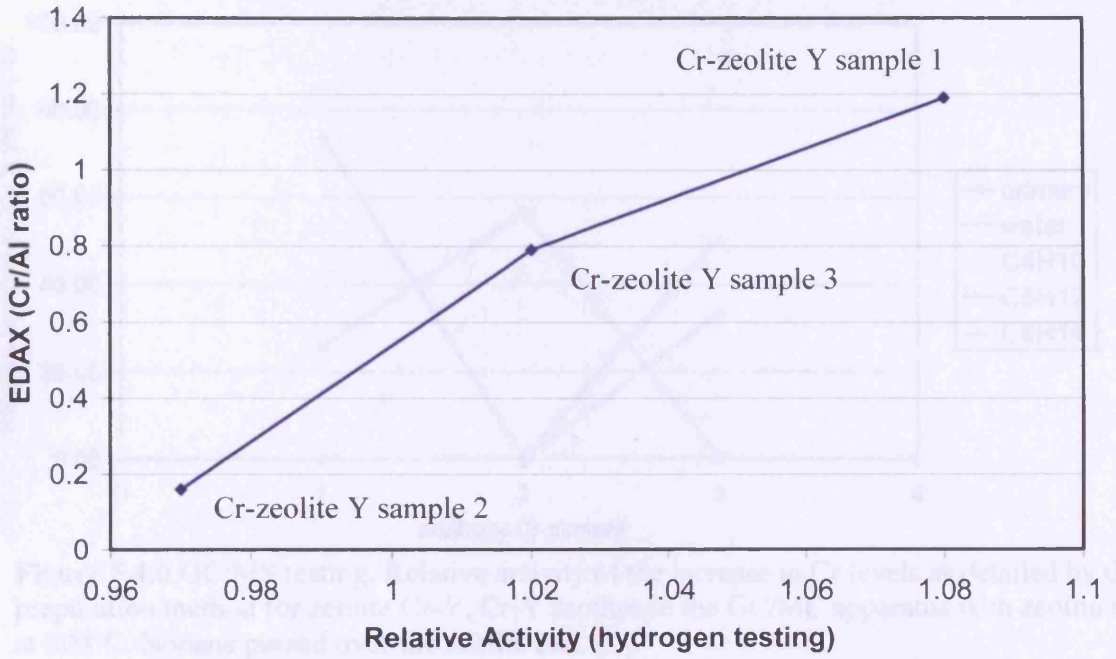

Figure 5.4.5 Graph relating the Cr/Al ratio obtained by EDAX with relative activity (control, zeolite Y = 1) calculated from the hydrogen testing across the range of Cr-zeolites.

The three zeolite Cr-Y samples were tested in the zeolite bed/GC/MS rig at 300°C with nonane as the analyte. At 300°C (figure 5.4.6) it is quite apparent that Cr-Y-1 which has the arbitrary Cr content of 2 is clearly more active than the other two samples with more water being present and a high proportion of C_4H_{10} being produced. If the other two Cr levels are examined a difference can be seen in the catalytic activity between the high and low Cr levels. The low value is producing some water with a high proportion of the original nonane going through unreacted indicating some combustion but no cracking. Whereas the higher Cr content is performing catalytic cracking to C_4H_{10} and C_5H_{12}, with some nonane going through but no water. Along with evidence from the other temperatures it is indicating that the Cr may be in different forms within the structure due to the processing parameters, and perhaps in different locations due to migration during the calcination of the powder.

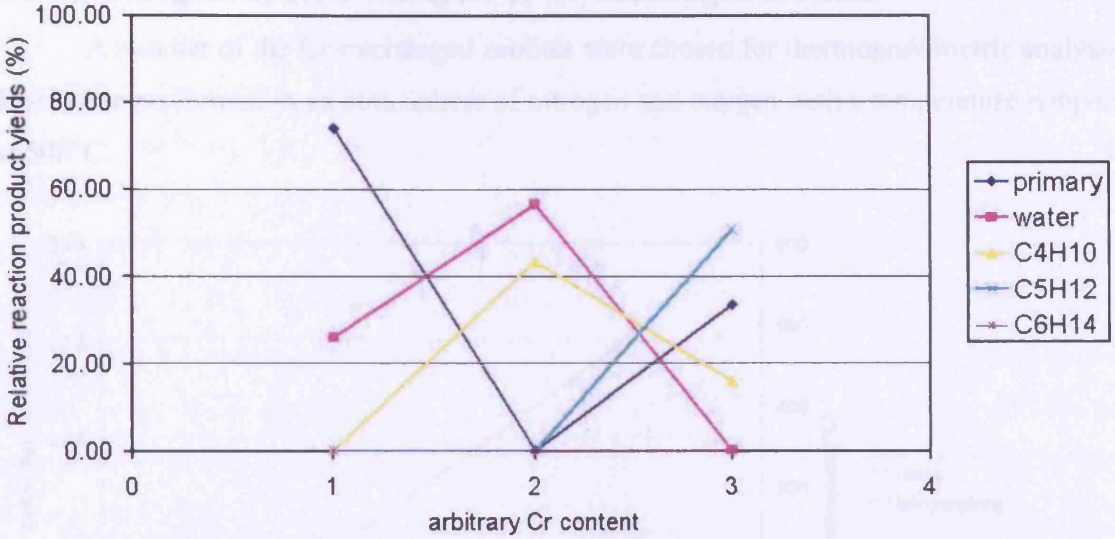

Figure 5.4.6 GC/MS testing. Relative activity of the increase in Cr levels as detailed by the preparation method for zeolite Cr-Y. Cr-Y zeolites in the GC/MC apparatus with zeolite bed at 300°C. Nonane passed over the zeolite bed.

5.5 Thermogravimetric Analysis of Cr-exchanged zeolites

A number of the Cr-exchanged zeolites were chosen for thermogravimetric analysis. Tests were performed in an atmosphere of nitrogen and oxygen with a temperature ramp up to 500°C.

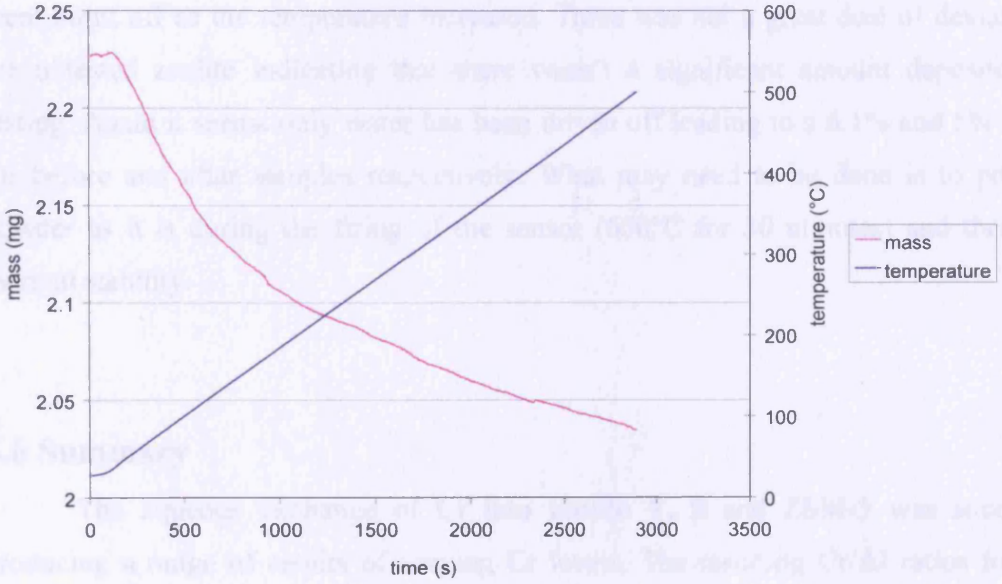

Figure 5.5.1 Change in mass as temperature increases in N_2 over time. For Cr-zeolite Y sample 2.

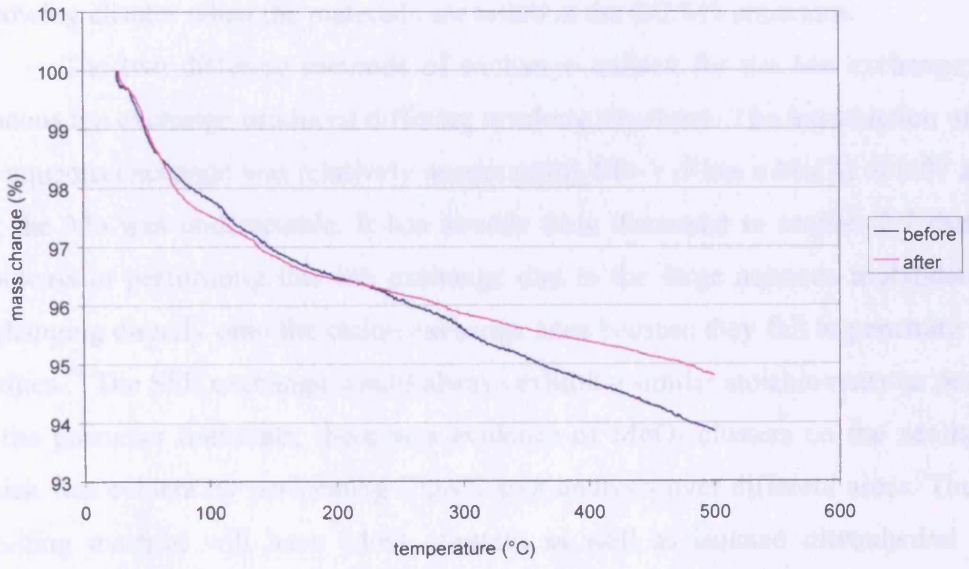

Figure 5.5.2 Change in mass as temperature increases in O_2. Samples are Cr-ZSM5-5 before and after being tested in zeolite bed-GC/MS apparatus.

Figure 5.5.1 shows the mass loss of Cr-Y-2 over time as it is heated in a nitrogen atmosphere. There is approximately a 9% loss in mass of the sample upon reaching 500°C from room temperature. This is consistent with the hydrophilic nature of the material as it loses water as the temperature increases. In figure 5.5.2, Cr-ZSM5-5 was tested in O_2 to see whether any possible carbonaceous materials deposited during zeolite bed-GC/MS testing, were burnt off as the temperature increased. There was not a great deal of deviation from the untested zeolite indicating that there wasn't a significant amount deposited during testing. Again it seems only water has been driven off leading to a 6.1% and 5% reduction for before and after samples respectively. What may need to be done is to process the powder as it is during the firing of the sensor (600°C for 30 minutes) and then test for thermal stability.

5.6 Summary

The aqueous exchange of Cr into zeolite Y, β and ZSM-5 was successful in producing a range of results of varying Cr levels. The resulting Cr/Al ratios for the Cr-zeolite Y samples produced a good spread of Cr levels (0.06, 0.16, 0.79, 1.19). Therefore, there will be the ability to observe how the Cr content affects the catalytic activity in the following chapter when the materials are tested in the GC/MS apparatus.

The two differing methods of exchange utilised for the Mo exchange; SSE and aqueous ion exchange produced differing resulting structures. The introduction of Mo using the aqueous exchange was relatively unsuccessful, Mo-Y-5 has a Mo/Al of 0.07 and in Mo-β-2 the Mo was undetectable. It has already been discussed in section 2.7 that there are problems in performing this ion exchange due to the large aqueous molybdate ions not exchanging directly onto the cation exchange sites because they fail to penetrate the zeolite cavities.[74] The SSE exchange would always exhibit a similar stoichiometry as per the ratios of the precursor materials; there was evidence of MoO_3 clusters on the zeolite particles which was evident by performing EDAX spot analysis over different areas. Therefore the resulting material will have MoO_3 clusters as well as isolated ditetrahedral $[Mo_2O_7]^{2-}$ dimers which contain framework oxygen associated with two Al sites.

The aqueous exchange of W into zeolite Y and β using ammonium paratungstate was successful for zeolite Y but not for zeolite β due to the narrow pore openings and the complexity of the zeolite structure in zeolite β.

6. Catalytic property testing using zeolite bed & GC/MS

6.1 Introduction

The purpose of this chapter is to understand the relationship between the zeolite type, the exchanged metal ion present, and the metal loading with reference to the reaction products that are detected.

A standard method was used to quantify and display the results from the zeolite bed – GC/MS set-up. From the MS data, relative amounts of reaction products were determined thus totalling 100%. Included in this data were the proportions of the original analyte which was passed through the zeolite bed and is labelled as the "primary analyte" on the relevant graphs. Thus when there is 100% of the primary analyte, no reaction has taken place in the zeolite bed as the analyte has passed through unreacted. All materials were tested to a series of linear alkanes, which are used as a simple determining method to establish whether any variation in activity through a simple molecular series is seen before moving onto different organic groups and flavour compounds.

6.2 Effects of experimental set-up

A number of parameters were defined in the experimental set-up for consistent comparative results between materials. Before fixing these parameters for the bulk of the experiments each parameter was varied to assess best experimental practice and to obtain further information regarding material properties.

6.2.1 Flow rate effects through the zeolite bed

Figure 6.2.1.1 describes the catalytic activity of Mo-zeolite Y sample 5 at 350°C. The analytes were flowed through at two different flow rates, 10 ml (standard) and 20 ml to assess the effect of residence time in the zeolite bed. The branched alkanes only occur at 20 ml. Water occurs at both flow rates but at a greater magnitude at 20 ml, and there is a heptane peak at C8 for both flow rates.

Therefore the residence time of the analytes within the zeolite bed has an important impact on the reaction products. This will have important consequences for the testing of the sensors as there will be two thicknesses fabricated of the zeolite filter layer.

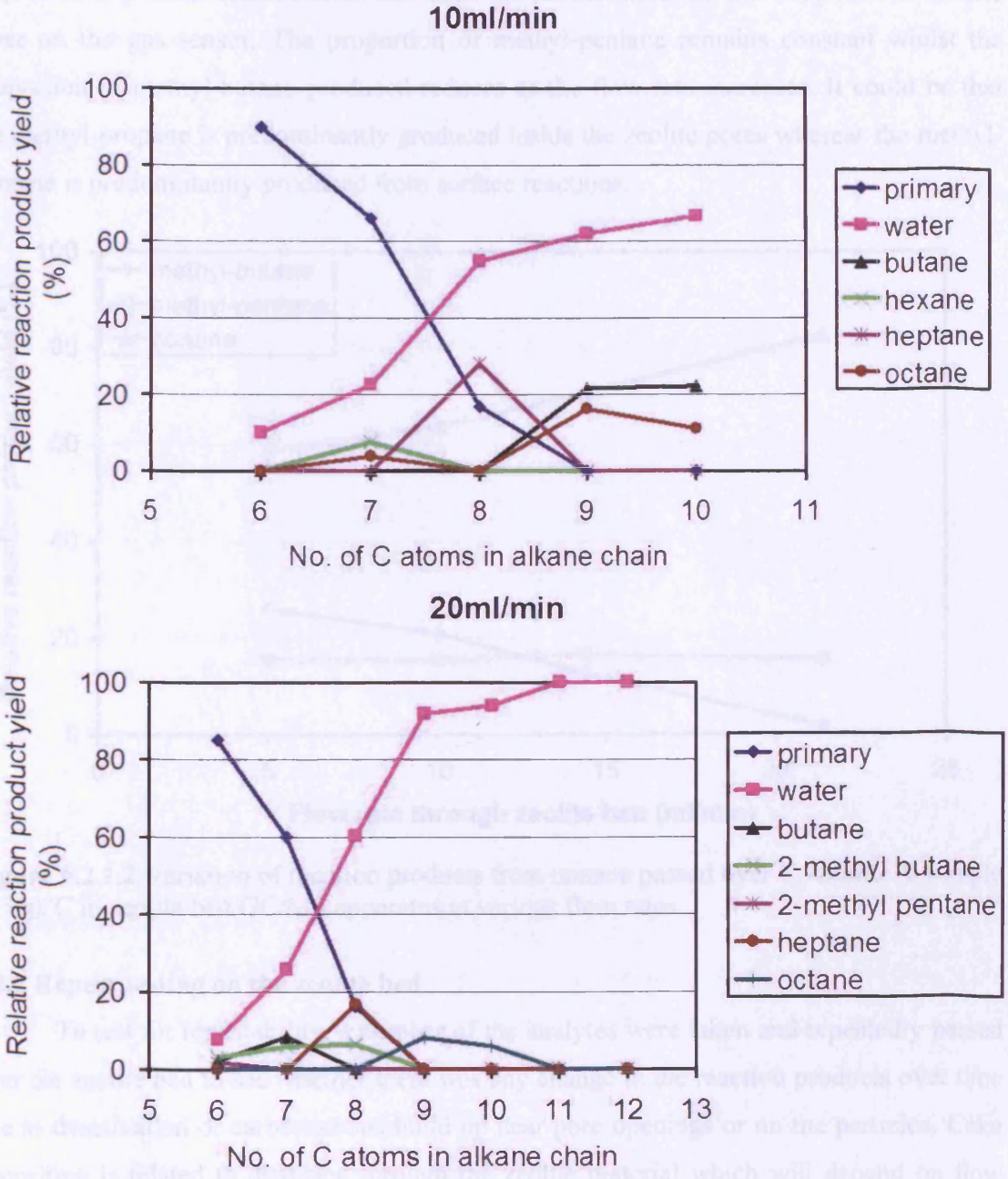

Figure 6.2.1.1 Catalytic activity of Mo-zeolite Y sample 5 at 350°C in the zeolite bed/GC/MS apparatus. Comparing flow characteristics through the zeolite bed at 10 ml/min and 20 ml/min flow rates of air.

Another example of the flow rate characteristics is exhibited in figure 6.2.1.2 in which nonane was passed through Cr-zeolite Y sample 1 at various flow rates. This shows how the residence time in the zeolite bed varies as a function of the flow rate through it. This is an important consideration for when the zeolite materials are integrated as a filter layer on the gas sensor. The proportion of methyl-pentane remains constant whilst the proportion of methyl-butane produced reduces as the flow rate increases. It could be that the methyl-propane is predominantly produced inside the zeolite pores whereas the methyl-pentane is predominantly produced from surface reactions.

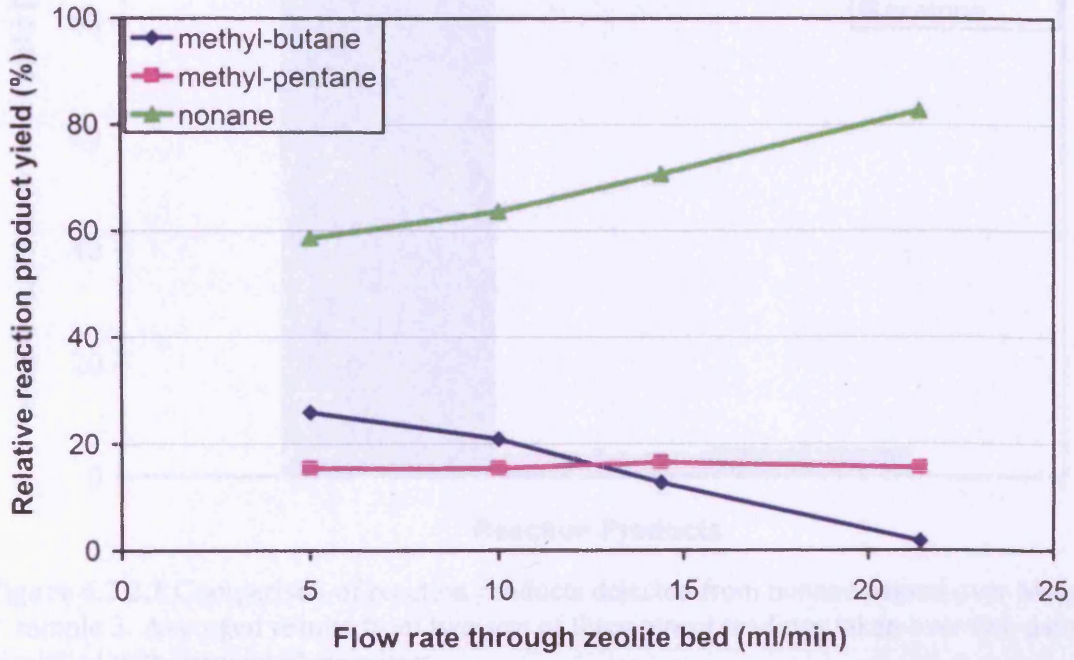

Figure 6.2.1.2 Variation of reaction products from nonane passed over Cr-zeolite Y sample 1 at 300°C in zeolite bed/GC/MS apparatus at various flow rates.

6.2.2 Repeat testing on the zeolite bed

To test for repeatability, a number of the analytes were taken and repeatedly passed over the zeolite bed to see whether there was any change in the reaction products over time due to deactivation or carbonaceous build up near pore openings or on the particles. Coke deposition is related to diffusion through the zeolite material which will depend on flow rate and concentration, and if coke ends up being deposited it becomes the diffusion barrier itself. Coke deposition and any associated reduction in catalytic activity will be easily

observable when the materials are integrated into a sensor (sensor results discussed in chapter 7) resulting in a change in sensitivity.

Figure 6.2.2.1 displays the reaction products from nonane after two sets of three tests taken over two days. The repeatability is good although the associated error could be an issue when comparing reaction products with low yields.

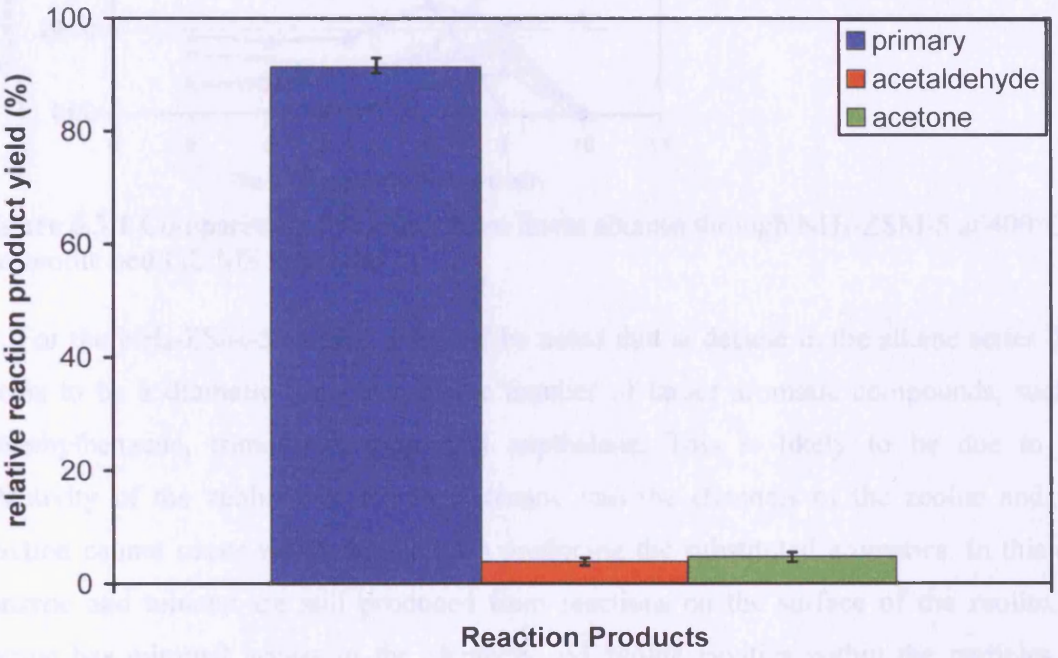

Figure 6.2.2.1 Comparison of reaction products detected from nonane passed over Mo-zeolite Y sample 3. Averaged results from two sets of three repeat readings taken over two days displayed with associated error bars.

6.3 Unmodified zeolite testing – effects of zeolite type

Both the NH_4-ZSM-5 and H-Y samples had a tendency towards aromatisation of the longer linear alkanes at high temperatures. If we analyse the data shown in figures 6.3.1 and 6.3.2 we can see the relative similarities between the two materials, in general as the chain length increases, less of the primary analyte is seen yet more benzene is produced. Substituted aromatics make up the remainder of the products.

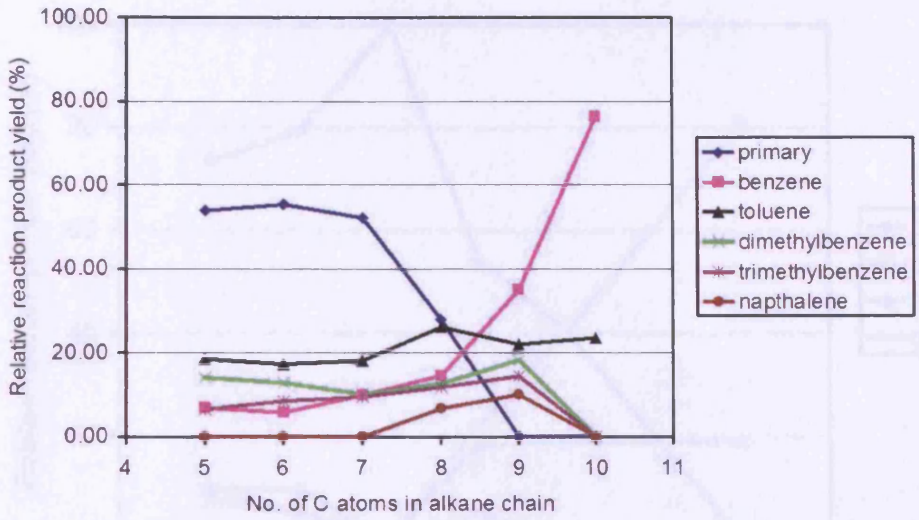

Figure 6.3.1 Comparison of products from linear alkanes through NH_4-ZSM-5 at 400°C in the zeolite bed/GC/MS apparatus.

For the NH_4-ZSM-5 sample it should be noted that at decane in the alkane series there seems to be a dramatic reduction in the number of larger aromatic compounds, such as dimethylbenzene, trimethylbenzene and napthalene. This is likely to be due to size selectivity of the zeolite not allowing decane into the channels of the zeolite and thus reaction cannot occur within the cavities producing the substituted aromatics. In this case benzene and toluene are still produced from reactions on the surface of the zeolite, but decane has minimal access to the channels and zeolite cavities within the particles and therefore more complex aromatics are not seen in the reaction products. Thus it can be assumed that the substituted aromatics are only produced in the zeolite channels and cavities by way of the surface topology and slower diffusion through these channels as compared to the macroporous diffusion around the particles allowing further reaction.

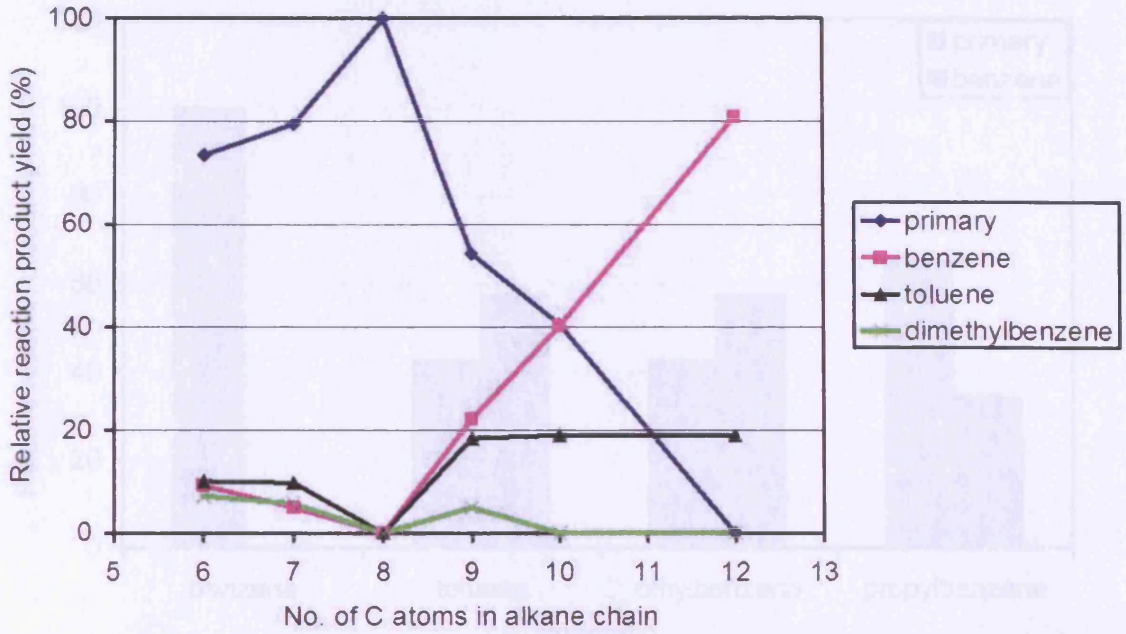

Figure 6.3.2 Comparison of reaction products from linear alkanes passed through H-zeolite Y in GC/MS apparatus. Zeolite bed at 400°C.

If we take the zeolite Y outlined in figure 6.3.2 there are not a large amount of reaction products until we get to nonane whereupon reaction products increase whilst with the ZSM-5 it is after heptane that more reaction products are seen. The channel size in zeolite Y is larger than that of ZSM-5 therefore it is at a longer chain length that the reaction products become more prevalent. Also there are no large aromatic compounds in the reaction products indicating an easier diffusion through the zeolite channels for the primary analyte, reaction intermediates and products. There seems to be a selective result at octane where no reaction products were detected. In the case of octane the analyte is passing through the zeolite unreacted which will be related to the molecular size of octane and the zeolite pore size.

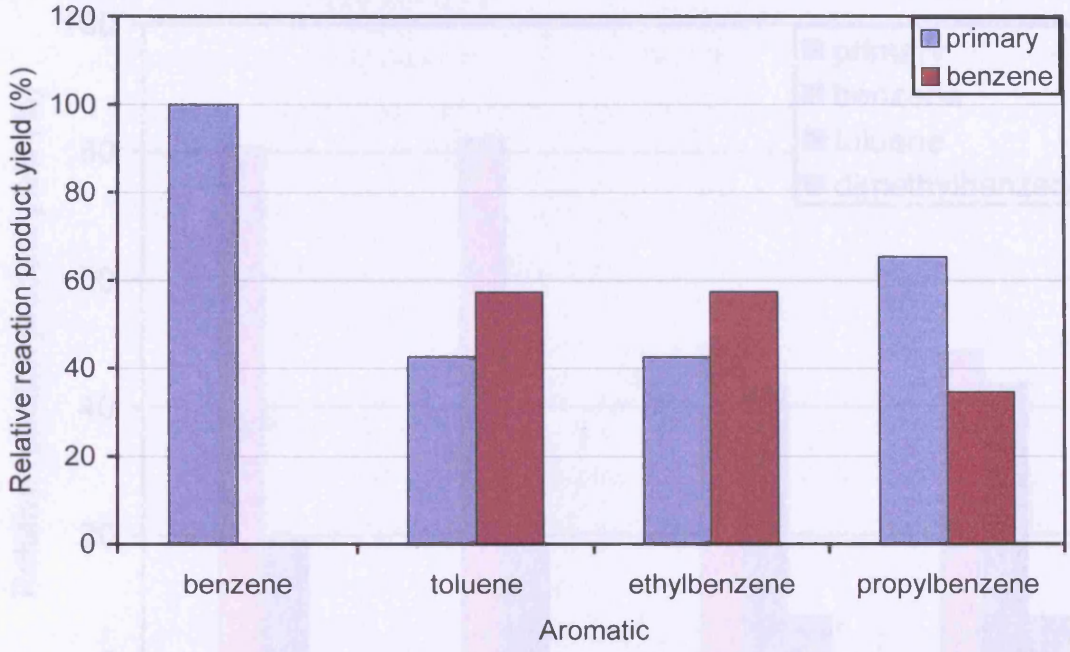

Figure 6.3.3 Comparison of reaction products from series of aromatic compounds through H-zeolite Y in GC/MS apparatus. Zeolite bed at 400°C.

A series of aromatic compounds were also passed through the zeolite bed/GC/MS apparatus as displayed in figure 6.3.3. Benzene passes through unreacted whilst the rest of the series with additional functional groups have benzene as a reaction product but there were no other reaction products detected. Toluene and ethylbenzene both have benzene as a reaction product in the same proportion however for propylbenzene the proportion of benzene produced is lower. The propylbenzene has difficulty entering the zeolite pores due to the propyl group on the benzene ring.

Two flavour compounds of interest were also tested through zeolite Y, namely benzyl acetate and linalool. In figure 6.3.4, in the comparison of products from linalool with another large molecule, in this case dodecane, there is a measurable difference. Also note that they were both tested with a standard 3µl input sample and also a 6µl input sample to establish any differences associated with the input concentration, repeatability and the mathematical interpretation of the MS data. The interpretation is good but many repeat samples would need to be done for consistency of the zeolite over time and to establish the associated error.

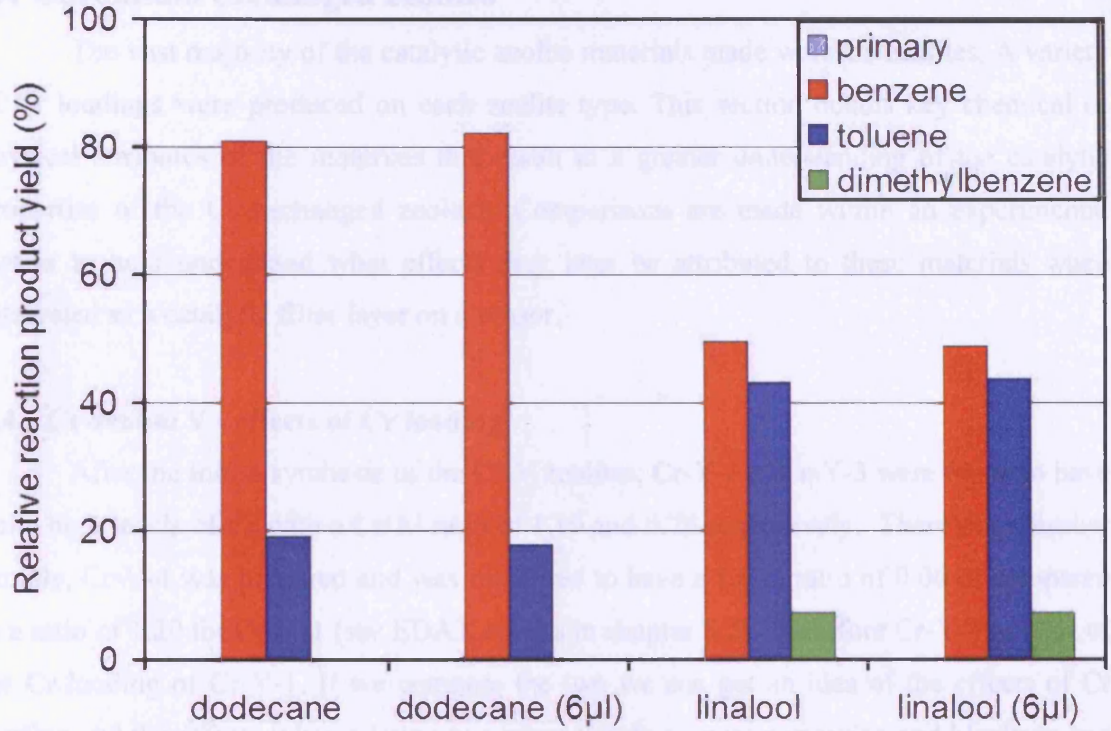

Figure 6.3.4 Comparison of products from dodecane and linalool passed through H-zeolite Y in the GC/MS apparatus. Zeolite bed at 400°C.

LTA zeolite was also tested in the zeolite bed/GC/MS apparatus however for all samples tested no observable reaction products were detected. The LTA zeolite is void of Brönsted protons and has a small pore size of 4 Å in this instance therefore there will be no pore interaction with any of the analytes tested.

6.4 Chromium exchanged zeolites

The vast majority of the catalytic zeolite materials made were Cr-zeolites. A variety of Cr loadings were produced on each zeolite type. This section details key chemical or physical attributes of the materials that result in a greater understanding of the catalytic properties of the Cr exchanged zeolites. Comparisons are made within an experimental matrix to help understand what effects may later be attributed to these materials when integrated as a catalytic filter layer on a sensor.

6.4.1 Cr-zeolite Y - effects of Cr loading

After the initial synthesis of the Cr-Y zeolites; Cr-Y-1 to Cr-Y-3 were found to have quite high levels of Cr with a Cr/Al ratio of 1.19 and 0.79 respectively. Therefore a further sample, Cr-Y-4 was prepared and was measured to have a Cr/Al ratio of 0.06 as compared to a ratio of 1.20 for Cr-Y-1 (see EDAX results in chapter 5.2). Therefore Cr-Y-4 has 5% of the Cr loading of Cr-Y-1. If we compare the two we can get an idea of the effects of Cr loading and the effects it has relating to surface topology, pore narrowing and blockage and the catalytic species present as discussed in the literature review. With the high levels of Cr in Cr-Y-1 and Cr-Y-3 there will be a high proportion of Cr_2O_3 on the surface of the zeolite.

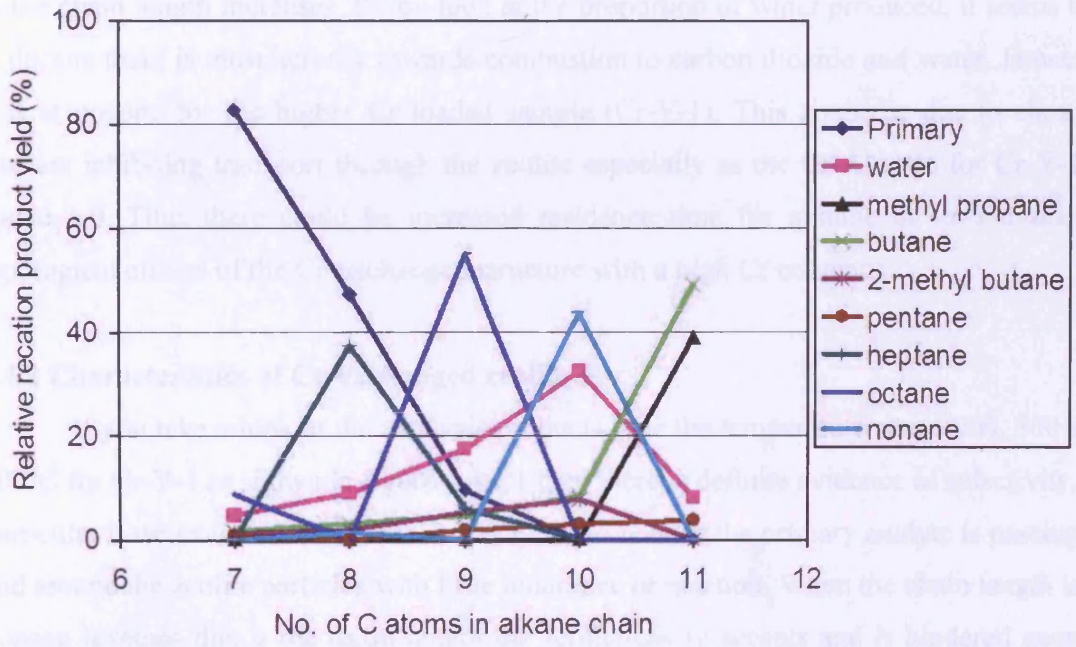

Figure 6.4.1 Catalytic reaction products from a series of linear alkanes through Cr-zeolite Y sample 4 (Cr/Al = 0.06) at 300°C in the GC/MS set-up.

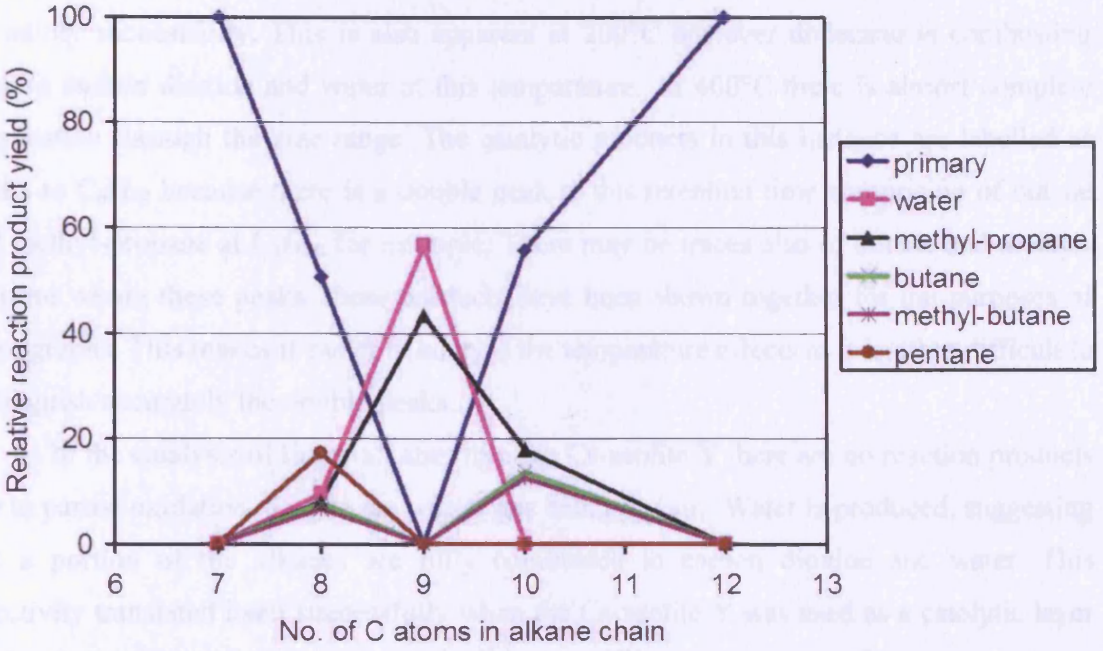

Figure 6.4.2 Catalytic reaction products from a series of linear alkanes through Cr-zeolite Y sample 1 (Cr/Al = 1.2) at 300°C in the GC/MS set-up.

The GC/MS results of the Cr-exchanged zeolite with a low Cr content shown in figure 6.4.1 show the importance of the residence time of the molecule through the zeolite as the chain length increases. If you look at the proportion of water produced, it seems that at decane there is most activity towards combustion to carbon dioxide and water. However it is at nonane for the higher Cr loaded sample (Cr-Y-1). This could be due to chromia clusters inhibiting transport through the zeolite especially as the Cr/Al ratio for Cr-Y-1 is above 1.0. Thus there could be increased residence time for nonane in Cr-Y-1 due to topological effects of the Cr-exchanged structure with a high Cr content.

6.4.2 Characteristics of Cr-exchanged zeolite Y

If you take a look at the catalysis products over the temperature range 200, 300 and 400°C for Cr-Y-1 as shown in figure 6.4.2.1 then there is definite evidence of selectivity. In particular if we examine the results at 300°C, up to nonane the primary analyte is passing in and around the zeolite particles with little hindrance or reaction. When the chain length is at nonane it seems this is the chain length the zeolite cavity accepts and is hindered enough for catalytic cracking to occur. Larger than nonane and the primary analyte is finding an

alternate route through the zeolite as it is in powder form and the molecules are not entering the cavity successfully. This is also apparent at 200°C however dodecane is combusting fully to carbon dioxide and water at this temperature. At 400°C there is almost complete combustion through the size range. The catalytic products in this instance are labelled as C_4H_{10} to C_6H_{14} because there is a double peak at this retention time comprising of butane and methyl-propane at C_4H_{10} for example. There may be traces also of butene and methyl-propene within these peaks, these products have been shown together for the purposes of these graphs. This makes it easier to analyse the temperature effects as it is often difficult to distinguish accurately the double peaks.

In the catalysis of linear alkanes through Cr-zeolite Y there are no reaction products due to partial oxidation, despite the carrier gas being dry air. Water is produced, suggesting that a portion of the alkanes are fully combusted to carbon dioxide and water. This selectivity translated itself successfully when the Cr-zeolite Y was used as a catalytic layer on the sensor within the electronic nose in chapter 7.4.

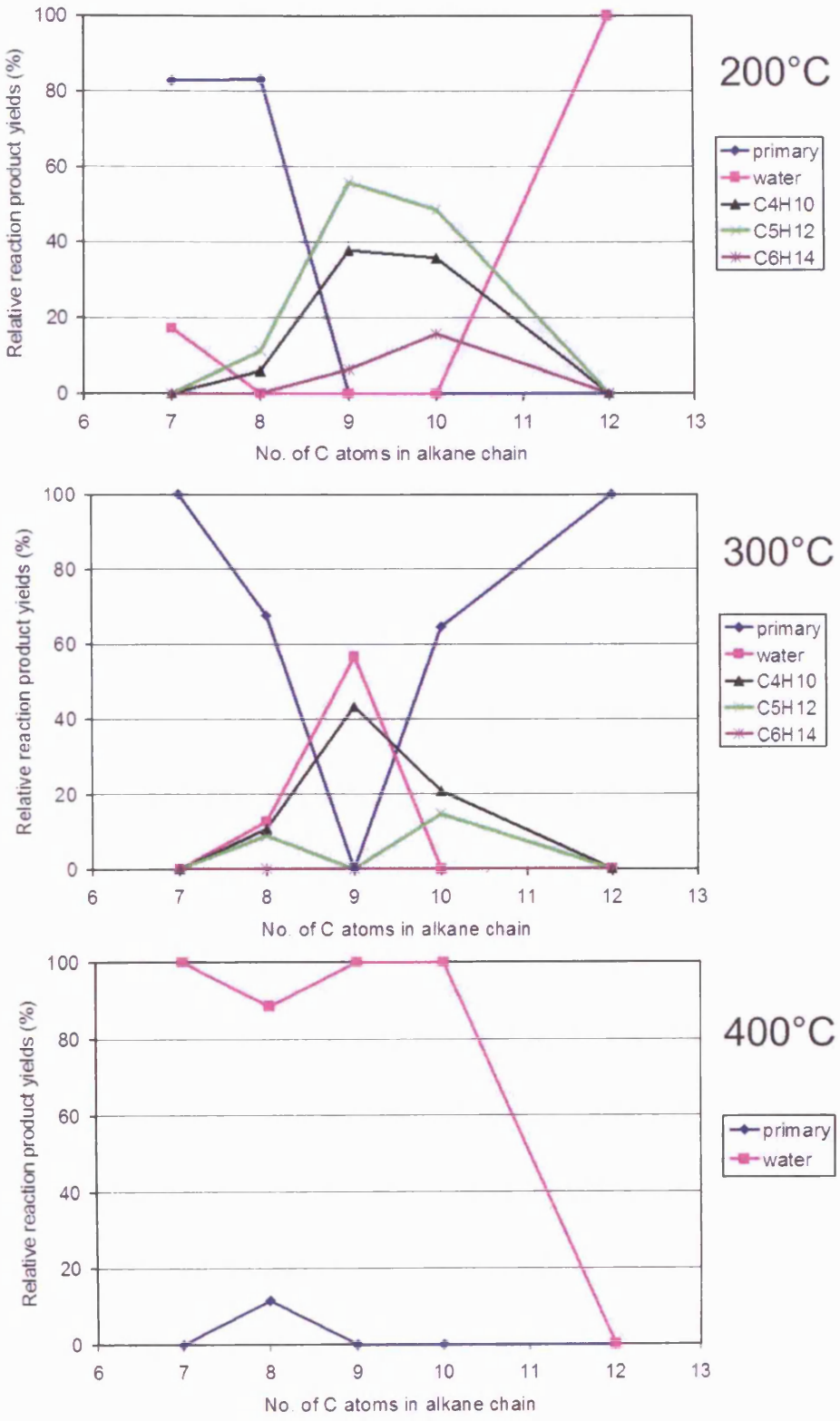

Figure 6.4.2.1 Catalytic reaction products from a series of linear alkanes through Cr-zeolite Y sample 1 (Cr/Al = 1.19) at various temperatures in the GC/MS set-up.

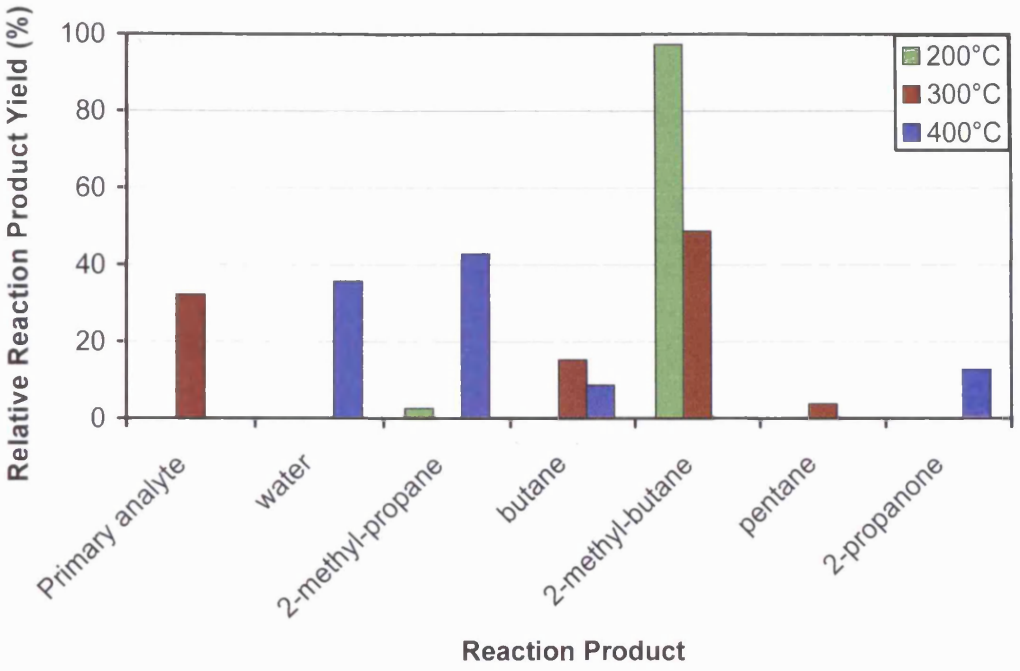

Figure 6.4.2.2 Catalytic reaction products from nonane passed through Cr-zeolite Y sample 3 (Cr/Al = 0.79) in the GC/MS apparatus at the temperatures indicated in the legend.

Figure 6.4.2.2 displays the reaction products of nonane passed through Cr-zeolite Y sample 3 at 200°C, 300°C and 400°C. At 400°C the increase in catalytic activity is evident with the production of 2-propanone and water suggesting further combustion than at the lower temperatures. There is also a high proportion of 2-methyl-propane at 400°C whilst at 200°C and 300°C a large proportion of 2-methyl-butane predominates.

6.4.3 Characteristics of Cr-exchanged zeolite β

Upon testing samples of Cr-zeolite β, it was found that depending on the temperature the reaction products were either the unreacted primary analyte or water indicating full combustion. This was true for all analytes tested. There could be a small temperature range where we might see any cracking and/or partial oxidation of the analyte. However in this instance this could not be established. The form of the Cr complexes within this zeolite structure could be different from that of the Cr exchanged zeolites Y and ZSM-5. After the ion exchange the Cr-zeolite β samples had a yellow colour whereas the Cr-zeolite Y and ZSM-5 samples were a pale green. Cr-zeolite beta sample 1 had x-ray diffraction performed on it to establish the presence of Cr (VI) complexes or CrO_3 to

account for the increased catalytic activity. The results indicated the presence of Cr (VI) but it was not conclusive.

Figure 6.4.3.1 illustrates the propensity towards full combustion exhibited by Cr-zeolite β sample 1 as the temperature increases.

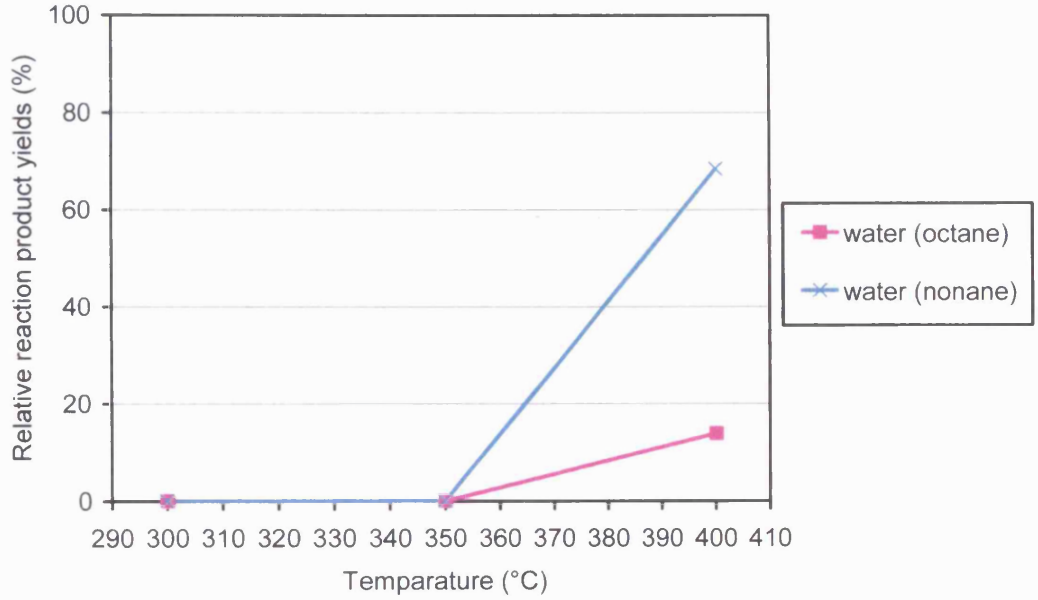

Figure 6.4.3.1 Analysis of reaction products as a function of temperature for Cr-zeolite β sample 1. Shows two analytes, octane and nonane and the subsequent increase in water as a reaction product as the temperature increases.

6.4.4 Characteristics of Cr-exchanged ZSM-5

For the Cr-ZSM5 samples there has been no evidence of cracking activity, but more activity than the standard ZSM5 samples. If we take Cr-ZSM5-5 at 300°C in figure 6.4.4.1 then there is aromatisation at the lower chain lengths but as you get to nonane and decane full combustion of the primary analyte is apparent. Then there is a trend towards further longer chain aromatic production at dodecane.

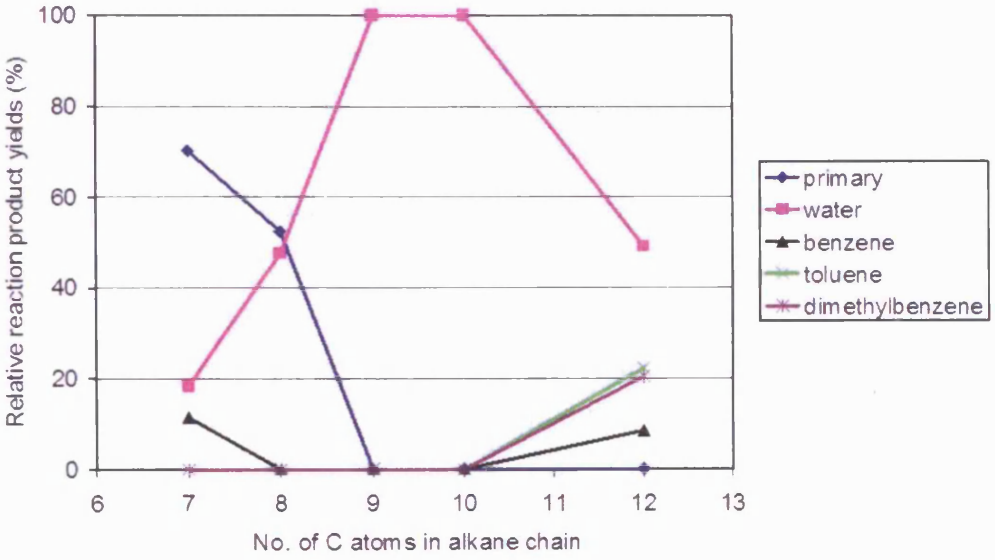

Figure 6.4.4.1 Catalytic reaction products from a series of linear alkanes through Cr-ZSM-5 sample 5 at 300°C in the GC/MS set-up.

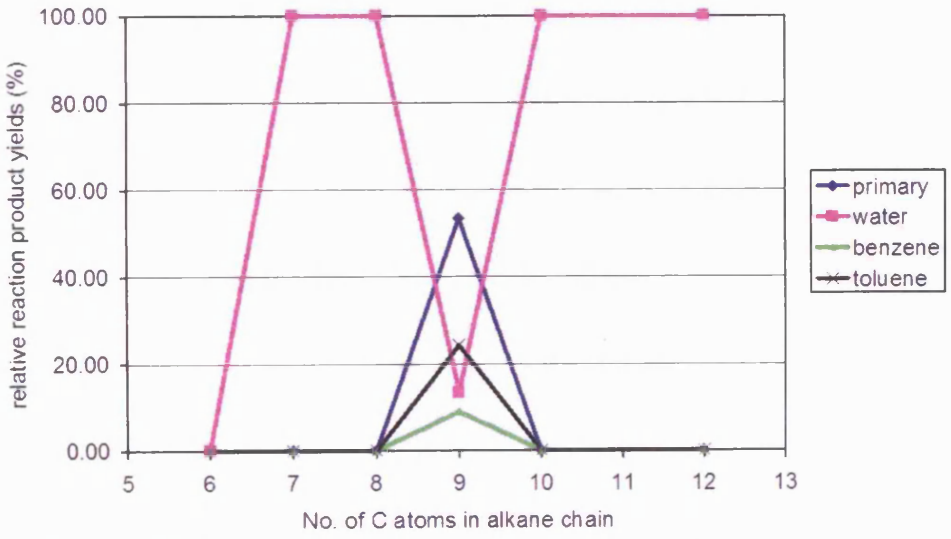

Figure 6.4.4.2 Catalytic reaction products from a series of linear alkanes through Cr-ZSM-5 sample 4 at 400°C in the GC/MS set-up.

Figure 6.4.4.2 shows the reaction products from linear alkanes through Cr-ZSM5 sample 4 at 400°C. There is a large amount of water due to full combustion and there is evidence of selectivity at nonane.

6.4.5 Summary of chromium exchanged zeolites

The catalytic activity shown by the differing zeolite structures after Cr ion exchange depends on a number of factors:

The main factor is the success of the ion exchange – details of transition metal levels are detailed in table 5.2.1, and the morphology of the resulting structure. The ideal is to replace the cations or protons with Cr species evenly throughout the zeolite pores but there has probably been more exchange at the outer surface of the material as opposed to within the zeolite channels. [34] There is also a question as to which sites the Cr species occupy and in which oxidation state.

Another factor is the thermal stability of the material after the ion exchange. The sensors are fired at 600°C for 30 mins to burn off the organic vehicle and partially sinter the sensing material. This may however cause defects in the crystal structure and there may have been expansion of the zeolite pore size due to the temperature. This may also explain why the electronic nose data is slightly different from the GC/MS data as the material has gone through this extra process. However, thermogravimetric analysis showed that the Cr modified zeolites were thermally stable up to 600°C.

6.5 Molybdenum exchanged zeolites

With the molybdenum exchanged zeolites, two different types of ion exchange were performed on the zeolites and subsequently what is shown in this chapter is the differing reaction products associated with the two types of exchange. Also what is observed is the differing catalytic properties associated with the varying levels of Mo introduced as observed for the Cr-zeolites.

6.5.1 Mo-zeolite Y – effects of Mo loading

The first sample to be tested was the Mo-zeolite Y sample 3 to linear alkanes and flavour compounds over temperatures of 300°C, 350°C and 400°C.

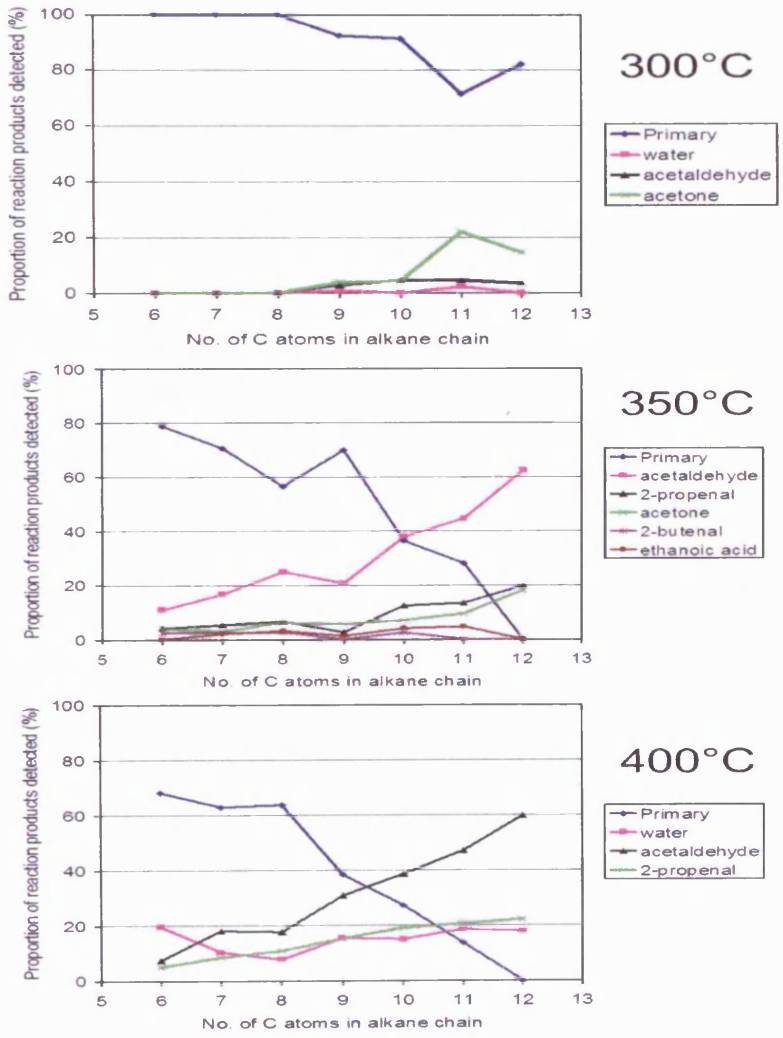

Figure 6.5.1.1 Catalytic reaction products from a series of linear alkanes through Mo-zeolite Y sample 3 (Mo/Al = 0.83) at various temperatures in the zeolite bed/GC/MS apparatus.

Mo-zeolite Y sample 1 (Mo/Al ~ 0.2) was also tested to the range of alkanes to see the effects of the Mo loading on the catalytic activity.

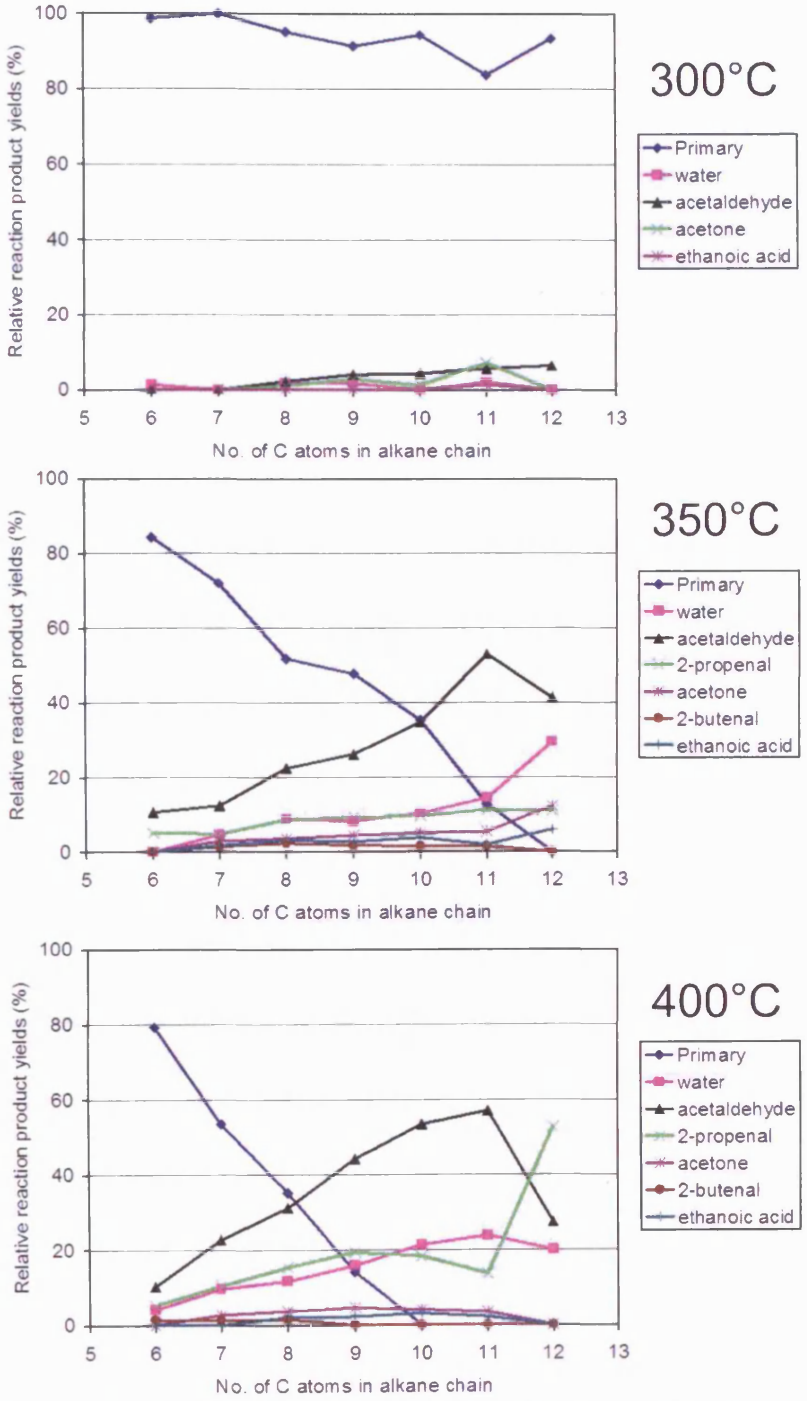

Figure 6.5.1.2 Catalytic reaction products from a series of linear alkanes through Mo-zeolite Y sample 1 (Mo/Al = 0.2) at various temperatures in the GC/MS apparatus.

Of the two solid state exchange Mo-zeolite Y samples tested (Mo-Y-1 and Mo-Y-3), Mo-Y-1 with a lower Mo ratio showed no significant loss in activity however there is a noticeable change in activity after undecane at 350°C and 400°C. There is significant difference in reaction products from the Cr-zeolites. Thus Mo-Y-3 was subsequently integrated into a sensor as a filter layer.

Figure 6.5.1.1 describes the catalytic activity of Mo-Y-3 at 300, 350 and 400°C. In general the reaction products are water, small aldehydes and ketones and a trace of ethanoic acid at 350°C. The presence of water indicates full combustion of the analyte to carbon dioxide and water (CO_2 cannot be detected using this apparatus). The proportion of products seems to change linearly across the molecular chain length range although there is some deviation at each temperature. Namely at chain lengths of C11, C9 and C8 in the series at the temperatures of 300, 350 and 400°C respectively.

Figure 6.5.1.2 describes the catalytic activity of Mo-Y-1 at 300, 350 and 400°C under the same conditions as Mo-Y-3. Again there is a similar range of reaction products. There is ethanoic acid present at all three temperatures. Deviations across the chain length range are less apparent but are occurring at C11 for 300°C, 350°C and C12 for 400°C.

With regards to these solid state exchange (SSE) samples, Mo-Y-3 and Mo-Y-1, figures 6.5.1.1 and 6.5.1.2 respectively there does not seem to be a great difference between the two samples with regards to catalytic activity. For example at 400°C the amount of water detected across the alkane series for Mo-Y-1 is comparable to that of Mo-Y-3 whereas Mo-Y-1 has approximately 20% of the Mo content of Mo-Y-3 suggesting that the level of Mo has already reached excess in sample Mo-Y-1. The sample has a Mo/Al ratio of 0.2 however due to the method of exchange (SSE) there will be a predominance of MoO_3 clusters present as well as the intended exchange of MoO_x crystallites with the protons of the zeolite. Mo-Y-3 in situ on a sensor has been observed under SEM, figures 5.3.5 and 5.3.6, and there seems to be clusters of MoO_3 on the surface of the zeolite particles. There was also clear evidence of large distinct particles of MoO_3 still present. The powders of Mo-Y-1 and Mo-Y-3 were also observed in the SEM during the EDAX analysis and both were showing clusters on the surface of the zeolite particles with high levels of Mo indicating MoO_3.

If you take a look at the reaction products of Mo-Y-3 at 350°C in figure 6.5.1.1 it is observed that primarily the reaction products are aldehydes and ketones with acetaldehyde

(CH_3CHO) being predominant and there is a general increase in products, when you increase the chain length there is a decrease in the amount of the original analyte (primary). This is indicating that cracking and partial oxidation of the analyte is occurring - cracking occurring at the still existing acidic sites on the zeolite, and partial oxidation by the supported Mo clusters and MoO_3. At 350°C there is also a slight deviation from the linear behaviour of the magnitude of reaction products at nonane. This could be an indication of the zeolites selectivity at this chain length as observed with the Cr-zeolites. At 400°C the increase in catalytic activity at this temperature can clearly be seen as the only reaction products are water (indicating full combustion), acetaldehyde and propenal.

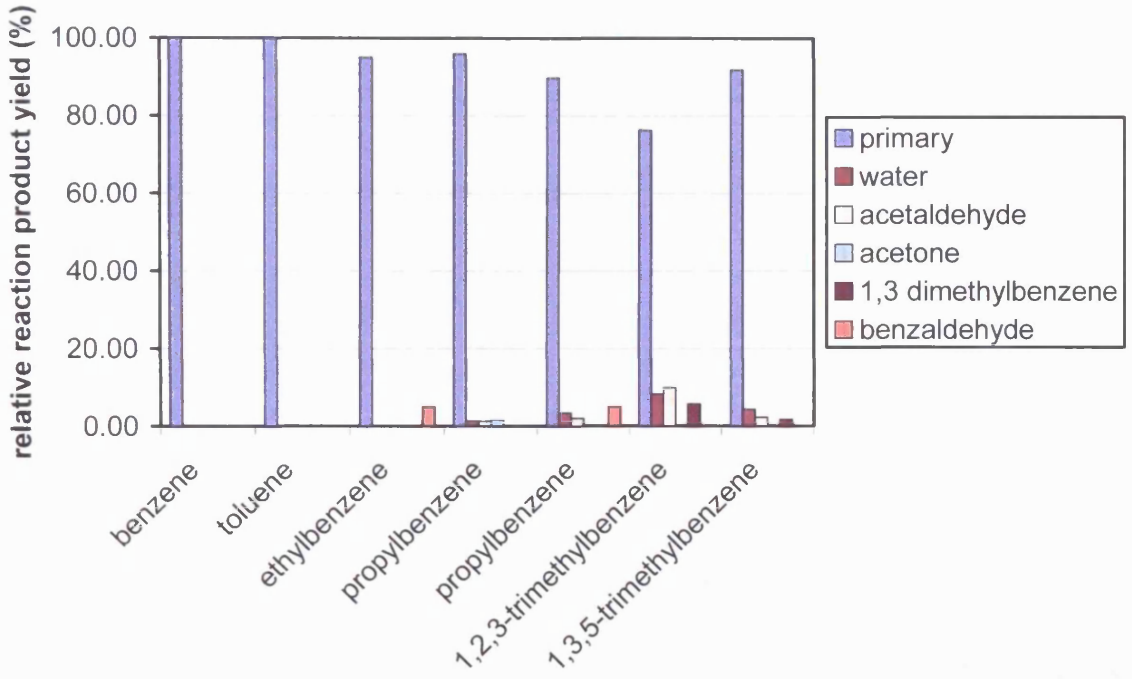

Figure 6.5.1.3 Catalytic reaction products from a series of aromatic compounds through Mo-zeolite Y sample 3 (Mo/Al = 0.83) at various temperatures in the GC/MS apparatus.

From the series of aromatics shown in figure 6.5.1.3 benzene and toluene pass through the Mo-zeolite Y unreacted. For the other compounds there are small amounts of aldehydes and ketones being detected such as acetaldehyde and benzaldehyde. These partially oxidised reaction products correlate with the findings from the alkane series as shown in figures 6.5.1.1 and 6.5.1.2 for the Mo-zeolite Y samples that have been solid state ion exchanged. For the two trimethylbenzene samples there are also traces of

dimethylbenzene suggesting methyl group removal which has subsequently been involved in secondary reactions to produce further reaction products.

6.5.2 Mo-zeolites – effects of ion exchange method

Figure 6.5.2.1 describes the catalytic activity of Mo-zeolite Y sample 5 (Mo-Y-5) at 350°C. Mo-Y-5 was prepared by the aqueous ion exchange method (AQ). In this instance the reaction products are linear and branched alkanes of a smaller size than the original analyte.

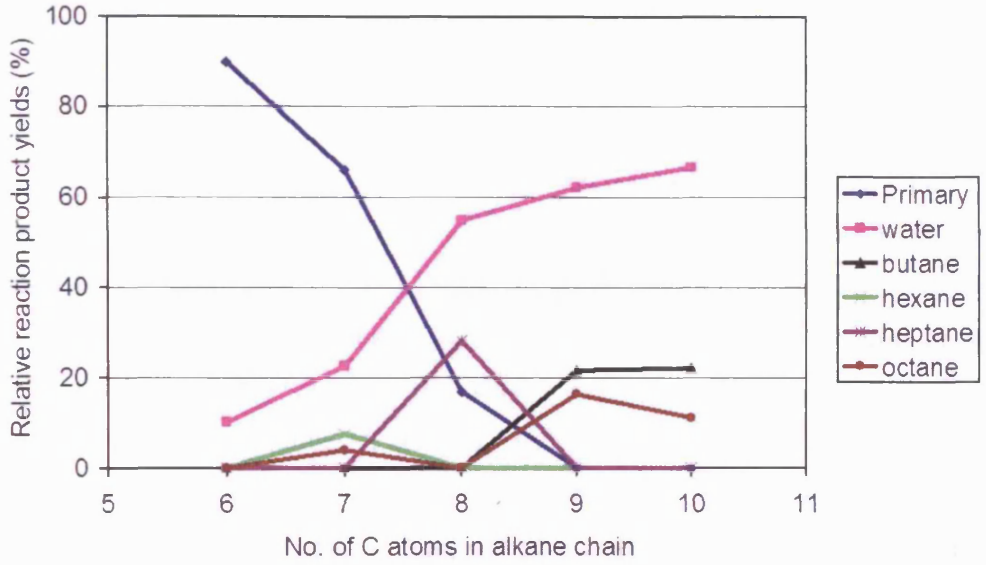

Figure 6.5.2.1 Catalytic reaction products from a series of linear alkanes through Mo-zeolite Y sample 5 at 350°C in the zeolite bed/GC/MS apparatus.

In the comparison between the SSE samples Mo-Y-3 and Mo-Y-1 at 350°C there is a distinct difference in reaction products. We are seeing the cracking of the linear alkanes to shorter chain lengths akin to the Cr-zeolites which also underwent an aqueous exchange, but there are no branched alkanes unless we increase the flow rate as outlined in chapter 6.2. For Mo-Y-5 there is a general increase in activity down the linear alkane series as there is an increase in water production. The other reaction products are linear alkanes indicating a general cracking of species and reduction in chain length; hence butane gets quite predominant at C9 and C10. We know that the Mo loading of this zeolite after ion exchange is not very high which indicates that most of this activity observed is probably

due to the proton sites of the zeolites. There does not appear to be much indication of selectivity although at octane there is a variation in the trend of reaction products.

6.5.3 Mo-zeolites – Comparison with Cr-zeolites

A comparison can be made between Cr-zeolite Y sample 4 and Mo-zeolite Y sample 5. Both these materials are aqueous exchanged zeolite Y's with similar transition metal loadings thus we can compare the effects due to the transition metal exchanged, Cr-Y-4 has a Cr/Al loading of 0.06 and Mo-Y-5 has a Mo/Al loading of 0.07. The success of the exchange will also have an effect as to the extent of the catalysis. During the aqueous exchange the size of the aqueous complex will determine how much exchange has occurred within the zeolite pores, as the Mo complex is larger than the Cr complex it could be expected that more exchange may have occurred within the zeolite pores for the Cr-exchanged sample.

In figure 6.5.3.1 a larger proportion of water was detected from the Cr-zeolite Y sample in contrast to the Mo-zeolite Y sample indicating more full combustion of the alkanes. There is catalysis occurring on the Mo-zeolite Y sample to smaller alkanes such as butane and hexane. On both samples there is evidence of chain length reduction and chain length addition, therefore showing the activity of the metal complexes to the terminal methyl group. For the Cr-zeolite Y there is production of nonane from hexane, heptane and octane showing the selectivity towards nonane to this zeolite type. The amount of the primary analyte reduces towards nonane whilst the amount of water detected increases as the residence time increases within this material as the chain length increases.

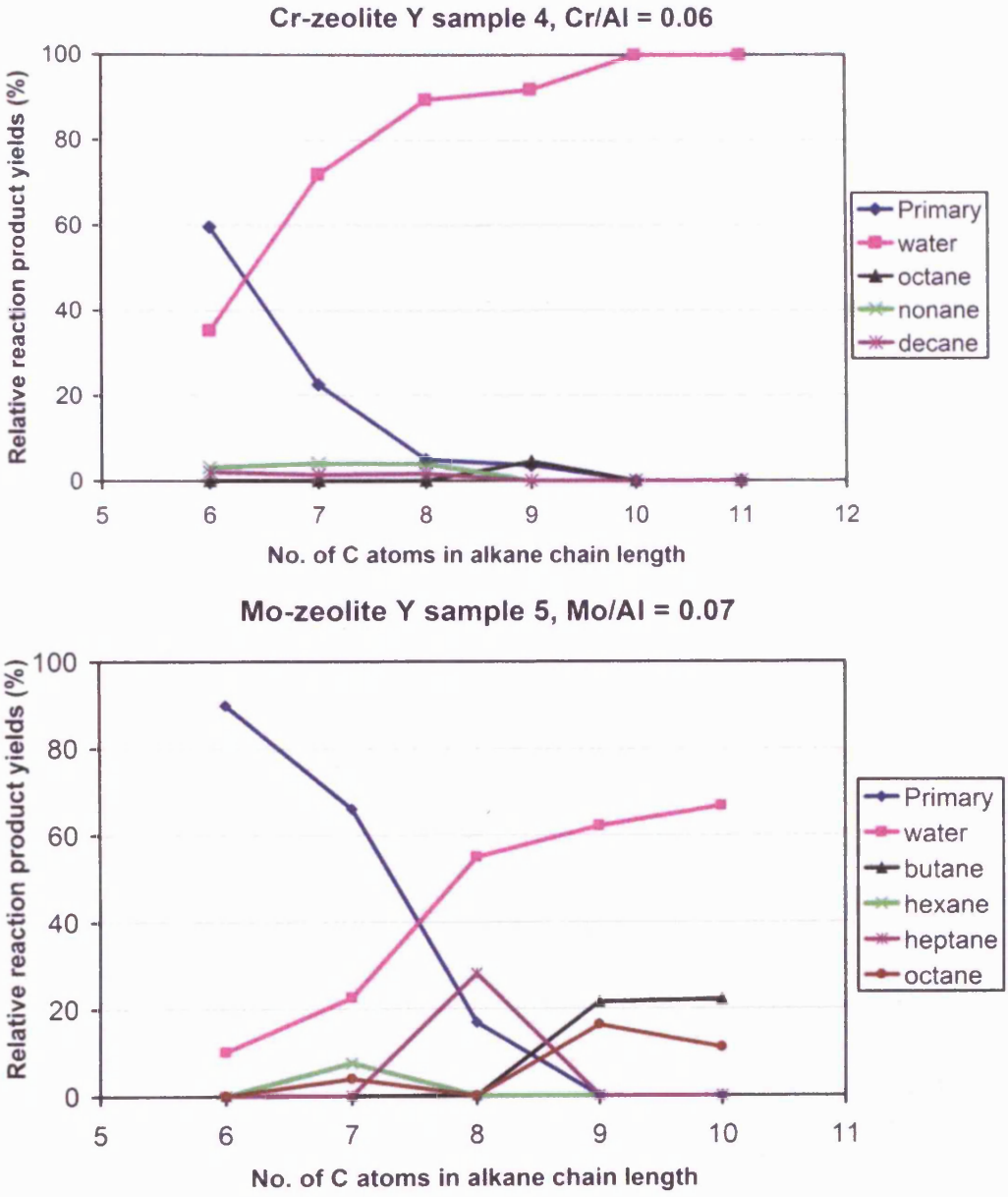

Figure 6.5.3.1 Cr-zeolite Y sample 4 and Mo-zeolite Y sample 5 tested in the GC/MS apparatus at 350°C. Series of alkanes in increasing chain length tested through both samples.

6.6 Tungsten exchanged zeolites

GC/MS results for W-zeolite Y:

W-zeolite Y sample 1 (W-Y-1) was initially tested to a series of linear alkanes at 300°C and 350°C to establish some initial characteristics of this materials catalytic activity. The W/Al ratio for W-Y-1 was determined to be 0.12 by EDAX.

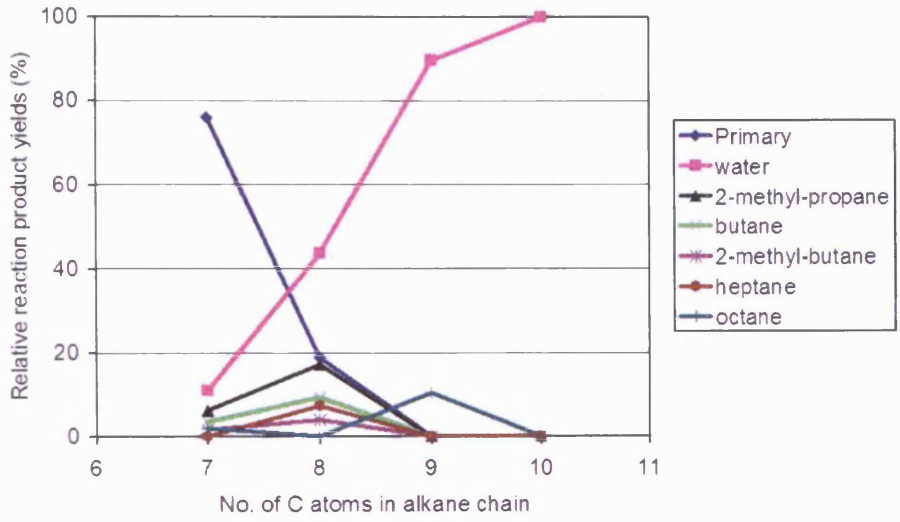

Figure 6.6.1 Catalytic reaction products from a series of linear alkanes through W-zeolite Y sample 1 (W/Al = 0.12) at 300°C in the zeolite bed/GC/MS apparatus.

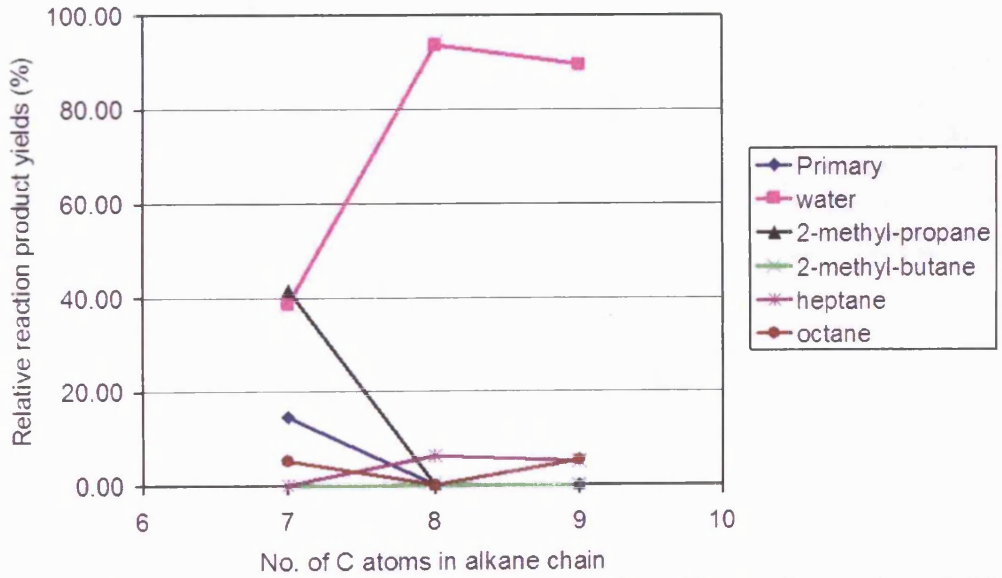

Figure 6.6.2 Catalytic reaction products from a series of linear alkanes through W-zeolite Y sample 1 (W/Al = 0.12) at 350°C in the zeolite bed/GC/MS apparatus.

This is a relatively low loading of W compared to previous tests using Cr and Mo yet we have some significant catalytic activity. We can see an interesting effect illustrated in figure 6.6.2. At 350°C heptane is producing a significant amount of 2-methyl-propane suggesting cracking and skeletal isomerisation. When W-Y-1 is at 300°C, figure 6.6.1, using the same conditions as set for 350°C the production of 2-methyl-propane is more apparent at octane. These reactions are taking place under the constraints imposed by the size of the channels. As a result, unique products are formed as a function of reaction temperature and residence time in the zeolite bed.

If we increase the loading of the W in the zeolite we can observe a change in catalytic activity as observed in figure 6.6.3. The loading of W-Y-2 is only slightly higher than W-Y-1 however the main reaction product is now 2-methyl-butane and there seems to be a greater variety of cracked products as compared to the lower loading as shown in figure 6.6.1. There is little water evident in the cracked products of W-Y-2 suggesting a lower propensity for full combustion to carbon dioxide and water compared to sample W-Y-1.

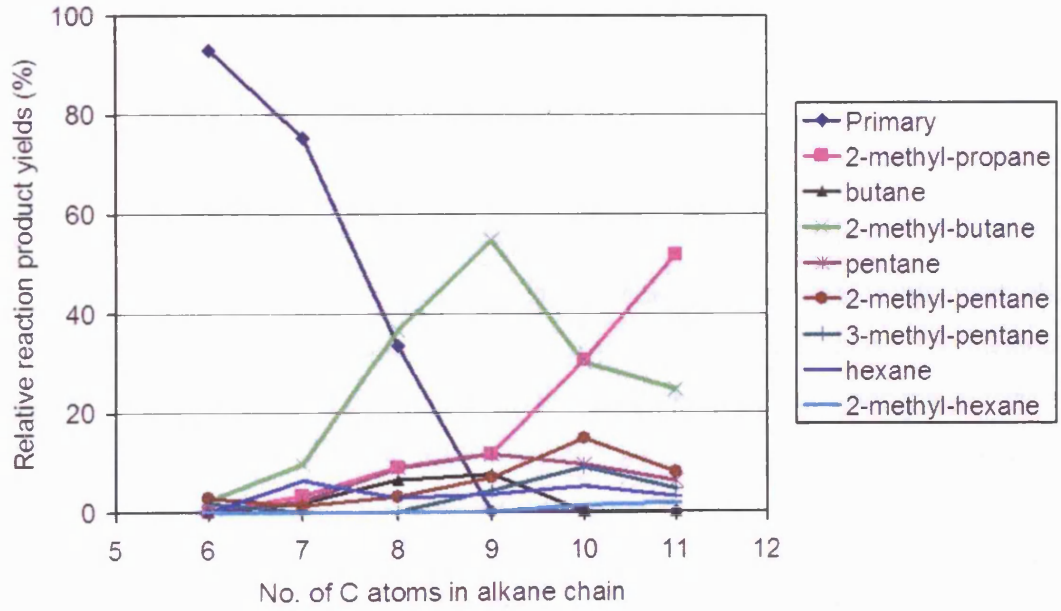

Figure 6.6.3 Catalytic reaction products from a series of linear alkanes through W-zeolite Y sample 2 (W/Al = 0.14) at 300°C in the GC/MS set-up.

6.7 CTO and Cr_2O_3

Powders of CTO and Cr_2O_3 were also put in the material bed and tested in the GC/MS set-up. All tests were performed at 400°C. There was no real pattern of activity for either material and hence no graphical representation is displayed in this section.

However for the CTO there was a large amount of primary analyte that was detected. It could be possible that due to the particle size of the CTO in the material bed a large proportion of analyte was managing to pass over the particles with no interaction with the surface. Volatile analytes such as heptane and 2-methyl-hexane had traces of propanone and propenal in the reaction products indicating reaction to smaller aldehydes and ketones. This would indicate that in the context of the material being fabricated into a gas sensor we can now ascertain that the linear alkanes are most probably catalysed on the surface of the CTO to smaller aldehydes and ketones which subsequently are responsible for further reactions on the surface of the CTO and causing the response.

The Cr_2O_3 which is used as a filter layer on CTO sensors towards volatile organic compounds also had a large proportion of the primary analyte being detected along with a large proportion of water as would be expected indicating combustion to carbon dioxide and water. For some of the smaller alkanes tested such as pentane, hexane, heptane as well as benzene, there were some small alkanes present along with traces of small ketones in the reaction products.

6.8 Summary of catalytic property testing

Despite the complexity of the experimental set-up, consistent results were obtained that exhibited the catalytic characteristics of each zeolite material tested. The methodology produced a clear idea of the characteristics that might be expected when the materials were subsequently integrated into the fabrication of a gas sensor, and could also be utilised to confirm findings in the subsequent sensor testing in the injection rig.

The effects of transition metal loading were established on zeolite Y. Characteristics of materials type were established for the Cr-zeolites and the methods of introducing the transition metals was assessed by the Mo-zeolites.

The differing methods of introducing Mo into the zeolite structure were by aqueous exchange and solid state exchange. For all the solid state exchange samples the reaction

products were aldehydes, ketones and ethanoic acid from linear alkanes. Whilst for the aqueous exchange samples the reaction products are cracked linear alkanes, which is the same for the Cr and W exchanged zeolites.

7. Sensor Testing and Array Development in Injection Rig

7.1 Introduction

The zeolite materials assessed using the techniques described in chapters 5 and 6 were fabricated as integrated filter layers into a variety of gas sensors as described in chapter 4. All sensor details are listed in Appendix 2. Initially using the injection rig, arrays of CTO sensors were used in conjunction with a heated zeolite bed that was identical to the one used in the GC/MS apparatus (see figure 7.3.1). This was to try and evaluate sensor responses as compared to the results described in chapter 6. Also the zeolite bed was used for a comparison with powdered samples of Cr_2O_3 and Cr-zeolites as shown in section 7.2 to establish the sieving effect of the Cr-zeolites.

After these initial tests, sensors were fabricated with the metal exchanged zeolites integrated as a layer on the sensor. Sensor arrays consisting of 3 sensors were tested which typically consisted of a control sensor, a sensor with 50 μm of zeolite material and a sensor with 100 μm of the same zeolite material. Therefore by normalising sensor response to the control sensor (see section 7.3) the effect of the zeolite filter layer on the sensor can be isolated and the deviation from the standard attributed to the effect of the zeolite can be visually seen.

To instil a sense of continuity and improvement on the methods of data analysis used in the commercial electronic nose the normalised data from the sensor array in the injection rig was also utilised in a statistical software package (SPSS 12.0). This was performed in order to understand the generics of the statistical discrimination embedded in the software utilised by the electronic nose. It also enables a different approach to be taken in terms of how we interpret and understand discrimination in terms of the function of an individual sensor response within an array.

To understand what is being achieved by placing the zeolite layer on the CTO sensor then there must be an understanding of the CTO sensing mechanism itself with regards to the original analyte and any reaction products that will be formed due to the catalytic nature of the zeolites. The sensor behaviour itself can initially be understood by realising the relative sensitivity of the sensor material to different classes of compound. In

general, the sensitivity to a particular gas is greater the higher the reactivity of the gas with oxygen. Thus, the order of sensitivity for different classes of compound is usually alcohols, ketones > aromatics > aliphatics. Thus if an aliphatic compound is cracked on the zeolite layer to give an aromatic, the sensor signal will be increased. The sensitivity is also a function of the aliphatic chain length. Figures 7.1.1 to 7.1.3 show the transient responses of CTO to three groups of compounds; alcohols, aromatics and alkanes.

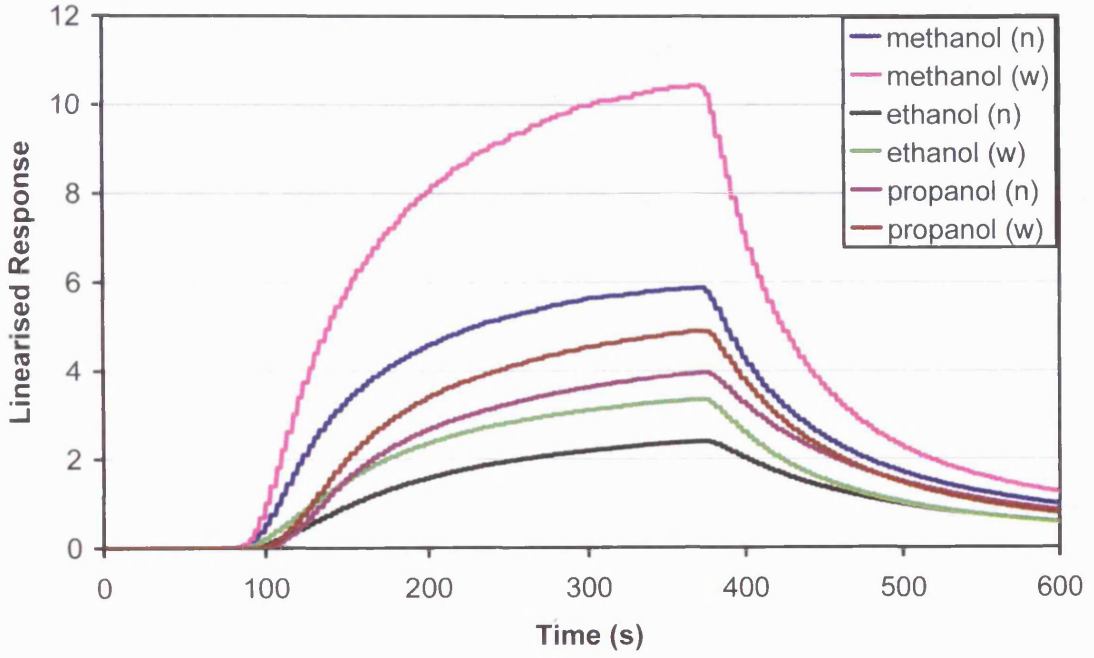

Figure 7.1.1 Linearised CTO response to alcohols. Sensor operating at 400°C. 300 s injection of analyte. (n) – narrow electrode gap, (w) – wide electrode gap

The CTO sensors have an order of sensitivity of methanol > propanol > ethanol. Propanol will be getting partially combusted on the surface thus providing further reaction products the CTO is sensitive to. This will be significant as to the reaction products produced from the zeolite layer as to any further reaction on the surface of the CTO.

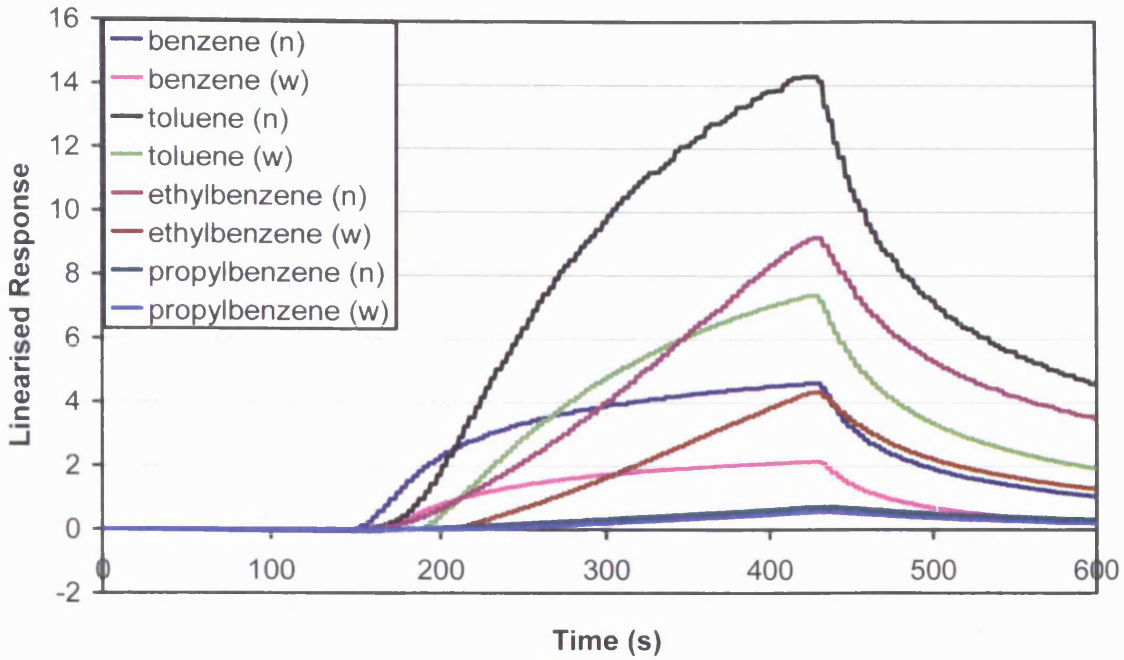

Figure 7.1.2 Linearised CTO response to aromatic series. Sensor operating at 400°C. 300 s injection of analyte.

For the aromatic series, there is some transient shape differences evident and the sensitivity scale is toluene > ethylbenzene > benzene > propylbenzene. The transient shape change is progressive through the series of the aromatics as the response curve tends towards the x-axis.

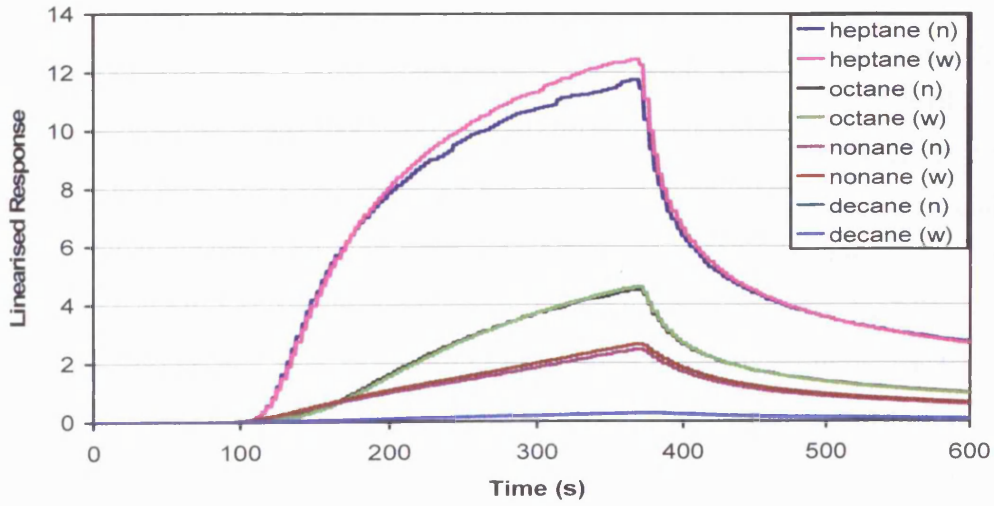

Figure 7.1.3 Linearised CTO response to alkane series. Sensor operating at 400°C. 300 s injection of analyte.

The CTO response to the alkane series is shown in figure 7.1.3 and the sensitivity decreases as the chain length increases, heptane > octane > nonane > decane.

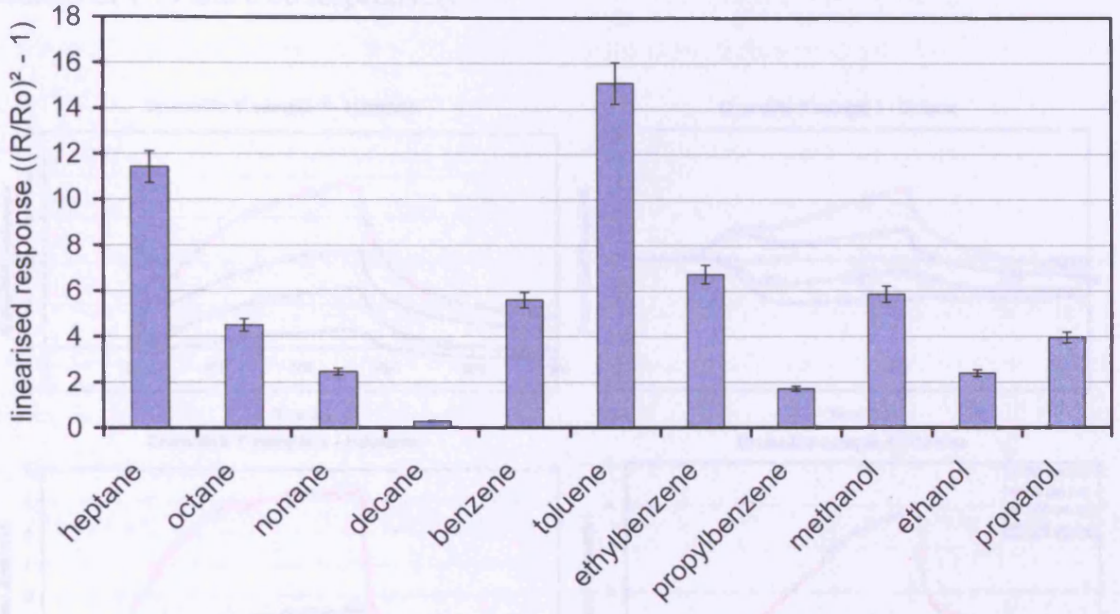

Figure 7.1.4 Comparison of maximum response using standard CTO sensor after 300 seconds injection in the injection rig.

With the effect of introducing a catalytic layer onto the sensor, then there has to be an understanding of the behaviour of this layer if you are to gain anything from the response measured from the underlying CTO sensing material. For the zeolite layer there are two time scales for diffusion both of which are similar to the experiment time scale, therefore transients associated with non-steady state concentration profiles are observed on the experimental time scale. The two sensor time scales are the time scale for diffusion through the porous layers, and the time scale for diffusion of the gas if it is slowed by exchange into the zeolite pores. Second, if reaction products are formed within the zeolite pores, then there will be a delay before these are seen by the sensor material. If the products are aromatics or partially oxidised compounds, then there could be a significant response associated with their presence. If reaction products are formed on oxide particles outside the zeolite pores, then the delay before the effect of the products on the sensor response is

seen will be shorter. Therefore for most results displayed in this chapter the sensor response has been normalised to a control sensor. Therefore these diffusion/reaction effects can clearly be observed along a transient (see chapter 7.3). This can easily be seen if two contrasting loadings of Cr-zeolite Y are compared, Cr-Y-1 and Cr-Y-4 which have Cr/Al loadings of 1.19 and 0.06 respectively.

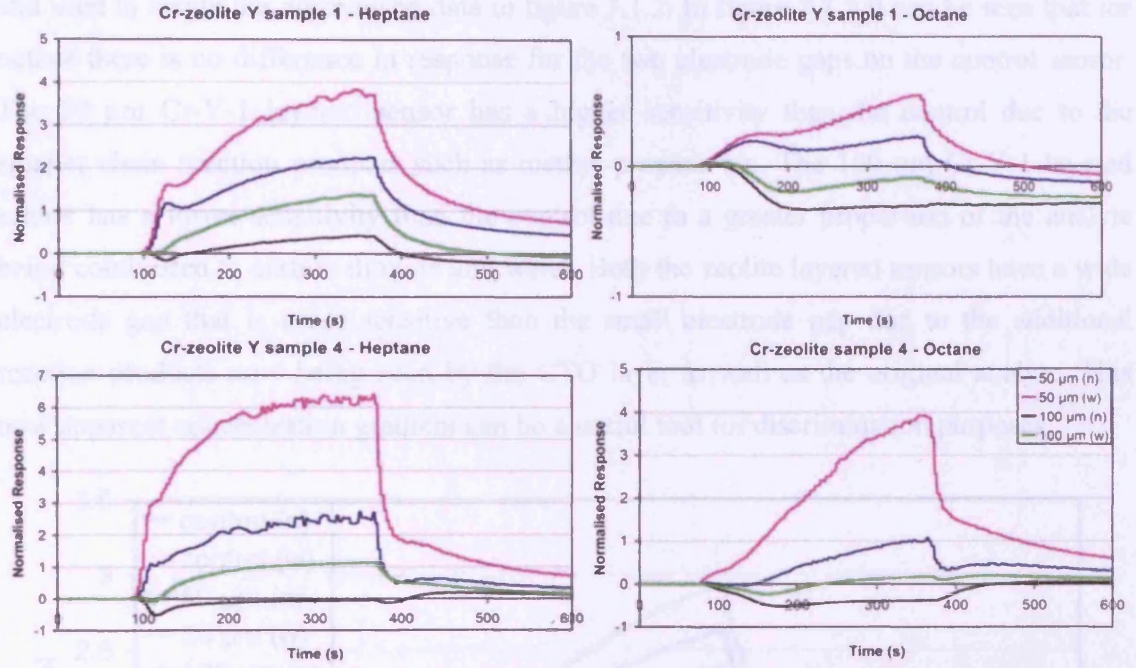

Figure 7.1.5 Comparison of heptane and octane normalised responses for Cr-zeolite Y-1 and Cr-zeolite Y-4 sensor arrays operating at 400°C in the injection rig. 500 s sample injection.

If the injection rig results as shown in figure 7.1.2 are compared with the zeolite bed/GC/MS results it suggests that the Cr-Y-1 layer will have higher cracking activity than the Cr-Y-4 layer due to the Cr loading. If the heptane results are compared; the Cr-Y-4 50 µm layered sensor has a higher normalised response than the Cr-Y-1 50 µm layered sensor due to a greater proportion of cracked hydrocarbons from the original heptane. As the normalised sensor response decreases and some transients have gone below the sensitivity of the control sensor (x-axis) the amount of fully combusted reaction products increases.

In figure 7.1.2 it is clear that there is an obvious variation in transient shape at the start of the transient between 100 and 200 s. The Cr-zeolite Y sample 1 (Cr-Y-1) layered sample has an initial peak for both heptane and octane. If we relate this back to the zeolite

bed-GC/MS data (figures 6.4.1 and 6.4.2) then we can ascertain that the CTO sensing layer is likely to be seeing reaction products such as methyl-propane, butane and methyl-butane. Also full combustion will be occurring so there will be a proportion of carbon dioxide and water which the CTO is insensitive to. This initial peak seen for the Cr-Y-1 layered sensors may be due to surface cracked reaction products that CTO is sensitive to being detected. In the case of octane, figure 7.1.3 shows the sensor responses that were obtained for this test and used to create the normalised data in figure 7.1.2. In figure 7.1.3 it can be seen that for octane there is no difference in response for the two electrode gaps on the control sensor. The 50 µm Cr-Y-1 layered sensor has a higher sensitivity than the control due to the smaller chain reaction products such as methyl-propane etc. The 100 µm Cr-Y-1 layered sensor has a lower sensitivity than the control due to a greater proportion of the analyte being combusted to carbon dioxide and water. Both the zeolite layered sensors have a wide electrode gap that is more sensitive than the small electrode gap due to the additional reaction products now being seen by the CTO layer as well as the original analyte. This now apparent concentration gradient can be a useful tool for discrimination purposes.

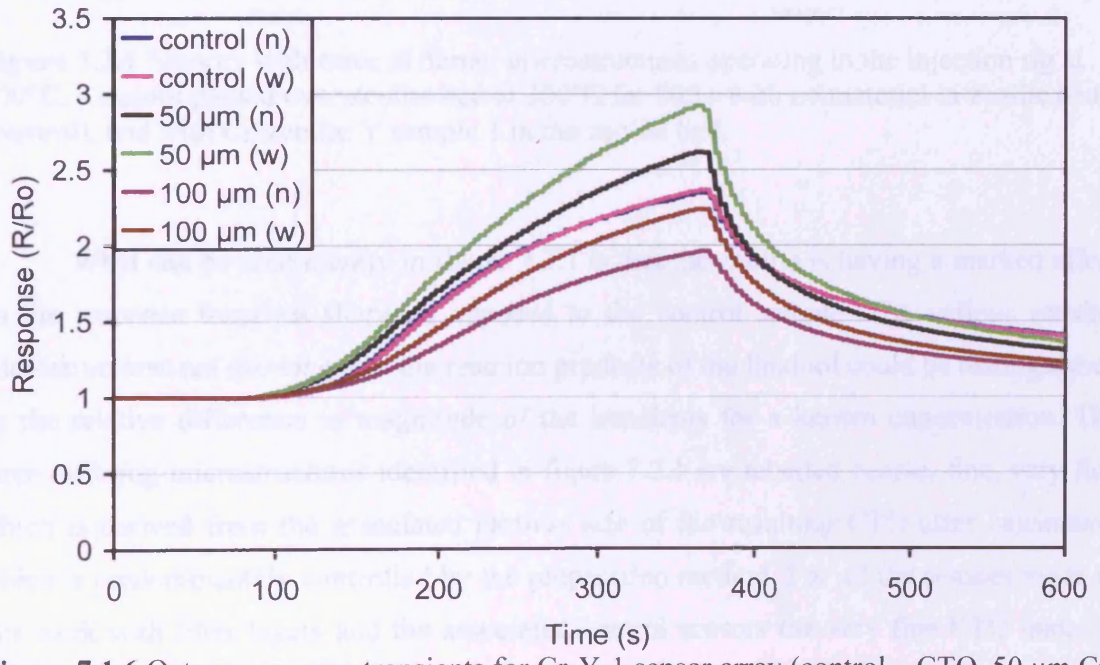

Figure 7.1.6 Octane response transients for Cr-Y-1 sensor array (control – CTO, 50 µm Cr-Y-1 layer on CTO, 100 µm layer on CTO) operating at 400°C.

7.2 Testing with zeolite bed and standard CTO sensors

Initially some testing was done using three sensors with differing CTO microstructures in the sensor chamber and various Cr-exchanged zeolites in powder form as per the GC/MS set-up in the sample chamber to various alkenes and flavour compounds. A good example of the differences seen can be observed below for linalool (3,7-Dimethyl-6-octadien-3-ol) testing by comparing the sensor responses of the control and Cr-zeolite Y sample 1 at 300°C. The transients have been displayed as response (R/Ro) transients as all the sensors are CTO with no catalytic overlayer. Therefore a direct comparison can be made between the response characteristics of the various CTO microstructures.

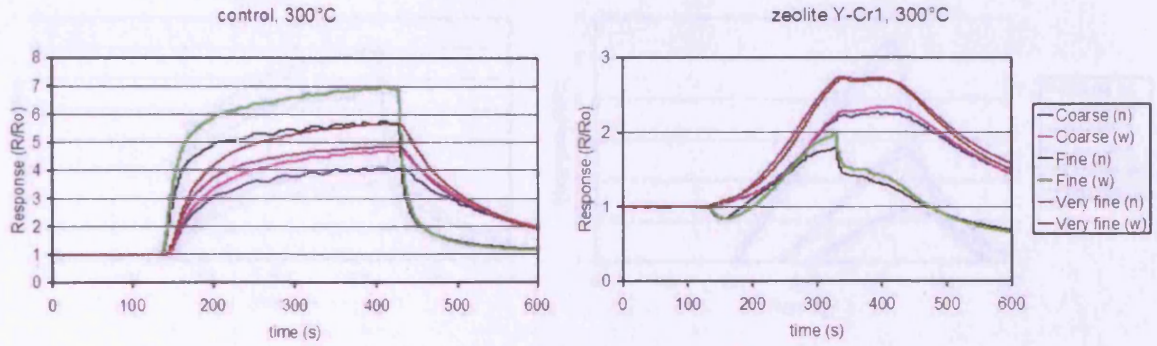

Figure 7.2.1 Sensors with three different microstructures operating in the injection rig at 400°C. Linalool passed over zeolite bed at 300°C for 500 s with no material in zeolite bed (control), and with Cr-zeolite Y sample 1 in the zeolite bed.

What can be seen clearly in figure 7.2.1 is that the zeolite is having a marked effect on the response transient shape as opposed to the control sample. The various sensing microstructures are showing that the reaction products of the linalool could be distinguished by the relative difference in magnitude of the transients for a known concentration. The three differing microstructures identified in figure 7.2.1 are labelled coarse, fine, very fine which is derived from the associated particle size of the resulting CTO after calcination which is predominantely controlled by the preparation method. For all the sensors made in this work with filter layers and the associated control sensors the very fine CTO material was used. Whilst for the control there does not seem to be any correlation between particle size and response it is interesting to note how the difference between the narrow and wide electrode gaps after the analyte has passed over the Cr-zeolite Y. This indicates that there is

no concentration gradient evident through the CTO sensing material for all three microstructures. This is clearly evidence of the catalytic cracking that is occurring on the Cr-zeolite Y material and thus the reaction products are exhibiting fast macroporous diffusion through the CTO and no further reactions are occurring within the CTO layer.

If you look at the response to octane using the same set-up over Cr_2O_3 and Cr-Y-1 both at 200°C the sieving characteristic of the zeolite can clearly be seen in the transient shape. The octane is interacting with the zeolite pore structure thus affecting the transient shape.

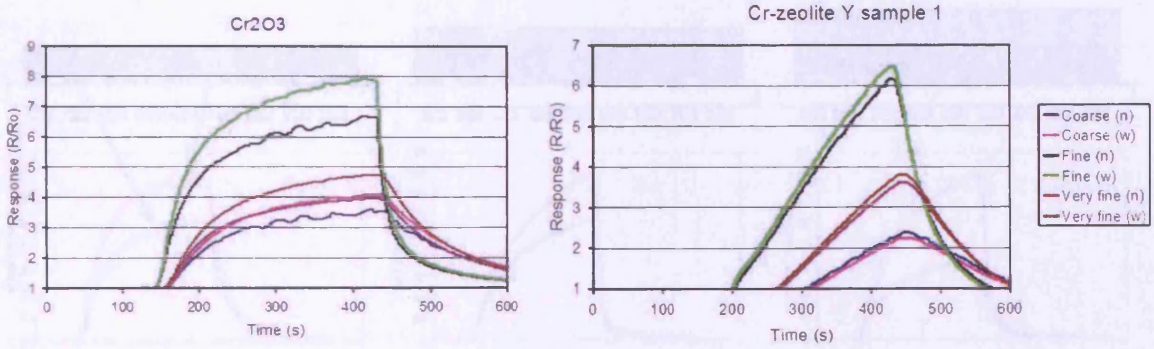

Figure 7.2.2 Sensors with three different microstructures operating in the injection rig at 400°C. Octane passed over zeolite bed at 200°C for 500 s with Cr_2O_3, and with Cr-zeolite Y sample 1 in the zeolite bed.

7.3 Introduction to results interpretation using normalisation method for sensor arrays

With three sensors in the array the sensor responses were obtained using the Pico ADC16 data logger via the in-house constructed potentiostat circuits. The principal is outlined in figure 7.3.1 below and the methodology behind going from the sensor responses (which are illustrated below each sensor) to the normalised transient graph are as follows.

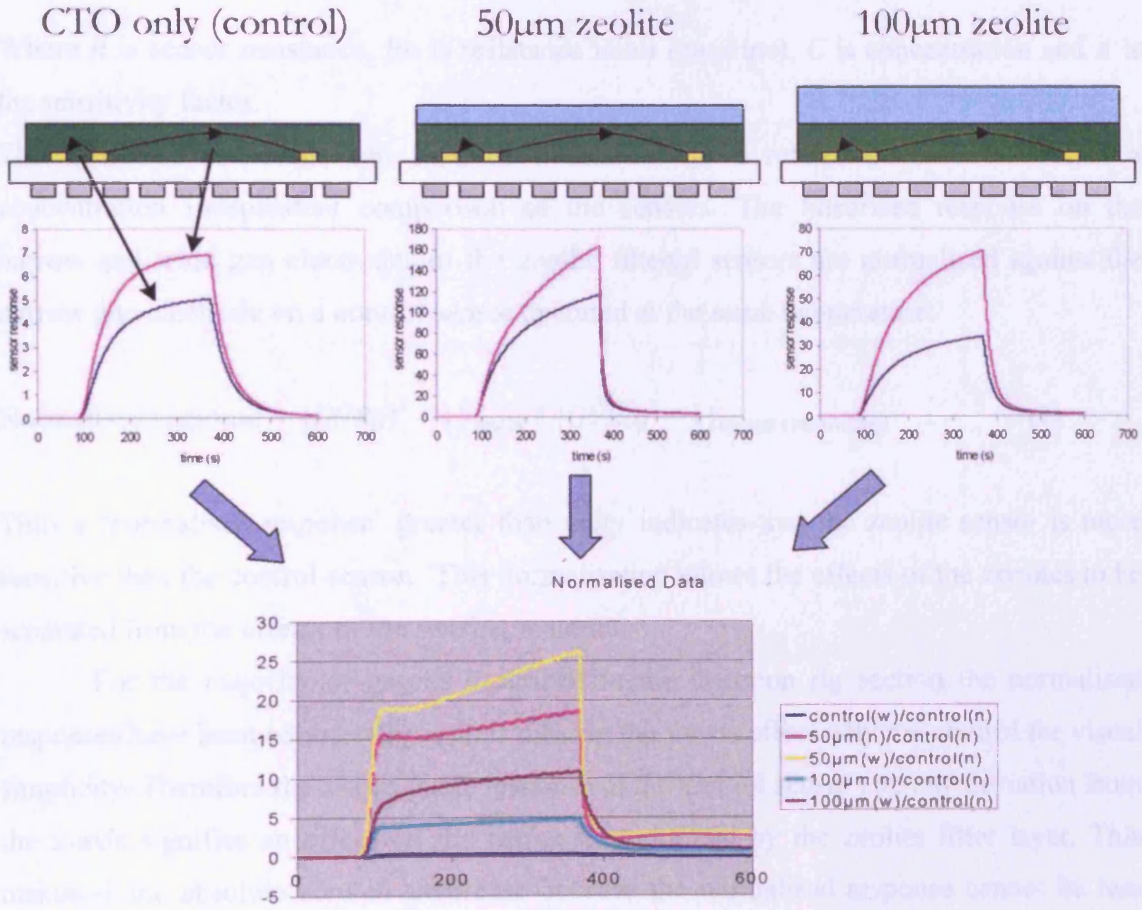

Figure 7.3.1 Diagram representing sensor array and the methodology behind obtaining normalised response graph from a test. Sensor array consists of CTO sensor, CTO with 50 µm zeolite, CTO with 100 µm zeolite. Sensors operating at 400°C responding to methane.

Figure 7.3.2 describes the progression of results analysis that were taken to compare "normalized" sensor transients. The response was first linearised to remove their square root concentration dependence and to obtain transients that were directly proportional to concentration. It has been shown previously that the following equation is a good approximation to the sensor response law, for small responses[75]:

$$(R/Ro)^2 - 1 = AC \qquad (1)$$

Where R is sensor resistance, Ro is resistance in air (baseline), C is concentration and A is the sensitivity factor.

The linearised responses can then be normalized to a reference sensor to obtain a concentration independent comparison of the sensors. The linearised response on the narrow and wide gap electrodes of the zeolite filtered sensors are normalised against the narrow gap electrode on a control sensor operated at the same temperature:

$$\text{Normalised response} = \{(R/Ro)^2 - 1\}_{\text{zeolite}} / \{(R/Ro)^2 - 1\}_{\text{control (narrow gap)}} \qquad (2)$$

Thus a 'normalised response' greater than unity indicates that the zeolite sensor is more sensitive than the control sensor. This normalisation allows the effects of the zeolites to be separated from the effects of the sensing material.

For the majority of graphs described in the injection rig section the normalised responses have been adjusted by -1 thus making the x-axis effectively the control for visual simplicity. Therefore the x-axis is the response of the control sensor and any deviation from the x-axis signifies an effect on the response performed by the zeolite filter layer. This makes -1 the absolute zero in each case because the normalised response cannot be less than -1.

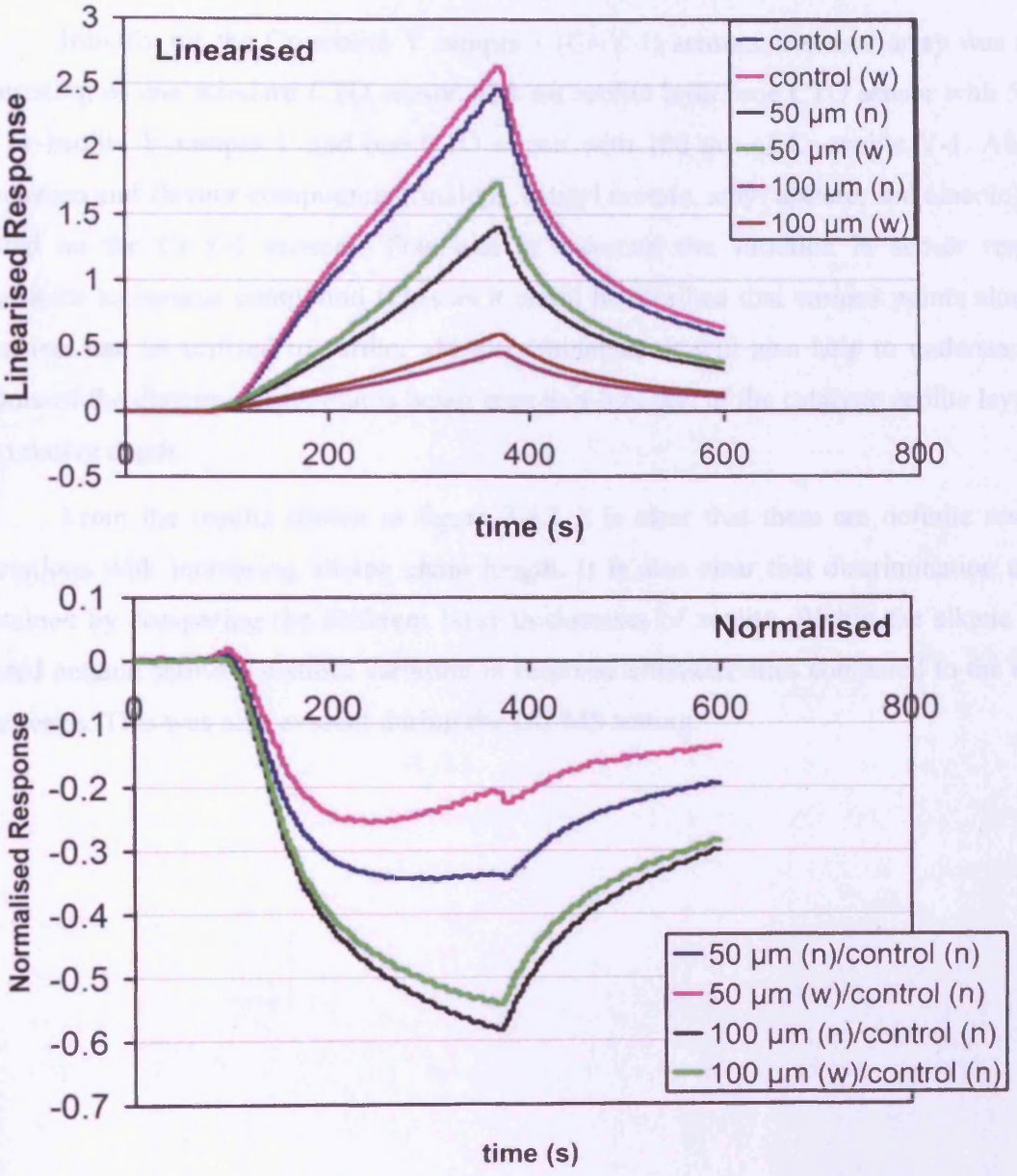

Figure 7.3.2 Injection rig Cr-Y-1 sensor response transients after results processing. Sensors operating at 400°C exposed to nonane for 300s.

7.4 Evaluation of Cr-zeolite Y sensors using injection rig

Initially for the Cr-zeolite Y sample 1 (Cr-Y-1) sensors, a sensor array was tested consisting of one standard CTO sensor with no zeolite layer, one CTO sensor with 50 μm of Cr-zeolite Y sample 1, and one CTO sensor with 100 μm of Cr-zeolite Y-1. Alkanes, aromatics and flavour compounds (linalool, benzyl acetate, amyl acetate, and cineole) were tested on the Cr-Y-1 sensors. This was to ascertain the variation in sensor response transients to various compound types as it could be ascribed that various points along the transient can be utilised to further aid discrimination. It will also help to understand the nature of the discrimination that is being seen as a function of the catalytic zeolite layer and its relative depth.

From the results shown in figure 7.4.1 it is clear that there are definite response variations with increasing alkane chain length. It is also clear that discrimination can be obtained by comparing the different layer thicknesses of zeolite. Within the alkane series tested nonane shows a distinct variation in response characteristics compared to the rest of the series. This was also evident during the GC/MS testing.

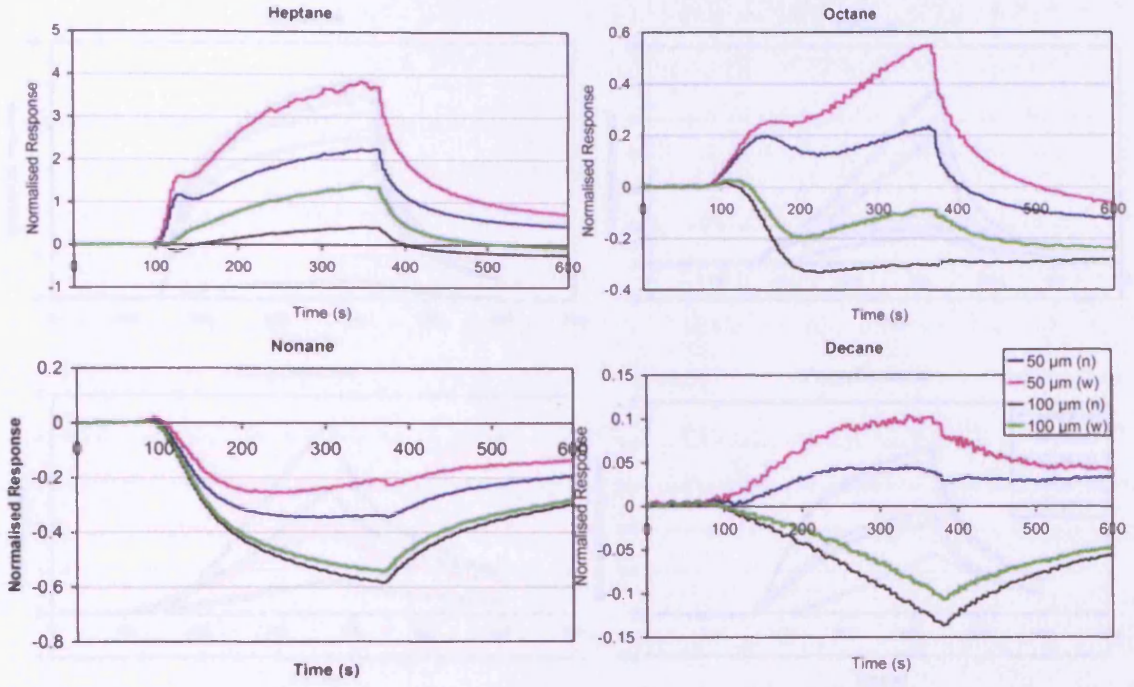

Figure 7.4.1 Comparison of normalised sensor response transients of Cr-zeolite Y sample 1 (Cr/Al = 1.2) layered sensors (50 and 100 µm) when tested to linear alkanes.

It is clear in this series that each compound in the series can be identified by its transient when related to the control sensor. It is also clear that by having two thicknesses of layer helps the discrimination further. This can also be seen for flavour compounds as shown in figure 7.4.2.

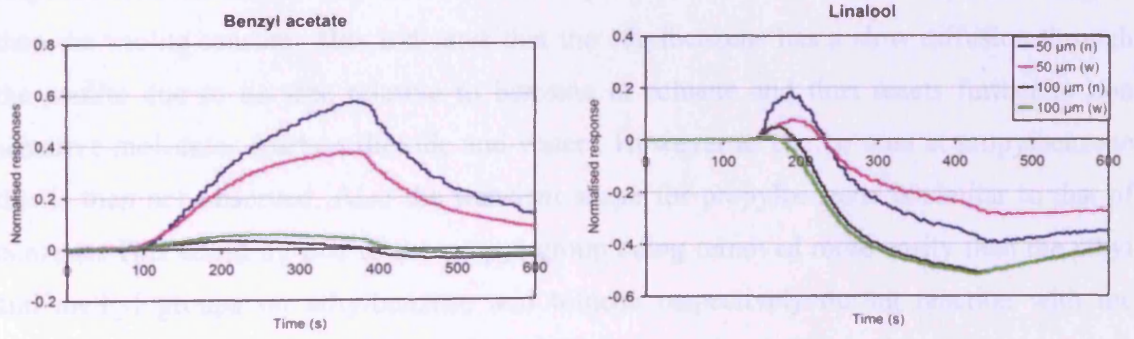

Figure 7.4.2 Comparison of normalised sensor response transients of Cr-zeolite Y sample 1 (Cr/Al = 1.2) layered sensors (50 and 100 µm) when tested to benzyl acetate and linalool.

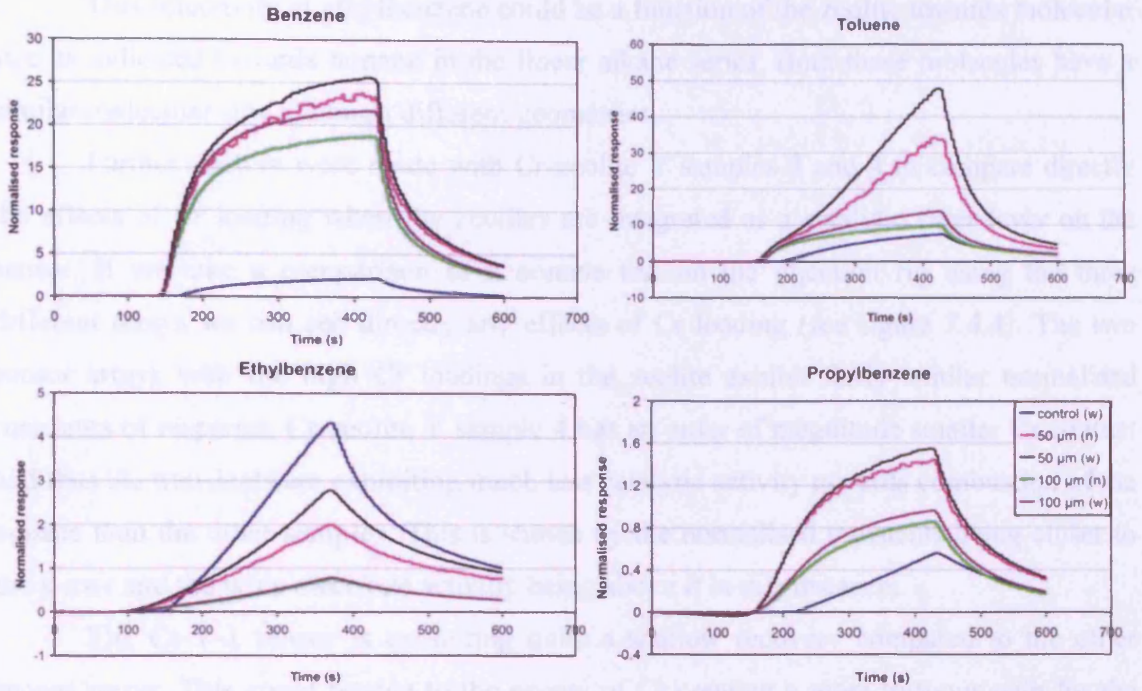

Figure 7.4.3 Comparison of normalised sensor response transients of Cr-zeolite Y sample 1 (Cr/Al = 1.2) layered sensors (50 and 100 µm) when tested to aromatics.

When the Cr-Y-1 sensor array was tested to aromatics as shown in figure 7.4.3 the difference in transient shape can clearly be seen. There is an interesting comparison with the normalised wide gap on the control sensor which has been displayed on these graphs. In most instances the wide electrode gap on the control has a similar but slightly higher response than the narrow gap however for ethylbenzene the normalised response is higher than the zeolite sensors. This indicates that the ethylbenzene has a slow diffusion through the zeolite due to its size relative to benzene or toluene and thus reacts further to non sensitive molecules (carbon dioxide and water). However as can be seen at propylbenzene this is then not observed. Also the transient shape for propylbenzene is similar to that of benzene. This could by due to the propyl group being removed more easily than the ethyl and methyl groups on ethylbenzene and toluene respectively during reaction with the zeolite and/or the effects of reaction and diffusion associated with molecular access to the zeolite pores. Note that the transients for the zeolite sensors towards ethylbenzene are very shallow to start with before rising more rapidly indicating higher sensitivity but slower response than the control sensor.

This selectivity at ethylbenzene could be a function of the zeolite towards molecular size as indicated towards nonane in the linear alkane series. Both these molecules have a similar molecular size although different geometries.

Further sensors were made with Cr-zeolite Y samples 3 and 4 to compare directly the effects of Cr loading when the zeolites are integrated as a catalytic filter layer on the sensor. If we take a comparison of a nonane test on the injection rig using the three different arrays we can see directly any effects of Cr loading (see figure 7.4.4). The two sensor arrays with the high Cr loadings in the zeolite exhibit fairly similar normalised transients of response. Cr-zeolite Y sample 4 has an order of magnitude smaller Cr content and thus the transients are exhibiting much less catalytic activity towards combustion of the nonane than the other samples. This is shown by the normalised transients being closer to the x-axis and the wide electrode actually being above it in this instance.

The Cr-Y-1 sensor is exhibiting quite a shallow recovery compared to the other sensor arrays. This could be due to the excess of Cr creating a more tortuous path for the gas in this zeolite and thus reactant molecules are thus having a longer residence time within the layer as opposed to the samples with less Cr. Remember that the Cr could be causing a narrowing of pore dimensions due to the bulk of the species exchanged onto the surface of the zeolite.

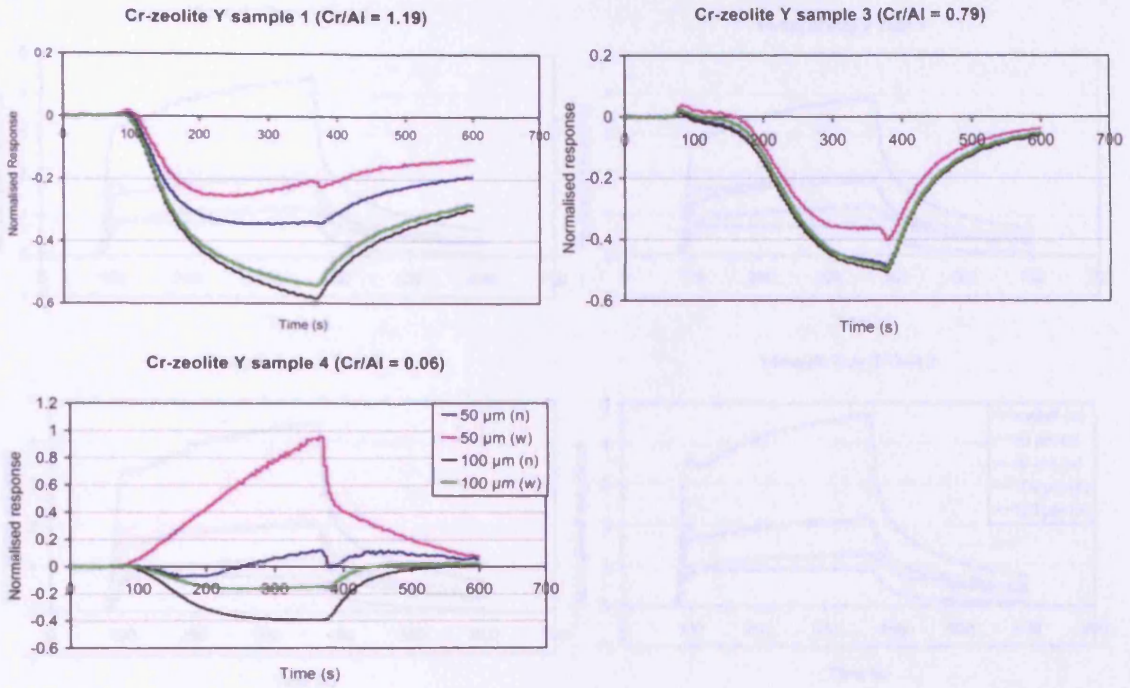

Figure 7.4.4 Nonane tested under the same conditions in the injection rig to 3 different Cr-zeolite Y sensor arrays as indicated operating at 400°C.

Further to these studies the repeatability of the injection rig also needed to be ascertained and periodically an array of sensors was subjected to numerous repeat tests using the same analyte either consecutively or periodically. Figure 7.4.5 shows a series of ethanol tests performed on using the Cr-Y-4 array operating at 400°C. The repeatability is very good even comparing the first sample performed the day before and a number of tests performed in between. Therefore for this array the zeolites did not seem to be deteriorating over time due to any carbonaceous build up causing the catalytic sites to become inactive. This is good considering the low amount of Cr exchanged on this sample of zeolite (Cr/Al = 0.06).

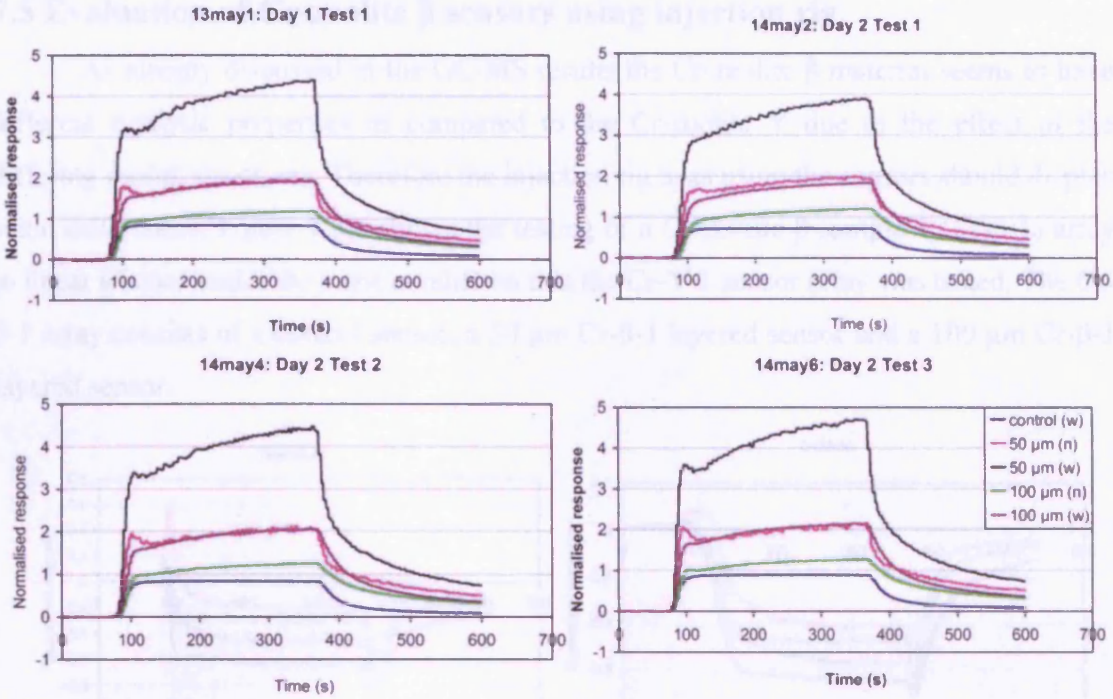

Figure 7.4.5 Repeat ethanol testing using the Cr-zeolite sample 4 array consisting of a control sensor, 50 µm Cr-Y-4 layered sensor and a 100 µm Cr-Y-4 layered sensor. All sensors operating at 400°C.

7.5 Evaluation of Cr-zeolite β sensors using injection rig

As already discussed in the GC/MS results the Cr-zeolite β material seems to have different catalytic properties as compared to the Cr-zeolite Y due to the effect of the differing zeolite structures. Therefore the injection rig tests using the sensors should display some differences. Figure 7.5.1 shows the testing of a Cr-zeolite β sample 1 (Cr-β-1) array to linear alkanes under the same conditions that the Cr-Y-1 sensor array was tested. The Cr-β-1 array consists of a control sensor, a 50 μm Cr-β-1 layered sensor and a 100 μm Cr-β-1 layered sensor.

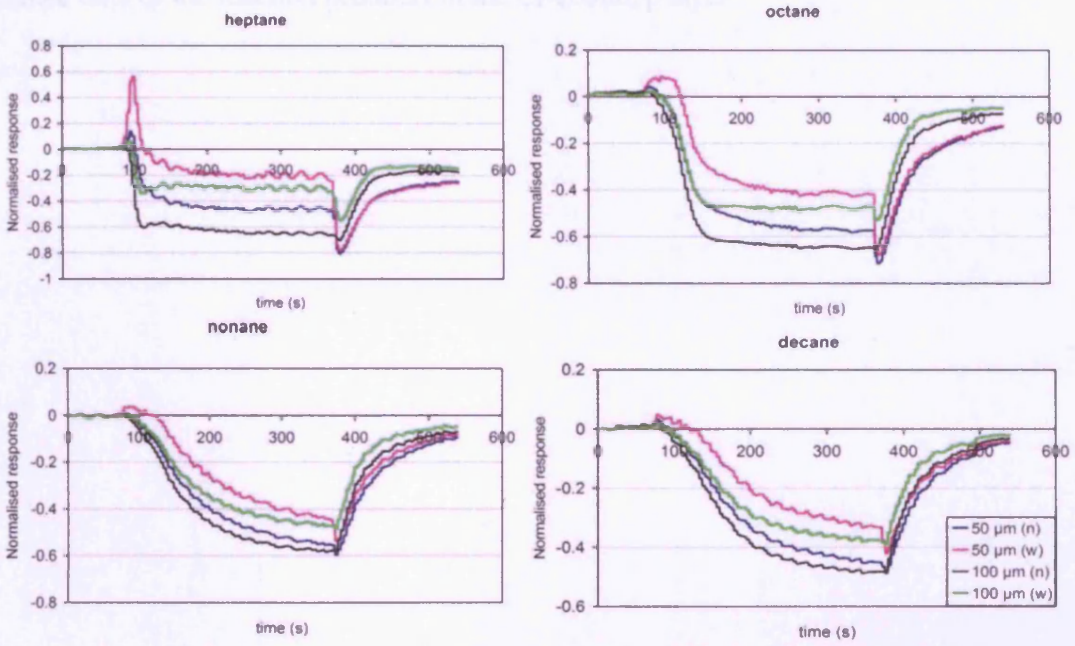

Figure 7.5.1 Cr-zeolite β sample 1 array operating at 400°C in the injection rig under standard test conditions. Tested to linear alkanes.

The transients in figure 7.5.1 show some similarities to those in figure 7.4.1 in terms of progression in increasing the chain length of the linear alkane. However what is apparent is the difference in response towards heptane and octane. The transients for both zeolite sensors operating at 400°C are below the x-axis therefore the responses are less than the control. This can be related back to the GC/MS data and the fact that at this temperature most analytes were getting fully combusted to water and carbon dioxide. Therefore this translation can be seen directly with the effect on the sensor response as compared to the Cr-zeolite Y sensors in figure 7.5.1. Despite the high catalytic activity of this zeolite

towards the analytes there is a definite change in transient shape as you go from octane to nonane. Where selectivity was observed at nonane for Cr-zeolite Y it could now be observed at octane for Cr-zeolite β as it has a smaller pore size and tortuous pathways therefore also making it difficult for the analytes to interact with the zeolite pores. In all of the normalised transients there is a small kink tending towards -1 just before the sensors recover after the analyte has stopped being injected. This will be due to the control sensor recovering faster than the zeolite sensors, there is probably still some desorbing of reaction products from the zeolite after the after the analyte has stopped being injected due to residence time of the reaction products in the Cr-zeolite β layer.

7.6 Evaluation of Mo-zeolite Y sensors using injection rig

Figure 7.6.1 describes the progression of normalised transients down the alkane series using Mo-zeolite Y sample 3 (Mo-Y-3 – solid state ion exchange) sensors operating at 400°C. There is a noticeable transient shape change down the alkane series. Heptane is showing an initial peak in the transient which is also slightly apparent at octane. It is more prominent for the 50 µm zeolite layered sample. The 50µm Mo-zeolite layered sample is showing a greater degree of sensitivity for all alkanes in the series.

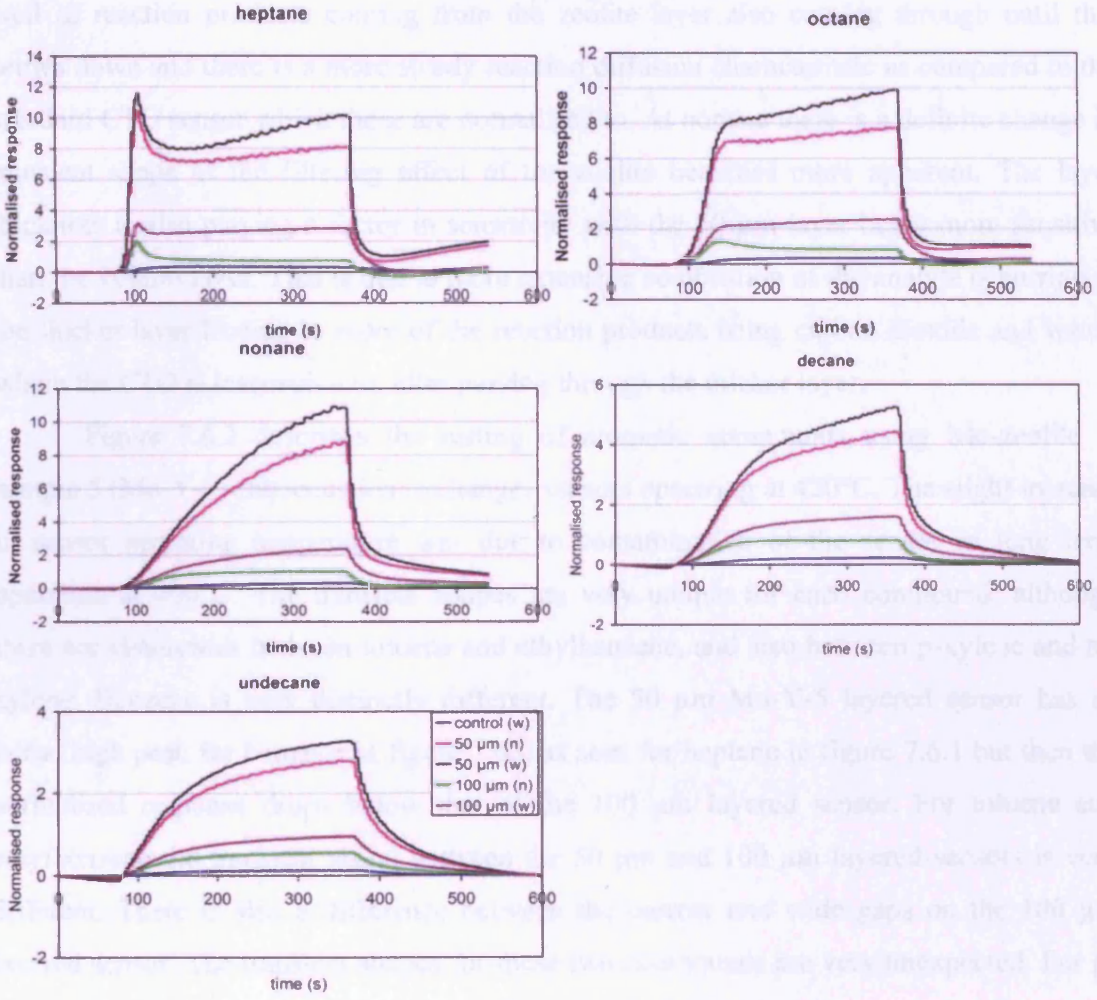

Figure 7.6.1 Normalised sensor transients of Mo-Y-3 sensors operating at 400°C and tested to linear alkanes

It can be observed that a number of characteristics on the normalised transient response in figure 7.6.1 can be related back to the GC/MS results at 400°C in figure 6.5.1.1. There is an initial peak to the normalised transient for heptane and octane. If you take a look at figure 6.5.1.1 you can see that there is a large amount of the primary analyte getting through the zeolite bed at C7 and C8. It must be considered that the GC/MS test uses a pulse of the initial analyte rather than a continuous stream which may affect the results. Therefore this initial peak observed in figure 7.6.1 could be due to an initial burst of the primary analyte coming through the zeolite layer and reacting on the surface of the CTO as well as reaction products coming from the zeolite layer also coming through until this settles down and there is a more steady reaction diffusion characteristic as compared to the standard CTO sensor which these are normalised to. At nonane there is a definite change in transient shape as the filtering effect of the zeolite becomes more apparent. The layer thickness is also playing a factor in sensitivity with the 50 μm layer being more sensitive than the 100μm layer. This is due to more extensive combustion of the analyte occurring in the thicker layer leading to more of the reaction products being carbon dioxide and water, which the CTO is insensitive to, after passing through the thicker layer.

Figure 7.6.2 describes the testing of aromatic compounds using Mo-zeolite Y sample 5 (Mo-Y-5 – aqueous ion exchange) sensors operating at 420°C. The slight increase in sensor operating temperature was due to contamination of the sensor in long term operation at 400°C. The transient shapes are very unique for each compound, although there are similarities between toluene and ethylbenzene, and also between p-xylene and m-xylene. Benzene is very distinctly different. The 50 μm Mo-Y-5 layered sensor has an initial high peak for benzene in figure 7.6.2 as seen for heptane in figure 7.6.1 but then the normalised response drops below that of the 100 μm layered sensor. For toluene and ethylbenzene the transient shape between the 50 μm and 100 μm layered sensors is very different. There is also a difference between the narrow and wide gaps on the 100 μm layered sensor. The transient shapes for these two compounds are very unexpected. For p-xylene and m-xylene again there is a difference in transient shape between the 50 μm and 100 μm layered sensors.

For the Mo-Y-5 sensors tested to aromatics as indicated in figure 7.6.2 there is a clear indication of functional group selectivity. These sensors had to be run at 420°C as opposed to 400°C for the Mo-Y-3 sensors. This was due to the Mo-Y-5 sensors experiencing a drop

in sensitivity over time most likely attributed to a carbonaceous build up in the zeolite pores during catalysis remembering that this material does not have a high loading of Mo.

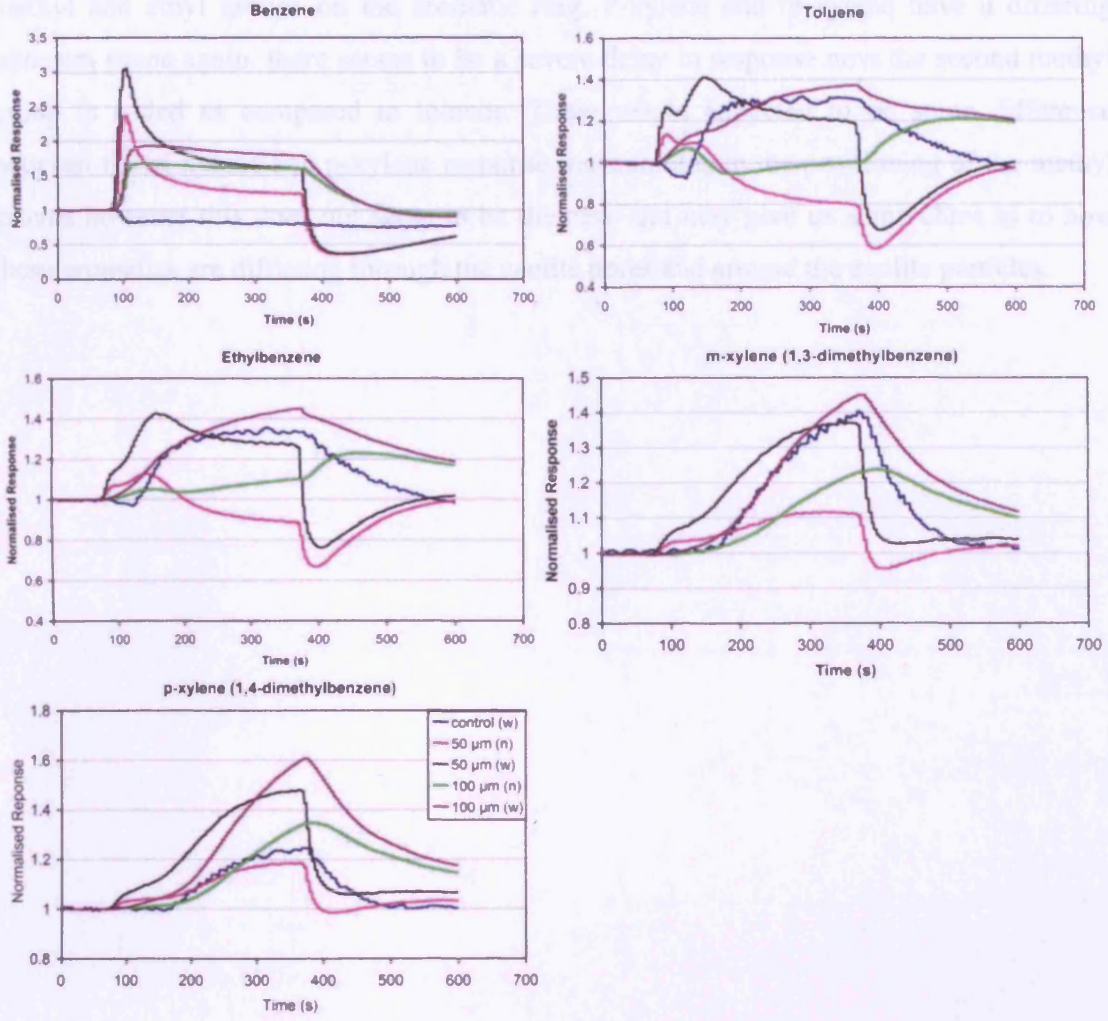

Figure 7.6.2 Normalised sensor transients of Mo-Y-5 sensors operating at 420°C and tested to aromatics

The selectivity of the Mo-Y-5 sensors is clearly observed in the transient shape. Benzene is very distinct from the others and again has an initial peak which may be due to the amount of the primary analyte the CTO is seeing initially as well as reaction products as observed for heptane in figure 7.6.1. The transient shapes for toluene and ethylbenzene are very unusual when normalised against the standard CTO sensor. It can be assumed that there are a variety of reaction and diffusion effects occurring within the zeolite layer to the

original analyte and the reaction products as they pass through the zeolite layer. What is clear is the distinction between these and benzene indicating the selectivity attributed to the methyl and ethyl groups on the aromatic ring. P-xylene and m-xylene have a differing transient shape again, there seems to be a severe delay in response now the second methyl group is added as compared to toluene. There would expected to be some difference between the m-xylene and p-xylene response transient due to the positioning of the methyl groups however this does not seem to be the case and may give us some clues as to how these aromatics are diffusing through the zeolite pores and around the zeolite particles.

7.7 Evaluation of W-zeolite Y sensors using injection rig

The injection rig sensor array consisted of a control sensor (CTO only), 50 μm layered W-zeolite Y sample 1 (W-Y-1) sensor and 100 μm layered W-Y-1 sensor.

Testing to the linear alkane series at 400°C is shown in figure 7.7.1. With an increase in chain length the molecule will travel more slowly through the zeolites and hence the transient behaviour relative to the control sensor is slower. Increasing the thickness of the zeolite layer enhances the effect.

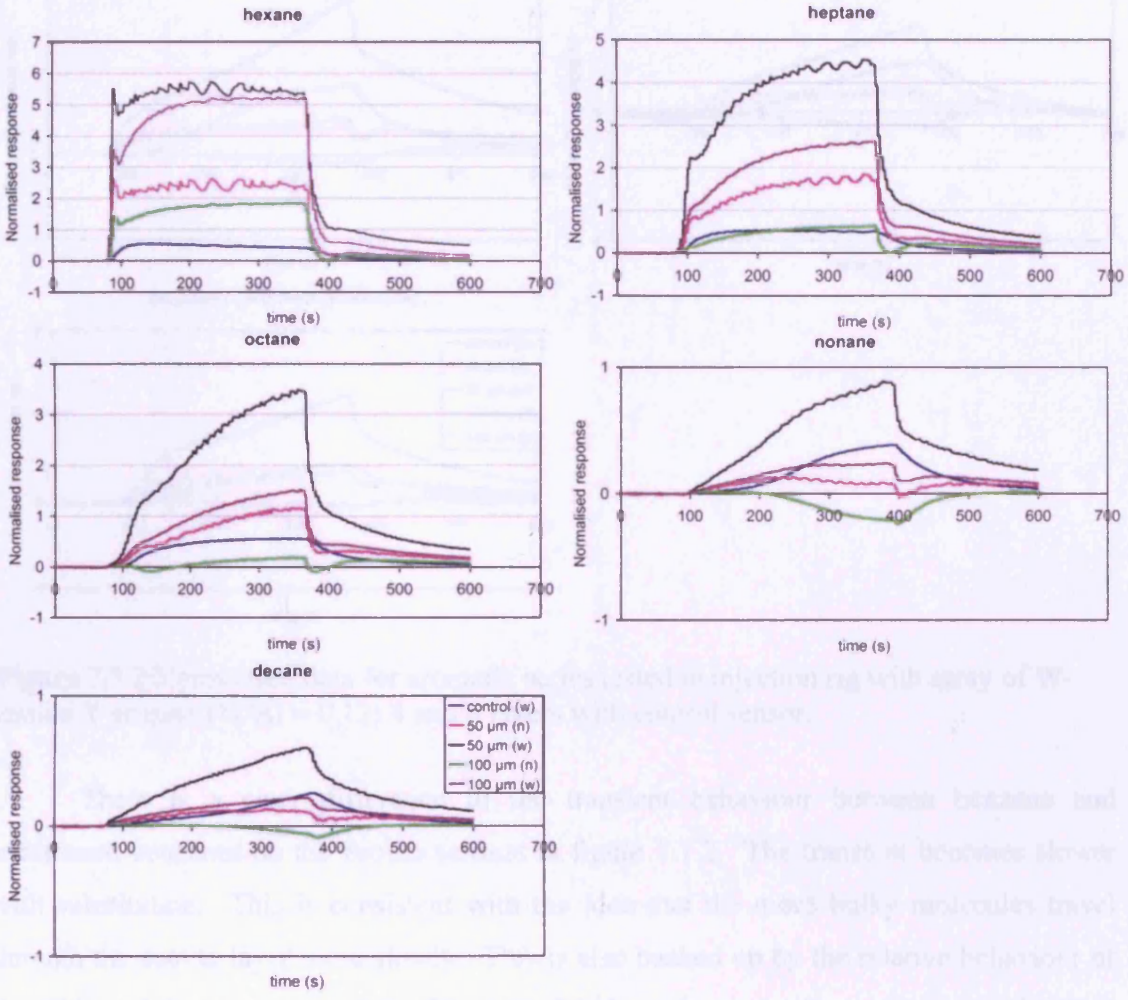

Figure 7.7.1 Normalised data for alkane series tested in injection rig with array of W-zeolite Y sensors (W/Al = 0.12) 4 and 8 layers with control sensor.

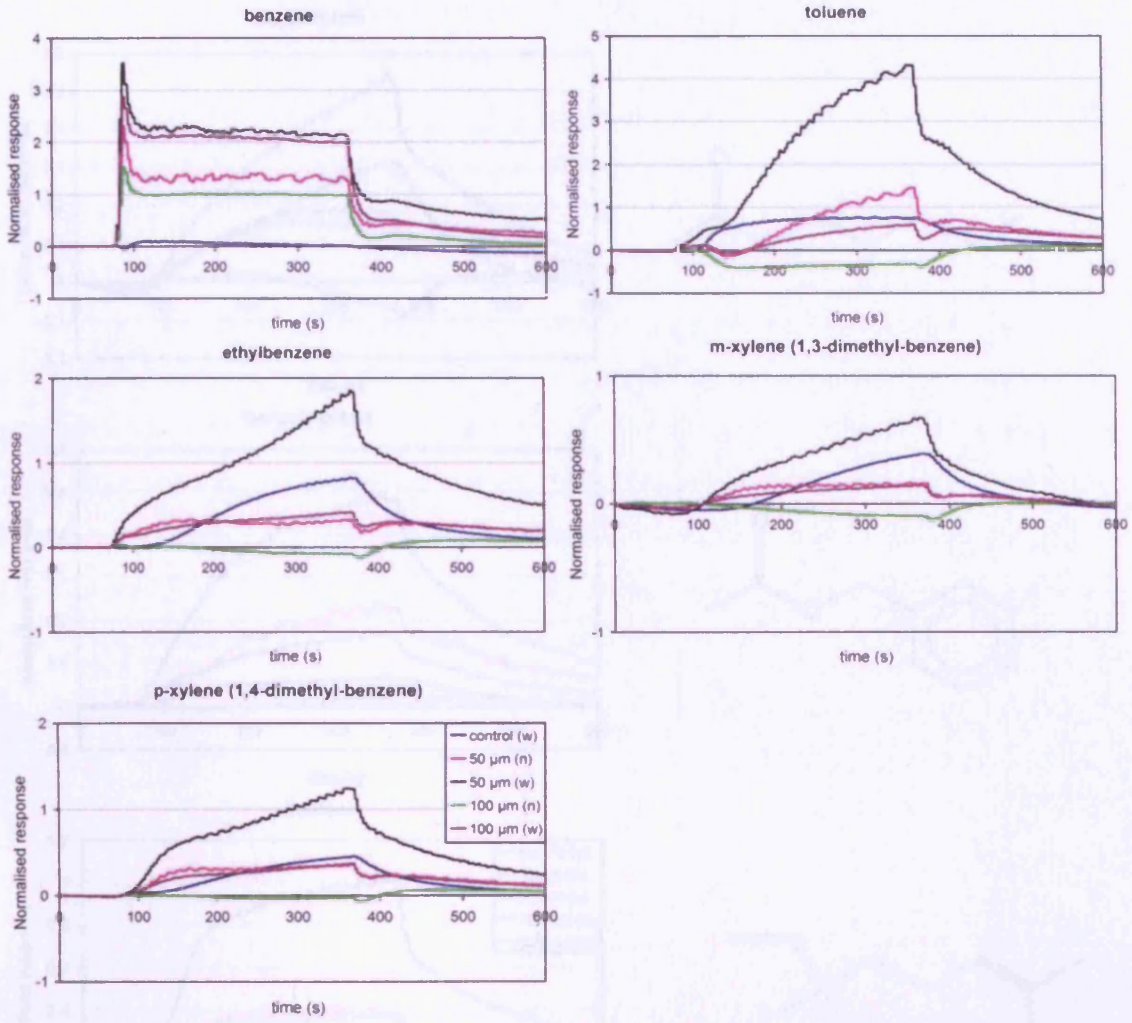

Figure 7.7.2 Normalised data for aromatic series tested in injection rig with array of W-zeolite Y sensors (W/Al = 0.12) 4 and 8 layers with control sensor.

There is a clear difference in the transient behaviour between benzene and substituted benzenes on the zeolite sensors in figure 7.7.2. The transient becomes slower with substitution. This is consistent with the idea that the more bulky molecules travel through the zeolite layer more slowly. This is also backed up by the relative behaviour of the wide and narrow gaps and the 50 µm and 100 µm layer zeolites respectively. Namely that the wide gaps give larger responses than the narrow gaps, i.e. there is a concentration gradient, and this becomes steeper, even with benzene, with the 100 µm layer showing a larger effect than the 50 µm layer.

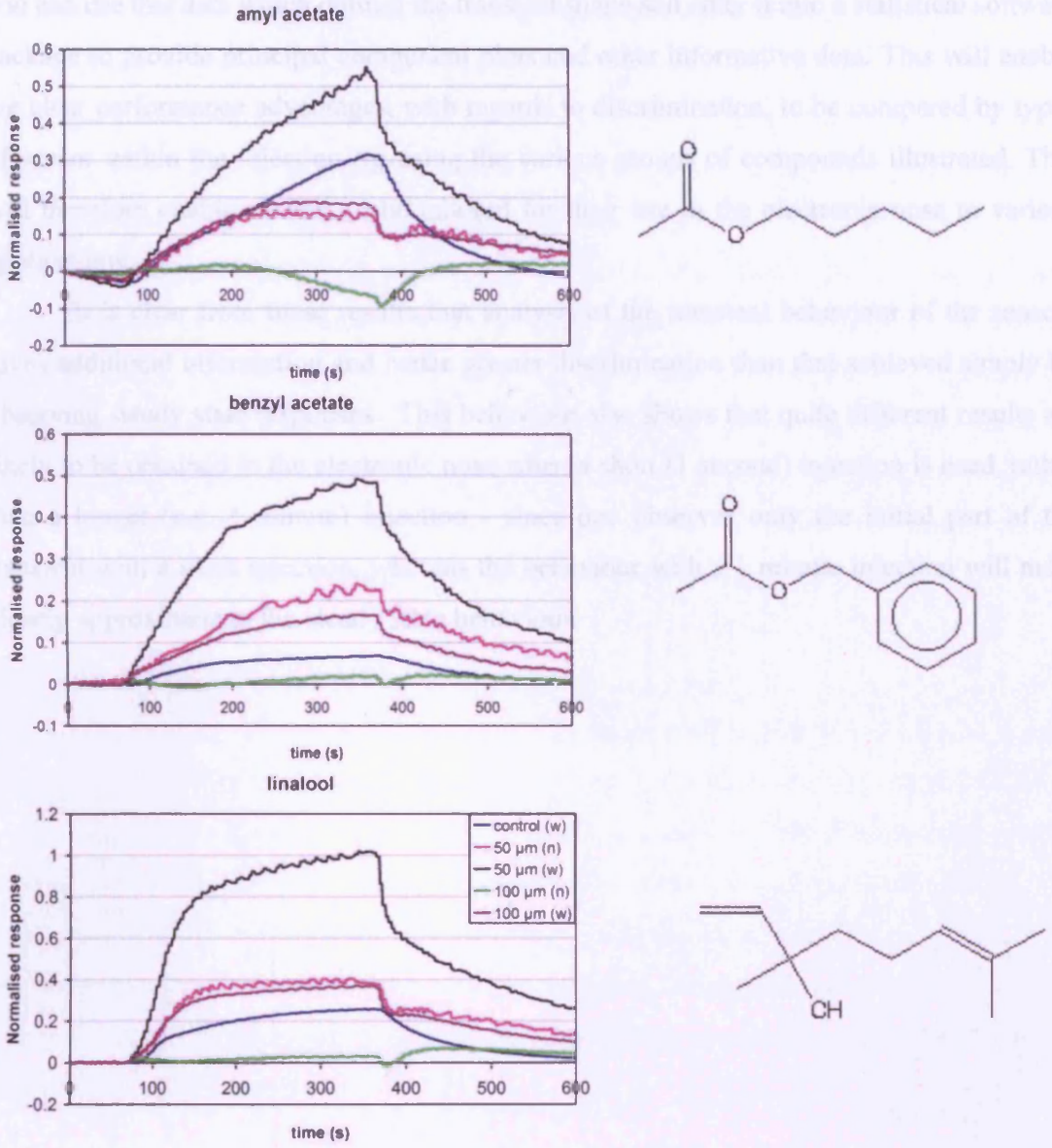

Figure 7.7.3 Normalised data for flavour samples tested in injection rig with array of W-zeolite Y sensors (W/Al = 0.12) 4 and 8 layers with control sensor. Y-axis describes the difference in the linearised response normalised to the narrow gap on the control sensor. X-axis describes the time in s.

The flavour testing transients shown in figure 7.7.3 are of particular interest with regard to the ylang-ylang testing as linalool and benzyl acetate are two of the flavour compounds that vary the most with respect to the different grades of ylang-ylang (see chapter 8.4). The transient shape can easily be exploited to differentiate the compounds. For instance if we take points along the transient at say 100, 200, 300 s and at the maximum

you can use this data which defines the transient shape and enter it into a statistical software package to provide principal component plots and other informative data. This will enable the clear performance advantages, with regards to discrimination, to be compared by types of sensor within the injection rig using the various groups of compounds illustrated. This will therefore enable sensors to be tailored for their use in the electronic nose to various applications.

It is clear from these results that analysis of the transient behaviour of the sensors gives additional information and hence greater discrimination than that achieved simply by observing steady state responses. This behaviour also shows that quite different results are likely to be obtained in the electronic nose when a short (1 second) injection is used, rather than a longer (e.g. 1 minute) injection - since one observes only the initial part of the transient with a short injection, whereas the behaviour with a 1 minute injection will more closely approximate to the steady state behaviour.

7.8 Statistical analysis of injection rig transient data using SPSS

This section evaluates the discriminatory effectiveness of the sensors using a statistical software package (SPSS 12.0). Data were taken from the transient responses taken from the injection rig. Data were taken from either a maximum response along the 500 s transient or from periods along the transient – 100, 200, 300 s for example. The advantage of taking points from periods along the transient is that it can take into account transient shape as a determinant for the discrimination. This will hopefully add another dynamic to the discriminant function analysis performed to help aid and improve the methods employed by an electronic nose. In the Fox 2000 electronic nose that has also been utilised in this work (see chapter 8) the usual analysis is to take the maximum responses from a sample to perform the analysis which means the first component is directly related to the volatility of the sample which may hinder the discriminatory analysis.

7.8.1 Evaluation of Cr-zeolite Y sensor array

The sensor array used consisted of a CTO sensor with no zeolite layer which is used as the control, a CTO sensor with a 50 μm Cr-Y-1 zeolite layer, and a CTO sensor with a 100 μm Cr-Y-1 zeolite layer, all operating at 400°C. Figure 7.8.1.1 highlights the problem of taking the maximum point along the transient for discriminant analysis. Many of the compounds are clustered together and only volatile species seem to have been discriminated against such as heptane, benzene, toluene and ethylbenzene. It does however give a good working example of the methods employed by the electronic nose whilst using a standard sensor testing rig.

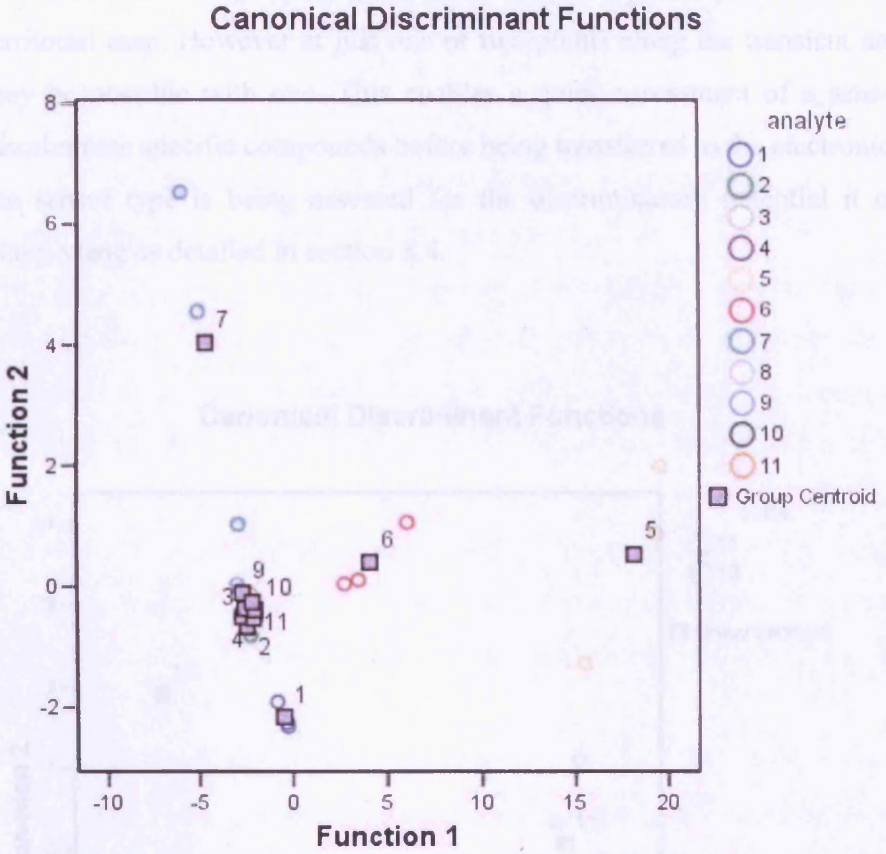

Key: 1 - heptane 1ml, 2 - octane 1ml, 3 - nonane 1ml, 4 - decane 1ml, 5 - benzene 1ml, 6 - toluene 1ml, 7 - ethylbenzene 1ml, 8 - linalool 1ml, 9 - benzyl acetate 1ml, 10 - amyl acetate 1ml, 11 - cineole 1ml

Figure 7.8.1.1 Discriminant function analysis map using three repeated samples of each analyte indicated in the key. Produced from data obtained from the injection rig containing a Cr-zeolite Y sample 1 sensor array (CTO – control, CTO + 50 µm Cr-Y-1, CTO + 100 µm Cr-Y-1) operating at 400°C.

7.8.2 Evaluation of W-zeolite Y sensors

Points along the transient were taken at 100, 200, 300s and the maximum from the transients normalised to narrow gap on the control CTO sensor. Thus there were effectively four streams of data input for each time along the transient. Using a simple discriminant analysis as shown in figure 7.8.2.1 a simple territorial map can be produced from the flavour compounds whose transients are highlighted in figure 7.7.3. In this case each point represents a different time along the transient. In this instance all four data streams were

needed for clear discrimination. It is basically comparing the relationship between the points thus the variation in normalised sensor response across an array to provide the territorial map. However at just one or two points along the transient and repeat results it may be possible with one. This enables a quick assessment of a sensors capabilities to discriminate specific compounds before being transferred to the electronic nose. In this case the sensor type is being assessed for the discriminatory potential it may have towards ylang-ylang as detailed in section 8.4.

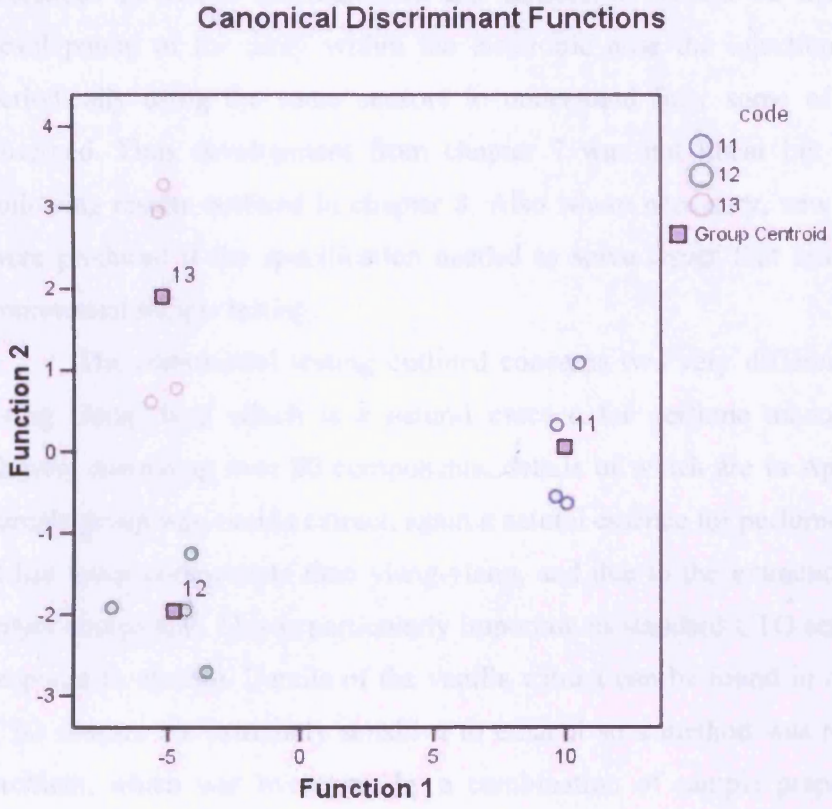

Figure 7.8.2.1 Discriminant function analysis map using three repeated samples of each analyte indicated in the key. Produced from data obtained from the injection rig containing a W-zeolite Y sample 1 sensor array (CTO – control, CTO + 50 µm W-Y-1, CTO + 100 µm W-Y-1) operating at 400°C.

Key: 11 – Amyl Acetate
12 – Benzyl Acetate
13 - Linalool

8. Electronic nose development

8.1 Introduction

This final results section deals with the integration of the zeolite filtered sensors within the electronic nose thus enabling an assessment of the sensors themselves and their discriminatory capabilities towards groups of commercial samples. Initial testing was done using single component organic compound groups such as linear alkanes, alcohols and aromatics to assess the materials and sensors. It should be made clear that for the development of the array within the electronic nose the injection rig was also utilised periodically using the same sensors to understand fully some of the results that were observed. Thus development from chapter 7 was not linear but ran in parallel to the following results outlined in chapter 8. Also where necessary, new catalytic zeolite types were produced if the specification needed to solve issues that arose during some of the commercial sample testing.

The commercial testing outlined concerns two very different sample groups. One being ylang-ylang which is a natural essence for perfume manufacture obtained from flowers containing over 80 components, details of which are in Appendix V. The second sample group was vanilla extract, again a natural essence for perfume manufacture however it has fewer components than ylang-ylang, and due to the extraction process ethanol is a major component. This is particularly important as standard CTO sensors give a significant response to ethanol. Details of the vanilla extract can be found in Appendix IV. Standard CTO sensors are extremely sensitive to ethanol so a method was required to combat this problem, which was overcome by a combination of sample preparation and discerning sensor combinations. The sample preparation consisted of applying 20 μL of sample to a 2 cm^2 piece of filter paper and letting it stand for 30 mins to allow some of the ethanol to evaporate as it is the most volatile component within the vanilla extract. Then the samples were placed in the 10 ml sample vials and the standard procedure for testing was undertaken.

In most of the testing the 'MICS' chambers containing the zeolite sensors were compared to the standard 'C' sensor chamber as supplied by Alpha-MOS, details of which

are in Appendix III. (MICS relates to the title of the European Project which sponsered this work).

8.2 Integration of sensors into Fox 2000 electronic nose

By initially using 6 SEMDEC sensors across 2 chambers in the electronic nose a method was established for determining the best combination of sensors for a 3 sensor array. Initially the sensors were operated at 400°C and then the temperature was reduced or raised to gauge whether there is any advantage of running at a different temperature for a specific material. A three sensor array that is highly discriminatory to alkanes and alcohols was initially established. For the alkanes and alcohols it was established that an array comprising of Cr-zeolite β sample 1 - 8 layers, Mo-zeolite Y sample 3 – 8 layers, Cr_2O_3 8 layers all operating at 400°C provided good discrimination. The resulting principal component analysis plot is shown in figure 8.2.1, the axes describe the 3rd and 4th principal components.

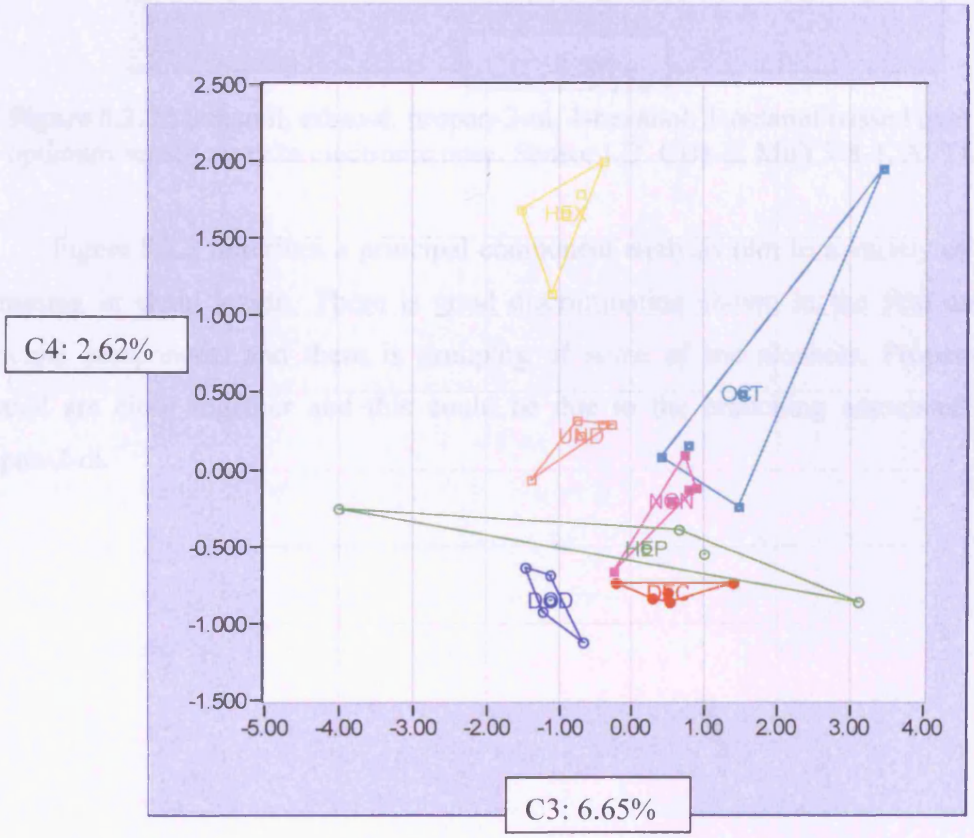

Figure 8.2.1 Hexane to dodecane passed over optimum sensor array in electronic nose. Sensor I.D. CB8-3, MoY3-8-1, AFT8-1.

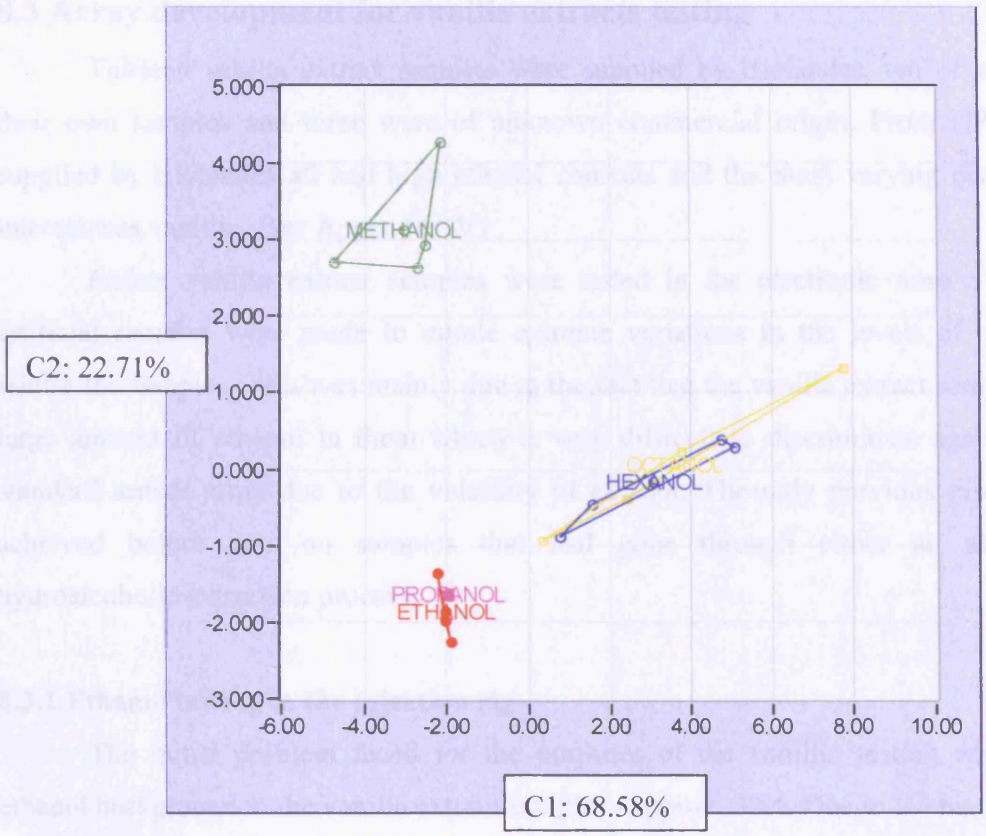

Figure 8.2.2 Methanol, ethanol, propan-2-ol, 1-hexanol, 1-octanol passed over optimum sensor array in electronic nose. Sensor I.D. CB8-3, MoY3-8-1, AFT8-1.

Figure 8.2.2 describes a principal component analysis plot to a variety of alcohols, increasing in chain length. There is good discrimination shown in the first and second principal components and there is grouping of some of the alcohols. Propan-2-ol and ethanol are close together and this could be due to the branching associated with the propan-2-ol.

8.3 Array development for vanilla extracts testing

Thirteen vanilla extract samples were supplied by Biolandes, ten of which were their own samples and three were of unknown commercial origin. From HPLC results supplied by Biolandes all had high ethanol contents and the main varying constituent of interest was vanillin. (see Appendix IV)

Before vanilla extract samples were tested in the electronic nose a variety of artificial samples were made to mimic extreme variations in the levels of components within the samples. This was mainly due to the fact that the vanilla extract samples have a large amount of ethanol in them which is very difficult to discriminate against using a standard sensor array due to the volatility of ethanol. The only previous discrimination achieved before was on samples that had gone through either an alcoholic or hydroalcoholic extraction process.

8.3.1 Ethanol testing in the injection rig

The initial problem faced for the purposes of the vanillin testing was the large ethanol background in the vanilla extract samples - approx. 30%. Due to the high sensitivity of CTO to ethanol we initially need to find sensors with a low sensitivity to ethanol. (See figure 8.3.1.1)

The following sensor arrays were used:

Cr-Y-1 Chromium exchanged (aqueous) zeolite Y sample 1, Cr/Al = 1.20 (EDAX)

Cr-B-1 Chromium exchanged (aqueous) zeolite β sample 1

Cr-ZSM5-4 Chromium exchanged (aqueous) zeolite ZSM-5 sample 4

Mo-Y-1 Molybdenum exchanged (solid state) zeolite Y sample 1, Mo/Al = 0.20 (EDAX)

Mo-Y-3 Molybdenum exchanged (solid state) zeolite Y sample 3, Mo/Al = 0.83 (EDAX)

Mo-Y-5 Molybdenum exchanged (aqueous) zeolite Y sample 5, Mo/Al = 0.07 (EDAX)

W-Y-1 Tungsten exchanged (aqueous) zeolite Y sample 1, W/Al = 0.12 (EDAX)

Other Sensors used:

AFT Cr_2O_3 filter layer (100 μm (8 printed layers) on CTO)

LTA Linde Type A zeolite (3Å) (50 μm (4 printed layers) on CTO)

A 100 s ethanol exposure was performed and repeated on each subsequent sensor array and the transients were assessed to ascertain suitability for vanilla extract testing. This

was based on the sensitivity to ethanol and transient shape as normalised to the narrow gap on the control sensor in each array.

It was generally observed that a lot of the sensors had a heightened sensitivity to ethanol due to the catalytic nature of the zeolite filters enhancing sensitivity further.

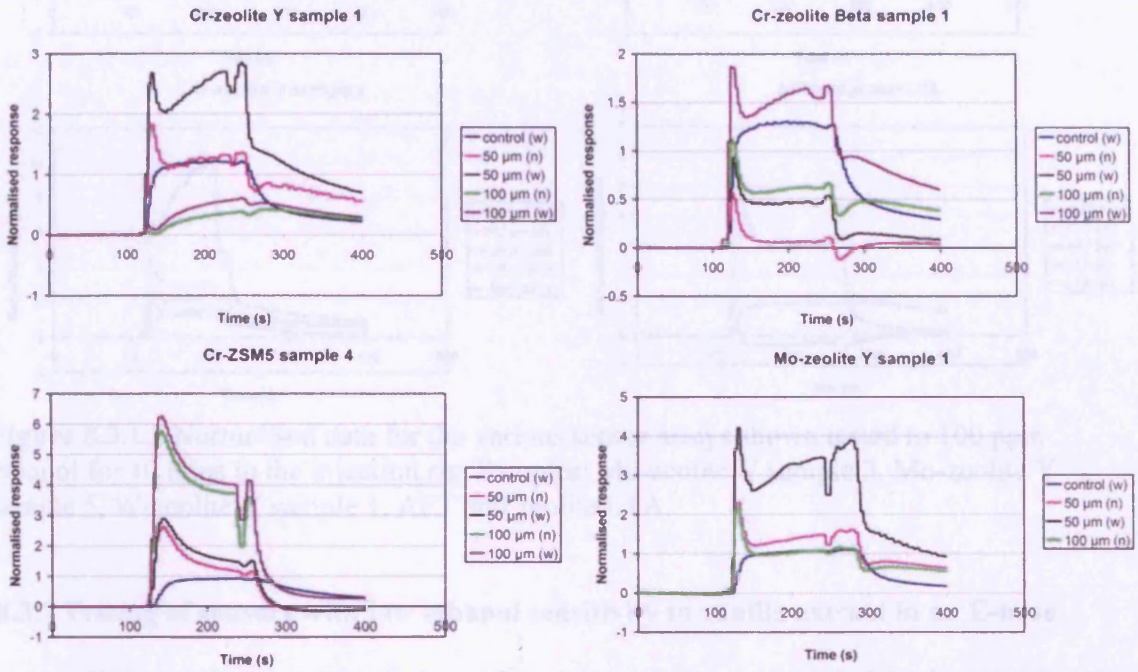

Figure 8.3.1.1 Normalised data for the various sensor arrays shown tested to 100 ppm ethanol for 10 mins in the injection rig. Samples: Cr-zeolite Y sample 1, Cr-zeolite beta sample 1, Cr-ZSM5 sample 4, Mo-zeolite Y sample 1.

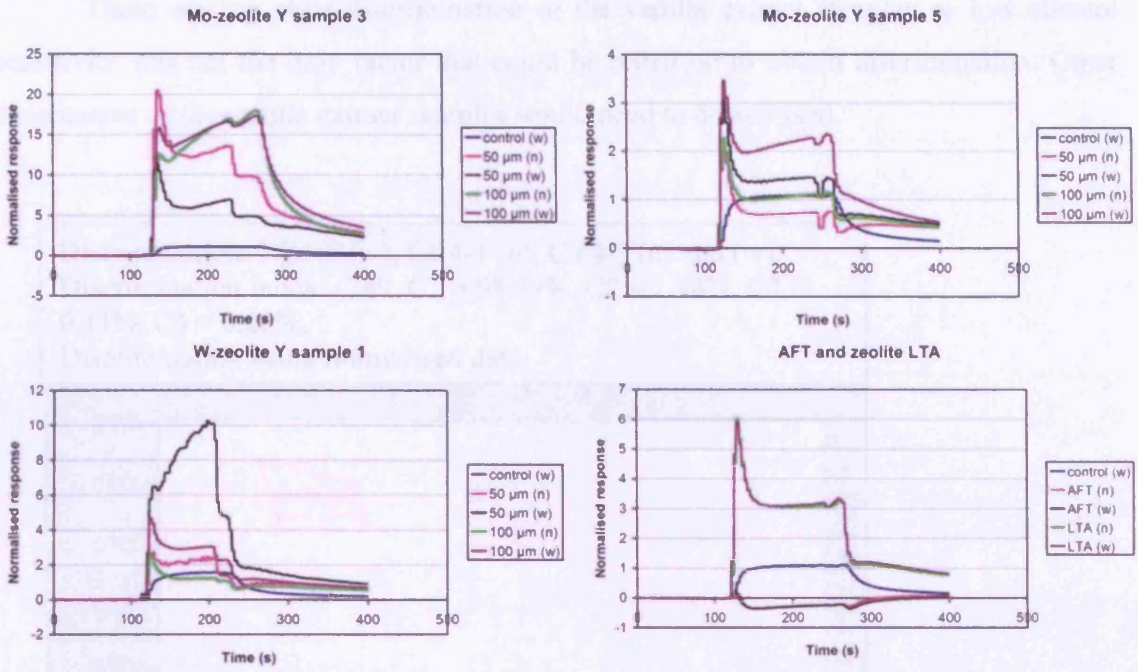

Figure 8.3.1.2 Normalised data for the various sensor arrays shown tested to 100 ppm ethanol for 10 mins in the injection rig. Samples: Mo-zeolite Y sample 3, Mo-zeolite Y sample 5, W-zeolite Y sample 1, AFT and zeolite LTA.

8.3.2 Testing of sensors with low ethanol sensitivity to vanilla extract in an E-nose

Utilising the sensors with low ethanol sensitivity, as identified in the injection rig testing, initial tests were performed on the electronic nose with the vanilla extract samples. The following conditions were set-up for testing:

Sensors in zeolite sensor chamber – NZ4-2 (no zeolite layer), CB4-1 (Cr-zeolite beta 50 µm layer), CY8-4 (Cr-zeolite Y 100 µm layer).

Testing - Vanilla extracts A – O, ethanol, vanillin (Aldrich), UCL synthetic vanilla extract (4 samples of each)

The synthetic vanilla extract sample was produced in accordance to the quantities of constituents of a typical sample from HPLC results supplied by Biolandes. From figure 8.3.2.1 below it can be observed that the synthetic sample is very different from the vanilla extract samples implying that the other constituents of the vanilla extract samples have a distinct effect on discrimination however it is unsure as to how they vary if at all from sample to sample.

There was no clear discrimination of the vanilla extract samples so low ethanol sensitivity was not the only factor that could be relied on to obtain discrimination. Other constituents of the vanilla extract samples would need to be assessed.

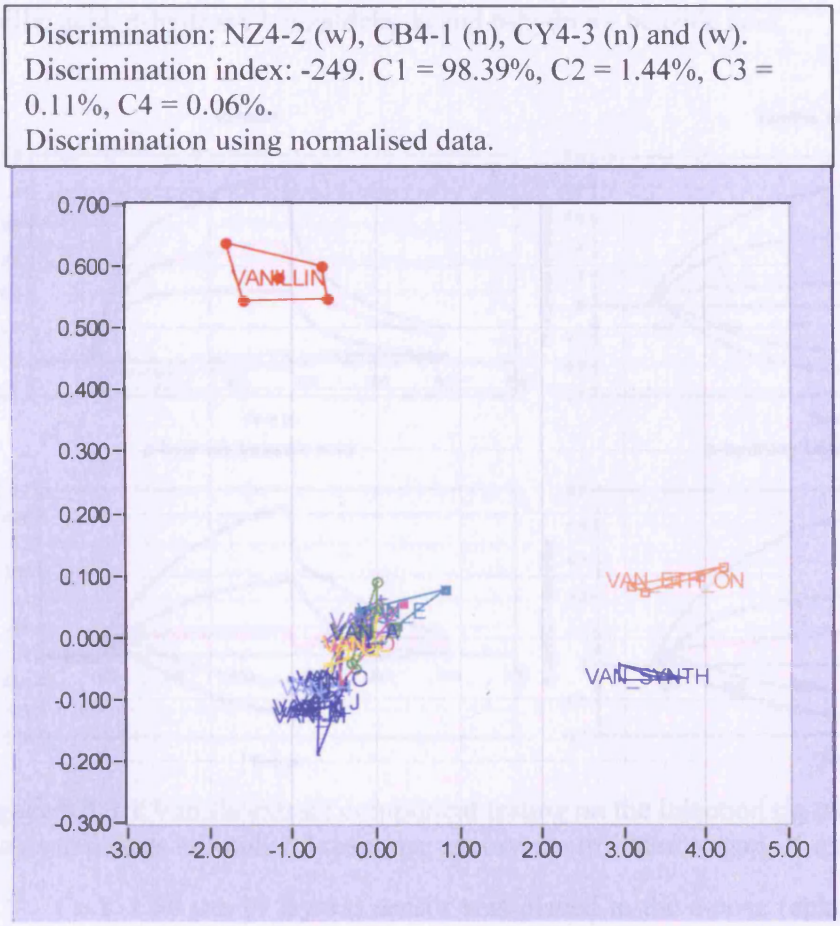

Figure 8.3.2.1 Vanilla extract testing on E-nose using initial array (NZ4-2, CB4-1, CY8-4) all operating at 400°C.

8.3.3 Vanilla extract constituent testing

Following from the initial electronic nose testing a number of the key arrays that had a relatively low sensitivity to ethanol within the parameters set were tested to other important constituents of the vanilla extract samples as indicated by Biolandes; vanillin, vanillic acid, p-hydroxy benzaldehyde and p-hydroxy benzoic acid.

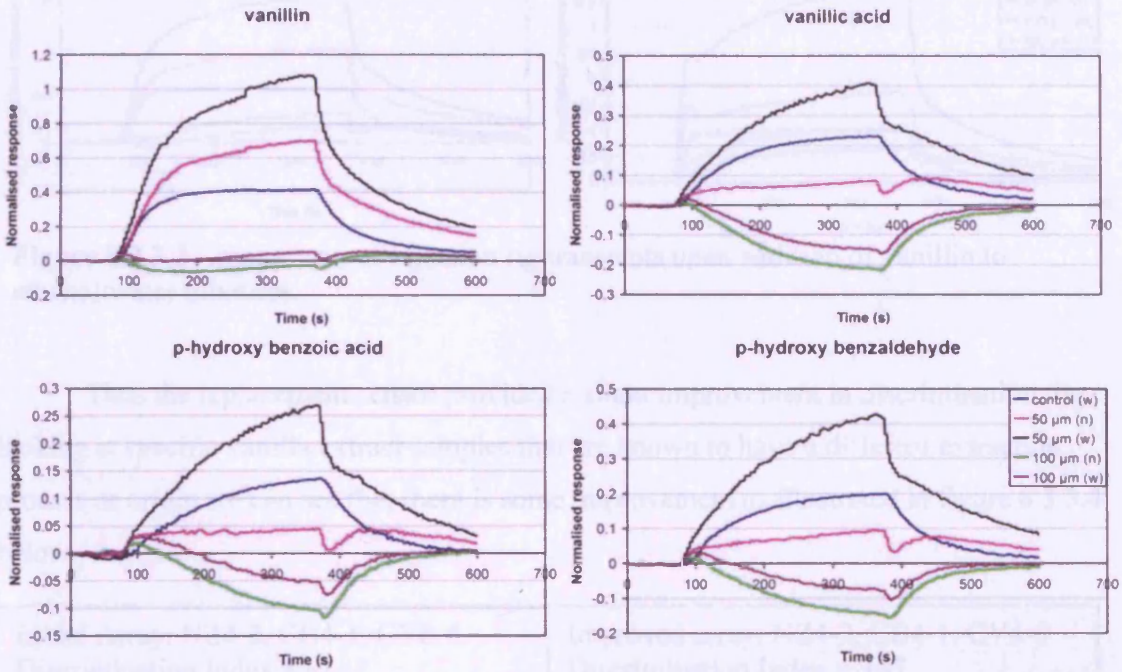

Figure 8.3.3.1 Vanilla extract component testing on the injection rig using CrY1 array. Y-axis describes normalized response against control narrow gap. X-axis: time (s).

Cr-Y-1 50 µm (4 layers) sensor was placed in the e-nose replacing the Cr-Y-1 100 µm (8 layers) sensor as it showed a large variation in response between the wide and narrow gap and differing transient shape. Although the 50 µm Cr-Y-1 zeolite layered sensor enhances ethanol sensitivity more than the 100 µm Cr-Y-1 zeolite layered sample it is expected that the discrimination will be improved as one of the remaining sensors in the zeolite sensor chamber has low ethanol sensitivity.

In addition, to assess the possible effects of vanillin content variation vanillin mixtures were made to assess the effect of vanillin in a background of ethanol with the new sensor. The injection rig transients are displayed in figure 8.3.3.2. The results indicate a definite difference in transient shape and magnitude of response after the 5 minute

injection. There is an initial peak in the normalised response difference on the vanillin added sample. This is due to the catalytic effect of the zeolite cracking the vanillin and producing reaction products that CTO is very sensitive to in addition to the response due to ethanol.

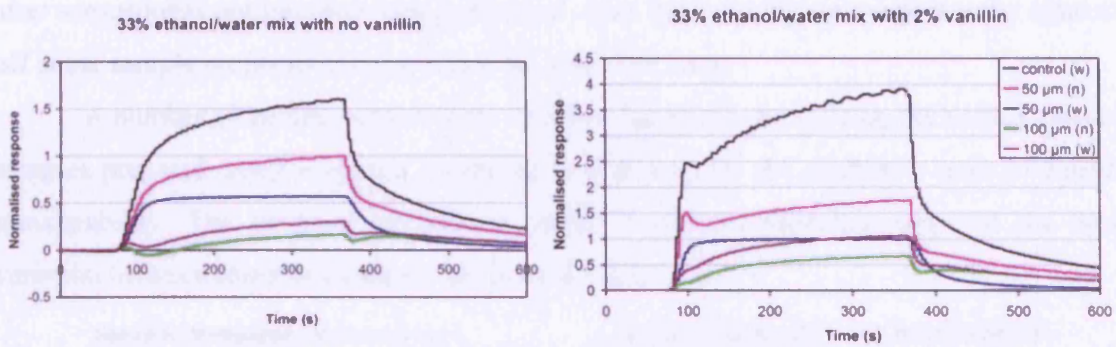

Figure 8.3.3.2 Comparison of injection rig transients upon addition of vanillin to ethanol/water mixtures.

Thus the replacement sensor provided a slight improvement in discrimination. By looking at specific vanilla extract samples that are known to have a different extraction process or origin we can see that there is some improvement as illustrated in figure 8.3.3.4 below.

Initial Array: NZ4-2, CB4-1, CY8-4. Discrimination Index = -2.	Improved array: NZ4-2, CB4-1, CY4-3 Discrimination Index = +87

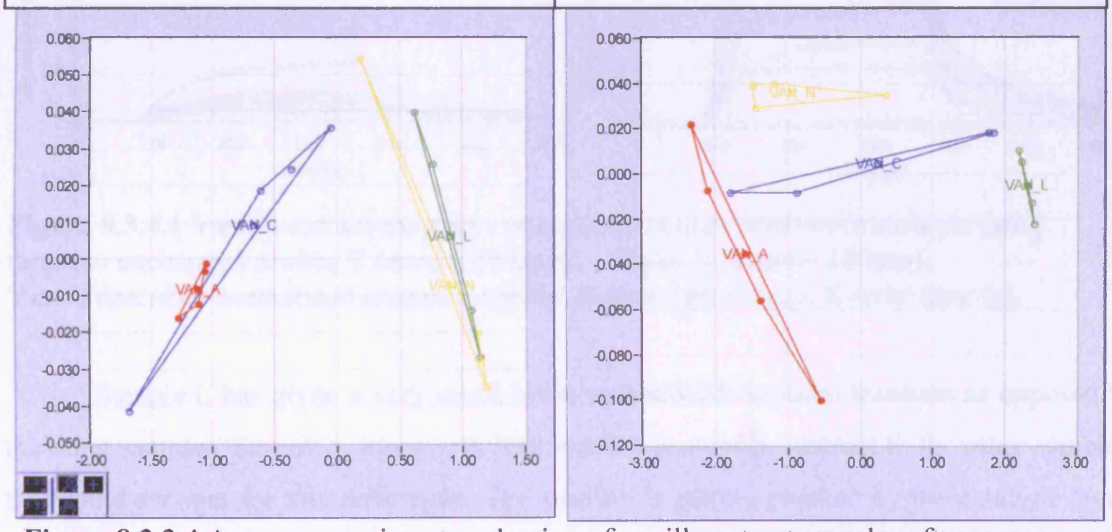

Figure 8.3.3.4 Array comparison to selection of vanilla extract samples after sensor change.

8.3.4 Integration of Tungsten exchanged zeolite filtered sensor into MICS chamber

Following the vanilla extract testing performed on the electronic nose as outlined in the previous section it was deemed that the Cr-B-4 (Cr-zeolite beta 50 µm layer) sensor should be replaced as it now seemed to be providing little of the discrimination in the array after sensor/mass optimisation was performed. Also due to trying to evaporate the ethanol off at the sample preparation stage it may be less of an issue.

A number of zeolite sensors were tested in the injection rig using the vanilla extract samples prepared using a similar technique to that used on the electronic nose to ensure transferability. The tungsten exchanged zeolite Y sensors produced some of the best variation between samples as shown in figure 8.3.4.1.

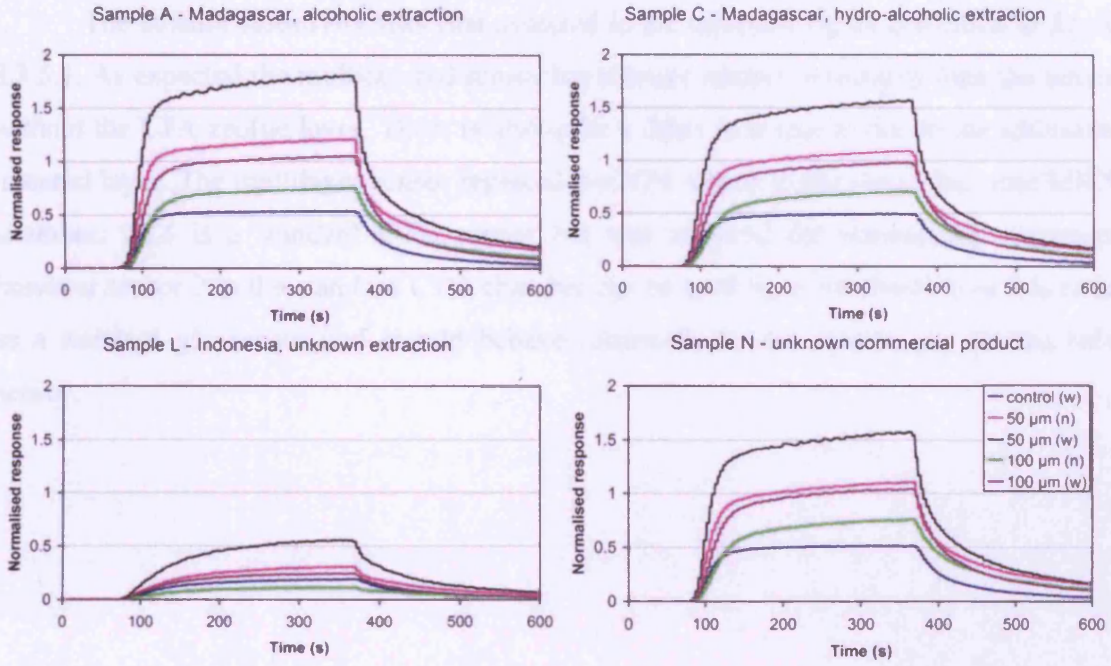

Figure 8.3.4.1 Vanilla extract samples - normalised sensor response transients using tungsten exchanged zeolite Y sensors (4 layers – 50µm, 8 layers – 100µm).
Y-axis describes normalized response against control narrow gap. X-axis: time (s).

Sample L has given a very much lower normalised response transient as opposed to the other samples. Sample L has a very low vanillin content in contrast to the other samples that could account for this difference. The vanillin is getting cracked by the catalytic layer which is producing an enhancement in response due to the increased sensitivity induced by these additional cracked products that the CTO is sensing.

8.3.5 Integration of multilayered sensor into MICS chamber

As described in chapter 4.7 the idea of a multilayered sensor was put forward to aid discrimination by adding a filter layer for reaction products between the catalytic zeolite layer and the sensing CTO layer. Thus creating a sandwich structure as shown in figure 4.7.1.

From observations regarding the improvements in discrimination obtained by using a sensor with a 50 μm layer of Cr-zeolite Y as the catalytic layer as described in the previous section. Thus a multilayered sensor was fabricated using the same catalytic layer to see what effect an additional layer of LTA zeolite material might have considering it will absorb a large number of small molecules.

The ethanol sensitivity was first assessed in the injection rig as described in figure 8.3.5.1. As expected the multilayered sensor has a lower ethanol sensitivity than the sensor without the LTA zeolite layer. There is also quite a delay in response due to the additional material layer. The multilayer sensor replaced the NZ4 sensor in the electronic nose MICS chamber. NZ4 is a standard CTO sensor but was required for normalising responses however sensor 2 in the standard CTO chamber can be used for normalisation as it is rated as a standard gas sensor and should behave identically to the narrow gap on the NZ4 sensor.

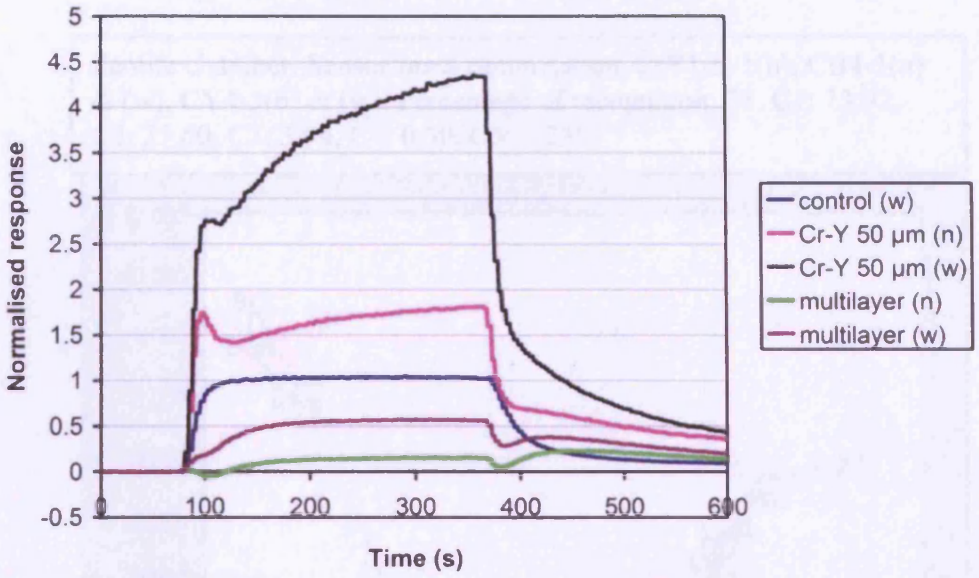

Figure 8.3.5.1 Comparison between multilayered and standard Cr-zeolite Y sensor under ethanol exposure in injection rig tested to ethanol.

8.3.6 Vanilla extract testing using optimised sensor array in MICS chamber

The following set-up was used in the electronic nose:
Chamber 1 – CrY1-L-1 (400°C), CB4-1(400°C), CY4-3(400°C)
Chamber 2 – Standard 'C' chamber.

Four samples of each vanillin extract sample type were tested (except M, N and O) in a random order.

All the plots shown below are DFA plots produced from the raw data taken from the electronic nose and no further manipulation was undertaken to correlate with testing undertaken at Biolandes.

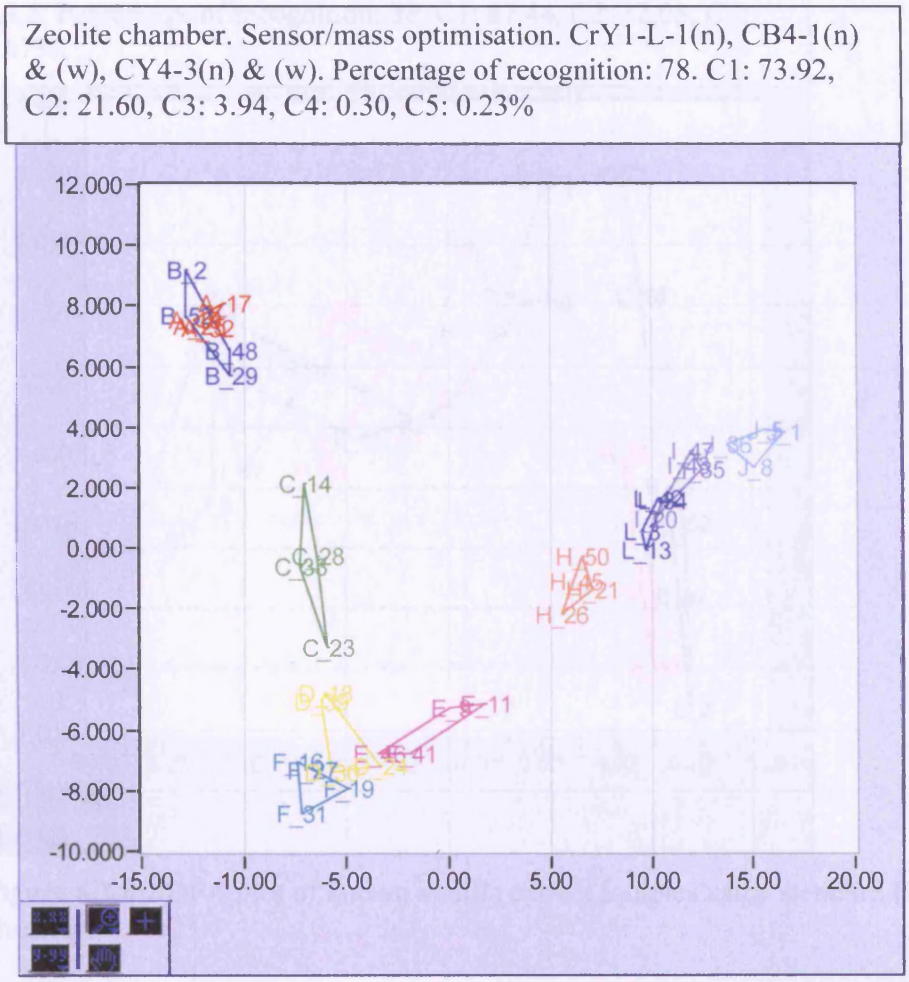

Figure 8.3.6.1 DFA plot of known vanilla extract samples using zeolite sensors chamber. All sensors operating at 400°C.

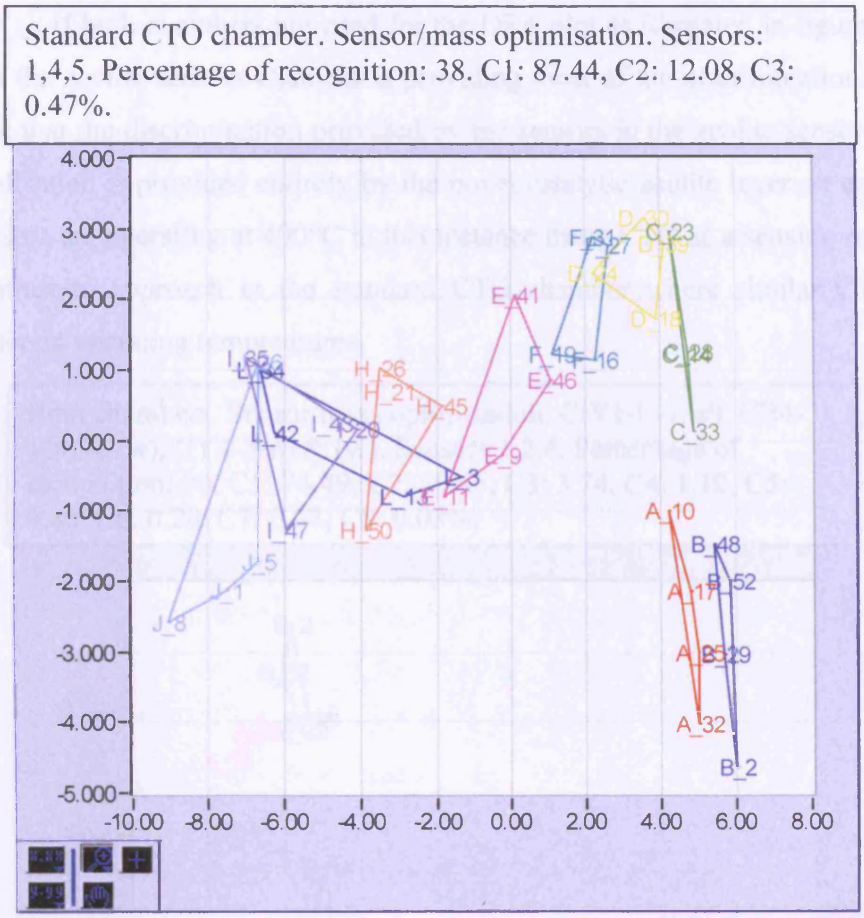

Figure 8.3.6.2 DFA plot of known vanilla extract samples using standard CTO chamber.

In figure 8.3.6.1 the zeolite sensor chamber is discriminating the various samples relatively successfully. It does not seem to be able to distinguish between samples A and B which the standard CTO array seems to be able to do. The HPLC data suggests samples A and B are very similar and are both produced by an alcoholic extraction process however there must be other constituents that vary in magnitude which the zeolite sensors are unable to distinguish. The zeolite sensor chamber is using five of the six channels for the discrimination in this instance so all three sensors are being fully utilised. I and L are also not very well discriminated between because despite being from different origins both have low vanillin contents. However H also has a low vanillin content but is discriminated against. This could be due to the higher ethanol content H has compared to I and L which implies that ethanol content could still play quite a factor despite trying to evaporate it off during sample preparation.

If both chambers are used for the DFA plot as illustated in figure 8.3.6.3 it is clear that the zeolite sensors chamber is providing most of the discrimination. It is important to note that the discrimination provided by the sensors in the zeolite sensors chamber for this application is provided entirely by the novel catalytic zeolite layer on each sensor. All the sensors are operating at 400°C in this instance using CTO as a sensing material which is in contrast to approach in the standard CTO chamber where similar CTO sensors are at different operating temperatures.

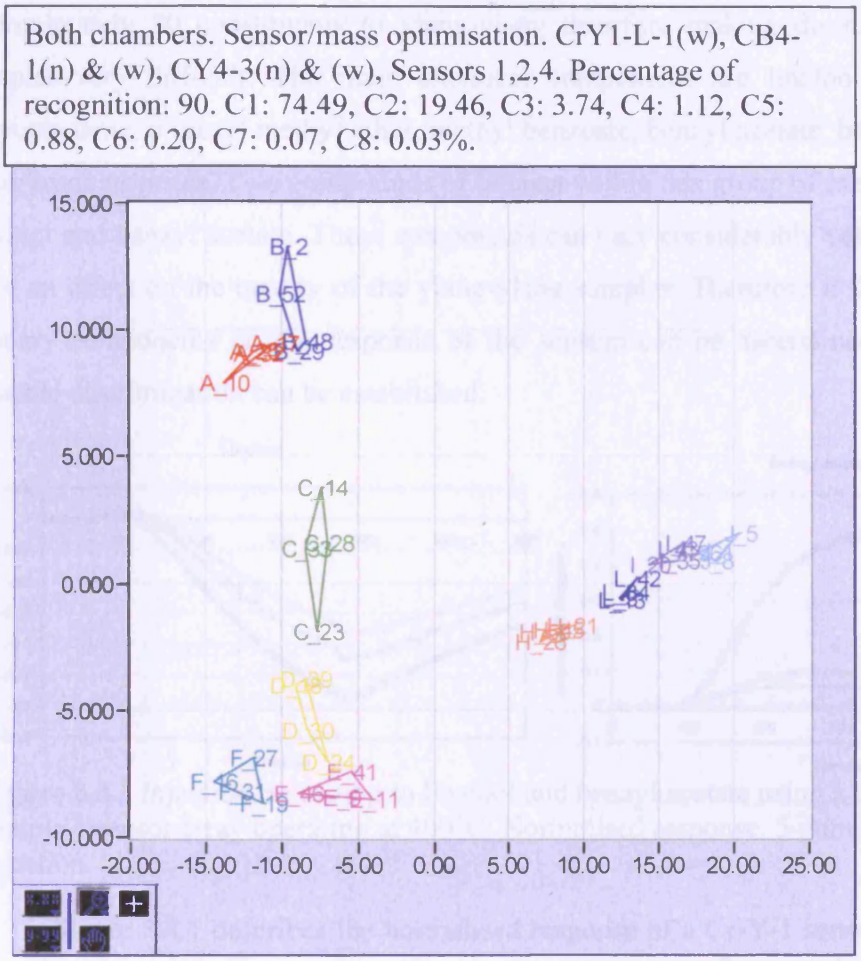

Figure 8.3.6.3 DFA plot of known vanilla extract samples using both chambers.

8.4 Development of array for Ylang-ylang testing

Ylang-ylang oil is extracted from the freshly picked flowers by water or steam distillation. There are different 'pressings' of ylang-ylang oil - called 'extra' and then 1st, 2nd and 3rd pressing. The extra is the very first pressing and contains the highest amounts of esters and therefore has the sweetest odour while the later pressings have a less-sweet odour. Details of the samples used in this work are available in Appendix V. Ylang-ylang has a more complex mixture of components than the vanilla extract samples; there are approximately 80 constituents to ylang-ylang therefore making discrimination between samples very difficult. The main chemical components are linalool, geranyl acetate, caryophyllene, p-cresyl methyl ether, methyl benzoate, benzyl acetate, benzyl benzoate and other sesquiterpenes. Two compounds of interest within this group of main components are linalool and benzyl acetate. These compounds can vary considerably between samples and have an effect on the quality of the ylang-ylang samples. Therefore if the effects of these primary components on the response of the sensors can be ascertained then a basis for possible discrimination can be established.

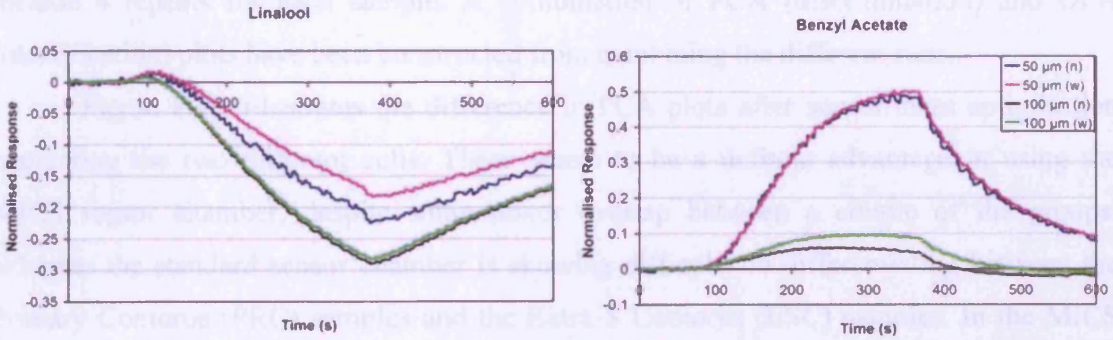

Figure 8.4.1 Injection rig testing to linalool and benzyl acetate using a Cr-zeolite Y sample 1 sensor array operating at 400°C. Normalised response, 5 minute gas injection.

Figure 8.4.1 describes the normalised response of a Cr-Y-1 sensor array to linalool and benzyl acetate. The difference in normalised response is apparent between the two different compounds. For the linalool sample the normalised response is negative due to the catalytic effect of the Cr-zeolite combusting a proportion of the sample to carbon dioxide and water. In contrast the normalised benzyl acetate response is positive thereby the Cr-zeolite layered sensors are showing greater sensitivity than the control, the 50 µm layered sensor is more sensitive than the 100 µm layered sensor. The enhanced response will be

due to the benzene ring within the benzyl acetate structure, the compound will be catalysed to a mixture of ketones and benzene. Benzene can easily pass through the zeolite structure unreacted and therefore this product compound along with the possible ketones has created the enhanced response. In contrast the linalool does not have a benzene ring within its structure and therefore is more easily fully combusted to carbon dioxide and water through the Cr-zeolite overlayer. The large difference in relative sensitivity between the 50 μm and the 100 μm overlayered sensors to benzyl acetate can be attributed to the effect of the thicker overlayer producing more fully oxidised reaction products.

30 samples of ylang-ylang from two sources (Comoros and Madagascar) were obtained from Biolandes to establish correlation of results with results from their electronic nose containing an equivalent sensor chamber containing the sensor array (CTO + 100 μm Cr-zeolite β sample 1, CTO + 100 μm Mo-zeolite Y sample 3, CTO + 100 μm Cr_2O_3). The same method of analysis used by Biolandes was utilised and all the samples were placed randomly in the autosampler's trays to avoid systematic errors.

Due to the large number of samples a number of runs had to be undertaken to include 4 repeats for each sample. A combination of PCA (discrimination) and DFA (identification) plots have been constructed from combining the different runs.

Figure 8.4.1 illustrates the difference in PCA plots after sensor/mass optimisation comparing the two different cells. There seems to be a definite advantage in using the MICS sensor chamber, despite some minor overlap between a couple of the groups. Whereas the standard sensor chamber is showing difficulty in differentiating between the Primary Comoros (PRC) samples and the Extra S Comoros (ESC) samples. In the MICS chamber it is again evident that the first two sensors in the chamber are doing most of the discrimination (Mo-zeolite Y sample 1 sensor and Cr-zeolite beta sample 1 sensor).

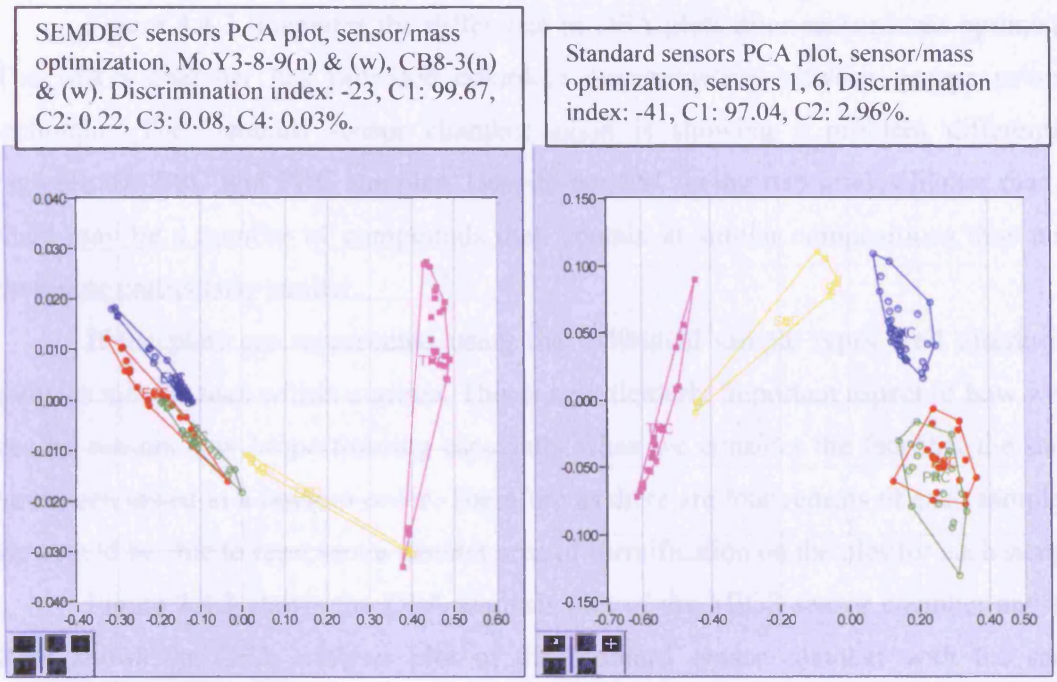

Figure 8.4.1 Principal Component Analysis (PCA) plots of the raw data from all Comoros samples labelled in groups – ESC, EXC, PRC, SEC, TRC.

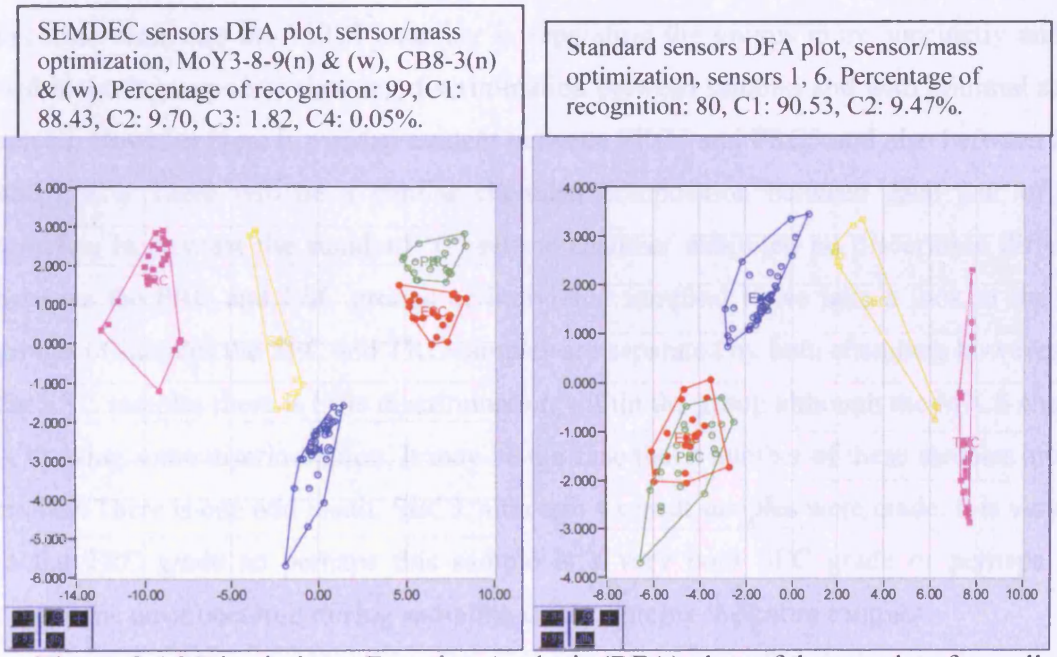

Figure 8.4.2 Discriminant Function Analysis (DFA) plots of the raw data from all Comoros samples labelled in groups - ESC, EXC, PRC, SEC, TRC.

Figure 8.4.2 illustrates the difference in DFA plots after sensor/mass optimisation. The MICS chamber has provided complete discrimination between groups using this technique. The standard sensor chamber again is showing a problem differentiating between the ESC and PRC samples. Despite the ESC being two grades higher than PRC there may be a number of compounds they contain at similar compositions thus making their note particularly similar.

If the plots are represented using the individual sample types well discriminated samples may be seen within a group. This is a particularly important aspect of how well the zeolite sensors may be performing especially when we consider the fact that the samples have been tested in a random order. Therefore as there are four repeats of each sample type we should be able to represent a distinct area of identification on the plot for each sample.

Figure 8.4.3 shows the DFA analysis plot of the MICS sensor chamber and figure 8.4.4 shows the DFA analysis plot of the standard sensor chamber with the samples grouped individually. Again we see that the ESC and PRC samples are grouped together however if a closer look is taken at the results as indicated in each plot respectively then it becomes clear that the MICS chamber is separating the groups more succinctly and also within those groups it is showing discrimination between samples and with minimal sample spread. However there is overlap evident between PRC1 and PRC3 and also between ESC1 and ESC7. There will be a similar chemical composition between each pair of these samples. In contrast the standard 'C' sensor chamber exhibited no discernible difference between the PRC and ESC groups or individual samples. If we take a look at the other groups of samples the SEC and TRC samples are separated by both chambers however with the EXC samples there is little discrimination within the group although the MICS chamber is showing some discrimination. It may be the case that a number of these samples are very similar. There is one odd result, SEC3, although 4 repeat samples were made. It is very near to the TRC grade so perhaps this sample is a very poor SEC grade or perhaps some systematic error occurred during sampling contaminating the entire sample.

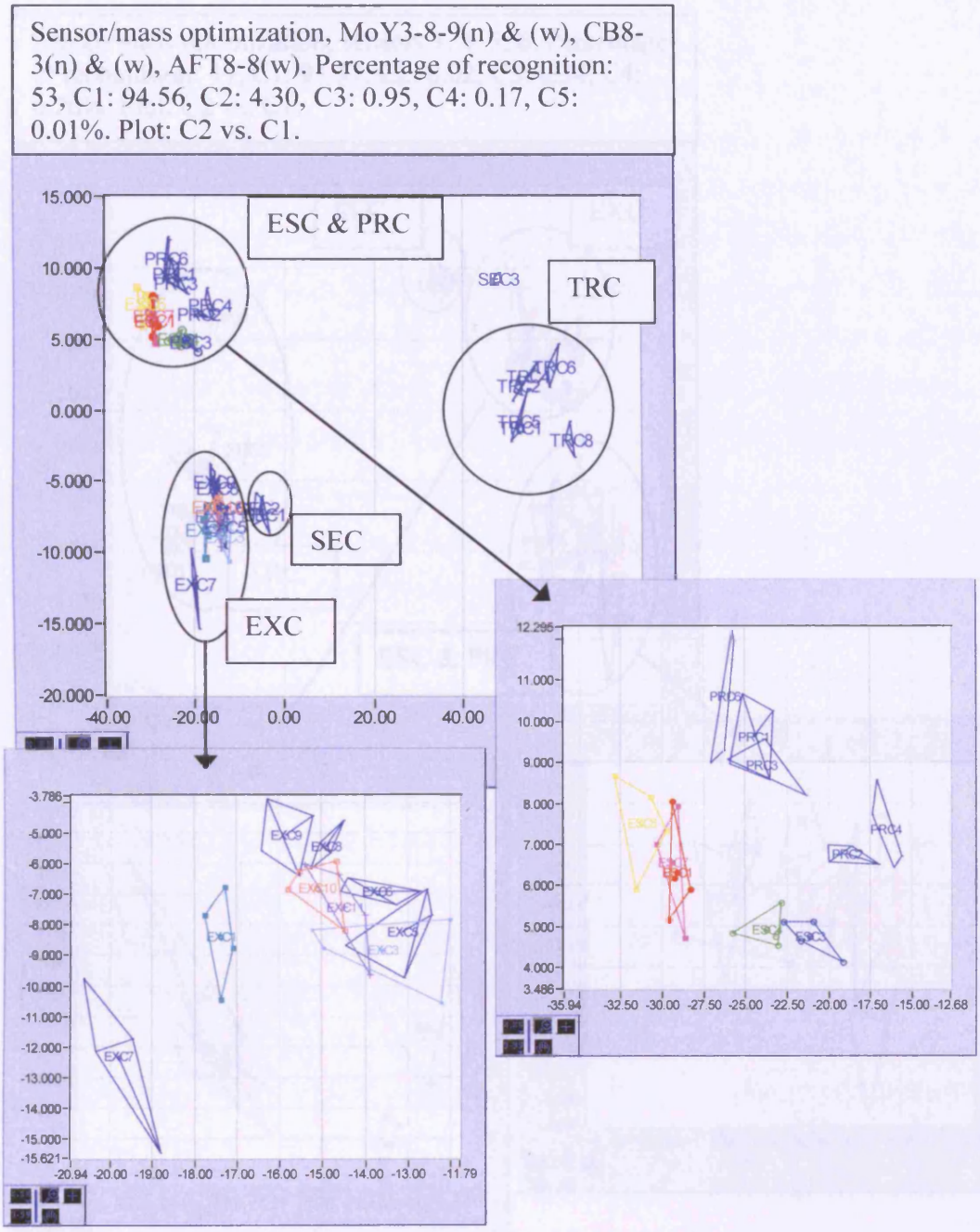

Figure 8.4.3 MICS chamber DFA analysis plots of raw data from all Comoros samples labelled individually.

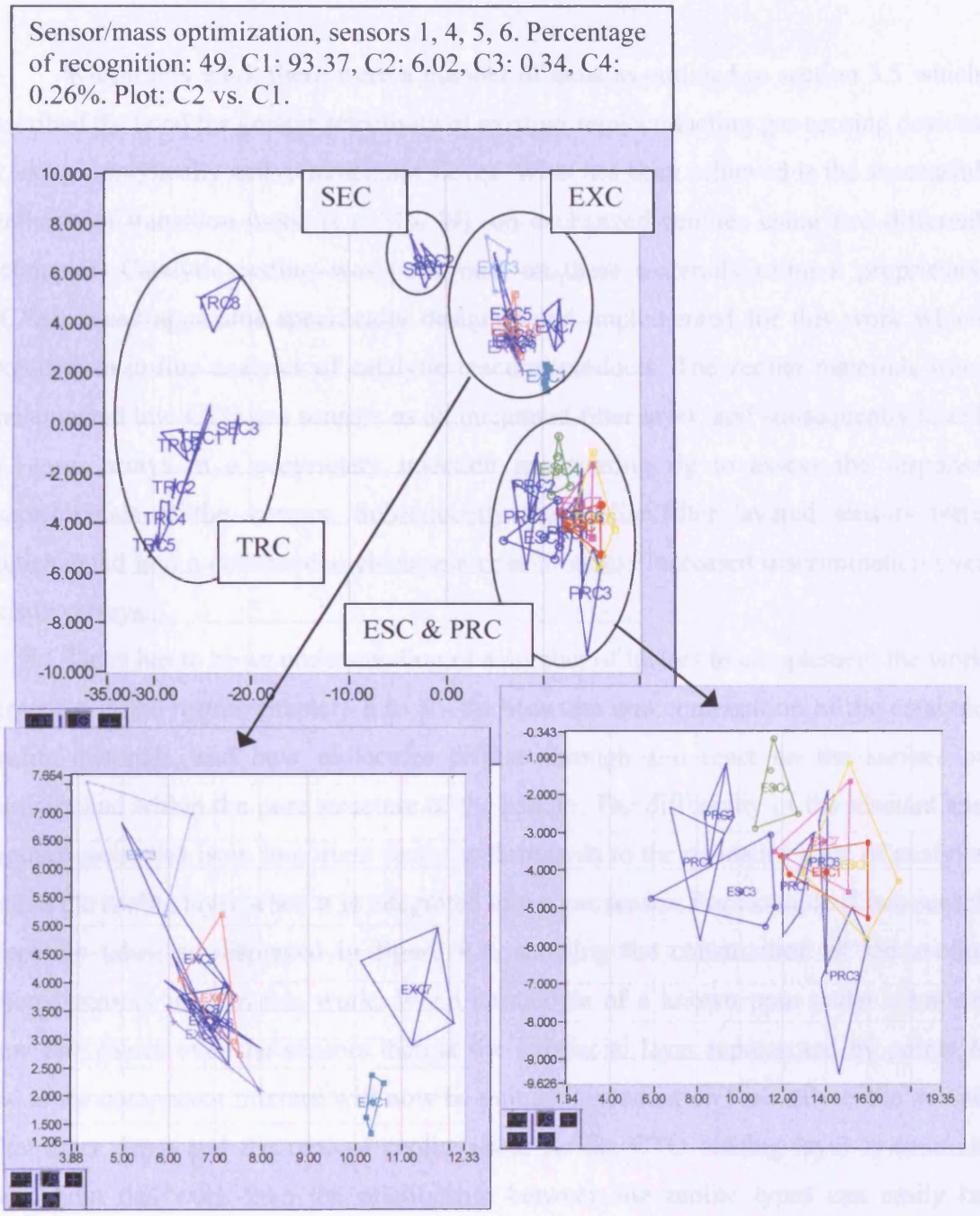

Figure 8.4.4 Standard sensor chamber DFA analysis plots of raw data from all Comoros samples labelled individually.

9. Discussion

Within this work there were a number of aims as outlined in section 3.5 which described the need for greater selectivity of existing semiconducting gas sensing devices by using catalytically active molecular sieves. What has been achieved is the successful synthesis of transition metal (Cr, Mo, W) ion exchanged zeolites using two different techniques. Catalytic testing was performed on these materials using a proprietary GC/MS based apparatus specifically designed and implemented for this work which provided an in-line analysis of catalytic reaction products. The zeolite materials were implemented into CTO gas sensors as an integrated filter layer, and subsequently tested in sensor arrays in a proprietary injection gas sensing rig to assess the response characteristics of the sensors. Subsequently the zeolite filter layered sensors were implemented into a commercial electronic nose to assess increased discrimination over existing arrays.

There has to be an understanding of a number of factors to complement the work presented in the results chapters 5 to 8 - the structure and composition of the catalytic zeolite materials, and how molecules diffuse through and react on the surface of particles and within the pore structure of the zeolite. The diffusivity of the reactant and product molecules is an important factor with regards to the residency time of analytes within the zeolite layer when it is integrated into a gas sensor. For example if two sensor types are taken as displayed in figure 9.1, showing the construction of the zeolite filtered sensors used in this work. When an analyte of a known ppm under a known flow rate passes over the sensors then at the interfacial layer represented by points A and B the component mixture will now be unique dependent on the analyte, the zeolite filter layer depth and the type of zeolite used. As the CTO sensing layer is constant throughout this work then the relationship between the zeolite types can easily be assessed on chip as described in chapter 7 after the normalisation of data to the control. Therefore after the normalisation of data this is an excellent way of testing the effectiveness of a catalyst. The surface area is constant for all sensors made and material depth is known and thus there is a known volume of material undertaking catalysis which is effectively being assessed by the underlying CTO layer.

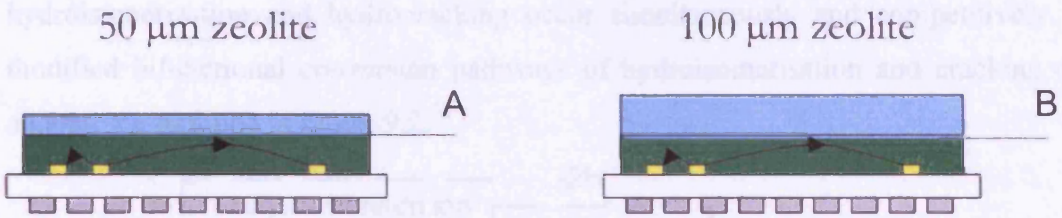

Figure 9.1 Schematic representation of a 50 μm layered sensor and 100 μm layered CTO sensor.

Materials characterisation to assess the levels of transition metal incorporated into the zeolites was primarily by EDAX (results displayed in table 5.2.1). This produced a good comparison of the materials and the associated M/Al ratio after exchange. Other methods of analysis could have been used to characterise the molecular structure of the supported metal ions as it can be complicated. The deposition of chromium ions on a support, for example, can result in (a) isolated chromium ions, (b) a two-dimensional chromium oxide overlayer, or (c) three-dimensional chromium oxide crystallites, and each phase can possess several different molecular structures. [33, 64] Thus if quantitative information is required, techniques which can provide detailed information about the molecular structure of the supported chromium oxide must be capable of discriminating between these different states, and of quantifying the individual oxidation states. Useful spectroscopic characterisation techniques for this type of characterisation are ESR (electron spin resonance), DRS (diffuse reflectance spectroscopy), RS (Raman spectroscopy), IR (infrared spectroscopy), and XPS (X-ray photoelectron spectroscopy). In this work one technique was chosen to provide qualitative details of dispersion to be defined as the ratio of the amount of metal over the total amount present on the surface. There was no need to fully characterise the transition metal exchanged zeolites with a range of techniques as only a comparison in metal loadings is required and information on the homogeneity of the samples. As long as there is a comparative difference in metal loadings the catalytic properties thus ascertained on the GC/MS and the subsequent sensor properties can then be related back to the findings from the EDAX measurements.

The catalytic property testing presented in chapter 6 provided useful information regarding the reaction products, along with the relative activity of the different samples. It was clear from the results regarding the Cr, Mo and W exchanged samples that were all exchanged using an aqueous ion exchange that the reaction products consisted of a mixture of linear and branched alkanes if the feed analyte was an n-alkane. The transition metal exchanged zeolites are acting as bifunctional catalysts,

hydroisomerisation and hydrocracking occur simultaneously and competitively. The modified bifunctional conversion pathways of hydroisomerisation and cracking of n-alkanes are outlined in figure 9.2.[76]

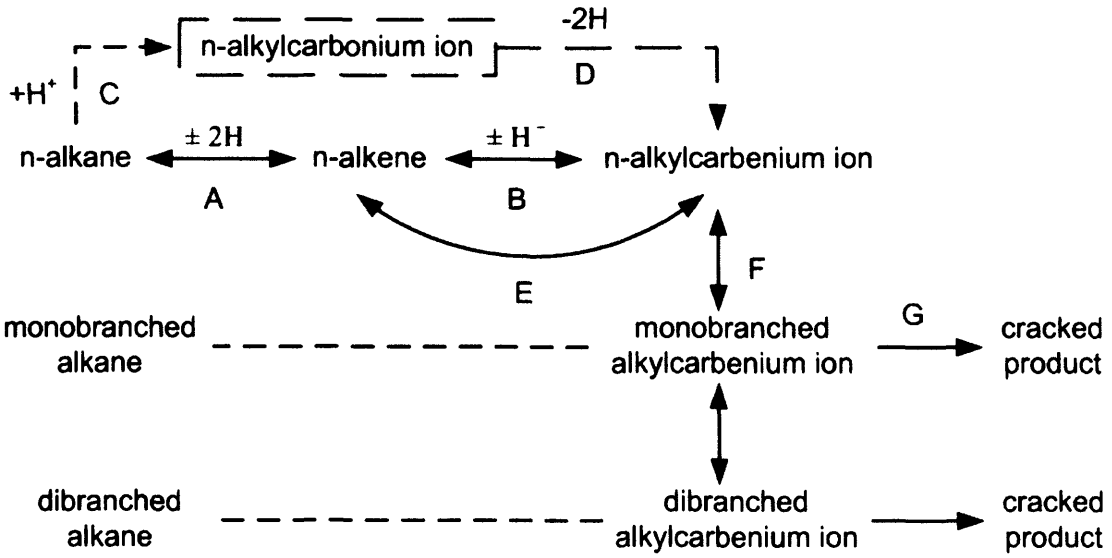

Figure 9.2 Modified bifunctional pathways of hydroisomerisation and cracking of n-alkane

A: hydrogenation-dehydrogenation on metallic sites

B: protonation-deprotonation on acid sites

C: addition of proton to form alkylcarbonium ion on acid sites

D: dehydrogenation to form alkylcarbenium ion

E: competitive adsorption-desorption of alkene and carbenium ion on acid sites

F: rearrangement of alkylcarbenium ion

G: cracking of alkylcarbenium ion

Alkenes are generated through dehydrogenation of alkane on metallic sites (Path A). The carbonium ions can also be generated by addition of protons to alkanes on acid sites (Path C). The carbenium ions are generated through protonation of alkenes on acidic sites (Path B) or dehydrogenation of carbonium ion (Path D). Alkylcarbenium ions can either rearrange themselves (Path F) or undergo cracking through β-scission (Path G) which gives rise to a smaller carbenium ion and an alkene fragment, which is immediately hydrogenated.

Octane through Cr-zeolite Y sample 1 at 300°C, for example, produced methyl-propane, butane, methyl-butane and pentane. Octane first goes through dehydrogenation to octene on the metallic sites, followed by protonation to an alkylcarbenium ion which is rearranged to a monobranched alkylcarbenium which gets cracked to a smaller carbenium ion and an alkene fragment, which is immediately hydrogenated. For octane

and the other linear alkanes tested at this temperature there was no evidence of dibranched alkanes as products, due to the shape selectivity of the zeolites, as the dibranched alkanes cannot be formed in the zeolite pores. The proportions of products identified in the aforementioned GC/MS test were as follows: methyl-propane 8 %, butane 8 %, methyl-butane 7 %, and pentane 17 %. The proportion of products will depend on the diffusivity of the analyte and reaction products through the zeolite and the relationship this has with access to the catalytic sites and the catalytic rate.

With regard to the injection rig testing there are certain constants that can be assumed to help understand the relationship between the transition metal loading, the depth of catalytic material on the sensor and the transient characteristics. In figures 9.3 and 9.4 this fundamental relationship has been displayed by utilising the sensor responses to nonane using three sets of sensor arrays – CrY1 (Cr/Al = 1.20), CrY3 (Cr/Al = 0.79) and CrY4 (Cr/Al = 0.06) over a number of repeat tests. Figure 9.3 details the responses from the wide gap electrode and figure 9.4 details responses from the narrow gap electrode. The normalised responses have been used to provide a ratio of response as a function of zeolite layer height per μm depth of material as shown by the y-axis. The x-axis displays the Cr content. When y = 0 there is no difference from the control sensor thus this indicates that there is no effect from the catalytic layer.

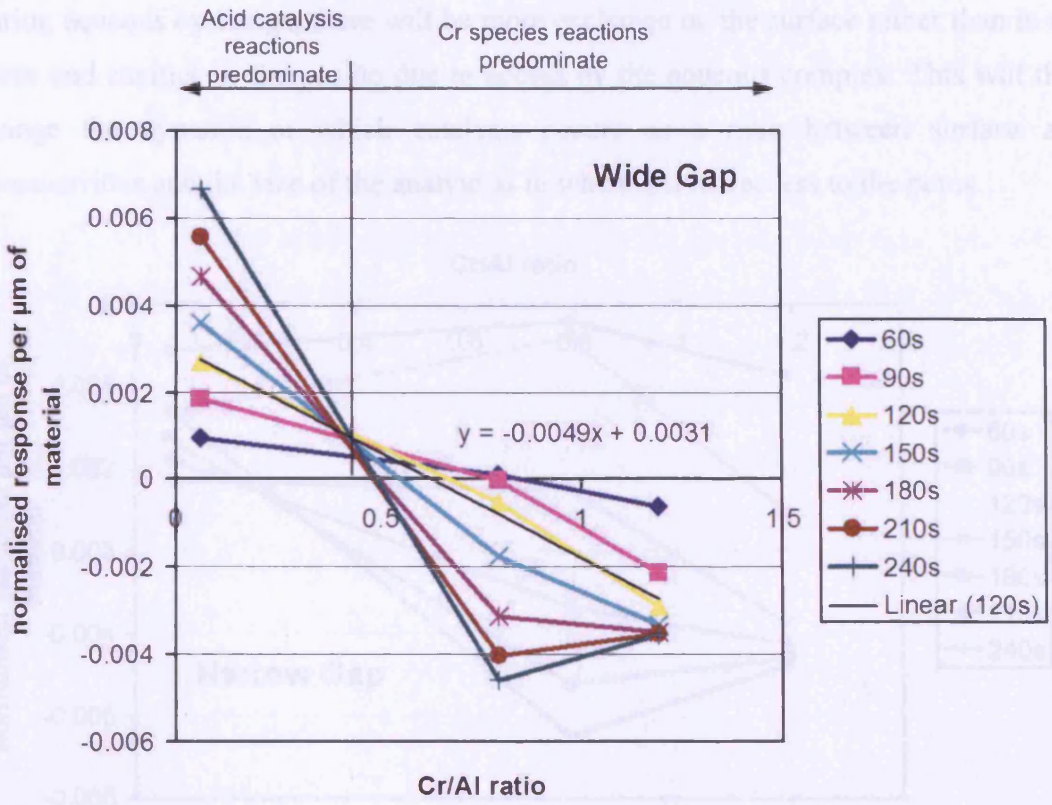

Figure 9.3 Plot showing the relationship between the Cr/Al ratio in Cr-zeolite Y and the normalised response from the wide gap per µm of material. CrY1, CrY3 and CrY4 sensors tested to nonane in the injection rig. Points taken from along the transient responses as indicated in the legend.

Figure 9.3 shows the variation in response per µm of material for varying Cr levels in Cr-zeolite Y. The wide gap is a good indicator of the catalytic effect of the zeolite filter layer only as it interrogates the upper portion of the CTO layer, as opposed to the narrow gap (see figure 9.4) which interrogates the lower portion. There will be lower normalised responses across the narrow gap as there will be a certain depth of CTO to provide further reaction.

In Figure 9.3 the variation in Cr content affects the catalysis type and efficiency as it increases. Typical acid catalysis is dominant below a Cr/Al ratio of approximately 0.4, thereafter the effects of Cr species predominates. Typically transition metals are introduced into zeolites to enhance the catalytic effect and it is clear in figure 9.3 that at the Cr level of 0.79 there is greater catalytic activity combusting more of the analyte to carbon dioxide and water hence $y < 1$. As you go over a Cr/Al ratio of 1 it is speculated that there are more numerous Cr_2O_3 clusters blocking pore openings and therefore a reduction in catalytic effectiveness. Also residency time may be playing a factor in reaching equilibrium throughout the zeolite filter layer. It could also be suggested that the acid catalysis is effective only until a Cr/Al ratio 0.4 rather than at 0.5, because

during aqueous exchange, there will be more exchange on the surface rather than in the pores and cavities in the zeolite due to access by the aqueous complex. This will thus change the dynamic at which catalysis occurs as a ratio between surface and pores/cavities and the size of the analyte as to whether it has access to the pores.

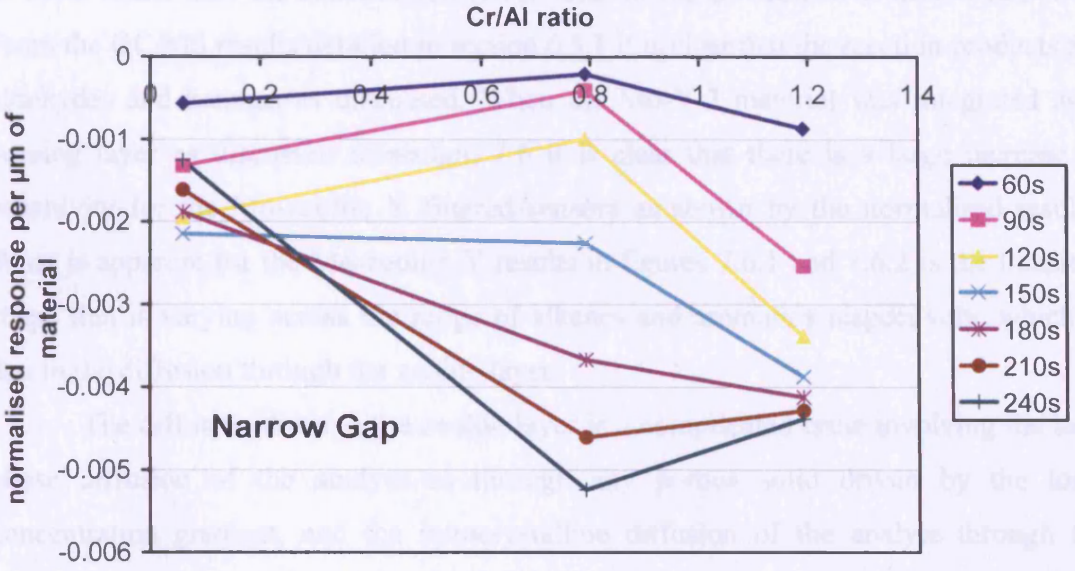

Figure 9.4 Plot showing the relationship between the Cr/Al ratio in Cr-zeolite Y and the normalised response from the narrow gap per µm of material. CrY1, CrY3 and CrY4 sensors tested to nonane in the injection rig. Points taken from along the transient responses as indicated in the legend.

Figure 9.4 shows the averaged responses across the narrow gap. All points are below y = 0 indicating that across the Cr-zeolite Y material range displayed the narrow gap is always less sensitive than the control. It would have helped if there were further Cr-zeolites made with different Cr/Al levels for both figures 9.3 and 9.4 to provide a clearer picture. With varying Cr/Al levels some of the reaction steps may be catalysed by one kind of site, and others by a second kind of site. This could occur in series and both kinds of sites must be in proximity to one another in order for the overall reaction to occur and usually they are both on the same catalyst particle. This for example explains the presence of the branched alkanes in some of the reaction products as discussed earlier. The alkane is first dehydrogenated to an alkene, the alkene isomerises to an isoalkene, which is hydrogenated to an isoalkane. The hydrogenation and dehydrogenation steps occur on the Cr complex, the isomerisation steps on an acid site. This also emphasises the change in reaction kinetics observed in figure 9.3 whereupon the change in reaction site distribution affects reaction product distribution and ultimately the sensor response.

The solid state exchanged Mo-zeolites in contrast to the aqueous exchanged Cr-zeolites produced partially oxidised organic species from the alkane feedstock. With the type of exchange there will be a high proportion of MoO_3 clusters as discussed in chapter 5 using the EDAX analysis. Therefore there are two distinct phases for reaction to occur rather than the combination effect seen for the Cr-zeolites as described above. From the GC/MS results detailed in section 6.5.1 it is clear that the reaction products are aldehydes and ketones as discussed. When the Mo-Y-3 material was integrated as a sensing layer as discussed in section 7.6 it is clear that there is a large increase in sensitivity for the Mo-zeolite Y filtered sensors as shown by the normalised results. What is apparent for the Mo-zeolite Y results in figures 7.6.1 and 7.6.2 is the transient shape that is varying across the range of alkanes and aromatics respectively, which is due to the diffusion through the zeolite layer.

The diffusion through the zeolite layer is a complicated issue involving the bulk phase diffusion of the analyte as through any porous solid driven by the local concentration gradient, and the intracrystalline diffusion of the analyte through the zeolite pores. Mass transport in the intracrystalline space of the zeolites is strongly influenced by interactions between diffusing molecules and the walls of the zeolite channels, therefore the diffusivity, D, can vary over a range from 10^{-4} to 10^{-16} cm^2s^{-1}.

If the system in the GC/MS apparatus is observed the bulk diffusivity can be ascertained through the volume of the material from the experimental set-up.

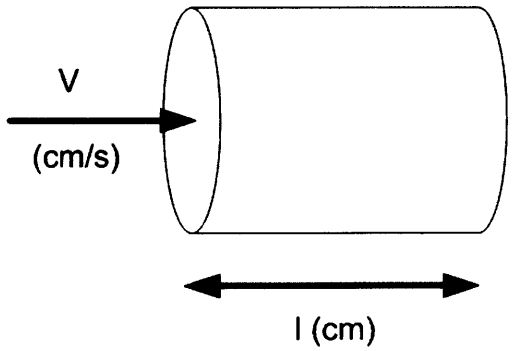

Figure 9.5 Schematic of diffusion parameters for diffusion of analytes through zeolite bed associated with GC/MS apparatus.

So the time for diffusion, $\tau_l = l / v$ (1)

where linear velocity, v = flow rate into zeolite bed / cross sectional area

$v = 10$ ml/min / $\pi.r^2$

$v = 31.5$ cm/min

bed depth, l = 0.5 cm

therefore, $\tau_1 = 0.95$ s

Time for particle interaction, $\tau_2 = r^2 / D`$ where r is particle radius and D` is the diffusivity.

For the sensor the diffusion system can be simplified because of the nature of the sensor construction as outlined in figure 9.1 therefore for depth h of material:

$$\tau = h^2 / D` \qquad (2)$$

Therefore for a depth of 100 μm, $\tau = 10^{-4}$ cm^2 / D`. The diffusivity through a porous sensor structure of this type has been measured experimentally to be in the order of, D` ~ 10^{-3} to 10^{-4} cm^{2}s^{-1}. [77] Therefore $\tau \sim 0.1$ to 1 s.

Therefore the results from materials in the reactor bed in the GC/MS apparatus can be directly related to the sensor construction. It should be noted that in the reactor bed powdered material is used as opposed to sintered material in the sensor, so there will be a surface area difference however it will not be any order of magnitude different. [77]

Knowing the diffusion characteristics of both systems is useful for assessing the response characteristics of the CTO sensing layer to all the analytes tested as outlined in section 7.1. The difference between the two electrode responses can be assumed to be the height of the control sensor as they interrogate both the top and bottom sections of the sensor material.

If the normalised responses of the zeolite filtered sensors are taken it could be observed that information pertaining to the diffusivity can be obtained from the difference in response on the wide gap between the 50 μm and 100 μm sensors and thus obtain the diffusivity, D` for each analyte through the catalytic zeolite materials. The wide gap is monitoring the reaction products from the zeolite filter layer in real time therefore it may be possible to ascertain the time for diffusion, τ, from features in the response difference. By using the normalised responses we are ignoring the effects of concentration.

Therefore if the example of a heptane response in the injection rig is taken using the 100 μm and 50 μm Cr-zeolite Y sample 1 sensors as shown in figure 9.6 there is a difference in the transient response. There is a time for which the sensors reach equilibrium with each other until there is a constant difference.

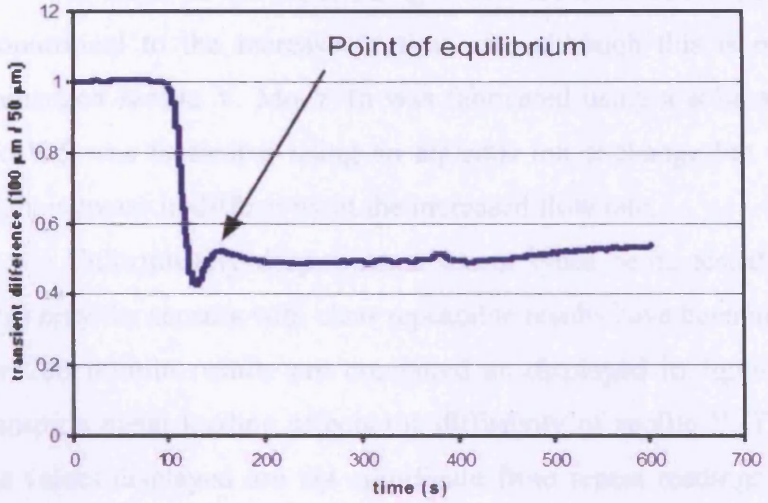

Figure 9.6 Difference in normalised transients between the wide gaps on the 100 µm and 50 µm Cr-zeolite Y sample 1 sensors. Heptane response in the injection rig. Air flow at 200 ml/min.

From the point of equilibrium the time, τ can be calculated from knowing the time of injection and by taking into account any time lag for analyte to reach the sensors at 100 ml/min through the heated tubing of the injection rig. The layer heights of the sensors are known as detailed in appendix II.

Therefore for the diffusivity of heptane through Cr-Y-1 from a rearrangement of equation (2):

$$D` = h^2 / \tau \qquad (3)$$

$$= (0.0057)^2 / 89$$

$$= 3.65 \times 10^{-7} \text{ cm}^2/\text{s}$$

Across the range of zeolite filtered sensors fabricated all were tested to 100 ppm ethanol at flow rates of 100 ml/min and 200 ml/min. Therefore from this data a comparison of diffusivities can be constructed.

Sample	M/Al ratio	Flow rate (ml/min)	D` (cm²/s)
Cr-Y-1	1.19	100	3.35E-07
Cr-Y-1	1.19	200	5.76E-07
Cr-Y-3	0.79	100	1.57E-07
Cr-Y-3	0.79	200	2.81E-07
Mo-Y-1a	0.2	100	5.1E-07
Mo-Y-1a	0.2	200	5.85E-07
Mo-Y-5	0.07	100	1.57E-07
Mo-Y-5	0.07	200	1.98E-07
W-Y-1	0.1	200	2.43E-07

Table 9.1 Table of calculated diffusivities of ethanol through the various transition metal exchanged zeolites. Calculated from normalised transients obtained from sensor arrays in the injection rig. All sensors operating at 400°C.

In table 9.1 the Cr exchanged zeolites have an increase in diffusivity which is proportional to the increase in flow rate although this is not exhibited by the Mo exchanged zeolite Y. Mo-Y-1a was fabricated using a solid state ion exchange whilst Mo-Y-5 was fabricated using an aqueous ion exchange but they both exhibit only a slight increase in diffusivity at the increased flow rate.

Unfortunately despite most sensor types being tested to ethanol to both flow rates only the sensors with clear repeatable results have been included in table 9.1. If all the 200 ml/min results are compared as displayed in figure 9.7 it is clear that the transition metal loading affects the diffusivity of zeolite Y. The errors associated with the values displayed are not significant from repeat readings. Also as you increase in metal ion size Cr < Mo < W this also affects the diffusivity. With further testing and by using a broad range of metal loadings it may be possible to calculate the constant for which a particular metal affects the diffusivity.

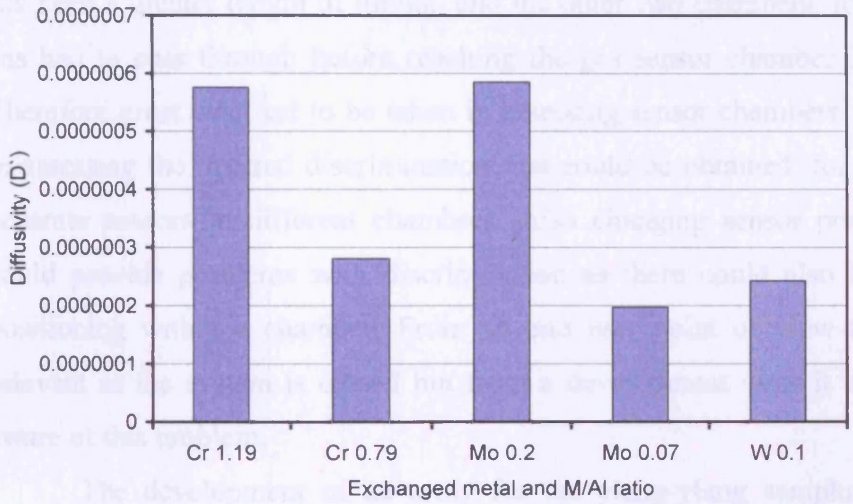

Figure 9.7 Diffusivity comparison of the transition metal exchanged zeolite Y as integrated as a filter layer on a CTO sensor. Tested to 100 ppm ethanol in the injection rig at 200 ml/min. All sensors operating at 400°C.

The diffusivity behaviour is also a characteristic concerning the plots in figure 9.2 which relates to the diffusion and reaction of nonane through the various loadings of Cr-zeolite Y. The trend line indicated whereupon the loading behaviour is linear will relate to the material type, i.e. zeolite Y. The gradient indicated at this point will be indicative of the zeolite type with regard to that particular exchanged metal ion and the analyte tested. Therefore there should be a relationship between this gradient relating to response per μm of material and the diffusivity calculation for each material.

When the sensors were entered into the electronic nose there were a number of interesting points that were discovered. The electronic nose has the option to have up to

three different sensor chambers (see figure 4.9.2) in the apparatus at any one time for increased discrimination possibilities. It was usual during this work to have one or two chambers containing the zeolite filtered sensors and one standard 'C' chamber which was factory standard from Alpha-MOS. Each chamber is interconnected with a length of PTFE tubing which differed from the injection rig in which all tubing was stainless steel heated to above the injection temperature. This difference was critical in the potential for transferability of the sensor technology between the injection rig and the electronic nose as the testing outlined in figure 9.8 outlines. The problem being that the unheated PTFE tubing acts as a capillary column within the electronic nose apparatus. In figure 9.8 a set zeolite filtered sensors were set up in chamber 1 and tested to a set of adulterated ylang-ylang samples and then the chamber was moved to be third in line within the electronic nose. The discrimination improves dramatically by moving the gas sensor chamber from the chamber 1 position to the chamber 3 position because there has been a greater length of tubing, and the other two chambers, for which the sample has had to pass through before reaching the gas sensor chamber 3rd in the sequence. Therefore great care had to be taken in assessing sensor chambers with each other and in assessing the optimal discrimination that could be obtained, for example, from two separate sensors in different chambers. Also changing sensor position within arrays could provide problems with discrimination as there could also be variation due to positioning within a chamber. From an end user point of view this problem is not relevant as the system is closed but from a development view it was necessary to be aware of this problem.

The development of an array for the ylang-ylang samples that had over 80 components proved very difficult due to the complexity of the samples and the minor variability in composition. However discrimination improvement was seen as outlined in section 8.4.

The vanilla extract testing had a successful development from the injection rig to the electronic nose. Vanilla extract has fewer components than ylang-ylang with the predominant one being alcohol therefore array development was accomplished successfully. The transfer of technology from the injection rig to electronic nose was methodically implemented from the testing of the main constituents; vanillin, vanillic acid, p-hydroxy benzoic acid and p-hydroxy benzaldehyde.

Chamber 1: Discrimination index: -18, C1: 89.02, C2: 10.55, C3: 0.43%. Discrimination using $(R/Ro)^2$-1. C2 vs. C1.

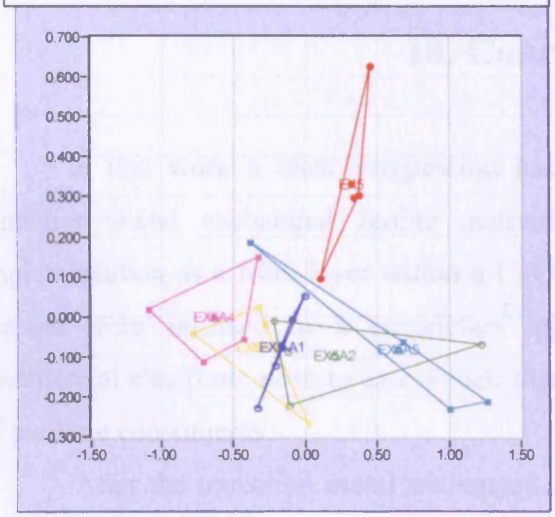

Chamber 3: Discrimination index: 71, C1: 99.53, C2: 0.46, C3: 0.01%. Discrimination using $(R/Ro)^2$-1. C2 vs. C1.

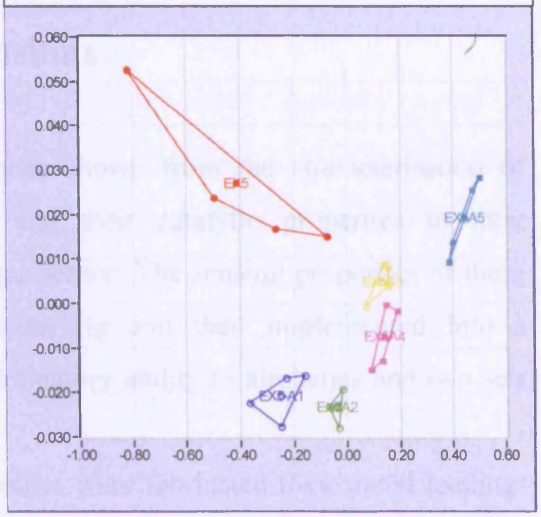

Key: EX5: control, EX5-A1: 10% farnesene, EX5-A2: 10% linalool, EX5-A3: 10% benzyl acetate, EX5-A4: 10% eugenol, EX5-A5: 10% 3-caryophyllene.

Figure 9.8 Comparison of discrimination of adulterated samples when two sensors (MoY3-8-2, CB8-3) are in the first chamber as opposed to the third chamber under the same conditions

10. Conclusions

In this work a clear progression has been shown from the characterisation of transition metal exchanged zeolite materials and their catalytic properties to their implementation as a filter layer within a CTO gas sensor. The sensing properties of these sensors were assessed in a proprietary injection rig and then implemented into a commercial electronic nose to assess their discriminatory ability to aliphatics and two sets of perfume constituents.

After the transition metal exchanged zeolites were fabricated their metal loadings were successfully assessed using EDAX and a suitable ratio M/Al was introduced to assess the loading as exchange occurs with the ion or proton present at the Al sites within the zeolite structure. Reactivity tests using hydrogen and a CTO sensor were also performed to give a simple activity assessment. This was a unique, simple and quick method to assess the relative activity of the zeolites and did correlate with the activity observed in the subsequent GC/MS testing.

The in-line zeolite bed/thermal desorber/GC/MS arrangement worked successfully in assessing the catalytic reaction products of a number of analytes through the range of zeolite materials. For the Cr and Mo exchanged zeolite Y samples there was evidence of specific selectivity at nonane in the aliphatic series. The different Mo exchanges - solid state exchange and aqueous, produced differing reaction products. Aldehydes and ketones were produced from the solid state exchange, linear and branched alkanes from the aqueous exchange.

The injection rig results complemented the GC/MS data therefore exhibiting a follow through of experimental technique and analysis from one system to another. The best example being the selectivity of nonane through Cr-zeolite Y sample as shown in figures 6.4.2 and 7.4.1 respectively. The transient information pertained from the injection rig data gave good indication of the discrimination within compound groups such as the aliphatics and aromatics tested. It proposed the idea that transient data can be used to identify or discriminate specific compounds in relation to compound mixtures. The

injection rig data were also utilised to calculate the diffusivity of compounds through the zeolite filter as mentioned in the discussion.

The electronic nose results showed the improved discrimination attainable using the zeolite filtered sensors over the standard 'C' chamber for both the ylang-ylang samples and the vanilla extract samples. Also transient data from the injection rig were utilised to create discriminatory graphs using a standard statistical software package. This shows progression in technique which can be used in the future to ascertain sensor suitability within an electronic nose.

11. Future Developments

The future possibilities for this work are wide ranging, the sensors developed have practical applications on a single component level and when integrated into an array for the purposes of discriminating mixtures.

If you take the analysis methods used in this work, these themselves can be utilised in the future to develop catalysts. The in line method using the thermal desorber and GC/MS proved difficult to establish a suitable working method but once implemented the results proved repeatable and conclusive. There are two ways in which the apparatus could be adapted to provide additional information. One is the use of a controlled injection such as that used for the injection rig to pass analyte through the zeolite bed instead of the pulsed injection used. The thermal desorber would need to be adjusted to allow for a large inlet time to collect the reaction products however this may not allow for collecting sufficient sample to subsequently transfer to the GC. The second improvement possible would be to implement a sensor itself within an outlet of the thermal desorber. The outline of the implementation is detailed in figure 11.1. This would allow for the excess sample that is not sent to the GC from the thermal desorber which is sent via the split tube to be sent via a sensor chamber. This would hopefully enable a monitoring of the reaction products using a standard CTO sensor as they are desorbed from the cold trap during the heated temperature ramp. Also this would create additional sensor transient data to correlate with the injection rig data when the material is integrated as a filter layer. The main possible problem with this system is the integration of the air supply into the sensor chamber along with the reaction products from the thermal desorber.

The development of the sensors with a catalytic zeolite filter layer provides future possibilities for commercial devices with improved sensitivity and selectivity for specific application purposes. Improved sensitivity devices such as the Mo-zeolite Y sensors where the zeolite material had undergone a solid state ion exchange could be used for detecting low ppm's of volatile hydrocarbons. There was an increase in sensitivity to heptane to an order of 10 times with the sensors operating at 400°C compared to the control sensor. When the sensors were operating at 420°C there was an increase in sensitivity to the

magnitude of 25 times. Thus the ability of the zeolite layer not only to enable the sensor to be more selective as was shown in chapter 7, but to facilitate the catalysis of large compounds into smaller compounds that CTO is more sensitive to, is an advantage over existing sensor devices. Also the transient information obtained from normalising sensor responses is key in determining component mixtures in the future.

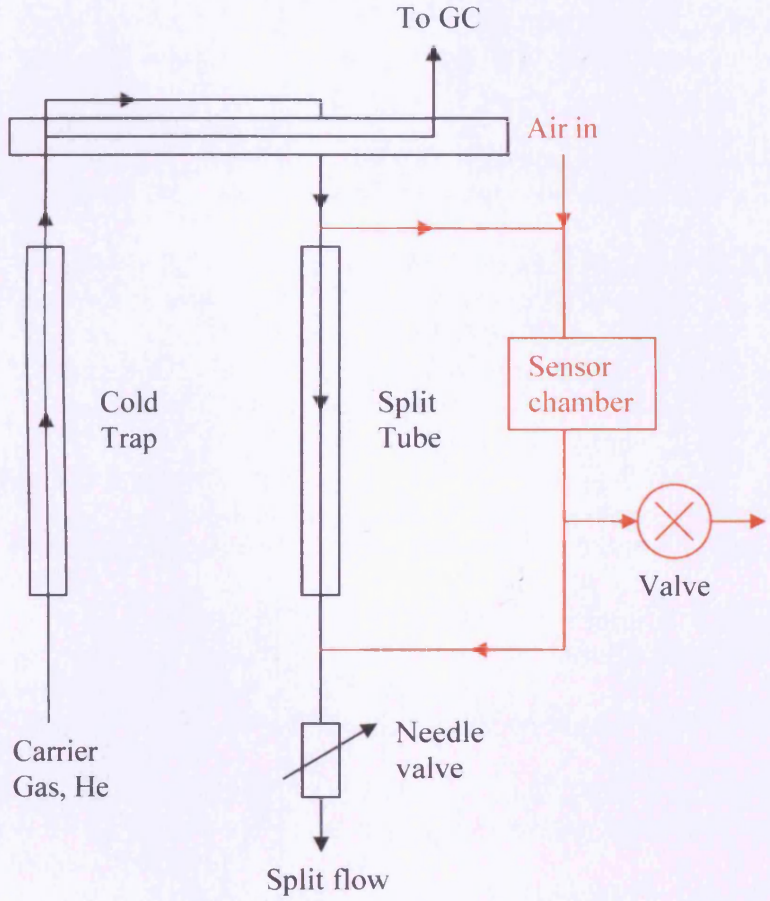

Figure 11.1 Schematic of thermal desorber operation and sample flow with possible sensor chamber addition highlighted in red.

The improved selectivity exhibited using the zeolite filtered sensors to analytes of similar organic structure is going to prove invaluable in the future development of electronic noses. Traditionally the metal oxide sensing arrays operate different sensing materials and/or operating temperatures. In this work the improved discrimination was achieved by using a materials based approach with the sensors operating at the same temperature and the sensing material being common throughout. From this standpoint it is clear that there are many factors that still need to be considered in the future developments of artificial olfactory systems. Further development is required to enable devices to break

away from the traditional standpoint of training such devices to provide qualitative comparison analysis and focus on a more quantitative first time approach to chemical analysis.

References

[1] Moseley P.T., Tofield B.C. (1987) *Solid State Gas Sensors.* Adam Hilger, Bristol.
[2] Moseley P.T., Norris J.O.W., Williams D.E. (1991) *Techniques and Mechanisms in Gas Sensing.* Adam Hilger, Bristol.
[3] Fairley P.D., Rutt H.N. (2001) A Novel gas concentration monitor using a solid state modulator. *Sensors and Actuators B: Chemical.* **75**, pp. 192-196.
[4] Janata J. (1989), *Principles of chemical sensors.* Plenum Press, New York.
[5] www.citytech.co.uk City Technology Ltd, Walton Road, Portsmouth, Hampshire, PO6 1SZ, UK.
[6] www.figarosensor.com
[7] Williams D.E., Pratt K.F.E. (2000) Microstructure effects on the response of gas-sensitive resistors based on semiconducting oxides. *Sensors and Actuators B: Chemical.* **70** pp.214-21.
[8] Williams D.E., Moseley P.T. (1991) Dopant Effects on the Response of Gas-sensitive Resistors Utilising Semiconducting Oxides. *J.Mater.Chem.* **1**, No.5, pp.809-14.
[9] Cronstedt A.F. (1756) *Akad. Handl.* Stockholm, **18**, p. 120.
[10] Cronstedt A.F. (1758) *Mineral*, Stokholm. p.120.
[11] Barrer R.M. (1938) The sorption of polar gases by zeolites. *Proc. Roy. Soc.*
[12] Meier, W. M., et al. The Atlas of Zeolite Structure Types, http://www.iza-structure.org/databases/
[13] King L.J., Campbell D.O., Collins E.D., Knauer J.B., Wallace R.M. (1984) *Proceedings of the 6th Intenational Zeolite conference.* Eds. Olsen D., Bisio A. Butterworths, Guildford. p. 660.
[14] Tynjala P., Pakkanen T.T. (1997) Shape selectivity of ZSM-5 zeolite modified with chemical vapor deposition of silicon and germanium alkoxides. *Journal of Molecular Catalysis A: Chemical.* **122**, pp.159-168.
[15] Dyer A. (1988). *Introduction to zeolite molecular sieves.* John Wiley &Sons Ltd., Chichester.
[16] Liu Z., Ottavianni M.F., Abrams L., Lei X., Turro N.J. (2004) Characterization of the external surface of silicalites employing electron parametric resonance. *J.Phys.Chem.A.* **108**, pp. 8040-8047.
[17] Babitz S.M., Williams B.A., Miller J.T., Snurr R.Q., Haag W.O., Kung H.H. (1999) Monomolecular cracking of n-hexane on Y, MOR, and ZSM-5 zeolites. *Applied Catalysis A: General.* **179**, pp.71-86.
[18] Milton (1968) *Molecular Sieves,* Soc. of Chem. Ind., London.
[19] Herreros, B. The X-ray Diffraction Zeolite Database http://chemmac1.usc.edu/bruno/zeodat/XRD.html
[20] Jacobs P.A., Martens J.A., Weitkamp J., Beyer H.K. (1982) *J. Chem Soc. Faraday Disc.* **72**, p. 353.
[21] Wielers A.F.H, Vaarkamp M., Post M.F.M. (1991). Relation between properties and performance of zeolites in paraffin cracking. *J. Catal.* **127**, pp.51-66.
[22] Narbeshuber, T.F., Brait A., Seshan K., Lercher J.A. (1997) Dehydrogenation of light alkanes over zeolites. *J. Catal.* **172**, pp.127-136.
[23] Meisel S.L., McCullogh J.P., Lechthaler C.H., Weisz P.B. (1976) Chem. Tech. **6**, p. 86.
[24] Sherman J.D. (1999) Synthetic zeolites and other microporous oxide molecular sieves. *Proc. Natl. Acad. Sci.* **96**. No. 7. pp. 3471 – 3478.

[25] Nagamori Y., Kawase M (1998) Converting light hydrocarbons containing olefins to aromatics. *Microporous and mesoporous materials.* **21,** pp. 439-435.
[26] Karge H.G., Weitkamp J. (Eds.). (2001) *Post synthesis modifications I, Vol. 3.* Springer-Verlag, Berlin.
[27] Paraskeva T. (2005) *Improving the performance of sensors using zeolites as selectivity modifiers.* PhD Thesis. University of London.
[28] Chintawar P.S., Greene H.L. (1997) Decomposition characteristics of chlorinated ethylenes on metal loaded zeolite Y and γ-Al_2O_3. *Applied Catalysis B: Environment.* **13,** pp. 81-92.
[29] Chintawar P.S., Greene H.L. (1997) Interaction of chlorinated ethylenes with chromium exchanged zeolite Y: An in situ FT-IR Study. *J. Catal.* **165,** pp.12-21.
[30] Parrillo D.J., Fortney J.P., Gorte R.J. (1995) A comparison of adsorption and reaction properties in Cu-ZSM-5 and Cu-Y. *J. Catal.* **153,** pp. 190-193.
[31] Rachapudi R., Chintawar P.S., Greene H.L. (1999) Aging and structure/activity characteristics of Cr-ZSM-5 catalysts during exposure to chlorinated VOCs. *J. Catal.* **185,** pp.58-72.
[32] Giannetto G., Garcia L., Papa J., Yanez F., Goldwasser M.R., Linares C., Moronta D., Mendez B., Urbina de Navarro C., Monque R. (1997). Synthesis and characterisation of [Cr,Al]-ZSM-5 zeolites. *Zeolites.* **19.** pp. 169-174.
[33] Weckhuysen B.M., Wang D., Rosyneck M.P., Lunsford J.H. (1998) Conversion of methane to benzene over transition metal ion ZSM-5 zeolites I. Catalytic characterisation. *J. Catal.* **175,** pp.338-346.
[34] Weckhuysen B.M., Wang D., Rosyneck M.P., Lunsford J.H. (1998) Conversion of methane to benzene over transition metal ion ZSM-5 zeolites II. Catalyst characterisation by X-ray photoelectron spectroscopy. *J. Catal.* **175,** pp. 347-351.
[35] Mosqueira L. and Fuentes G.A. (2002) Molecular selection of MoO_x species during migration on Al_2O_3 and zeolites Y and ZSM-5. *Molecular Physics.* **100,** No.9, pp. 3055-3057.
[36] Anderson J.A., Pawelec B., and Fierro J.L.G. (1993) Mo-USY zeolites for hydrodesulphurisation. 1. Structure and distribution of molybdenum oxide phase. *Applied Catalysis A: General.* **99,** pp. 37-54.
[37] Okamoto Y (1997) Preparation and characterisation of zeolite-supported molybdenum and cobalt-molybdenum sulfide catalysts. *Catalysis Today.* **39,** pp. 45-59.
[38] Egia B., Cambra J.F., Arias P.L., Guemez M.B., Legaretta J.A., Pawelec B., and Fierro J.L.G. (1997) Surface Properties and Hydrocracking activity of NiMo zeolite catalysts. *Applied Catalysis A: General.* **169,** pp. 37-53.
[39] Li D., Nishijima A., Morris D.E. (1999) Zeolite-supported Ni and Mo catalysts for hydrotreatments 1. Catalytic activity and spectroscopy. *Journal of Catalysis.* **182,** pp. 339-348.
[40] Ding M., Yuying S., Xinhe B., Yide X. (2000) Methane dehydro-armoatization under nonoxidative conditions over Mo/H-ZSM5 catalysts: EPR study of the Mo species on/in the H-ZSM5 zeolite. *Journal of Catalysis.* **189,** pp. 314-325.
[41] Ha V.T.T, Meriaudeau P., Naccache C., Tiep L.V (2002) Aromatization of methane over zeolite supported molybdenum: active sites and reaction mechanism. *Journal of Molecular Catalysis A: Chemical.* **181,** pp. 283-290.

[42] Li W., Meitzner D., Borry R.W., Iglesia E. (2000) Raman and X-ray absorption Studies of Mo Species in Mo/H-ZSM5 catalysts for non-oxidative CH_4 reactions. *Journal of Catalysis.* **191,** pp. 373-383.
[43] Borry R.W., Kim Y.H., Huffsmith A., Reimer J.A., Iglesia E. (1999) Structure and density of Mo and acid sites in Mo-exchanged H-ZSM5 catalysts for nonoxidative methane conversion. *J.Phys.Chem.B.* **103,** pp. 5787-5796.
[44] Almanza L.O., Narbeshuber T., Araujo P., Naccache C., Taarit Y.B. (1999) On the influence of the mordenite acidity in the hydroconversion of linear alkanes over Pt-mordenite catalysts. *Applied Catalysis A: General.* **178,** pp.39-47.
[45] de Lucas A., Valverde J.L., Canizares P., Rodriguez L. (1998) Partial Oxidation of methane to formaldehyde over W-H-ZSM5 catalysts. *Applied Catalysis A: General.* **172,** pp. 165-176.
[46] de Lucas A., Valverde J.L., Rodriguez L., Sanchez P., and Garcia M.T. (2001) Modified W/HZSM-5 catalysts: structure and catalytic properties. *Journal of Molecular Catalysis A: Chemical.* **171,** pp. 195-201.
[47] Armor J.N. (1998) Metal-exchanged zeolites as catalysts. *Microporous and mesoporous materials.* **22,** pp. 451-456.
[48] Blomsma E., Martens J.A., Jacobs P.A. 1996, Isomerization and hydrocracking of heptane over bimetallic bifunctional PtPd/H-Beta and PtPd/USY zeolite catalysts. *Journal of Catalysis.* **165,** pp. 241-248.
[49] Muller R., Lange E. (1986) Multidimensional sensor for gas analysis. *Sensors and Actuators.* **9,** pp. 39-48.
[50] Plog C., Maunz W., Kurzweil P., Obermeier E., Scheibe C. (1995) Combustion gas sensitivity of zeolite layers on thin film capacitors. *Sensors and Actuators B.* **24-25,** pp.403-406.
[51] Fukui K., Nishida S. (1997) CO gas sensor based on Au-La_2O_3 added SnO_2 ceramics with siliceous zeolite coat. *Sensors and Actuators B.* **45,** pp.101-106.
[52] Oliver J. (1999) Electronic Odour Sensing. In: Pybus D.H., Sell C.S. (Eds.) *The Chemistry of Fragrances.* The Royal Society of Chemistry, Cambridge.
[53] Faia P.M., Pereira M.A., Nunes A.M., Furtado C.S. (1999) Electronic noses, a different approach to the sensitivity and selectivity issues. *Journal of European Ceramic Society.* **19,** pp.883-886.
[54] Hatfield J.V., Hicks P.J., Neaves P., Persaud K.C., Travers P. An integrated approach to an artificial nose based on ASICs and conducting polymers. *Sensors VI: Technology, systems and applications.* pp.27-32.
[55] Muenchmeyer W., Walte A., Matz G. (2000) Improving electronic noses using a trap and thermal desorption unit. *Sensors and Actuators B.* **69,** pp.379-383.
[56] Moseley P.T., Williams D.E. (1991) Oxygen surface species on semiconducting oxides. In: Mosely P.T., Norris J.O.W., Williams D.E. (Eds.) *Techniques and mechanisms in gas sensing.* Adam Hilger, Bristol.
[57] Moseley P.T., Williams D.E. (1989) Gas sensors based on oxides of early transition metals. *Polyhedron.* **8,** No.13/14, pp.1615-1618.
[58] Gardner J.W., Bartlett P.N. (1994) A brief history of electronic noses. *Sensors and Actuators B: Chemical.* **18,** pp.210-211.
[59] Gardner J.W., Bartlett P.N. (1999) *Electronic Noses: Principles and Applications.* Oxford University Press. Oxford.

[60] Faia P.M. et al. (1999) Electronic Noses, a Different Approach to the Sensitivity and Selectivity Issues. *Journal of the European Ceramic Society.* **19**, pp.883-86.
[61] www.alpha-mos.com Alpha-Mos France, 20 Avenue Didier Daurat, 31400 Toulouse – France.
[62] Dyer A. (1988). *Introduction to zeolite molecular sieves.* John Wiley &Sons Ltd., Chichester.
[63] Baerlocher C., McCusker L.B., Database of Zeolite Structures: http://www.iza-structure.org/databases/
[64] Weckhuysen B.M., Wachs I.E., Schoonheydt R.A. (1996). Surface chemistry and spectroscopy of chromium in inorganic oxides. *Chem. Rev.* **96**, pp. 3327-3349.
[65] Anderson J.A., Pawelec B., Fierro J.L.G. (1993) Mo-USY zeolites for hydrodesulphurisation. 1. Structure and distribution of molybdenum oxide phase. *Applied Catalysis A: General.* **99**, pp. 37-54.
[66] Okamoto Y (1997) Preparation and characterisation of zeolite-supported molybdenum and cobalt-molybdenum sulfide catalysts. *Catalysis Today.* **39**, pp. 45-59.
[67] Borry R.W., Kim Y.H., Huffsmith A., Reimer J.A., and Iglesia E. (1999) Structure and density of Mo and acid sites in Mo-exchanged H-ZSM5 catalysts for nonoxidative methane conversion. *J.Phys.Chem.B.* **103**, pp. 5787-5796.
[68] de Lucas A., Valverde J.L., Rodriguez L., Sanchez P., and Garcia M.T. (2001) Modified W/HZSM-5 catalysts: structure and catalytic properties. *Journal of Molecular Catalysis A: Chemical.* **171**, pp. 195-201.
[69] Niemeyer D., Williams D.E., Smith P., Pratt K.F.E., Slater B., Catlow R.A., Stoneham A.M. (2002) Experimental and computational study of the gas-sensor behaviour and surface chemistry of the solid solution $Cr_{2-x}Ti_xO_3$ ($x \leq 0.5$). *J.Mater.Chem.* **12**, pp. 667-675.
[70] Agmet Ltd. (ESL Europe – www.electroscience.com), 8 Commercial Rd., Reading, RG2 0QZ, UK.
[71] Williams D.E., Pratt K.F.E. (1995) Theory of self-diagnostic sensor array devices using gas-sensitive resistors. *J.Chem.Soc., Faraday Trans.* **91**, No. 13 pp. 1961-66.
[72] Williams D.E. (1999) Semiconducting oxides as gas-sensitive resistors. *Sensors and Actuators B: Chemical.* **57**, No.1 pp. 1-16.
[73] www.alpha-mos.com Alpha-Mos France, 20 Avenue Didier Daurat, 31400 Toulouse – France.
[74] Anderson J.A., Pawelec B., and Fierro J.L.G. (1993) Mo-USY zeolites for hydrodesulphurisation. 1. Structure and distribution of molybdenum oxide phase. *Applied Catalysis A: General.* **99**, pp. 37-54.
[75] Williams D.E., Pratt K.F.E. (1996) Resolving combustible gas-mixtures using gas sensitive resistors with arrays of electrodes, *J. Chem . Soc., Faraday Trans*, **92**, no.22, pp.4497-4504
[76] Park K.-C., Ihm S.-K. 2000, Comparison of Pt/zeolite catalysts for n-hexadecane hydroisomerisation, *Applied Catalysis A: General*, **203**, pp. 201-209.
[77] Williams D.E., Henshaw G.S., Pratt K.F.E., Peat R. (1995) Reaction-diffusion effects and systematic design of gas-sensitive resistors based on semiconducting oxides, *J. Chem Soc. Faraday Trans.*, **91**, No. 21, pp. 4299-4307.

Appendix I: Frameworks of zeolite structures

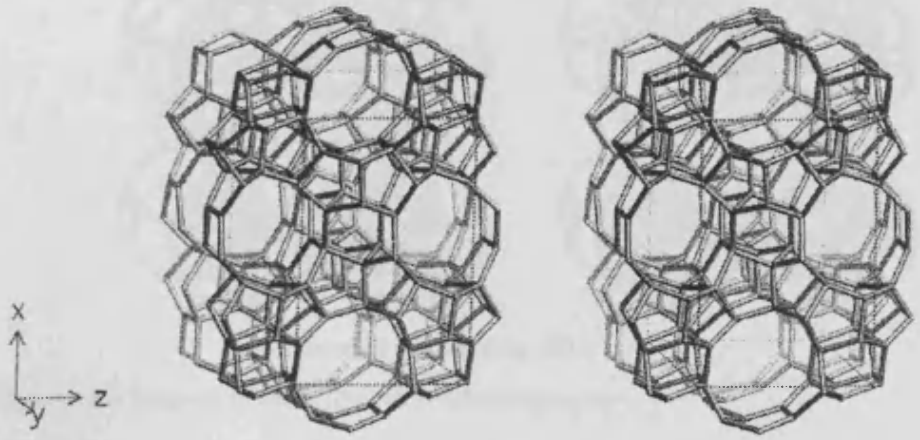

framework viewed along [010]

Figure A1.1 Diagram of ZSM-5 framework.

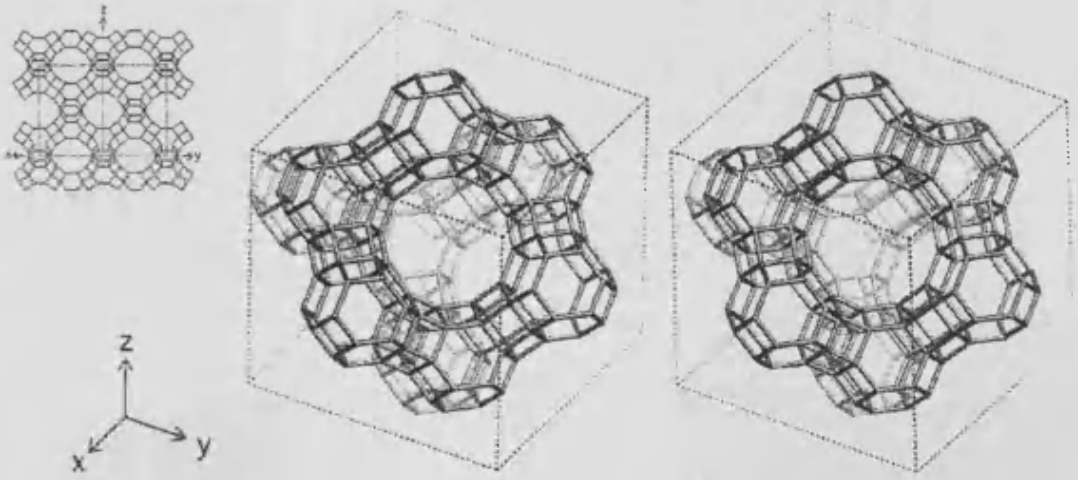

Figure A1.2 Diagram of zeolite Y framework.

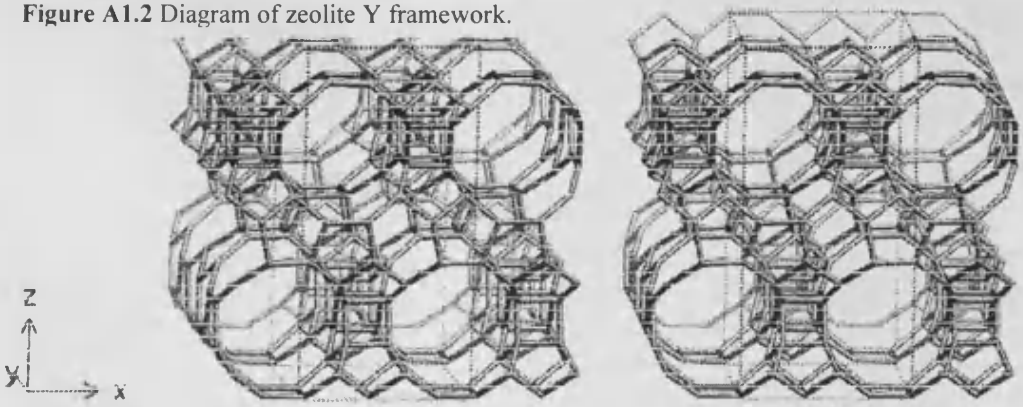

Figure A1.3 Diagram of zeolite β framework.

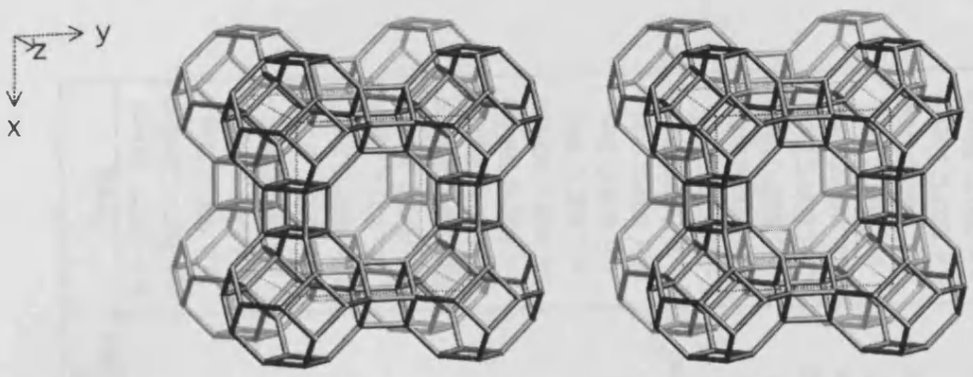

framework viewed along [001]

Figure A1.4 Diagram of Linde Type A zeolite framework.

Appendix II: Table of Sensors Constructed

Code	Date	Sensing oxide layer	Ink details	No. layers	Layer height (µm)	Filter layer	Ink details	No. layers	Layer height (µm)	Firing
AFT8-1	04/10/03	CTO	1:1 16/8/02	8		Cr2O3	1:1 9/4/03	8		o.c. 600°C 30mins
AFT8-2	04/10/03	CTO	1:1 16/8/02	8		Cr2O3	1:1 9/4/03	8		o.c. 600°C 30mins
AFT8-3	04/04/03	CTO	1:1 16/8/02	8		Cr2O3	1:1 9/4/03	8		o.c. 600°C 2hrs
AFT8-4	04/04/03	CTO	1:1 16/8/02	8		Cr2O3	1:1 9/4/03	8		o.c. 600°C 2hrs
AFT8-5	04/04/03	CTO	1:1 16/8/02	8		Cr2O3	1:1 9/4/03	8		o.c. 600°C 2hrs
AFT8-6	04/04/03	CTO	1:1 16/8/02	8		Cr2O3	1:1 9/4/03	8		o.c. 600°C 2hrs
AFT8-7	04/04/03	CTO	1:1 16/8/02	8		Cr2O3	1:1 9/4/03	8		o.c. 600°C 2hrs
AFT8-8	13/10/03	CTO	1:1 16/8/02	8		Cr2O3	1:1 9/4/03	8		o.c. 600°C 2hrs
CB4-1	18/09/03	CTO	1:1 16/8/02	8		Beta-Cr1	n/a	4		o.c. 600°C 30mins
CB8-1	2002	CTO	1:1 16/8/02	8		Beta-Cr1	n/a	8		o.c. 600°C 30mins
CB8-2	2002	CTO	1:1 16/8/02	8		Beta-Cr1	n/a	8		o.c. 600°C 30mins
CB8-3	04/01/03	CTO	1:1 16/8/02	8		Beta-Cr1	n/a	8		o.c. 600°C 30mins
CB8-4	04/01/03	CTO	1:1 16/8/02	8		Beta-Cr1	n/a	8		o.c. 600°C 30mins
CB8-5	04/01/03	CTO	1:1 16/8/02	8		Beta-Cr1	n/a	8		o.c. 600°C 2hrs
CB8-6	04/01/03	CTO	1:1 16/8/02	8		Beta-Cr1	n/a	8		o.c. 600°C 2hrs
CB8-7	04/04/03	CTO	1:1 16/8/02	8		Beta-Cr1	n/a	8		o.c. 600°C 2hrs
CrY1-L-1	26/04/04	CTO	1:1 10/4/03	8	100	LTA/CrY1	CrY1 - 1:2 1/4/04	4/4	45.5/42	o.c. 600°C 2hrs
CrY3-5-1	25/11/03	CTO	1:1 10/4/03	8	100	CrY3	1:2 13/11/03	5	71	o.c. 600°C 2hrs
CrY3-5-2	25/11/03	CTO	1:1 10/4/03	8	100	CrY3	1:2 13/11/03	5	71	o.c. 600°C 2hrs
CrY3-5-3	25/11/03	CTO	1:1 10/4/03	8	100	CrY3	1:2 13/11/03	5	71	o.c. 600°C 2hrs
CrY3-8-1	25/11/03	CTO	1:1 10/4/03	8	100	CrY3	1:2 13/11/03	8	106	o.c. 600°C 2hrs
CrY3-8-2	25/11/03	CTO	1:1 10/4/03	8	100	CrY3	1:2 13/11/03	8	106	o.c. 600°C 2hrs
CrY4-4-1	18/3/04	CTO	1:1 10/4/03	8	100	CrY4	1:2.5 18/3/04	4	53	o.c. 600°C 2hrs
CrY4-8-1	18/3/04	CTO	1:1 10/4/03	8	100	CrY4	1:2.5 18/3/04	8	102	o.c. 600°C 2hrs
CY4-1	2002	CTO	1:1 16/8/02	8		Y-Cr1	n/a	4		o.c. 600°C 30mins
CY4-3	30/4/03	CTO	1:1 16/8/02	8		Y-Cr1	n/a	4	74	o.c. 600°C 30mins
CY8-1	2002	CTO	1:1 16/8/02	8		Y-Cr1	n/a	8		o.c. 600°C 30mins
CY8-3	30/4/03	CTO	1:1 16/8/02	8		Y-Cr1	n/a	8	131	o.c. 600°C 30mins

Code	Date	Sensing oxide layer	Ink details	No. layers	Layer height (µm)	Filter layer	Ink details	No. layers	Layer height (µm)	Firing
CY8-4	7/1/04	CTO	1:1 16/8/02	8		Y-Cr1	n/a	8	131	o.c. 600°C 2hrs
CY8-5	7/1/04	CTO	1:1 16/8/02	8		Y-Cr1	n/a	8	131	o.c. 600°C 2hrs
CZ4-1	2002	CTO	1:1 16/8/02	8		ZSM5-Cr4	n/a	4		o.c. 600°C 30mins
CZ4-3	15/4/03	CTO	1:1 16/8/02	8		ZSM-5-Cr4	n/a	4		o.c. 600°C 30mins
CZ4-4	04/11/03	CTO	1:1 16/8/02	8		ZSM-5-Cr4	n/a	4		o.c. 600°C 30mins
CZ8-1	2002	CTO	1:1 16/8/02	8		ZSM5-Cr4	n/a	8		o.c. 600°C 30mins
LTA4-1	13/11/03	CTO	1:1 10/4/03	8	100	LTA	1:3 12/11/03	4	46	o.c. 600°C 2hrs
LTA4-2	13/11/03	CTO	1:1 10/4/03	8	100	LTA	1:3 12/11/03	4	46	o.c. 600°C 2hrs
MoY1a-4-1	25/11/03	CTO	1:1 10/4/03	8	100	MoY1a	1:2 16/11/03	4	62	o.c. 600°C 2hrs
MoY1a-8-1	25/11/03	CTO	1:1 10/4/03	8	100	MoY1a	1:2 16/11/03	8	116	o.c. 600°C 2hrs
MoY3-4-1	30/5/03	CTO	1:1 10/4/03	8	100	MoY3	1:2 30/05/03	4	54	o.c. 600°C 30mins
MoY3-4-2	18/09/03	CTO	1:1 10/4/03	8	100	MoY3	1:2 30/05/03	4	54	o.c. 600°C 2hrs
MoY3-4-3	18/11/03	CTO	1:1 10/4/03	8	100	MoY3	1:2 30/05/03	4	54	o.c. 600°C 2hrs
MoY3-8-1	31/05/03	CTO	1:1 10/4/03	8	100	MoY3	1:2 30/05/03	8	97	o.c. 600°C 30mins
MoY3-8-2	17/06/03	CTO	1:1 10/4/03	8	100	MoY3	1:2 30/05/03	8	97	o.c. 600°C 2hrs
MoY3-8-3	28/07/03	CTO	1:1 10/4/03	8	100	MoY3	1:2 30/05/03	8	97	o.c. 600°C 2hrs
MoY3-8-4	28/07/03	CTO	1:1 10/4/03	8	100	MoY3	1:2 30/05/03	8	97	o.c. 600°C 2hrs
MoY3-8-5	28/07/03	CTO	1:1 10/4/03	8	100	MoY3	1:2 30/05/03	8	97	o.c. 600°C 2hrs
MoY3-8-6	28/07/03	CTO	1:1 10/4/03	8	100	MoY3	1:2 30/05/03	8	97	o.c. 600°C 2hrs
MoY3-8-7	28/07/03	CTO	1:1 10/4/03	8	100	MoY3	1:2 30/05/03	8	97	o.c. 600°C 2hrs
MoY3-8-8	18/08/03	CTO	1:1 10/4/03	8	100	MoY3	1:2 30/05/03	8	97	o.c. 600°C 2hrs
MoY3-8-9	18/09/03	CTO	1:1 10/4/03	8	100	MoY3	1:2 30/05/03	8	97	o.c. 600°C 2hrs
MoY5-4-1	20/11/03	CTO	1:1 10/4/03	8	100	MoY5	1:2 13/11/03	4	57	o.c. 600°C 2hrs
MoY5-4-2	20/11/03	CTO	1:1 10/4/03	8	100	MoY5	1:2 13/11/03	4	57	o.c. 600°C 2hrs
MoY5-4-3	20/11/03	CTO	1:1 10/4/03	8	100	MoY5	1:2 13/11/03	4	57	o.c. 600°C 2hrs
MoY5-8-1	20/11/03	CTO	1:1 10/4/03	8	100	MoY5	1:2 13/11/03	8	97	o.c. 600°C 2hrs
MoY5-8-2	20/11/03	CTO	1:1 10/4/03	8	100	MoY5	1:2 13/11/03	8	97	o.c. 600°C 2hrs
MoY5-8-3	20/11/03	CTO	1:1 10/4/03	8	100	MoY5	1:2 13/11/03	8	97	o.c. 600°C 2hrs
NZ1	2002	CTO	1:1 16/8/02	8		-	-	-		o.c. 600°C 30mins
NZ1-1	21/2/03	CTO	1:1 16/8/02	8		-	-	-		o.c. 600°C 30mins

Code	Date	Sensing oxide layer	Ink details	No. layers	Layer height (µm)	Filter layer	Ink details	No. layers	Layer height (µm)	Firing
NZ1-10	27/3/03	CTO	1:1 16/8/02	8		-	-	-		o.c. 600°C 30mins
NZ1-2	21/2/03	CTO	1:1 16/8/02	8		-	-	-		o.c. 600°C 30mins
NZ1-3	21/2/03	CTO	1:1 16/8/02	8		-	-	-		o.c. 600°C 30mins
NZ1-4	03/03/03	CTO	1:1 16/8/02	8		-	-	-		o.c. 600°C 30mins
NZ1-5	03/03/03	CTO	1:1 16/8/02	8		-	-	-		o.c. 600°C 30mins
NZ1-6	03/03/03	CTO	1:1 16/8/02	8		-	-	-		o.c. 600°C 30mins
NZ1-7	03/06/03	CTO	1:1 16/8/02	8		-	-	-		o.c. 600°C 30mins
NZ1-8	03/06/03	CTO	1:1 16/8/02	8		-	-	-		o.c. 600°C 30mins
NZ1-9	27/3/03	CTO	1:1 16/8/02	8		-	-	-		o.c. 600°C 30mins
NZ2	2002	CTO	1:1 16/8/02	8		-	-	-		o.c. 600°C 30mins
NZ2-1	03/12/03	CTO	1:1 16/8/02	8		-	-	-		o.c. 600°C 30mins
NZ2-2	03/12/03	CTO	1:1 16/8/02	8		-	-	-		o.c. 600°C 30mins
NZ3-1	03/12/03	CTO	1:1 16/8/02	8		-	-	-		furn 600°C 30 mins
NZ4-1	18/09/03	CTO	1:1 10/4/03	8	100	-	-	-	-	o.c. 600°C 2hrs
NZ4-2	7/1/04	CTO	1:1 10/4/03	8	100	-	-	-	-	o.c. 600°C 2hrs
TH4-DM1	20/5/03	CTO-ZSM5	2002	8		-	-	-		o.c. 600°C 30mins
TH5-DM1	20/5/03	CTO-Y	2002	8		-	-	-		o.c. 600°C 30mins
TH6-DM1	20/5/03	CTO-Beta	2002	8		-	-	-		o.c. 600°C 30mins
WY1-4-1	25/11/03	CTO	1:1 10/4/03	8	100	WY1	1:2 14/11/03	4	68	o.c. 600°C 2hrs
WY1-4-2	25/11/03	CTO	1:1 10/4/03	8	100	WY1	1:2 14/11/03	4	68	o.c. 600°C 2hrs
WY1-4-3	25/11/03	CTO	1:1 10/4/03	8	100	WY1	1:2 14/11/03	4	68	o.c. 600°C 2hrs
WY1-8-1	25/11/03	CTO	1:1 10/4/03	8	100	WY1	1:2 14/11/03	8	116	o.c. 600°C 2hrs
WY1-8-2	25/11/03	CTO	1:1 10/4/03	8	100	WY1	1:2 14/11/03	8	116	o.c. 600°C 2hrs

Appendix III: Sensor details for standard 'C' chamber

Sensor Label	Position	Sensor Material	Heater Resistance R_H	Operating Temperature (°C)
LY/LG	1	Tungsten Oxide	37.30	unknown
LY/G	2	CTO	38.59	379
LY/AA	3	CTO	39.76	397
LY/Gh	4	CTO	41.75	391
LY/gCTL	5	CTO	42.73	406
LY/gCT	6	CTO	41.51	390

Information supplied by Alpha-MOS.

Alpha-Mos France,
20 Avenue Didier Daurat,
31400 Toulouse – France.

Appendix IV: Details of Vanilla Extract Samples and HPLC data

Sample	Botanical Origin	Country Origin	Extraction Process	HPLC Quantification (%)				
				Vanillin	Ac PHB	Ald PHB	Vanillic acid	Ethanol
A	Bourbon	Madagascar	Alcoholic	1.49	0.03	0.11	0.13	33
B	Bourbon	Madagascar	Alcoholic	1.64	0.04	0.12	0.12	31
C	Bourbon	Madagascar	Hydro-alcoholic	1.99	0.05	0.16	0.16	27
D	Bourbon	Madagascar	Hydro-alcoholic	1.62	0.04	0.12	0.12	27
E	Bourbon	Madagascar	Alcoholic	1.71	0.04	0.10	0.21	33
F	Bourbon	Madagascar	Alcoholic	1.87	0.04	0.12	0.17	33
H	Tahitensis	Tahiti		0.38	0.39	0.08	0.03	31
I	Tahitensis	Tahiti		0.51	0.28	0.10	0.01	25
J	Bourbon	Uganda		1.72	0.03	0.10	0.09	32
L	Bourbon	Indonesia		0.09	0.01	0.01	0.02	30
M	Unknown	Unknown		0.92	0.01	0.06	0.06	28
N	Unknown	Unknown		0.74	0.03	0.05	0.11	29
O	Unknown	Unknown		1.48	0.02	0.09	0.17	32

Samples and information supplied by:

Biolandes
Zac Du Font De L'Orme
855 A V M Donat – BP 11
06252 Mougins

www.biolandes.com

Appendix V: Details of Ylang-Ylang Samples

Grade	Abbreviation	Comoros samples	Madagascar samples
Extra S	ES	ES1, ES3, ES4, ES10	
Extra	EX	EX1, EX5, EX8, EX11	
Third	TR	TR5, TR6, TR8	TR7, TR9, TR10, TR11
Second	SE	SE1, SE3, SE5	SE4, SE6
Biolandes' VOP	VO	VO1, VO2	
First	PR	PR1, PR3, PR4, PR6	PR5, PR7
"adulterated" products	CO	CO7, CO8, CO12	

Note: For some Comoros samples the abbreviation would have and added suffix and read, for example, ESC for an extra S grade.

Samples and information supplied by:

Biolandes
Zac Du Font De L'Orme
855 A V M Donat – BP 11
06252 Mougins

www.biolandes.com

Appendix VI: Publications arising from this work

1 IEEE sensors, Vienna University of Technology, 24th to 27th Oct 2004 – paper presented entitled "Metal oxide semiconductor gas sensors utilising modified zeolite catalysts to improve selectivity".

2 Patent entitled "Gas Sensor" filed with UK patent office on 26th June 2003, published on 29th December 2004. GB2403295.

3 1st International Workshop on Smart Gas Sensors: Technology and Application, 17th March 2005 – poster presented entitled "Zeolite layers for Selectivity Enhancement of Metal Oxide Gas Sensors".

4 Mann D.P., Paraskeva T., Pratt K.F.E., Parkin I.P., Williams D.E. (2005) Metal Oxide Semiconductor Gas Sensors utilising a Cr-zeolite catalytic layer for improved selectivity. *Measurement Science and Technology.* **16** p.1193-1200. (Published online 11th April 2005).